Physical Properties of Concrete and Concrete Constituents

Physical Properties of Concrete and Concrete Constituents

Jean-Pierre Ollivier
Jean-Michel Torrenti
Myriam Carcassès

ISTE WILEY

First published 2012 in Great Britain and the United States by ISTE Ltd and John Wiley & Sons, Inc.

ISTE Ltd
27-37 St George's Road
London SW19 4EU
UK

www.iste.co.uk

John Wiley & Sons, Inc.
111 River Street
Hoboken, NJ 07030
USA

www.wiley.com

Library of Congress Cataloging-in-Publication Data

Ollivier, Jean-Pierre, 1946 Apr. 19-
Physical properties of concrete / Jean Pierre Ollivier, Jean Michel Torrenti, Myriam Carcasses.
p. cm.
Includes bibliographical references and index.
ISBN 978-1-84821-330-2
1. Concrete. 2. Concrete--Analysis. I. Torrenti, Jean Michel. II. Carcassés, Myriam III. Title.
TP882.3.O45 2012
666'.893--dc23

2012003201

British Library Cataloguing-in-Publication Data
A CIP record for this book is available from the British Library
ISBN: 978-1-84821-330-2

Printed and bound in Great Britain by CPI Group (UK) Ltd., Croydon, Surrey CR0 4YY

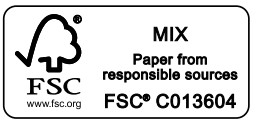

Table of Contents

Introduction xi

Chapter 1. Description of Granular Materials, Definitions 1

1.1. Introduction 1
1.2. Density 2
1.2.1. At the grain scale 2
1.2.2. At the granular material scale 4
1.3. Porosity of granular material 4
1.4. Compactness 4
1.5. Void ratio 5
1.6. Relative compactness 6
1.7. Saturation point 7
1.8. Moisture content 7
1.8.1. Measurement of moisture content 7
1.8.2. Comparison of methods of measurement 10
1.9. Ratio between the different densities 12
1.10. Absorption of water 12
1.11. Bibliography 13
1.12. Exercises 13

Chapter 2. Granulometry 19

2.1. Introduction 19
2.2. Characterization of the shape of grains 21
2.3. Methods of granulometric analysis 22
2.3.1. Sieving 23
2.3.2. Granulometric methods based on sedimentation 30
2.3.3. Coulter counter 37

2.3.4. Laser granulometer (NF ISO 13320-1) 38
2.3.5. Analysis of images coupled by microscopic observations 39
2.4. Granularity: presentation of results 40
2.4.1. Granular cumulative curves 40
2.4.2. Granular frequency curves 43
2.4.3. Other presentations of granularity 43
2.5. Granularity of a mixture of aggregate 46
2.6. Bibliography 47
2.7. Exercises. 48

Chapter 3. Specific Surface Area of Materials 55

3.1. Definition 55
3.1.1. The importance of this parameter: Portland cement hydration 56
3.2. Calculating the specific surface area of a granular material. 57
3.2.1. Powder consisting of identical grains of known shape 57
3.2.2. Homogeneous powder containing grains of non-uniform size 58
3.3. Methods based on permeability and porosity measurements 59
3.3.1. Kozeny-Carman equation. 59
3.3.2. Lea and Nurse apparatus 65
3.3.3. Blaine apparatus 67
3.4. Methods based on the adsorption of a gas 70
3.4.1. Adsorption kinetics. 70
3.4.2. Adsorption isotherms 71
3.4.3. Determination of specific surface area from isotherm adsorption 75
3.4.4. Determination of the specific surface area from an isotherm point 77
3.4.5. Comparison of techniques 78
3.5. Methylene blue test for the characterization of fine particles 78
3.6. Bibliography 79
3.7. Exercises. 79

Chapter 4. Voids in Granular Materials and the Arrangement of Grains 87

4.1. Introduction 87

4.2. Sphere packing (one-dimensional: $\Phi = 2R$): theoretical approach and experimental data . . . 88
4.2.1. 3D packing of square-based layers . . . 88
4.2.2. 3D packing of rhombic-based layers . . . 90
4.2.3. Porosity of identical spherical packing . . . 90
4.3. Experimental data . . . 95
4.4. Influence of grain shape . . . 97
4.5. Search for maximum compactness . . . 98
4.5.1. Mixture of two one-dimensional aggregates . . . 100
4.5.2. Theoretical analysis of the variation of compactness with volume fractions of grains of different sizes . . . 102
4.5.3. Model with interaction . . . 106
4.5.4. Consideration of the vibration, compressible packing model . . . 109
4.5.5. Mixture of three one-dimensional aggregates . . . 113
4.6. Bibliography . . . 121
4.7. Exercises . . . 121

Chapter 5. Voids in Concrete . . . 129

5.1. Definitions . . . 129
5.2. Characterization of heterogeneous materials . . . 133
5.3. Specific surface area of porous solids . . . 136
5.4. Measurements of the porosity of consolidated materials . . . 139
5.4.1. Measurement of total porosity . . . 139
5.4.2. Measurement of open porosity . . . 142
5.4.3. Determination of closed porosity . . . 144
5.5. Porometry . . . 145
5.5.1. Mercury porosimetry (or Purcell porosimetry) . . . 145
5.5.2. Image analysis . . . 164
5.5.3. Method based on the adsorption of a gas . . . 165
5.5.4. Dynamic porosimeter: the Brémond porosimeter . . . 172
5.5.5. Thermoporometry . . . 172
5.5.6. Small angle X-ray scattering and small angle neutron scattering . . . 174
5.5.7. Innovative techniques in development . . . 175
5.6. Bibliography . . . 175
5.7. Exercises . . . 177

Chapter 6. The Fundamentals of Diffusion . . . 195

6.1. The basics of diffusion . . . 195
6.1.1. Microscopic approach to diffusion . . . 195

6.1.2. Diffusion and transport of matter at the macroscopic level: Fick's first law . . . 201
6.1.3. A thermodynamic approach to molecular diffusion . . . 203
6.1.4. The diffusion of ions in solution . . . 205
6.1.5. Fick's second law . . . 210
6.1.6. The concentration profile of diffusing species . . . 211
6.2. Diffusion in porous media . . . 219
6.2.1. Molecular diffusion . . . 219
6.2.2. Ionic diffusion . . . 222
6.2.3. The penetration kinetic of a species by diffusion: Fick's second law . . . 222
6.3. Measurement of the effective diffusion coefficient in porous matter . . . 228
6.3.1. Diffusion cell method . . . 228
6.3.2. Electric field migration tests . . . 233
6.3.3. Measurement of the apparent diffusion coefficient by immersion . . . 240
6.3.4. Principle of methods of measuring the effective diffusion coefficient based on measurements of conductivity . . . 241
6.3.5. Orders of magnitude of the diffusion coefficient in concrete . . . 243
6.4. The relationship between the effective diffusion coefficient and porous structure . . . 245
6.4.1. Empirical models . . . 246
6.4.2. Polyphasic models . . . 249
6.5. Gaseous diffusion . . . 256
6.5.1. The diffusion of a gas in an infinite medium . . . 256
6.5.2. The diffusion of a gas in a pore . . . 258
6.5.3. The diffusion of a gas in a porous material . . . 259
6.5.4. The diffusion of a gas in a reactive porous environment . . . 261
6.6. Bibliography . . . 262
6.7. Exercises . . . 266

Chapter 7. Permeability . . . 279

7.1. Introduction . . . 279
7.2. Definition of the permeability of a material . . . 280
7.3. Measurement of permeability . . . 282
7.3.1. Constant head permeameters . . . 282
7.3.2. Analysis of results: validity of Darcy's law . . . 286
7.3.3. Methods of measuring gas permeability . . . 294
7.3.4. Variable head permeameters . . . 295

7.4. The relationship between permeability and porous structure . . 296
7.4.1. Empirical models 297
7.4.2. Physical models 297
7.5. The drying of concrete 303
7.5.1. Physical mechanisms 304
7.5.2. Simplified modeling of drying. 305
7.6. Physical parameters and performance-based approach 307
7.7. Bibliography 309
7.8. Exercises. 312

Index 333

Introduction

Concrete is manufactured at the plant or on site from various components: cement, water and different granular materials such as sand, gravel and various mineral additions. It may also contain admixtures intended to modify its properties from its fresh state (for example retarding or accelerating admixtures, superplasticizer) or its properties in its hardened state (for example air entraining agents). Properties introduced in this material are varied. They concern both its fresh state through its ability to be transported and poured in forms that are more or less fluid, as well as in its hardened state. Properties include its performances, for example mechanical resistance, resistance to aggressive environments, and acoustic or heat insulation. The formulation of concrete consists of finding components and their proportions to meet specific requirements, which may be very different. All of this should be done keeping in mind that concrete is a widely used material, its cost should be limited, and it is prepared and implemented on site in variable environmental conditions.

Understanding the rheological properties of fresh concrete, the hydration phenomenon of cement responsible for structuration, the relationship between the characteristics of the porous solid obtained and its mechanical performances or resistance to the aggressive penetration requires a complex knowledge of the physicochemistry of reactive porous materials. The development of simple formulation rules therefore requires the assimilation of this knowledge and a good command of the properties of these materials.

The purpose of this book is to provide the “mix designer” with useful knowledge on granular and porous materials, which will enable the innovative design of concrete. Topics covered include the characterization of

granular materials, the concepts of porosity and specific surface area, and the transport properties (diffusion and permeation) of concrete. Some of these topics are already covered in other general books dedicated to granular or porous materials. The objective here is to bring them together in one book by adapting them for use by concrete specialists.

Simulations in the form of exercises are offered at the end of each chapter to enable readers to assimilate theoretical knowledge and to apply such knowledge to specific problems encountered in civil engineering.

Chapter 1

Description of Granular Materials, Definitions

1.1. Introduction

We call a set of grains "*aggregate*". We also refer to this as *granular material*. Several civil engineering materials are granular materials: soil, road-building materials or concrete before the setting the binder, etc.

Let us consider a *grain*, as shown in Figure 1.1. This grain consists of a solid phase, voids or open pores and voids or closed pores. The former communicates with the outside, and the latter are included in the solid phase.

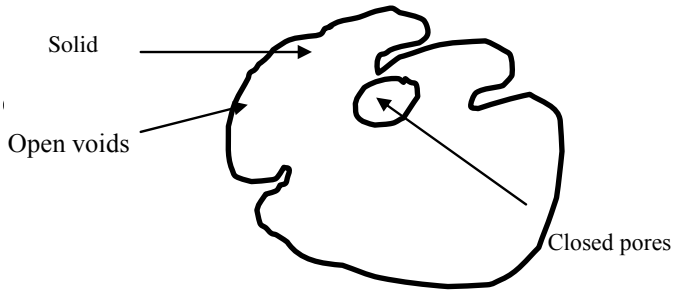

Figure 1.1. *Definition of a grain*

Physical Properties of Concrete and Concrete Constituents Jean-Pierre Ollivier, Jean-Michel Torrenti and Myriam Carcassès

By definition, the *grain volume* is the sum of the volume of a grain in its solid phase and the volume of the closed pores.

Let us now consider *a set of grains*. v_g is the *grain volume* of this set.

Different volumes are defined:

– V_a is the *apparent volume of granular material*. This is, for example, the volume of the container that holds all of the material or the volume of the stack of material if it is in bulk (which is the bulk volume).

– v_s is the volume of the total solid phase.

– v is the *void volume*: the total volume of the intergranular voids and open voids of grains. The geometric definition of the open void volume of a grain is not simple, as it necessitates the prior definition of the envelope of the grain. In practice, we speak of the void volume accessible to water. In the case of a granular material, the definition of void volume is simpler: it is the difference between the apparent volume and the grain volume.

$$V_a = v_g + v$$

The void volume is wholly or partially full of air or water.

1.2. Density

1.2.1. *At the grain scale*

We distinguish:

– The *solid density*: $\rho_s = \frac{m_s}{v_s}$ where m_s is the solid mass. This mass is ordinarily measured after drying, where the water contained in the open pores evaporates. We also refer to it as *dry mass*.

– The *density of grains*: $\rho_g = \frac{m_s}{v_g}$. This density is less than or equal to ρ_s according to the presence or absence of closed pores in the grains.

For example, in the case of cements these two densities are identical. Their measurement is taken using a volumeter (or hydrometer), known as the Chatelier, in accordance with standard EN 196-6.

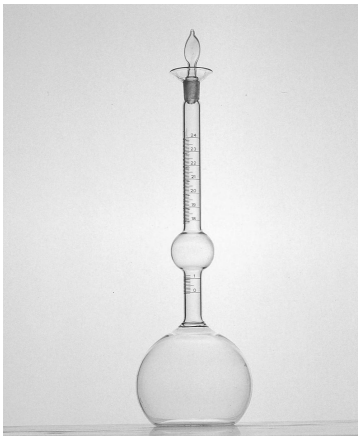

To characterize cement, it is placed in a glass container raised in a graduated cylinder (the volumeter), which contains oil (cement being reactive with water, it is advisable to choose an inert liquid). The change in volume is measured by the displacement of the oil in the graduated cylinder and the mass of the cement is obtained by weighing the volumeter twice: before and after adding the cement.

Figure 1.2. *The Chatelier volumeter or hydrometer (CONTROLAB)*

In the case of concrete aggregates, the NF EN 1097-6 standard defines four densities[1]. The latter definitions complicate the landscape slightly, but they are subject to requirements. They are subject to standard methods of measurement (NF EN 1097-6), which can be found in the exercises presented at the end of this chapter.

1 *The actual density determined after drying in an oven,* ρ_{rd}: the ratio between the mass of grains dried in an oven and the volume that they occupy in water, including closed pores and those accessible to water.
The absolute density, ρ_a: the ratio between the mass of grains dried in an oven and the volume that they occupy in water, including closed pores but excluding those accessible to water. This definition corresponds to the density of the grains.
The actual density of saturated surface dry, ρ_{ssd}: the ratio between the mass of a sample of grain, including the mass of water present in the pores that are accessible to water, and the volume that they occupy in water, including closed pores and those accessible to water.
The actual pre-dried density, ρ_p: the dry grain mass per unit volume (the volume is determined as the volume of the particles, including closed pores and those accessible to water).

1.2.2. *At the granular material scale*

The *density of granular material*, also known as the *bulk density*, ρ, is defined as the apparent mass per unit volume of aggregate:

$$\rho = \frac{m_s + m_e}{V_a}$$

where m_s is the mass of grains (it is also the mass of solid) and m_e is the mass of water contained in the voids.

When the material is dry ($m_e = 0$), the density is called the "dry density" and is written as ρ_d.

The density of a granular material depends on:

– the density of grains,

– the arrangement of the grains in space; and

– the quantity of water present in the voids.

Before being more specific about it (see section 1.8), we must define the variables characterizing the arrangement of the grains and the presence of water in the voids.

1.3. Porosity of granular material

This is the ratio between the void volume and the apparent volume:

$$p = \frac{v}{V_a}.$$

1.4. Compactness

This is the ratio between the volume of grains and the apparent volume:

$$c = \frac{v_g}{V_a} = \frac{V_a - v}{V_a} = 1 - p$$

1.5. Void ratio

This is the ratio between the void volume and the volume of grains:

$$e = \frac{v}{v_g} = \frac{v}{V_a\text{-}v} = \frac{p}{1\text{-}p}$$

Porosity, compactness and the void ratio are the three quantities that characterize the relative volume fractions of voids and grains of a granular material. Relationships exist between them and knowledge of one enables us to calculate the other two. For example, the measurement of the porosity of an aggregate is taken by weighing the quantity of the dry material, m_s, filling a container of a known volume, V_a. Knowing the density of the grains, ρ_g, the porosity is calculated using the formula:

$$p = \frac{v}{V_a} = \frac{V_a - V_g}{V_a} = 1 - \frac{m_s}{\rho_g V_a} = 1 - \frac{\rho_d}{\rho_s} = c.e$$

These three quantities depend on the shape and size of the grains of the granular material. To manufacture concrete, different granular materials are mixed in order to achieve a compact granular skeleton. This important objective is discussed in detail in Chapter 3. Let us compare the orders of magnitude of the porosities of granular materials:

– Sand: 21–50% (for example 35% of great Erg sand, 31% of Albien sand from the Parisian basin (l'Albien du Bassin Parisien), 24% of sand from the Barremian of the Parisian Basin (Barrémien du Bassin Parisien).

– Gravel: 25–40%.

– Clay: 44–50%.

– Cement: approximately 66%.

– Silica fume in grains: approximately 95%.

Porosity also depends on how the grains of the material arrange themselves in space. Under the effect of compression or vibration, porosity can be reduced (see section 1.6). It is therefore not a variable intrinsic to the material because it depends on the conditions of its "implementation". In the case of cement and of silica fume, it is noted that the porosities are very high: if silica fume was being transported in grain form, 95% of the volume

of the load would consist of voids! These very high values will be discussed in Chapter 2. They arise from strong electrostatic repulsions due to the superficial electric charges of the grains, which repel each other.

1.6. Relative compactness

The void ratio of a given aggregate may vary in accordance with the way the grains are arranged in space against one another. For example, if sand is poured very slowly into a container that is leveled, we obtain a loose arrangement corresponding to the maximum void ratio, e_{max}. If the container is shaken, the apparent volume of the material is reduced, as is the void ratio. Gradually, as the vibration energy increases, the void ratio approaches a lower limit, e_{min}.

The compactness or the relative *compactness index* enables a void ratio e to be collected that is in the range of possible values:

$$C_r = \frac{e_{max} - e}{e_{max} - e_{min}}$$

The relative compactness of a given aggregate, sometimes called the "compactness index", only depends upon its implementation.

We can distinguish conventionally between two categories of materials:

– *coherent materials* (e.g. clays) whose minimum void ratio depends on the applied stress (or even the speed of application of the stress); and

– *non-coherent materials* whose minimum void ratio does not depend on the applied stress. Granular materials used in the manufacture of concrete fall into this second category and in this book we limit ourselves to just such materials.

The voids of granular materials may contain water. Two quantities – one density (saturation point) and the other weight (moisture content) – are defined to characterize the quantity of water present in an aggregate.

1.7. Saturation point

This is the ratio between the volume of water, v_e, contained in the voids and the void volume:

$$s = \frac{v_e}{v}$$

The saturation point varies between 0 (dry material) and 1 (saturated material).

1.8. Moisture content

This is the ratio between the mass of water, m_e, and the mass of *dry material* (or mass of grains):

$$w = \frac{m_e}{m_s}$$

The moisture content is equal to 0 in the case of a dry material and in some instances may be greater than 1 (particularly in the case of some clays).

1.8.1. *Measurement of moisture content*

Measurement of the moisture content of aggregates used in the manufacture of concrete is essential, because if the methods of formulation enable determination of the efficient dosage of water (standard NF EN 206-1) of concrete (typically expressed as L/m^3 or as kg/m^3), it should take into account the water contained within the aggregates to determine the quantity of water that needs to be added. The measurements must be simple, as they must be routinely applied upon receipt of the aggregates.

The reference method is the gravimetric method. There are also a chemical method, electrical methods and a method based on the absorption of neutrons. These methods are outlined briefly in the following sections.

1.8.1.1. *Gravimetric method*

The mass of water contained in the aggregate is determined by the difference in the wet mass of a sample of aggregate and its dry mass obtained after drying at 105°C ±5°C to constant mass (two successive weighings, separated by at least one hour, should not differ by more than 0.1%). Generally the aggregate must be dried for approximately 24 hours [CAL 04]. To speed up the drying, an alternative source of heat can be used such as infrared lamps or halogen lamps. The aggregate can even be dried in the microwave.

The moisture content of aggregates can also be measured with the method known as "the frying pan", according to the standards NF P94-049-2 and NF P18-554.

Figure 1.3. *The frying pan method, also known as the frying stove method (CONTROLAB)*

1.8.1.2 *Chemical method*

A chemical method can be implemented using a "Speedy" or "Super Speedy" moisture meter (26 g or 142 g respectively), depending on the quantity of material tested. The wet aggregate is placed in the presence of excess calcium, which reacts with water according to the reaction:

$$C_2Ca + 2H_20 \rightarrow Ca(OH)_2 + C_2H_2$$

The amount of acetylene, C_2H_2, produced is proportional with the mass of water contained in the aggregate. The moisture content is read directly from the device, which in fact measures the pressure of the acetylene. Given the small mass of aggregate tested, the use of this device is only recommended for fine materials (sand), see Chapter 2 for the definition.

Figure 1.4. *Calcium carbide moisture meter (CONTROLAB)*

1.8.1.3. *Electrical methods*

These methods are based on the influence of the liquid water contained in a granular material on its resistivity (or conductivity). Thus, for a moisture content ranging from 5 to 25%, the resistivity of sand is divided by a factor of 10. The measurements are taken with probes immersed in the granular material. The measurements are also sensitive to temperature, the presence of dissolved salts and the shapes and sizes of the grains.

Water also has a strong influence on the permittivity of a granular material. The relative permittivity (the ratio between the absolute permeability of a medium and of air) is thus in the range of 5 for a solid grain and approximately 80 for water. The permittivity of a wet aggregate therefore depends on the water it contains and this property is used for measuring the moisture content [PAQ 71].

1.8.1.4. *Method based on the absorption of slow neutrons*

If a probe is immersed in fast neutrons (several km/s) of high energy (several MeV) in a granular material, the neutrons undergo elastic collisions (without energy loss) when they meet the heavy atoms of the grains. In a collision with a light atom, such as hydrogen whose mass is practically that of a neutron, the loss of energy is significant. After a number of collisions with hydrogen atoms, the neutron possesses energy in relation to its mass and the temperature of the medium: it reaches the thermal or slow state.

Measurement of the concentration of slow neutrons, after calibration, enables the assessment of hydrogen concentration, and therefore the moisture content of the wet aggregates. The fast neutron source (radium-beryllium or polonium-beryllium) and the slow neutron sensor are placed in the same probe because the result depends on the distance between the transmitter and receiver.

1.8.1.5. *Method based on the radiation of an infrared ray*

Infrared radiation wavelengths centered at the absorption peak of water are emitted towards the granular material. The reduction in radiation measured is based on the humidity and the moisture content. This is inferred from the specific calibration of the material as the wavelength of the infrared beam depends on the optical properties of grains.

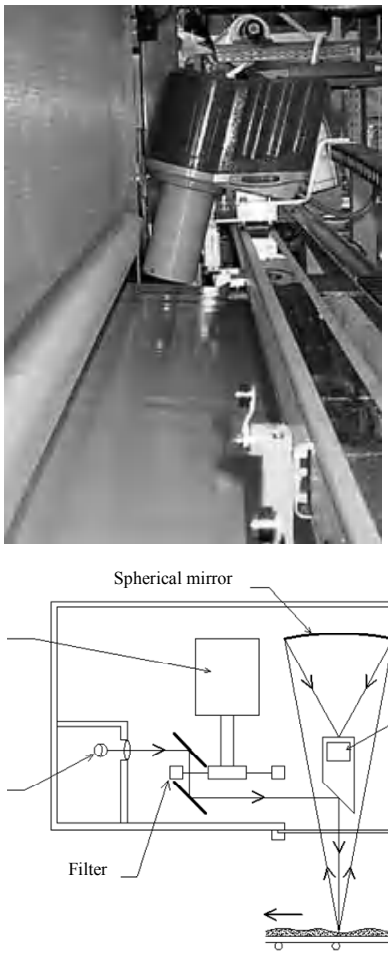

Figure 1.5. *Infrared moisture meter – flow chart [CAL 04]*

1.8.2. *Comparison of methods of measurement*

Methods of measuring the moisture content of aggregates are numerous and are based on very different principles. In [CAL 04], their implementation and their scope are described in detail. Table 1.1, taken from the same reference, gives the selection criteria for the methods listed above.

Measurement principle	Type of measure-ment concerned	Response time	Primary influencing factors	Measuring range	Type of moisture	Accuracy
Total drying Reference method Elimination of water in vapor form, weighing of the wet material then the dry material	Volume	Slow	Part of the mass loss may be due to the presence of volatile matter	0% up to saturation	Total water	±1%
Chemical	Volume	Fast	Dose of chemical agent. Small sample size. Limited to very fine grains.	0–12% (speedy) 0–20% (super speedy)	Surface water	±3%
Conductivity or resistivity (DC or low frequency <50 kHz)	Volume	Fast	Contact electrodes (polarization). Strong influence of dissolved salts. Strong influence of grain size and density.	3–12%	Intergranular water and water absorbed	Low accuracy
Permittivity	Volume, surface	Fast	Strong influence of dissolved salts. Influence of grain size and of temperature. Strong influence of density.	3–10% (sand); 4% (gravel)	Intergranular water and water absorbed	±1%
Neutronics	Volume	Fast	Influence of water content and hydrogen from organic matter. Strong influence of density.	1% up to saturation	Intergranular water and water absorbed*	±2% if duration = 1 mn ±1% if duration = 4 mn
Infrared	Surface	Fast	Strong influence of temperature and dust. Strong influence of nature and density.	0–30%	Surface water	±1%

*The water absorbed is fixed on the surface of grains. This concept is discussed in more detail in Chapter 3.

Table 1.1. *Selection criteria for different methods of measurement*

1.9. Ratio between the different densities

The density of a granular material depends on the grain density, porosity and saturation state.

It can be expressed in the following way:

$$\rho_d = \frac{m_s}{V_a} = \frac{\rho_s . v_s}{V_a} = \frac{\rho_s (V_a - v)}{V_a} = \rho_s (1 - p)$$

When the material is saturated, the density of the granular material (ρ_e = density of water) is:

$$\rho_{(s=1)} = \frac{m_s}{V_a} + \frac{m_e}{V_a} = \rho_s (1-p) + \frac{s.v.\rho_e}{V_a} = \rho_s (1-p) + p.\rho_e$$

In the general case, for any saturation point, s, we can write:

$$\rho = \frac{m_s + m_e}{V_a} = \frac{m_s}{V_a} + \frac{m_e}{V_a} = \rho_d + \frac{v_e \rho_e}{V_a} = \rho_d + sp\rho_e$$

Another ratio can express the density of an aggregate based on its moisture content:

$$\rho = \frac{m_s + m_e}{V_a} = \rho_d + \frac{m_e}{V_a}\frac{m_s}{m_s} = \rho_d (1 + w)$$

1.10. Absorption of water

The grains of a granular material have the capacity to absorb water by capillary action (see Chapter 5). This capability is characterized by a variable known as “water absorption” and is defined as the ratio between the dry mass and the increase in the mass of the sample of aggregates due to water penetration in the accessible pores.

Its measurement is subject to standard NF EN 1097-6.

1.11. Bibliography

[CAL 04] CALIBÉ, *Results and Recommendations of the National Project, Calibé, the Quality Control of Concrete*, ENPC Press, Paris, 2004.

[PAQ 71] PAQUET J., "Moisture measurement in situ for dielectric method of application to concrete", *Materials and Structures*, vol. 4, no. 2, pp. 67-124, March 1971.

1.12. Exercises

Exercise 1.1: *calculation of the density of grains in a mixture*

As is the case for concrete in civil engineering. aggregates are frequently combined to obtain mixtures of maximum compactness (see Chapter 2). This exercise aims to determine the density of grains in a mixture of two aggregates, with knowledge of the densities of the grains in the two aggregates and the proportions by volume or mass of the two aggregates in the mixture.

Two aggregates, 1 and 2, are mixed. The data are summarized in Table 1.2.

	Density of grains	**Mass of grains**	**Volume of grains**	**Proportion by weight**	**Proportion by volume**
Aggregate 1	ρ_{g1}	m_1	v_1	x_1	y_1
Aggregate 2	ρ_{g2}	m_2	v_2	x_2	y_2
Mixture	ρ_g	m	v		

Table 1.2. *Parameters of Exercise 1.1*

Show the relationship between the density of grains in the mixture ρ according to the densities of grains ρ_1 and ρ_2 and weight proportions x_1 and x_2.

$$\frac{1}{\rho_g} = \frac{x_1}{\rho_{g1}} + \frac{x_2}{\rho_{g2}}$$

Show the relationship between the density of grains in the mixture ρ according to the densities of grains ρ_1 and ρ_2 and volume proportions y_1 and y_2.

$$\rho_g = y_1\rho_{g1} + y_2\rho_{g2}$$

NOTE 1.1.– Note that due attention should be paid to this calculation on how we define the proportions of the mixture.

NOTE 1.2.– In Chapter 2, we will show that such a calculation cannot be carried out to determine the bulk density of a mixture of two aggregates.

Exercise 1.2: ***density measurement and pycnometer method***

The pycnometer consists of a glass funnel (1) equipped with a marker (2) on the vertical rod. This funnel is connected to a bottle (4) by means of an oiled part (3), see Figure 1.6.

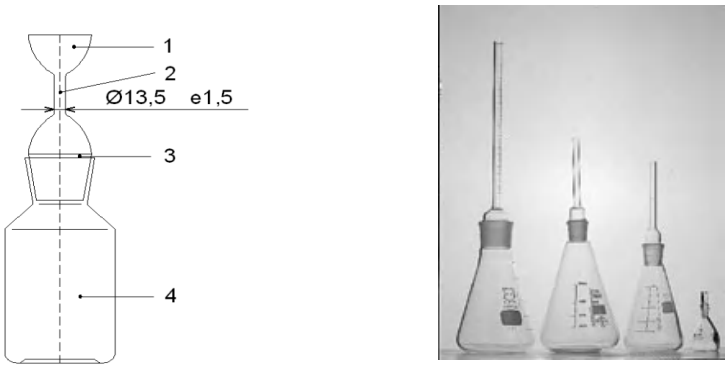

Figure 1.6. *Pycnometer according to standard NF P18-555 (CONTROLAB)*

The size of the pycnometer is adapted to the size of the grains to be characterized. A sample of the aggregate to be characterized is taken and placed in the flask of the pycnometer. The flask is filled with water and, after closing the funnel, the water level is adjusted to the level of the mark. After 24 hours of immersion, the pycnometer is weighed, with M_1 being the mass.

The pycnometer is drained while taking care to preserve the aggregate. It is then filled with water up to the mark, with M_2 being its mass.

The aggregate is spread out to form an even layer and is exposed to a weak stream of hot air to evaporate the surface moisture in order to reach the "saturated-surface dry" state, which is free of any trace of surface moisture and where the grains are not bonding to one another. M_3 is the mass of the dry grains of the saturated surface.

Finally the aggregate is dried in an oven at 110°C to constant mass, with M_4 being the dry mass.

Express:

– the absolute density, ρ_a;

– the real density determined by drying in an oven, ρ_{rd};

– the actual saturated surface dry density ρ_{ssd} according to masses M_1, M_2, M_3 and M_4; and

– the density of water, ρ_ε.

Knowing that the accuracy of the scale used is 0.01g and that the temperature of the trial is near to 20°C, but that it can vary by up to 4°C either side of this, calculate the accuracy of the measurement ρ_a.

Additional data: the variation of the density of water, ρ_ε, with temperature is given in Table1.3.

Temperature (°C)	16	20	24
ρ_ε (g/cm^3)	0.9990	0.9982	0.9973

Table 1.3. *Variation in the density of water according to temperature*

NOTE 1.3.– this method enables us to calculate the coefficient of water absorption:

$$WA_{24} = 100\frac{M_3 - M_4}{M_4}$$

Correcting factor:

$$\rho_a = \frac{M_4}{\left[M_4\text{-}(M_1\text{-}M_2)\right]\rho_e} \;;$$

$$\rho_{rd} = \frac{M_4}{\left[M_3\text{-}(M_1\text{-}M_2)\right]\rho_e} \;;$$

$$\rho_{ssd} = \frac{M_3}{\left[M_3\text{-}(M_1\text{-}M_2\right]\rho_e}$$

Exercise 1.3: ***measurement of the density of grains by hydrostatic weighing***

Figure 1.7. *Built for hydrostatic weighing (CONTROLAB)*

The grains to be characterized are deposited in a basket made of fine mesh wire (that holds the grains), see Figure 1.7. The basket is connected to the tray of a scale.

The basket containing a sample of aggregate to be tested is submerged in water. The result of the weighing is M_1. The basket is then emptied and weighed in a water vacuum, with M_2 being the result of the second weighing. The grains are spread and dried until the water is no longer visible, ensuring that the grain surface always appears wet. The grain mass in this state is M_3. The grains are then dried in an oven at 110°C to a constant mass (M_4).

Express:

– the absolute density, ρ_a;

– the actual density of drying in an oven ρ_{rd},

– the actual saturated surface dry density ρ_{ssd} according to masses M_1, M_2, M_3 and M_4; and

– the density of water, ρ.

NOTE 1.4.– this method enables us to calculate the coefficient of water absorption:

$$WA_{24} = 100\frac{M_1\text{-}M_4}{M_4}$$

Correcting factor:

$$\rho_a = \frac{M_4}{\left[M_4\text{-}(M_2\text{-}M_3)\right]\rho_e} \;;$$

$$\rho_{rd} = \frac{M_4}{\left[M_1\text{-}(M_2\text{-}M_3)\right]\rho_e} \;;$$

$$\rho_{ssd} = \frac{M_1}{\left[M_1\text{-}(M_2\text{-}M_3\right]\rho_e}$$

Exercise 1.4: ***preparation of a specimen with fixed characteristics.***

We want to prepare a cylindrical specimen of slag-sand[2] (with a height of 100 mm and diameter of 100 mm) using static compression. The proportions by weight of the different dry components are as follows:

– sand, S_1 = 80%;

– sand, S_2 = 10%;

– slag, L = 9%; and

– enzyme A = 1%

The characteristics of the components are summarized in Table 1.4.

Components	**Density of grains (g/cm^3)**	**Moisture (%)**
Sand S_1	2.64	0.3
Sand S_2	2.66	5.1
Slag	2.90	6.0
Enzyme	2.56	0.0

Table 1.4. *Density and moisture of the components*

The dry density of the material obtained after compression (made in a sealed mold) is $\rho_d = 2.21 \times 10^3$ kg/m^3 and the moisture is 6.5%.

1. What are the masses of the four solid and wet components and that of the water to be added to the mold?

2. What is the porosity and what is the saturation point of the specimen?

2 Slag-sand is a material used in the manufacture of road-building materials. It combines sand and a binder, the slag. This slag is a finely ground by-product of the steel industry. It reacts with water and an enzyme (e.g. lime) to make hydrates. The material structures itself and thus passes from the granular to the consolidated state, which enables the road-building materials to bear mechanical loads due to traffic.

Chapter 2

Granulometry

2.1. Introduction

Granulometry is used to determine the grain size of a granular material. Results of granulometric analysis (known as granularity) may be represented, for example, in the form of a distribution size curve.

Grains of different granular materials involved in the composition of concrete have very different shapes. Some are spherical, such as silica fumes, some have an angular shape, such as crushed aggregates, and others have a rounded shape, such as the grains of round aggregates from alluvial origins (see Figure 2.1). The shape of grains has a significant influence on the properties of concrete, particularly on the compactness of the granular mixture and the fluidity of concrete in its fresh state.

Given that most grains have a shape of some kind, the geometric definition of the "size" is initially very difficult. In practice, the definition of the "size" of a grain has a conventional character, which depends on the method of measurement implemented. Measurement may be direct, in which case the definition of the "size" is relatively simple. Measurements may also be taken by indirect methods, which provide equivalent sizes in relation to the physical property being measured. According to the method used, the granulometry result may change. It is therefore essential to carefully specify the experimental method used when we present the result of a granulometric analysis.

Physical Properties of Concrete and Concrete Constituents Jean-Pierre Ollivier, Jean-Michel Torrenti and Myriam Carcassès

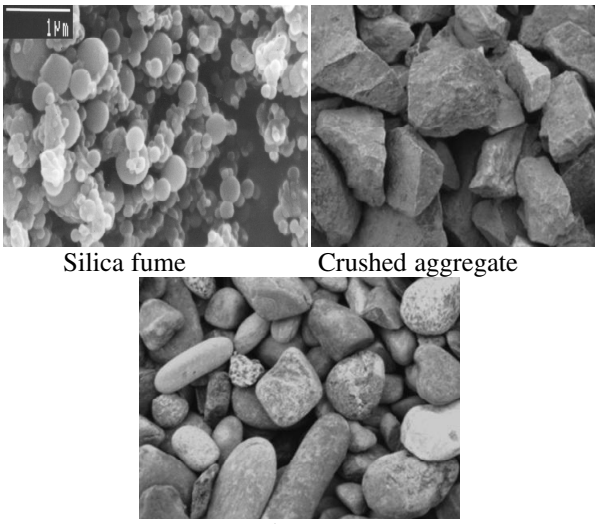

Figure 2.1. *Granular materials consist of grains of different shapes*

Generally, the size of a particular grain is of no interest. The information sought concerns how the grain size of a granular material is distributed. To obtain this information, a sample of the material is taken and due attention given to its representativeness. Methods of sampling exist for this: quartering or the use of a lane divider. In standard *NF EN 932-1, Tests to Determine General Properties of Aggregates*, parts 1 and 2 are devoted to the methods of sampling and methods of reduction of a laboratory sample, respectively.

Section 2.2 of this chapter describes variables. These enable us to characterize the shape of grains. Granulometry methods are discussed later in section 2.3. Sieving is used for particles with sizes larger than 100 μm. For smaller particles, methods based on different physical principles will be described. How to present granulometry results will be the subject of section 2.4.

During the granulometric analysis of a granular material, attention must be given to the dispersion of the particles. Fine particles in dry air tend to repel one another due to the effect of electrostatic forces because their surfaces frequently have charges of the same sign. As soon as moisture in the air accrues, the particles may agglomerate and the measurement of grain

size becomes more complicated. In the case of coarse grains this is not usually a problem, although sand and gravel have to be carefully prewashed to eliminate the smallest particles before carrying out granulometric analysis by sieving (see section 2.4). In the case of very small particles (less than 100 μm), the methods of analysis often require pre-dispersion in a liquid and we must ensure that the grains are properly separated from one another (we must deflocculate the grains, see Chapter 3).

2.2. Characterization of the shape of grains

In general, the shape of particles is characterized by the geometric quantities and, as in the case of the flattening coefficient for example, they may match the standard methods of measurement (see standard NF EN 933-3).

If a denotes the largest grain, c the smallest grain and b an intermediate size, we can define:

– *the flattening coefficient*: $FI = \frac{c}{b}$ [2.1]

– *the slenderness*: $\frac{b}{a}$ [2.2]

– *the shape factor*: $\frac{ac}{b^2}$ [2.3]

We can define two equivalent spheres: the isovolume sphere, which has the same volume as the grain; and the isosurface sphere, which has the same surface as the grain. If $\varnothing_1$ is the diameter of the isovolume sphere and $\varnothing_2$ the diameter of the isosurface sphere, the sphericity factor ψ is defined by the ratio:

$$\psi = \frac{\Phi_1}{\Phi_2} \quad [2.4]$$

The sphericity factor is also defined by the ratio between the surface of the isovolume sphere and the surface of the particle. These two definitions are equivalent.

The term $\frac{1}{\psi}$ is called the angularity factor. Its value is even larger than the grain in a shape that moves away from being spherical. For example, the angularity factor of the sphere is equal to 1, for a cube it is $\frac{1}{\psi}=1.11$ and for a parallelepiped (a × a × 2a) it is $\frac{1}{\psi}=1.14$.

Exercise 2.1 gives an application using an aggregate in the shape of an ellipsoid.

2.3. Methods of granulometric analysis

To illustrate the difficulty of associating grain size with a shape of some kind, let us consider two geometric definitions of the size of a particle. Figure 2.2a shows a grain on a projection plane. Note before proceeding that this projection depends on the chosen plane. We can define two "diameters" to characterize the size of the grain:

– *Feret's diameter* D_1 is the distance that separates two extreme tangents in the projected area brought parallel to a right angle.

– The *projected diameter* D_2 is the diameter of the circle with the same area, A, as the projection of the grain.

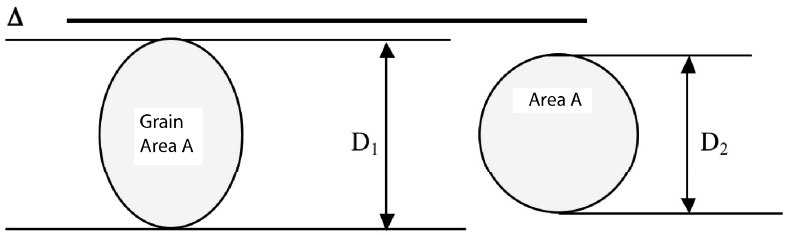

Figure 2.2. *Definition of Feret's diameter and the projected diameter*

Not only are these two diameters generally different, but Feret's diameter also depends on the direction of the projection line. This figure illustrates the

conventional character in the definition of the size of a grain. It shows us how important it is to clarify the definition retained. In general, the definition of the size of the grain is associated with an experimental method. It will serve us to clarify this.

2.3.1. *Sieving*

2.3.1.1. *Principle of sieving*

Sieving consists of sorting a granular material by granulometric denominations from different sieves.

The sieves are made of braided metallic wires or perforated sheets and have square side openings, d, see Figure 2.3. Value d is called the *opening* or *mesh size*.

Sieving a mass, m, of an aggregate on a sieve with an opening, d, separates the aggregate in two sets:

– Particles of a "size" greater than d, which remain in the sieve. This is the portion of particles *retained*.

– Particles of a "size" smaller than d that pass through the sieve. This is the *passing* or the *underflow*.

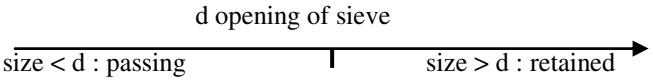

The sieve openings are standardized according to geometric progression. The geometric progression is characterized by the value of the base (d_0 = 1 mm) and by reason, r, which allows us to deduce the openings from one another by means of the ratio $d_{i+1} = r\,d_i$.

The value of the reason, r, in the series of recommended sieves according to standard NF EN 933-2 is near 2^1 and the values of the openings are as follows: 0.063 mm; 0.125 mm; 0.250 mm; 0.500 mm; 1 mm; 2 mm; 4 mm; 8 mm; 16 mm; 31.5 mm; 63 mm; and 125 mm.

---

1 The exact value is equal to $\left(\sqrt[10]{10}\right)^3$.

Sieving is done manually or mechanically using a sieve stack (see Figure 2.3). The sizes of the mesh and the number of sieves are chosen according to the nature of the sample and the accuracy required. It is not necessary to use all of the possible mesh sizes to proceed to granulometric analysis of a material. The more different sieves we use, however, the more accurate the results are. Standard NF ISO 565 specifies the sizes of the intermediate sieves that can be used.

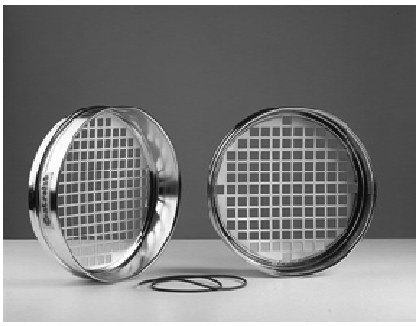

A

B

Figure 2.3. *(A) Sieve; and (B) a sieve stack used for mechanical sieving (CONTROLAB)*

In the stack, the overlaid sieves have decreasing mesh sizes and at the bottom of the stack a "background" is placed that is used to collect the particles passing through the mesh of the smallest sieve. For instance:

– M is the mass of the sample placed at the top;

– m_i is the weight of particles collected (retained) at the opening of sieve d_i; and

– m_f is the weight of particles collected on the bottom.

We say that an aggregate is of granular class d_1/d_2 (or granular size $[d_1, d_2]$) if its size is between the minimum value d_1 and the maximum value d_2. When the values of d_1 and d_2 are two successive openings in the series of standard sieves, it is known as elementary aggregate.

Masses, m_i, therefore correspond to granular classes d_{i-1}/d_i and it is possible to deduce the weight fractions of grains belonging to each granular class.

For example, the percentage of particles[2] in class d_{i-1}/d_i is $100.\frac{m_i}{M}$. The percentage of particles of a smaller size in the smallest sieve is $100.\frac{m_f}{M}$.

2.3.1.2. *Presentation of sieving results*

Typically, the results of granulometric analysis (*granularity*) by sieving are shown by the cumulative granular curve. It represents the variation in the grains passing (or underflow) through a sieve. These accumulate according to the size of the sieve openings in a semi-logarithmic axes system[3]. Figure 2.4 shows an example of the granularity of a material. Other modes of representation exist that are described at the end of this chapter.

---

2 Granulometric analysis results show the percentages of the number of particles. This is frequently the case with techniques that identify particles instead of weighing them (see section 2.3.1.3). The results are very different from those expressed in percentages by weight.

3 The successive openings of the two sieves are linked by the ratio $d_n = r.d_{n-1}$. In a logarithmic scale, the distance between the two markers d_n and d_{n-1} is proportional to $Ln\,d_n - Ln\,d_{n-1} = Ln\,r$. This term is a constant and the openings of the sieves are therefore equidistant.

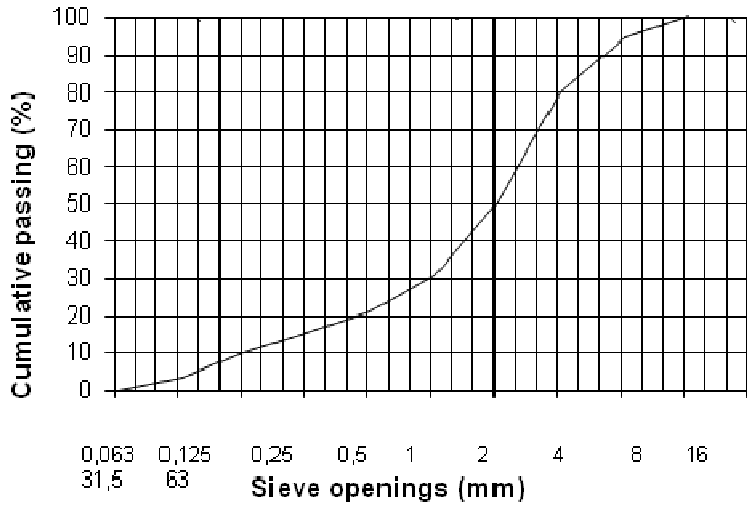

Figure 2.4. *Granularity of a material analyzed by sieving, showing its granular cumulative curve*

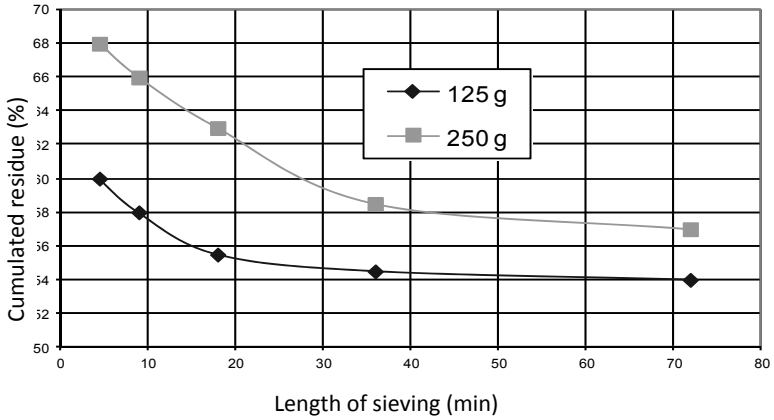

Figure 2.5. *Illustration of the efficiency of sieving*

2.3.1.3. *Efficiency of sieving*

For a grain to pass through a mesh, it must be smaller than the opening but it must also present itself at the opening and this opening must be free (and therefore not a clogged sieve). The efficiency of sieving therefore depends on the quality of material being sifted (weight of sieve). In fact, the better the quality is, the greater the chance there that the openings will be clogged at the end of sieving.

This is illustrated by the results of the experiment shown in Figure 2.5. In this experiment, different masses of the same material are sifted with TYLER, an American sieve with 200 mesh openings (200 openings per inch, i.e. approximately 74 μm per opening). The material is a mixture where 50% of the particles are smaller than this opening (between 200 and 270 mesh size) and 50% are larger than it (between 150 and 250 mesh size).

The theoretical result of the sieving is therefore that 50% of the grains will pass through. The experimental curves show that we obtain 40% passing over 4.5 minutes if the aggregate mass is 125 g; whereas it requires 27 minutes for an initial mass of 250 g, which is more than double the time. Furthermore, we may note that we do not reach 50% passing after 1 hour of sieving.

Efficiency diminishes greatly with the mass of material. In practice, we limit the mass of material by considering that the sieving must be completed in 10 min. The resulting mass limits in the sieves have values that are recorded in Table 2.1.

To avoid overloading the sieves, standard NF EN 933-2 recommends not exceeding sections A on each sieve and retaining opening d at the end of sieving:

$$retained\ max(g) = \frac{A(mm^2)\sqrt{d(mm)}}{200}.$$

Sample	Opening (mm)	Limited load (g)	Equivalent sieve diameter (mm)
17	0.040	50	0.050
18	0.050	-	0.063
19	0.063	-	0.080
20	0.080	-	0.100
21	0.100	-	0.125
22	0.125	-	0.160
23	0.160	-	0.200
24	0.200	-	0.250
25	0.250	-	0.315
26	0.315	-	0.400
27	0.400	100	0.500
28	0.500	-	0.630
29	0.630	-	0.800
30	0.800	-	1.00
31	**1.00**	**-**	**1.25**
32	1.25	-	1.60
33	1.60	200	2.00
34	2.00	-	2.50
35	2.50	-	3.15
36	3.15	400	4.00
37	4.00	-	5.00
38	5.00	-	6.30
39	6.30	-	8.00
40	8.00	2,500	10.00
41	10.00	-	12.50
42	12.50	-	16.00
43	16.00	-	20.00
44	20.00	-	25.00
45	25.00	-	31.50
46	31.50	-	40.00
47	40.00	5,000	50.00
48	50.00	-	63.00
49	63.00	-	80.00
50	80.00	-	100.00

Table 2.1. *Series of sieves according to standard NF EN 933 and limited mass on sieves*

When the size of the particles is very small, the sieving technique is no longer used. In fact regular weaving of sieves becomes increasingly difficult to do. Grains may agglomerate if they are not quite dry and, if they are, they may remain fixed on the sieves under the effect of the forces of electrostatic origin. The openings of sieves are therefore virtually limited to the smaller values, which are limited to this granulometric technique. For example, standard NF EN 933-2 recommends limiting the granulometric analysis by using a sieve with openings of 63 μm.

The sieving of aggregates is carried out when they are dry. Before starting to sieve, it is recommended that all small particles (smaller than 63 μm) are eliminated by sieving under water. The aggregates must be weighed after drying. Granulometric analysis is carried out on the remainder of the aggregate after drying at 110°C until a constant mass is reached.

To characterize materials whose grains are smaller, other methods must be used. They are discussed in the following sections.

The industrial preparation of aggregates requires the production of granular denominations with adapted materials: we use screens. Screening is the name of the process of granular denominations. The function here is not to characterize the materials, but to prepare them according to size criteria. Figure 2.6 shows a screening installation. The performance evaluation of screening is the subject of Exercise 2.5 at the end of the chapter.

Figure 2.6. *Screening installation*

2.3.2. *Granulometric methods based on sedimentation*

2.3.2.1. *Principle of granulometric sorting by sedimentation*

Let us consider the drop of a solid particle in a liquid:

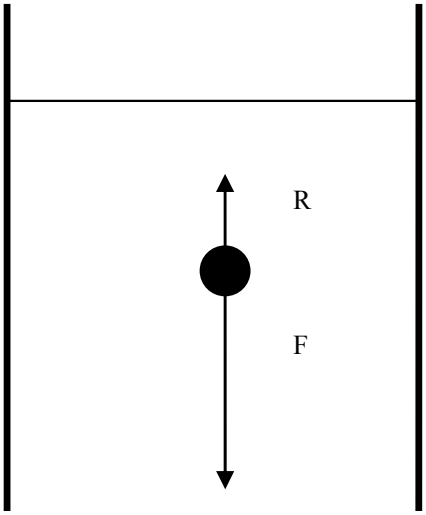

Figure 2.7. *Diagram of the solid particle gravity in a liquid*

The particle is subject to two vertical opposite forces:

– R: friction force; and

– F: apparent weight.

Apparent weight, F, is given by the following ratio:

$$F = (m_s - m_l)g = (\rho_s - \rho_l).V_p g \qquad [2.5]$$

where:

– m_s and m_l are the masses of the solid particle and that of the displaced liquid respectively;

– ρ_s and ρ_l are the densities of the solid and the liquid;

– V_p is the volume of the particle; and

– g is acceleration due to gravity.

The friction force may be expressed by the Stokes ratio if the particle is spherical (diameter $D = 2r$):

$$R = 6\pi \mu r u \qquad [2.6]$$

where μ is the viscosity (dynamic) of the liquid[4] (of size [M].[L]-1[T]-1) and u is the speed of the drop.

If the particle is spherical, the apparent weight is:

$$F = \frac{4}{3}\pi r^3(\rho_s\text{-}\rho_l)g \qquad [2.7]$$

Let us consider the drop of a spherical particle released without initial speed in the liquid. The motion of the particle is accelerated uniformly until F and R are equal and opposite. After that the motion becomes uniform. The speed limit, u_{lim}, is given by the ratio:

$$6\pi \mu r u_{\text{lim}} = \frac{4}{3}\pi r^3(\rho_s\text{-}\rho_l)g \qquad [2.8]$$

The speed limit is directly linked to the size of the particle. By introducing the diameter, D, it can be written:

$$u_{\text{lim}} = \frac{D^2}{18\mu}(\rho_s\text{-}\rho_l)g \qquad [2.9]$$

The speed limit reached by the spherical particles is proportional to the square of the diameter. If a particle of some shape drops in a liquid, it also reaches a speed limit. Considering that this speed limit is also that of a spherical particle expressed by the previous ratio, we can characterize the

4 In the international system, the unit of dynamic viscosity is the Poiseuille (Pl). In the ancient CGS system, the unit is the Poise (Po). 1 Pl = 10 Po.

particle of a shape by its size, known as its "Stokes diameter". This is the diameter of a spherical particle of the same density dropping at the same speed in the same liquid.

The previous ratio may be used to select particles dropping in a liquid provided that the density of all of the grains is the same, i.e. that we are dealing with a homogeneous material.

2.3.2.2. *Principle of granulometric analysis by sedimentation*

In practice, the acceleration phase is short (lasting a few milliseconds) and, at first approximation, we can consider that the speed limit is reached first time. This speed therefore represents the ratio between the distance traveled, h, and time of the drop, t. The diameter of the particle can therefore be expressed according to the ratio:

$$D = \sqrt{\frac{18\mu h}{(\rho_s - \rho_l) g t}} \qquad [2.10]$$

If the particles to be analyzed are dispersed in a liquid, the previous ratio expresses the distance traveled by each of them after t.

V is the volume of the suspension containing a total mass M of dispersed particles. X is the mass of particles that are smaller than D. For granulometric analysis of the material, we need to determine X for all possible values of D.

The elementary volume representative of the suspension v at the initial time contains a mass m of particles. If the suspension is homogeneous, whatever the position of the volume in the suspension it can be written:

$$\frac{m}{M} = \frac{v}{V}$$

At time t, particles of diameter D have travelled h. At this depth h, volume v (and all that is above it) no longer contains particles with a diameter that is larger than D. If x is the mass of particles contained in v at time t, we have:

$$\frac{x}{X} = \frac{v}{V} = \frac{m}{M} \Rightarrow X = x.\frac{V}{v} \qquad [2.11]$$

Knowing h and t, ratio [2.10] enables us to calculate the corresponding diameter, D. In renewing measurement x_i at different times t_i and at the same depth, we may therefore determine the values of X_i corresponding to decreasing diameters, D_i.

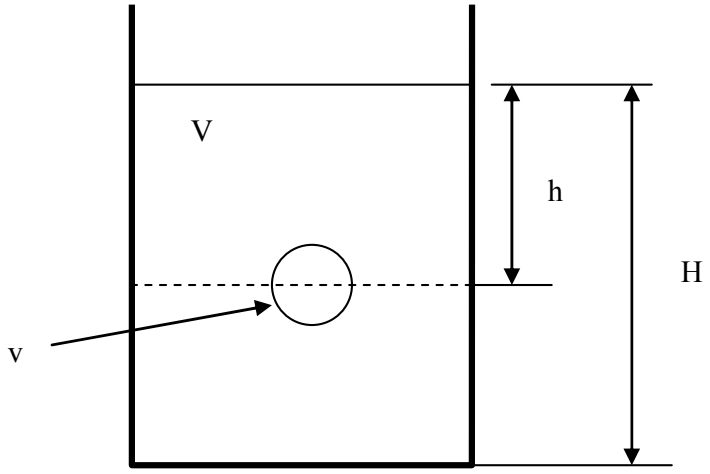

Figure 2.8. *Data concerning sedimentation principle*

Granulometric analysis based on the principle of sorting by sedimentation links a Stokes diameter, D, to particles having dropped in a liquid in distance h during time t according to ratio [2.10]. This calculation of D implies that the particles have the same densities, ρ_s, and consequently *measurements by sedimentation can therefore only be made with homogeneous particles.*

2.3.2.3. *Andreasen pipette*

Granulometric analysis using an Andreasen pipette (see Figure 2.9) is based on the principle of sedimentation, as discussed above.

A mass M of particles to be analyzed is dispersed in a liquid in the bottom of the graduated cylinder. Volume V of the suspension is measured. A vertical glass column is immersed in the suspension. Calibration allows us to know the depth h of the end where a small volume v (10–20 mL) of

suspension is taken by suction at time t. This sample is then decanted in a recipient and, after evaporation, the mass x of the particles contained in v is weighed. Ratio [2.11] allows us to calculate the mass X of the particles that are smaller than D, which given by equation [2.10], contained in the initial sample of mass M. By repeating the measurement at different times, granulometric analysis of the material can be carried out.

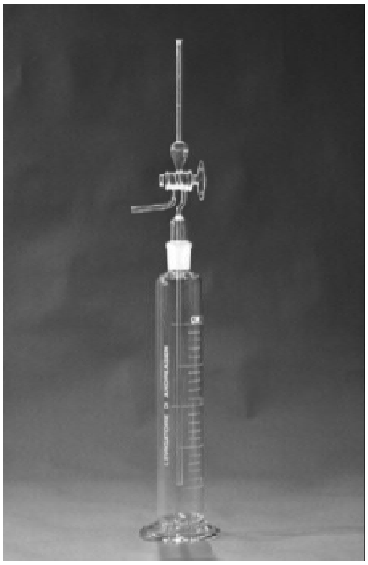

Figure 2.9. *Diagram of an Andreasen pipette (NF X31-107), (CONTROLAB)*

2.3.2.4. *Bouyoucos densimeter (or hydrometer) [MER 54]*

REMINDER 2.1.- the densimeter (or hydrometer) is a device consisting of a glass tube on top of a tank that allows us to measure the density of a liquid relative to water. Immersed in water, the tube is submerged to a depth h_{water}. When it is immersed in a liquid, the depth of the immersion is h_l.

If V_r is the volume of the reservoir, P the weight of the densimeter and s the section of the glass tube, it can be written that:

– case of water: $P = (h_{water} s + V_r)\rho_{water} g$; and

– case of liquid: $P = (h_l s + V_r)\rho_l = ([h_{water} + \Delta h]s + V_r)\rho_l$.

The density of liquid in relation to water is:

$$d = \frac{\rho_l}{\rho_{water}}$$
$$= \frac{h_{water}s + V_r}{h_l s + V_r}$$
$$= \frac{h_{water}s + V_r}{h_{water}s + V_r + \Delta hs}$$
$$= \frac{1}{1 + k.\Delta h}$$

Density is directly related to the difference in depression Δh: the glass tube can therefore be graduated with d values.

If the hydrometer is immersed in the suspension of particles in a liquid of density ρ_l, we can measure its density d every time at the depth of the reservoir. Thus at time t, if we note h as the depth of the reservoir (given by the depression measured), we know that particles that are larger than D do not exist at top of the reservoir, with D being given by ratio [2.10].

The measured density d of the suspension is given by:

$$d = \frac{X + (V - \frac{X}{\rho_s})\rho_l}{V\rho_{water}}$$

This ratio allows us to know X, which is the mass of particles that are smaller than D.

2.3.2.5. *Sedimentation scale*

This device allows the granulometric analysis of a powder by continuous recording of the sediment weight, which is deposited from a suspension on a scale pan. The apparent weight of particles being deposited on the right scale pan is balanced at all times so as to keep the beam horizontal. We propose to analyze the scale principle by means of an exercise discussed at the end of this chapter.

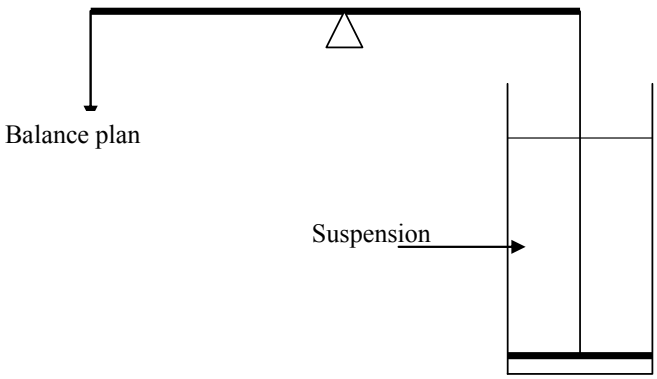

Figure 2.10. *Diagram of the sedimentation scale principle*

2.3.2.6. *Other methods based on sedimentation*

The three applications of sedimentation, which have been described above, are used sparingly because they require a lot of time and handling.

Granulometric analysis can also be automated, based on measurements of the physical properties of a suspension of particles, which are based on their content and size. We can use the variations of optical properties for this, such as the transmission of light (turbidity), diffusion of light, absorption or the diffusion of X rays. These methods are described in detail in the book by Jouenne [JOU 75].

Another, faster, method consists of selecting particles in air. The apparatus used is an elutriator in which the solid particles are subject to two opposing forces: a centrifugal force created by a disc turning at high speed on which there are particles to be selected; and a centripetal force created by a jet of air at controlled speed. Particles larger than a certain size are pushed to the outside of the disc and collected. The selection is achieved by the use of various speeds of air, which correspond to the different minimum sizes of selected particles. A diagram of the Bacho elutriator is shown in Figure 2.11. To carry out the granulometric analysis of a lot of particles in a dozen cuts, takes approximately 30 minutes as opposed to three to four hours with other methods.

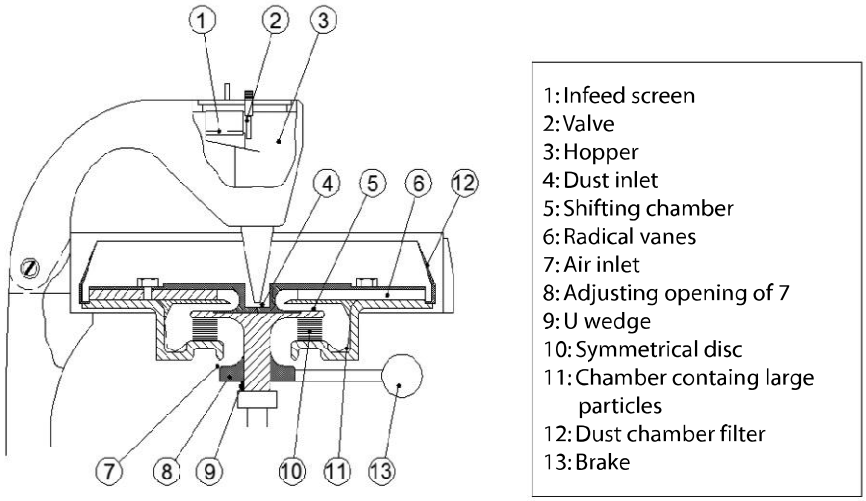

Figure 2.11. *Diagram of the Bahco elutriator*

2.3.3. *Coulter counter*

In the Coulter counter (see Figure 2.12), the sample to be analyzed is dispersed in an electrolyte (2). A tubular glass is immersed in the suspension with a calibrated inlet (3) and two platinum electrodes (1) are placed on either side of the chamber, which is powered by direct current.

The suspension is sucked into the tube through the calibrated inlet. When a particle passes through the inlet, it displaces its own electrolyte volume, thus changing its electrical resistance through the inlet. This change in resistance is converted into a pulse whose amplitude depends on the volume of the particle. The pulses are amplified and counted. The count is associated with amplitude discrimination. The correlation between the amplitude and the impulsions and the dimension of the particles is obtained by calibration. The passage of the suspension through the inlet is caused by an empty vacuum, which simultaneously causes the imbalance of a manometric column of mercury. The vacuum pump is isolated (which is the state described in Figure 2.12) and suction of the solution through the inlet continues under the influence of the depression in the manometer. The particles are automatically counted between two markers of the mercury column, which corresponds to a known volume of solution.

Proportionality between the variation of electric resistance and the volume of the particle is verified accurately if the section of the particle is weak compared to that of the inlet. In practice, this simplification leads to a restriction in the size of the particles counted to approximately 40% of the size of the inlet. Multiple inlet sizes are provided and selected according to the maximum size of the particles to be analyzed. The measuring system provides the numbers of particles belonging to diverse granular slices whose boundaries are initially chosen. Unlike the methods previously described, these are not masses but numbers of particles that are measured.

When several particles pass simultaneously in front of the electrodes, they are counted as one single particle whose size is the corresponding variation in intensity. Due attention must therefore be paid to making a suitable dilution to minimize this risk.

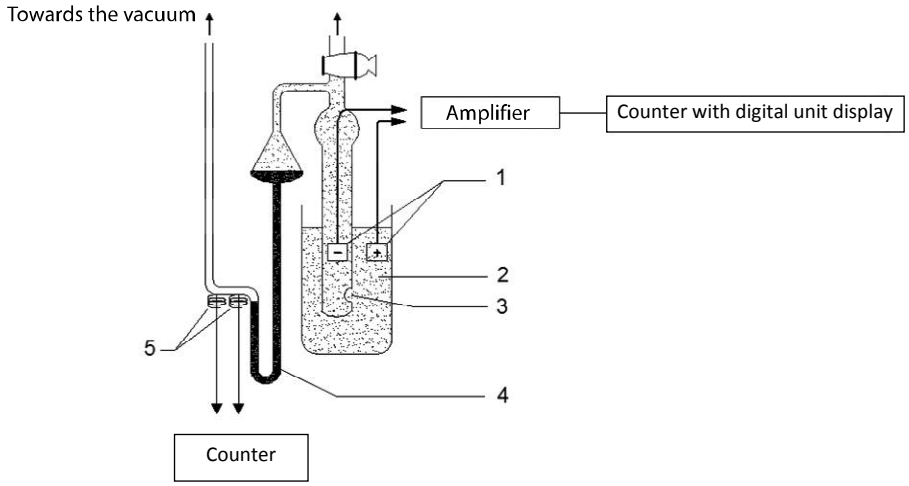

Figure 2.12. *Diagram of the principle of the Coulter counter*

2.3.4. *Laser granulometer (NF ISO 13320-1)*

This technique allows the analysis of granulometry of a mineral powder dispersed in a liquid, see Figure 2.13.

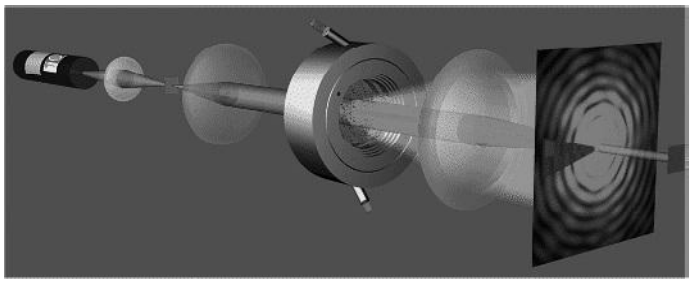

Figure 2.13. *Diagram of laser granulometer*

If we consider a large number of small, identical, circular, opaque screens, arranged randomly and intercepting a beam of coherent and monochromatic light (laser beam), there is *ad infinitum* (or in the focal plane of a lens) a diffraction pattern consisting of alternating light and dark concentric rings. According to the Fraunhofer theory, the brightness of the light rings is proportional to the number of screens present in the laser beam and the rays of the rings are inversely proportional to the diameter of the screens. When light is diffracted by a powder consisting of a set of particles of variable sizes, the diffracted figure obtained is the superposition of images corresponding to each diameter. From its mathematical analysis, we can determine the granular distribution of powder.

Particles are not screens and light is also diffused and reflected. These phenomena become ever more important than the particles, which are not opaque and whose size are small. Thus, we can consider that the Fraunhofer theory is no longer applicable for solid particles that are smaller than 3 μm. We can consider that the image collected results from the superposition of a diffracted image and the diffusion of light through the particles. This latter contribution is based on optical properties of the material analyzed, in the middle of which particles are dispersed (Mie theory). The means of calculation available enables us to take into account these two contributions and to determine the granulometry of a granular material whose sizes range from approximately 0.1 μm to several hundred micrometers.

2.3.5. *Analysis of images coupled by microscopic observations*

Microscopic methods have the advantage of enabling a direct observation of the particles to be analyzed. The analyzed images are projections of

particles in the observation plane and the definition of size is based on a convention. Practically speaking, some precautions should be taken:

– the particles have to be properly dispersed, otherwise particle agglomerates are measured;

– the sample should be representative of the set of particles (note that in 1 g, of cement whose grains are 5 μm in size, there are approximately 480×10^6 particles); and

– the representativeness of the sample is even more critical than having different sizes of particles: a particle 100 μm in diameter has the same mass as 106 particles of 1 μm.

It should also be noted that, for aggregate sizes ranging from approximately 1 mm to 50 mm, videogranulometers are used. These, by image processing of the passage of aggregates in front of a charge-coupled device (CCD) camera, are able to estimate the size and also the slenderness and flattening of aggregates. These types of apparatus are particularly useful in the continuous monitoring of a system where they can detect anomalies [DES 10].

2.4. Granularity: presentation of results

2.4.1. *Granular cumulative curves*

Granular cumulative curves are plotted against semi-logarithmic coordinates. The x-axis shows the limits of the chosen granular classes (e.g. sieve openings), and the y-axis shows *M*, the weight percentage of grains smaller than the sizes indicated by the corresponding x-axis (e.g. see Figure 2.4). These classic curves represent the passing (or underflow) accumulated according to grain size. Some granular curves may also represent the values of the granular material retained. The scale of sizes may also be inversed in relation to the classic representation, with values decreasing from left to right. This mode of representation is quite commonly used in documents related to road engineering.

Granular curves sometimes represent the number of grains of smaller sizes against the size represented in the x-axis. It is then easy to deduce the cumulative passing by supposing that the particles are spherical, see Figure 2.12. This mode of representation is more common when the

granulometric methods determine the number of particles, as is the case with a laser granulometer.

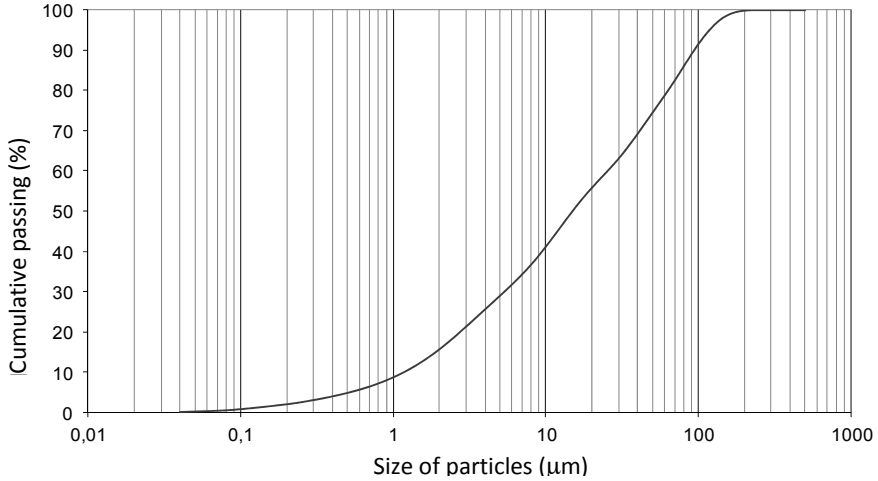

Figure 2.14. *Granular cumulative curve of dispersed silica fume*

2.4.1.1. *Efficient diameter*

The efficient diameter, D_i, is the size of particles that corresponds to an increased cumulative weight of i %.

According to this definition, the grain size of a material ranges from D_0 (the lowest value) to D_{100} (the highest value). The value of the efficient diameter, D_{50}, is often used to give an order of magnitude of the grain size of a material. Note that if 50% of the mass of particles are smaller than D_{50}, the corresponding number of grains is less than half (if all grains have the same density).

2.4.1.2. *Shape of granular cumulative curves*

Many granular materials have granular curves similar to that shown in Figure 2.15, where D_{50} is situated in the middle of the D_0–D_{100} range.[5] In this case, we call it "normal" distribution.

5 This does not mean that $D_{50} = \frac{D_0 + D_{100}}{2}$ because the x-axis scale is a logarithmic scale.

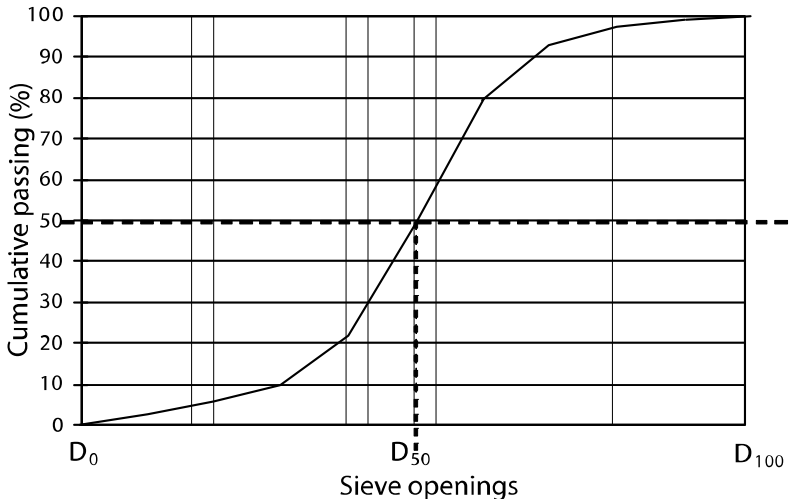

Figure 2.15. *"Normal" granular curve*

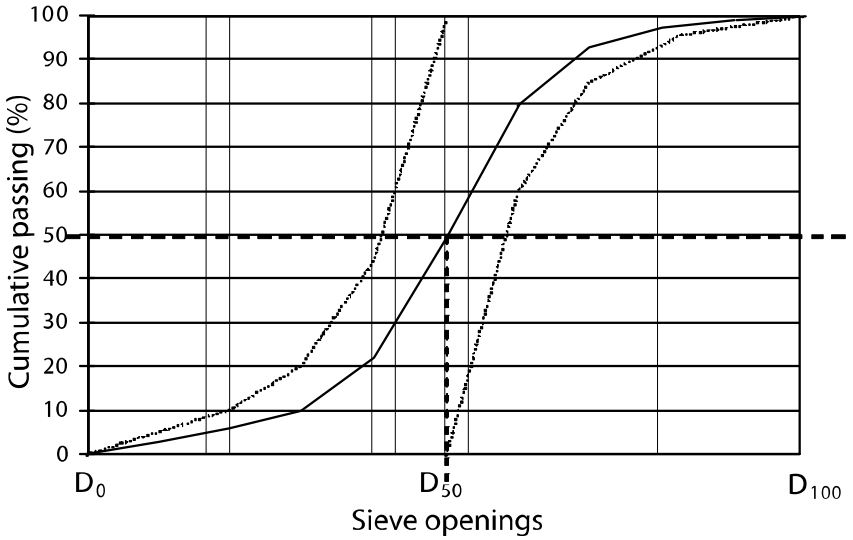

Figure 2.16. *Curves of granular materials obtained by cutting at D_{50} of an initial material may have very different shapes from those of the "normal" curves*

If D_{50} is close to D_0, this means that the grain mass mostly consists of fine grains. The granular cumulative curve may also have a very different shape to that shown in Figure 2.15. For example if we carry out a denomination of the material shown in Figure 2.15 in a sieve whose opening is equal to D_{50}, the shape of the granular curves of the two new materials will be very different to that of the original material (see Figure 2.16).

2.4.2. *Granular frequency curves*

Granular cumulative curves represent the function *M(log D)* point-by-point where *M* is expressed as a percentage. The granular frequency curve or the curve of granular distribution represent the derived function $\frac{dM}{d\log d} = f'(lod\ d)$. If we consider a granular class d_1–d_2 corresponding to two successive sieve openings (with $d_1 < d_2$), the value of *dM* is the mass of grains collected via the sieve opening d_1 expressed as a percentage of the total mass.

Granulometric results may also be presented by means of an experimental curve of granular distribution in which the value of *dM*, the mass of grains belonging to different granular classes, and the value of *log d* are recorded on the y-axis. The link between the different granular curves is summarized in Figure 2.17.

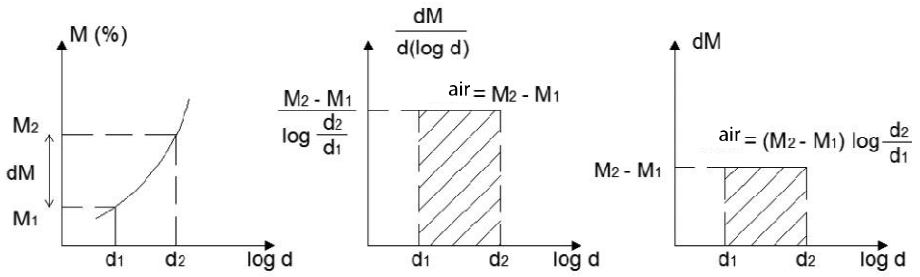

Figure 2.17. *Different granular curves*

2.4.3. *Other presentations of granularity*

The previous representations have provided detailed information on the grain size of an aggregate. Sometimes we may be satisfied with less detailed information, and for this we call upon various definitions that we will now give.

2.4.3.1. *Designation of aggregates according to the boundaries of granular class*

Aggregates *d/D* or *0/D* are noted if *d* is less than 1 mm. *d* is the size of the smallest grains and *D* the size of the largest grains. This designation is similar to that of the granular classes; however, standard NF EN 12620 admits that grains are out of range between *d* and D.

Depending on values *d* and *D*, concrete aggregates are designated in such a way as given in Table 2.2.

Filler	/D	$D < 2$ mm, at least 70% passing to 63 µm
Fines[6]	/D	Granular fraction passing through sieve of 63 µm
Sand	/D	$D \leq 4$ mm
Aggregate of natural class 0/8 mm	/D	$D \leq 8$ mm
Pebble	/D	$d \geq 2$ mm, 4 mm $\leq D \leq 63$ mm
Gravel	/D	4 mm $\leq D \leq 45$ mm

Table 2.2. *Designation of concrete aggregates (standard NF EN 12620)*

Granular characteristics are fixed by standard NF EN 12620 for these different aggregates and are summarized in Table 2.3.

6 The fines content is used to measure the properties of sand, aggregates of natural class 0/8 mm and of gravel. Maximum fine contents are measured by standard NF EN 12620.

Aggregate	Sizes	Mass of passing as a percentage					Category G*
		$2D$	$1.4D$[a,b]	D[c]	d[b]	$d/2$[a,b]	
Gravel	$D/d \leq 2$ or $D \leq 11.2$ mm	100	98–100	85–99	0–20	0–5	$G_C85/20$
		100	98–100	80–99	0–20	0–5	$G_C80/20$
	$D/d > 2$ and $D > 11.2$mm	100	98–100	90–99	0–15	0–5	$G_C90/15$
Sand	D = 4mm and d = 0	100	95–100	85–99	—	—	G_F85
Aggregate of natural class 0/8		100	98–100	90–99	—	—	$G_{NG}90$
Gravel		100	98–100	90–99	—	—	G_A90
		100	98–100	85–99			G_A85

[a] When the size calculated does not correspond to an exact size in the series R20 ISO565:1990 of sieves, the sieve having the closest size must be used.

[b] Additional requirements may be specified for discontinued granular concrete and for specific tasks.

[c] The percentage of the mass of passing to D may be greater than 99% but, in these cases, the provider must document and declare the granularity type of sieves D, d, $d/2$ and of intermediate sieves d and D of the principal series and of series 1 or of the principal series and of series 2. For the selection of intermediate sieves, it must ensure that the ratio in relation to the two successive sieves is equal to or greater than 1.4.

*Relative standards of other aggregate products fix different specifications.

Table 2.3. *Granular characteristics (standard NF-EN 12620)*

2.4.3.2. *Fineness modulus of concrete sand*

The fineness modulus (*FM*) is equal to the sum of the cumulate retained in the series of sieve openings 4 – 2 – 1 – 0.5 – 0.25 and 0.125 mm divided by 100:

$$\mathrm{FM} = \frac{\sum \text{cumulate retained in sieve (4.0-2.0-1-0.50-0.25-0.125 mm)}}{100}$$

In Figure 2.18, Sand 1 and Sand 2 have different granularities. The position of the granular cumulative curve in relation to the horizontal (M = 100%) is not the same and this is not reflected by the different fineness modulus. Sand 1 with fineness modulus FM_1 contains fewer small particles than Sand 2, with a fineness modulus of $FM_2 < FM_1$.

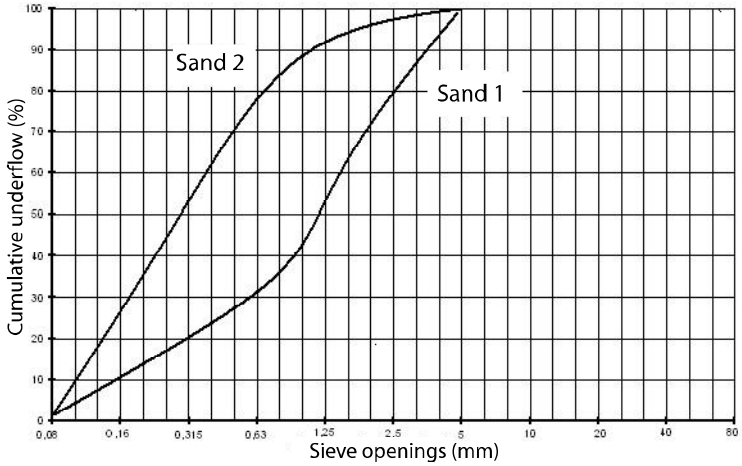

Figure 2.18. *Comparison of the granulometric curves of two sands of different fineness*

It is possible to describe sand (S) of fineness *FM* produced by mixing two sands, S_1 and S_2, of modulus FM_1 and FM_2 ($FM_1 > FM_2$). Abrams rule allows us to determine the proportions of S_1 and S_2:

$$\%S_1 = \frac{FM\text{-}FM_2}{FM_1\text{-}FM_2}.100$$

and

$$\%S_2 = \frac{FM_1\text{-}FM}{FM_1\text{-}FM_2}.100$$

2.5. Granularity of a mixture of aggregate

Granular materials such as concrete are manufactured by mixing different aggregates so as to obtain a compact mixture (see Chapter 4). To determine the granular cumulative curve of a mixture of known proportions of several

aggregates with known granular curves we use the law of mixtures for each sieve opening. This law is demonstrated by considering a denomination through a sieve opening, *D*.

The mass *m* resulting from the denomination of the mass m_1 of aggregate 1 and mass m_2 of aggregate 2 is:

$$m = m_1 M_1 + m_2 M_2$$

where M_1 and M_2 are the cumulative passing of the two aggregates.

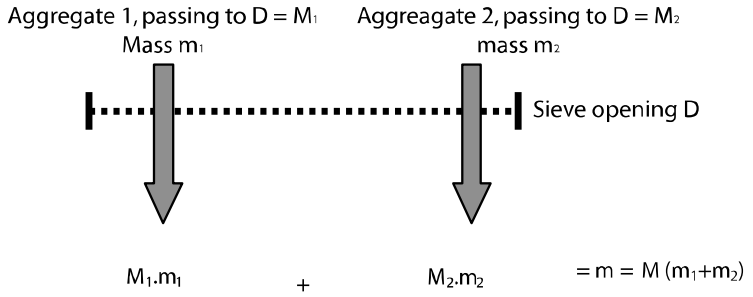

Figure 2.19. *Mixture of the two granulates*

The cumulative passing, *M*, of the mixture is given by the ratio:

$$M = \frac{m}{m_1 + m_2} = \frac{m_1 M_1 + m_2 M_2}{m_1 + m_2} = x_1 M_1 + x_2 M_2$$

where x_1 and x_2 are the weight proportions of aggregates 1 and 2 in the mixture. Exercise 2.3 gives an example of an application of this ratio.

2.6. Bibliography

[DES 10] DESCANTES Y., DUCASSOU J.B., BLOT G., "Videogranulometry VDG40 – Summary of past research and future prospects", *Recycling & Recovery*, vol. 31, pp. 45-54, 2010.

[JOU 75] JOUENNE C.A. *Treaty of Ceramic Materials and Mineral Materials*, Septima, Paris, 1975.

[MÉR 54] MÉRIAUX, S. *Annales Inst. Nat. Agro.*, pp. 149-205, 1954.

2.7. Exercises

Exercise 2.1: *Sedimentation scale (see Figure 2.8)*

This device allows the granulometric analysis of a powder by continuous recording of the weight of the sediment that is deposited, from a suspension to a scale pan. We will analyze the principle of this scale.

The suspension containing particles whose granulometry we hope to gather is placed in a cylindrical container. The right-hand scale pan is placed in this suspension and collects all of the sediment particles. The beam of the scale is kept horizontal with the means of a scale device. This device allows us to balance the force exerted on the right part. The weight result is typically expressed by a mass: one that balances the beam of the scale. If the right-hand pan is placed in air, it is known as weighing carried out in air. If the pan is placed in suspension, it is known as weighing carried out in liquid.

Here:

– M_0 is the total mass of the particles placed in suspension (weighing carried out in air);

– M is the result of the weighing (carried out in liquid) of the particles collected at the end of sedimentation;

– $m(t)$ is the mass of particles collected over time on the sedimentation plate (scale pan) and weighed in the sedimentation liquid. To simplify things, we will assume that $m(t) \in [0.M]$;

– ρ is the density of grains of the sample;

– ρ_l is the density of the sedimentation liquid and viscosity μ; and

– H is the height of the liquid column above the scale pan.

We will assume in this study that mass M_0 is low enough that each particle has an independent motion and the motion of each particle is uniform from zero where sedimentation starts, and that all particles are collected on the plate at the end of sedimentation.

1. Let us consider a set of identical spherical particles (with a diameter d_1) in suspension. Plot the curve $m(t)$. Give its equation.

2. We now have a sample consisting of two sets of homogeneous spherical particles:

– m_1 the mass of particles of diameter d_1 (as above);

– m_2 the mass of particles of diameter d_2 ($d_2<d_1$); and

– m_1 and m_2 are masses corresponding to weights in the sedimentation liquid.

a) Plot the *m(t)* curve and give its equation. How can we determine m_1 and m_2 from the *m(t)* curve?

b) Plot the *m(t)* curve in the case of a sample consisting of three sets: ($m_1(d_1)$, $m_2(d_2)$ and $m_3(d_3)$ – $d_3<d_2$).

c) How can we determine m_1, m_2, m_3 in relation to the *m(t)* curve?

3. Let us analyze the case of a sample consisting of (supposedly spherical) particles of continuous granulometry. The recording of *m(t)* has the shape given in Figure 2.20.

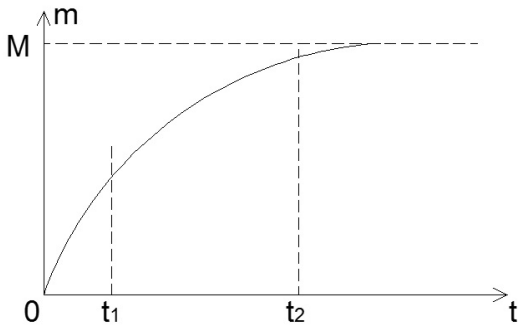

Figure 2.20. *Recording of m(t)*

a) Give the data d_1, the minimum value of the diameter of particles having been completely sedimented at time t_1; by analogy with the previous analysis, how can we determine the mass m_1 of all particles larger than d_1?

b) At time $t_2 > t_1$, all particles of size $d > d_2$ were sedimented. How do we determine the mass of particles whose size ranges from d_1 to d_2?

4. Application: We want to analyze a silicon carbide (ρ = 3.2 g/cm^3) by sedimentation in distilled water to 20°C (ρ_l = 1 g/cm^3).

Data:

– viscosity of water = 0.0102 g. cm^{-1} s^{-1};

– height of the sedimentation column H = 10 cm; and

– M_o = 728 mg.

The sedimentation curve recorded is shown in Figure 2.21.

a) Where M, the mass of grains collected at the end of sedimentation, is 500 mg. Justify this result.

b) What is the percentage of particles whose sizes range from 13.55 µm to 11.05 µm?

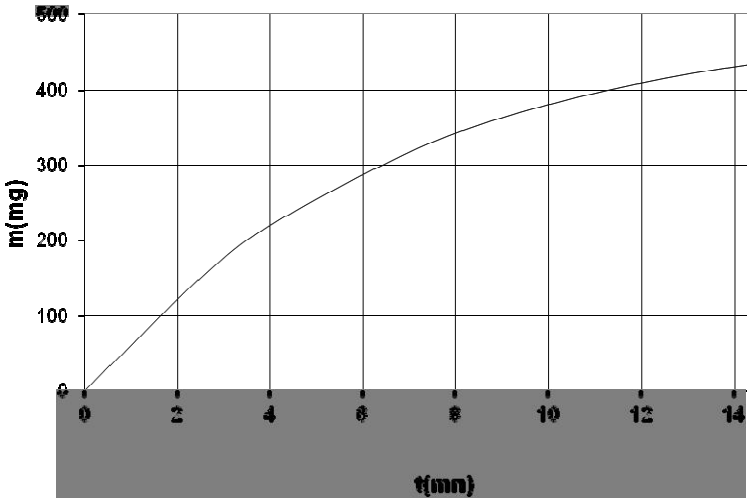

Figure 2.21. *Sedimentation curve of a silicon carbide*

Exercise 2.2

From the results of the following granulometric analysis (see Table 2.4), plot the granular cumulative curve and the experimental distribution curve. Calculate the fineness modulus of the material studied.

Mesh side of sieve (mm)	Mass retained on the sieve (g)	Retained mass (%)	Cumulative retained (%)	Cumulative passing (%)
1.00	0.0			
0.80	1.8			
0.63	3.2			
0.50	17.4			
0.40	20.5			
0.315	62.4			
0.250	40.6			
0.200	12.2			
0.100	8.0			
depth	0.0			

Table 2.4. *Results of granulometric analysis*

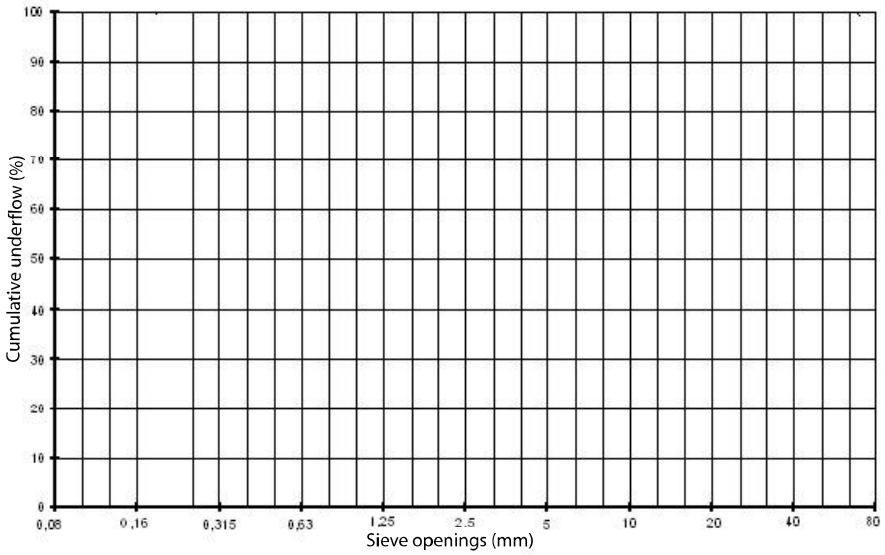

Figure 2.22. *Granulated curve*

Exercise 2.3: *granulometric mixtures and denominations*

The granulometry of aggregate A is carried out with the help of the AFNOR sieve series on a sample weighing 3,200 g. The grain mass collected in the sieves is shown in Table 2.4.

Sieve openings (mm)	16.0	10.0	5.0	2.5	1.25	0.63	0.315	0.16	0.08	depth
Mass collected (g)	0	96	416	320	320	512	832	352	128	224

Table 2.5. *Granulometry of aggregate A*

Aggregate A is mixed with two aggregates, B and C (defined in Table 2.6), and we want to check whether the cumulative curve of the mixture belongs to a given granulometric zone. The zone is an area defined in Table 2.6 by its boundary values (min and max) of the accumulated past.

The weight proportions of the mixture are as follows:

%A = 40%, %B = 50%, and %C = 10%

Plot the cumulative curve of A and of the mixture and check whether the mixture is within the zone imposed.

Sieve openings (mm)	25	20	16	10	5	2.5	1.25	0.63	0.315	0.16	0.08
Cumulative passing of B (%)	100	100	83	72	42	30	20	14	12	9	7
Cumulative passing of C (%)	100	55	0	0	0	0	0	0	0	0	0
Zone imposed (%)	100–100	80–100	-	60–100	48–65	35–50	-	19–30	13–23	7–15	1–8

Table 2.6. *Granulometry of aggregates B and C – zone imposed for the granular mixture*

Plot the granular cumulative curve A obtained after denominations in A of small elements (< 80 μm) and large elements (> 5 mm).

Exercise 2.4: *granular mixtures*

Demonstrate the Abrams equations (see section 2.4.3).

Exercise 2.5: *screening*

Granulometry of aggregate A is carried out with the help of the AFNOR sieve series on a sample weighing 3,200 g. The mass of grains collected in the sieves is shown in Table 2.7.

Sieve openings (mm)	16.0	10.0	5.0	2.5	1.25	0.63	0.315	0.16	0.08	depth
Mass collected (g)	0	96	416	320	320	512	832	352	128	224

Table 2.7. *Granulometry of aggregate A*

a) Plot the cumulative granular curve of A.

b) Screening is an industrial technique of granulometric denominations that aims to separate an aggregate 0/*D* such as A into two aggregates: B (0/*d*) and C (*d*/*D*).

In fact denomination *d* (a rhetorical denomination mesh) is never perfect and some grains of B are greater than *d*, a cumulative passing B less than 100%. Some grains of C are smaller than *d*, so we obtain a cumulative retained of less than 100% at opening *d*.

The ordinate of the intersection of cumulative passing B and of cumulative retained C is called the “screening efficiency”.

Aggregate A is screened with the theoretical mesh of 2.5 mm and, in 1 ton of aggregate A, we collect 800 kg of B (0/*d*) whose granularity is summarized in Table 2.8.

Sieve openings (mm)	0.08	0.16	0.315	0.63	1.25	2.50	5.00	6.30
Cumulative passing (%)	8.75	13.75	27.5	60	80	91	98	100

Table 2.8. *Granulometry of aggregate A after screening*

c) Plot the curve of cumulative retained C and determine the screening efficiency.

Exercise 2.6: *Shape of aggregates*

We have an aggregate with the shape of an ellipsoid whose three half-axes are $r_1 \leq r_2 \leq r_3$.

a) Calculate the flattening coefficient, the slenderness, the shape factor, the sphericity factor and the angular factor of this aggregate according to r_1, r_2 and r_3.

where:

– volume of ellipsoid = $4/3.\ r_1.r_2.r_3$;

– surface of ellipsoid

$\approx S \approx 2\pi\ [(r_1 r_2 + r_1 r_3 + r_2 r_3) - 3\ r_1 r_2 r_3 / (r_1 + r_{2+} r_3)]$; and

– numerical application: $r_1 = 5$ mm; $r_2 = r_3 = 10$ mm.

Chapter 3

Specific Surface Area of Materials

3.1. Definition

The specific surface area (or volume) of a material is the ratio expressed in m^{-1} between the outer surface S of the material and its volume. It can also be expressed in relation to its mass, m. This is known as the specific surface mass or specific surface area. It is this quantity, known as S_s, that we will consider later and that we will denote, as per current practice, by the term *specific surface area*.

The outer surface is the material surface in contact with the external environment, whether it is liquid or gas.

$$S_s = \frac{S}{m}$$

It is usually expressed in m^2/kg or in cm^2/g.

The specific surface area may be defined for granular materials and also for porous materials, which are studied in the second part of this book. For a granular material, the smaller the grains, the greater the ratio of outer surface to unit mass and so the larger the specific surface area. This quantity may therefore be used to account for the fineness of grains.

Physical Properties of Concrete and Concrete Constituents Jean-Pierre Ollivier, Jean-Michel Torrenti and Myriam Carcassès

The value of the specific surface area of a material generally depends on the method of measurement used, which must be specified. For example, we will thus speak of the Blaine or BET specific surface area, etc.

3.1.1. *The importance of this parameter: Portland cement hydration*

Portland cement is in the form of a powder. By mixing it with water, we obtain a fluid cement paste. Cement grains react with water to form hydrate compounds, which structure themselves over time. The cement paste stiffens then the solid formed progressively hardens. Cement hydration may be described by the degree of hydration, which, in a given time, is equal to the percentage of hydrated cement. Figure 3.1 shows the progression of this degree of hydration over time in relation to the fineness of the cement.

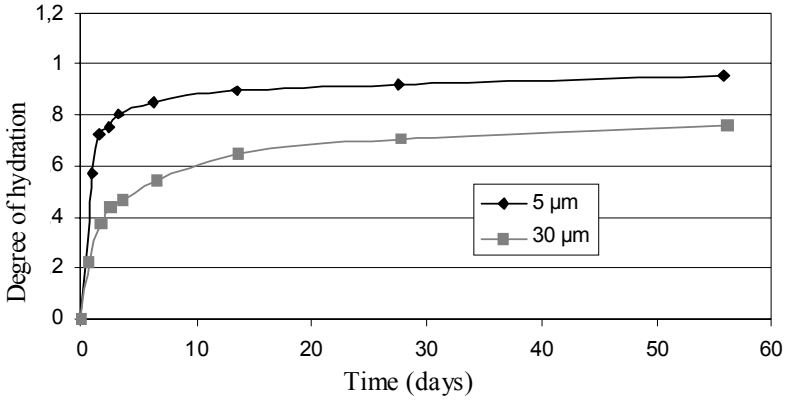

Figure 3.1. *Influence of the specific surface area of cement on the degree of hydration. The black dots correspond to cement whose grains have an average size of 5 µm and the gray dots to cement whose average size is 30 µm (according to [BEN 99])*

For a specific surface area of 3,500 cm^2/g, the reaction has a "dormant" period during which hydration is very slow. This period ends after approximately one to two hours. Hydrates then develop quickly and the cement paste structures itself: this is the setting. Concrete prepared with such cement may therefore be mixed, carried on site and poured into forms before setting. This is not the same with a thinner cement, whose specific surface area is 7,000 cm^2/g: the hydration is quicker and the setting of cement occurs

within minutes. The time during which this concrete has good workability properties is not compatible with its use on site.

Specific surface area determines the reaction rate of powder materials. Its control is therefore very important in the cement industry. This quantity is a global characteristic whose value is highly influenced by the smallest elements, which make up the powder. Specific surface area will also play a role on water demand: the smaller the cement grains are, the greater the quantity that needs to be added to the mixture to obtain a given consistency[1].

3.2. Calculating the specific surface area of a granular material

The specific surface area of a granular material depends on the grain size from which it is made. Thus, if a material is ground, its specific surface area increases. Monitoring the progression of specific surface area over time is also commonly used to determine the grinding efficiency.

If we look more closely, the outer surface of grains not only depends on the size of the grains but also on their roughness. To obtain a rough estimate of the specific surface area of a granular material, we can make a calculation from the granularity of the material by making an assumption on the shape of the grains. The value obtained will only be an order of magnitude of the specific surface area. To obtain a more accurate value, we must not be satisfied with such an estimate of the specific surface area. It must, however, be measured. The calculation deducted from the granularity is discussed in this section. More accurate methods of measurement are then discussed.

3.2.1. *Powder consisting of identical grains of known shape*

Let us first consider the simplest case: that of a homogeneous powder (all grains have the same density, ρ_g, and all particles the same shape and size). For a grain, let us write the ratio of the outer surface S to volume v_g:

$$\frac{S}{v_g} = \frac{c}{D}$$

1 According to standard NF 196-1, water demand corresponds to the quantity added to cement and is necessary to move from a state of pellets to a homogeneous paste in a cement mixer.

where c is a coefficient based on the grain shape and D is the size of the grain (diameter of a sphere, a cube edge, etc.).

If m is the grain mass, the specific surface area of the grain is given by: $S_S = \frac{S}{m} = \frac{c}{\rho_g D}$ where ρ_g is the density of the grain. The specific surface area of the grain is also that of the powder, as all grains are identical.

3.2.2. *Homogeneous powder containing grains of non-uniform size*

Let us consider a set of geometrically similar grains with the same constant density, ρ_g. That is:

– a narrow granular interval δD around size D_{mean}; and

– δm, the mass of powder grain belonging to this interval.

The surface δS of this granular interval is:

$$\delta S = \frac{c}{\rho_g D_{mean}} \delta m$$

For all the powder, whose grains have sizes ranging from D_0 to D_{100}, the surface is:

$$S = \sum_{D_0}^{D_{100}} \delta S = \sum_{D_0}^{D_{100}} \frac{c}{\rho_g D_{mean}} \delta m$$

If the powder is homogeneous, the density is constant. If the grains all have similar shapes, c is also constant. Therefore:

$$S = \frac{c}{\rho_g} \sum_{D_0}^{D_{100}} \frac{\delta m}{D_{mean}}$$

If M is the total mass of the powder, the specific surface area may be calculated in accordance with the following ratio:

$$S_S = \frac{c}{\rho_g M} \sum_{D_0}^{D_{100}} \frac{\delta m}{D_{mean}}$$

NOTE 3.1.– in the above formula, attention should be paid to the units: if M is in % (or g), δm must be expressed in the same unit. D_{mean} is the average size of the granular class containing a grain mass, δm. Given the gross oversimplification of equating all grains to spheres, the calculation only provides an order of magnitude of the specific surface area. Consequently, the value of D_{mean} is generally calculated in a much simpler way by the arithmetic average of the limits of each granular class.

3.3. Methods based on permeability and porosity measurements

Permeability is a quantity that characterizes the aptitude of a material to allow it to pass through a fluid under the effect of a pressure gradient. Its definition and the methods allowing its measurement are discussed in Chapter 7 of this book. The specific surface area of a powdered material can be calculated from a test measuring the airflow, which flows under pressure through a bed of compressed powder. The calculation is based on the Kozeny-Carman equation, which relies on the ratio of the surface area of a powdered material to the pressure gradient exerted on the powder bed and the resulting airflow. Having established this ratio, we will then discuss the two pieces of apparatus that allow us to determine the quantities involved in the Kozeny-Carman equation, namely that of Lea and Nurse and then that of Blaine.

3.3.1. *Kozeny-Carman equation*

Consider, for instance, a bed of pressed powder with height L and apparent section A. The upper surface is subjected to an air pressure $P+\Delta P$ and the lower surface to a pressure P. Under the pressure difference, a volume flow Q of air passes through the intergranular spaces (see Figure 3.2).

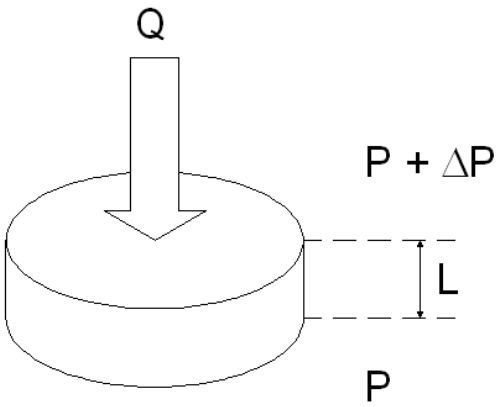

Figure 3.2. *Diagram of a powder bed prepared for the measurement of specific surface area*

It is assumed in what follows that the pressure difference between the two sides is small enough that we can ignore the compressibility of air between the two sides, which is equivalent to supposing that the volume flow is the same between the two sides under a stationary phase.

Here:

– v: intergranular void volume;

– M: mass of grain of the powder bed;

– ρ_g: grain density;

– $V_a = A.L$: apparent volume of the powder bed; and

– $p = \frac{v}{V_a}$: porosity of the powder bed.

The measurement of airflow into intergranular voids is complex. To simplify its study, we model the problem. For this, two assumptions allow us to simplify the geometry of the void space (see Figure 3.3). A third assumption relates to airflow:

– *Assumption 1*: voids are assimilated to a single channel of constant section a and length L_e. This assumption implies that the powder is uniformly compacted.

– *Assumption 2*: the volume of intergranular voids is equal to the volume of the channel ($v = a.L_e$) and the outer surface of the channel is equal to the external surface of the grains.

– *Assumption 3*: the flow phase is laminar. It is governed by Poiseuille's law.

The average flow velocity, u_e, is conveyed by a general form of Poiseuille's law:

$$u_e = \frac{Q_e}{a} = \frac{m^2}{h_0 \mu} . \frac{\Delta P}{L_e}$$

where:

– Q_e is the volume flow through the channel. It is equal to the flow Q through the material.

– m is the hydraulic radius of the channel. It is the ratio between the volume and the outer section of the channel.

– h_0 is a shape factor, which characterizes the shape of the channel section.

– μ is the air viscosity.

– L_e is the length of the flow or effective length of the channel.

The radius of the channel is:

$$m = \frac{v}{S_s . M} = \frac{v}{S_s \rho_g (V_a - v)} = \frac{p}{S_s \rho_g (1-p)}$$

Poiseuille's relation can be written as:

$$u_e = \frac{Q_e}{a} = \frac{m^2}{h_0 \mu} \cdot \frac{\Delta P}{L_e} = \frac{p^2}{S_s^2 \rho_g{}^2 (1\text{-}p)^2} \cdot \frac{1}{h_0 \mu} \cdot \frac{\Delta P}{L_e}$$

The voids volume can be expressed as:

$$v = a L_e = p V_a = pAL \Rightarrow a = pA \frac{L}{L_e}$$

where:

$$Q_e = a u_e = \frac{p^3}{S_s^2 \rho_g{}^2 (1\text{-}p)^2} \cdot \frac{AL}{h_0 \mu} \cdot \frac{\Delta P}{L_e^2}$$

or:

$$Q_e = \frac{p^3}{S_s^2 \rho_g{}^2 (1\text{-}p)^2} \cdot \frac{AL^2}{L_e^2 h_0 \mu} \cdot \frac{\Delta P}{L}$$

Therefore, by placing $\frac{1}{h} = \frac{1}{h_0} \cdot \frac{L^2}{L_e^2} = \frac{1}{h_0} \cdot \frac{1}{T^2}$, where T is the tortuosity of the model channel, the term h globally characterizes the channel's geometry through the ratio between the length of the flow and the height of the powder bed and the shape of the flow section. It is a number without size.

$$Q_e = \frac{p^3}{S_s^2 \rho_g^2 (1\text{-}p)^2} \cdot \frac{A}{h \mu} \cdot \frac{\Delta P}{L} \qquad [3.1]$$

This ratio is the Kozeny equation.

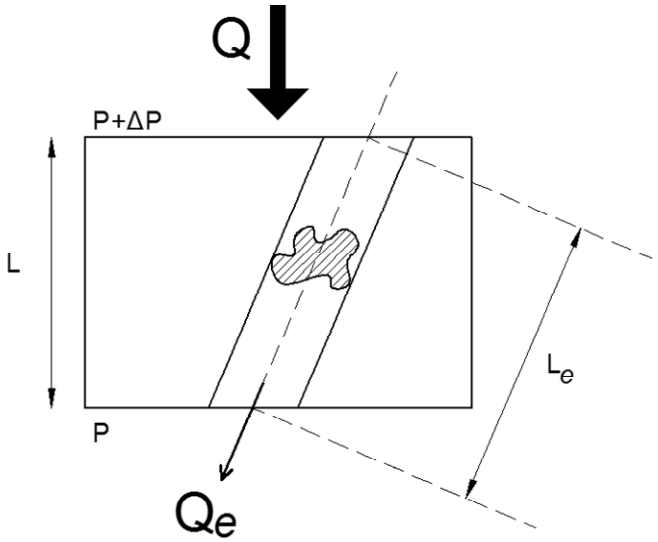

Figure 3.3. *Model of the intergranular porosity of a powder bed*

Carman has shown that for powder beds with porosity close to 0.5 and consisting of grains whose sizes range from 1 to 100 μm, the value of h is constant and equal to 5. Then relation [3.1] can be expressed as:

$$Q_e = \frac{p^3}{S_s^2 \rho_g^{\,2} (1-p)^2} \cdot \frac{A}{5\mu} \cdot \frac{\Delta P}{L}$$

and the specific surface area is given by:

$$S_s = \sqrt{\frac{p^3}{(1-p)^2} \cdot \frac{A}{5\mu\rho_g^2 L}} \cdot \sqrt{\frac{\Delta P}{Q}} \qquad [3.2]$$

The specific surface area can therefore be calculated from the powder bed characteristics (porosity, apparent surface and height), the grain density and the ratio between the airflow passing through the powder bed and the driving pressure. These quantities are easily measurable and the Kozeny-Carman relation can therefore easily be used to determine the specific surface area of a fine granular material, such as cement, filler or any other material whose grain size ranges from 1 to 100 μm.

Various pieces of apparatus have been designed to assist the measurement, particularly the determination of the ratio: $\frac{\Delta P}{Q}$. The Lea and Nurse apparatus functions with a constant pressure difference and the (more common) Blaine apparatus with a constant variable pressure difference. For these two pieces of apparatus, the powder bed is compressed with a piston in a cylindrical permeability cell. Figure 3.4 shows a permeability cell according to standard EN 196-6 for the surface area determination of cement using the Blaine apparatus.

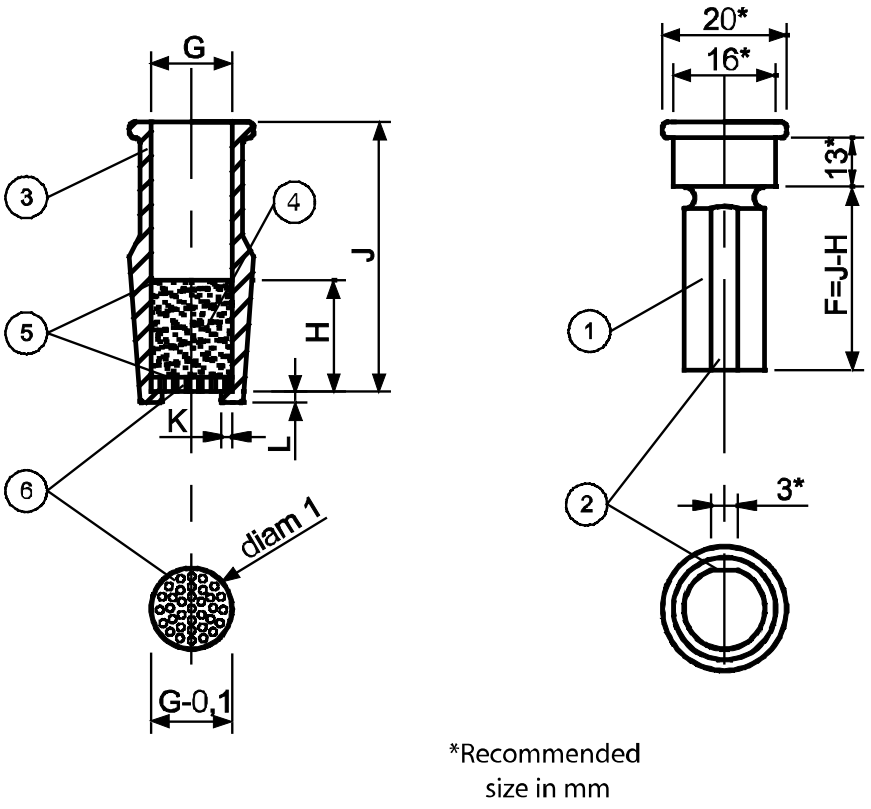

Figure 3.4. *Diagram of a permeability cell: the powder bed (4) is prepared by compression in the cylinder (3) with a piston (1). It rests on a perforated disc (6) that is covered with filter paper. The geometry of the powder bed is determined by section A of the inner cylinder (4) and by height H, which depends on sides J and F*

In this cell, grain mass M is measured to produce a powder bed with porosity equal to 0.5 and of known volume V_a in the cylinder. The porosity p of the powder bed is calculated according to:

$$M = \rho_g V_g = \rho_g (V_a - v) = \rho_g V_a (1 - p)$$

3.3.2. *Lea and Nurse apparatus*

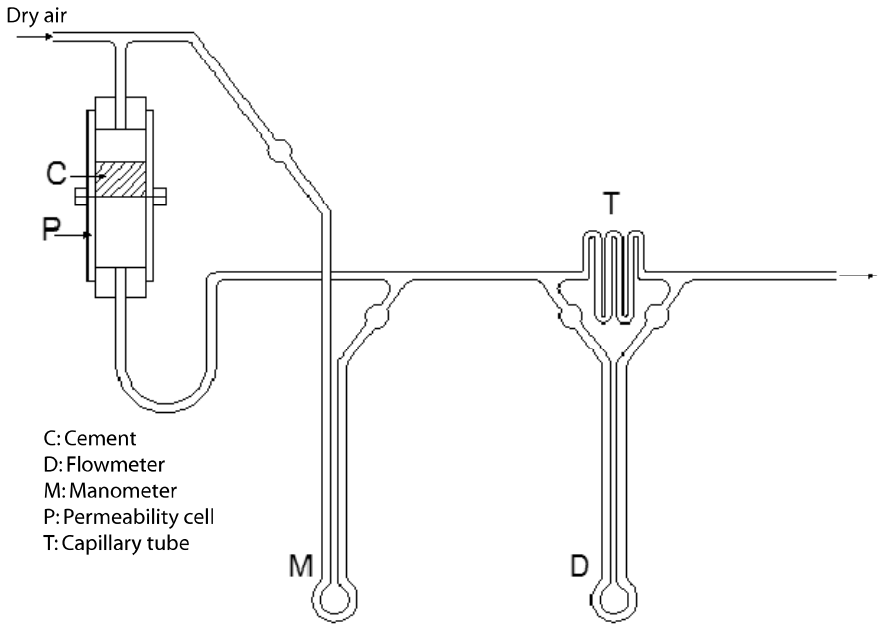

Figure 3.5. *Diagram of the principle of the Lea and Nurse apparatus*

During this test, the permeability cell is subjected to a constant pressure difference that is created by a hydraulic valve in this instance. ΔP, the pressure difference, is measured by a manometric tube, M. h_1 is the drop in the tube M containing a manometric liquid of density ρ_l. We therefore have:

$$\Delta P = h_1 \rho_l g$$

As a result of this driving pressure, an airflow Q passes through the powder bed. This flow is measured using a calibrated capillary tube T, at the ends of which a second manometric tube D is connected.

The flow in the capillary tube can be expressed using the Poiseuille equation (see Exercise 3.4):

$$Q = \frac{\pi r_c^4}{8\mu} \cdot \frac{\Delta P_2}{L_c}$$

in which:

– r_c and L_c are the respective radius and length of the calibrated capillary tube;

– μ is the air viscosity; and

– ΔP_2 is the pressure difference between the two ends of the tube.

The pressure difference ΔP_2 measured using the same manometric liquid as with M is given by:

$$\Delta P_2 = h_2 \rho_l g$$

where h_2 is the drop measured between the two parts of tube D.

Where:

$$Q = \frac{\pi r_c^4}{8\mu} \cdot \frac{\Delta P_2}{L_c} = \frac{K_c}{\mu} h_2 \rho_l g$$

K_c is a constant, which depends on the geometry of the capillary tube.

The Kozeny-Carman formula [3.2] can therefore be expressed as:

$$S_s = \sqrt{\frac{p^3}{(1\text{-}p)^2} \cdot \frac{A}{5\mu\rho_g^2 L}} \cdot \sqrt{\frac{\Delta P}{Q}} = \sqrt{\frac{p^3}{(1\text{-}p)^2} \cdot \frac{A}{5\mu\rho_g^2 L}} \cdot \sqrt{\frac{h_1}{K_c h_2}\mu}$$

$$= K_L \sqrt{\frac{p^3}{\rho_g^2 (1\text{-}p)^2 L}} \cdot \sqrt{\frac{h_1}{h_2}}$$

In this ratio, the term K_L is a constant, which characterizes the Lea and Nurse apparatus used. It depends on section A of the powder bed and of the capillary constant K_c. Value K_L is obtained by calibration with the known surface area of the powder. To calculate the surface area of the powder, we measure the height of the powder, the grain density, the porosity and the two drops in the manometric tubes. It is not necessary to know the density of the manometric liquids unless they are used in the two tubes.

3.3.3. *Blaine apparatus*[2]

During the test, the permeability cell is subjected to a variable difference in pressure. The permeability cell is connected to a U tube containing a manometric liquid (density ρ_l). A sidearm can draw air, which can raise the liquid in the left part. h_0 is the difference in the level between the two parts. The pressure difference between the two sides of the powder bed is $\Delta P = h_0 \rho_l g$.

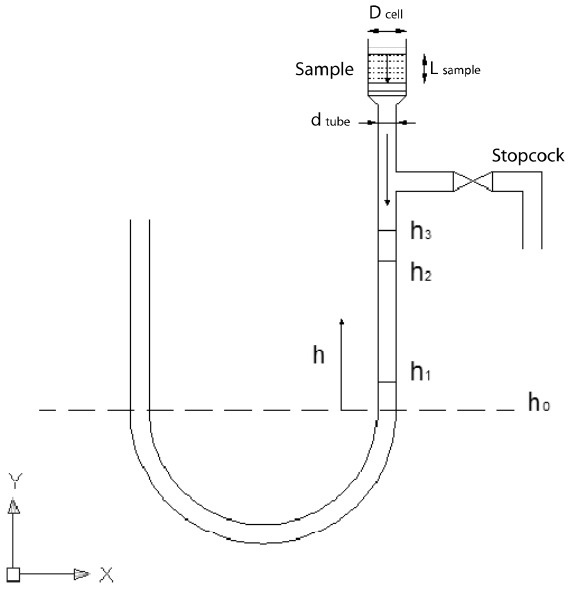

Figure 3.6. *Diagram of the principle of the Blaine apparatus*

2 Also known as “Blaine permeameter”.

We close the suction valve R. Under the effect of the pressure difference, air passes through the powder and drop h decreases. The pressure involved in the Kozeny-Carman relation therefore varies during the test. We will use the average value of the calculated pressure between the two positions marked on the tube. h_1 and h_2, are the two corresponding levels. We can express the average pressure as:

$$\Delta P_{moy} = h_{mean}\rho_l g = \frac{1}{\Delta t}\int_{h_1}^{h_2} h(t)\rho_l g dt$$

where Δt is the time taken for the manometric liquid to fall from the first mark to the second.

We can show[3] that h is the decreasing exponential function of time $h = h_0\, exp(-at)$:

$$dh = -ah\, dt \Rightarrow dt = -\frac{1}{a}\frac{dh}{h} \Rightarrow \int_0^{\Delta t} dt = \Delta t = -\frac{1}{a}\int_{h_1}^{h_2}\frac{dh}{h} = \frac{1}{a}\ln\frac{h_1}{h_2}$$

$$\int_{h_1}^{h_2} h(t)dt = \int_{h_1}^{h_2} h_0 \exp(-at)dt = -\frac{1}{a}(h_2 - h_1)$$

whereby:

$$\Delta P_{mean} = h_{mean}\rho_l g = \frac{h_1 - h_2}{Ln\frac{h_1}{h_2}}\rho_l g$$

The airflow that passes through the powder bed during time Δt is $Q_e = \frac{s(h_1 - h_2)}{2\Delta t}$ if s is the U section of the tube.

3 This ratio is determined in Chapter 7 on the permeability of materials.

Kozeny-Carman equation [3.2] therefore gives:

$$\frac{s(h_1\text{-}h_2)}{2\Delta t} = \frac{p^3}{S_s^2 \rho_g{}^2 (1\text{-}p)^2} \cdot \frac{A}{5\mu L} \cdot \frac{h_1\text{-}h_2}{\ln \frac{h_1}{h_2}} \rho_l g ?S_s$$

$$= \sqrt{\frac{p^3 \Delta t}{\rho_g{}^2 (1\text{-}p)^2 L}} \sqrt{\frac{A \rho_l g}{5\mu \ln \frac{h_1}{h_2}}}$$

By introducing constant K_B where the terms concerning the Blaine apparatus characteristics used are grouped,[4] we obtain:

$$S_s = K_B \sqrt{\frac{p^3 \Delta t}{\rho_g{}^2 (1\text{-}p)^2 \mu}}$$

Constant K_B of the apparatus is determined by calibration by carrying out a measurement using a standard cement whose surface area and grain density are known. Standard NF EN 196-6 indicates that the repeatability deviation[5] is approximately 50 cm^2/g and that of reproducibility[6] is approximately 100 cm^2/g.

It still remains to comply with the Kozeny-Carman model's conditions of validity, namely to regularly prepare a compacted powder bed with a porosity close to 0.5.

NOTE 3.2.– we must not forget that this measurement method can only be applied effectively for powders with sizes ranging from 1 to 100 μm. We must be vigilant in the case of fly ash because the preparation of the powder bed by compaction may break the hollow spheres of the ash and hence

4 In the standard Blaine apparatus, the height of the powder bed, noted here as L, is determined by the geometry of the cell and the height of the piston. It can therefore be included in the Blaine constant. If we use a different apparatus in which L is not inherently determined by the standard, the Blaine constant must be defined differently.

5 The repeatability of a measurement characterizes the quality of measurements made in one place with the same operator using the same measuring equipment.

6 The reproducibility of a measurement characterizes the quality of measurements made in different places by different operators using different measuring equipments.

modify the values of the outer surface. These remarks also apply to measurement using the Lea and Nurse apparatus.

3.4. Methods based on the adsorption of a gas

The adsorption phenomenon is the attachment of atoms (or molecules) of gas on solid surfaces. The links are chemical in nature (chemisorption) or of physical Van der Waals type (physisorption). This phenomenon concerns the attachment of atoms (or molecules) of gas to the surface and not the penetration of atoms (or molecules) into the solid (known as absorption). In what follows we only consider physical adsorption, because this phenomenon does not modify the solid being studied. We will show that it is possible to measure the specific surface area of a solid using a quantitative study of the adsorption phenomenon.

3.4.1. *Adsorption kinetics*

Let us consider a solid surface in a gaseous environment (see Figure 3.7). The collision of a gas atom can be followed either by an elastic shock or by a temporary attachment to the surface of the solid. The latter case is known as adsorption. This phenomenon allows the solid atoms at the interface with the gas to regain a steady balanced state. The gas is therefore called “adsorbate” and the solid “adsorbent”.

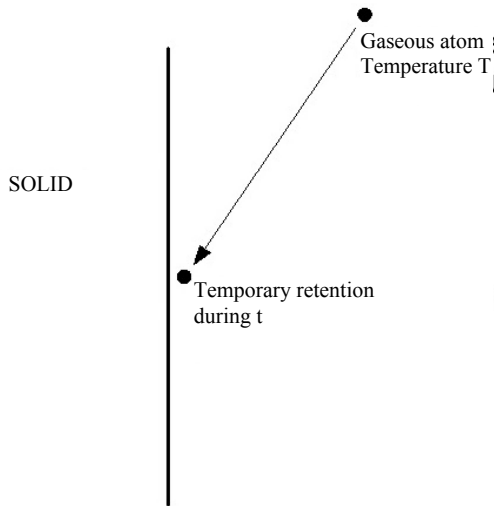

Figure 3.7. *Diagram of the adsorption principle of gas on a solid surface*

The retention time of a gas atom on the solid surface is:

$$t = t_0 \, exp(\frac{Q_a}{RT})$$

where Q_a is the adsorption heat, a gaseous characteristic, and t_0, a solid characteristic. After time t, the gas atom leaves the solid surface to return to the gaseous environment. Atoms adsorbed on the solid are constantly exchanged with the surrounding gas phase. If we consider the surface state at a given time t, atoms partially or totally overlap according to the value of the gas pressure, i.e. the number of shocks per unit time.

If n is the number of shocks per unit of time t and unit of surface, N_a, the number of adsorbed atoms per unit of surface is given by the relation:

$$N_a = n.t = n.t_0 \, exp(\frac{Q_a}{RT})$$

N_a is therefore based on: the nature of gas (Q_a); that of the solid (t_0); the pressure through its subsidiary n; and the temperature (T). A gas adsorption given on a solid depends on the gas pressure and the temperature.

To quantitatively describe the phenomenon of a gas adsorption on a solid, we generally set a value of the temperature and we use an "adsorption isotherm".

3.4.2. *Adsorption isotherms*

An adsorption isotherm is a graph showing the quantity of gas adsorbed on the surface of a solid at a given temperature T according to the gas pressure. Usually the quantity of gas adsorbed is expressed per unit mass of solid adsorbent or by the value of gas adsorbed per unit of solid mass m_s, reported in normal temperature and gas conditions. Pressure is most often expressed by the relative value $x = \frac{P}{P_0}$, where P_0 is the pressure of the saturation of gas at the considered temperature T. Several shapes of curve

can be obtained according to the texture of the materials studied. Figure 3.8 shows the classification adopted by IUPAC[7].

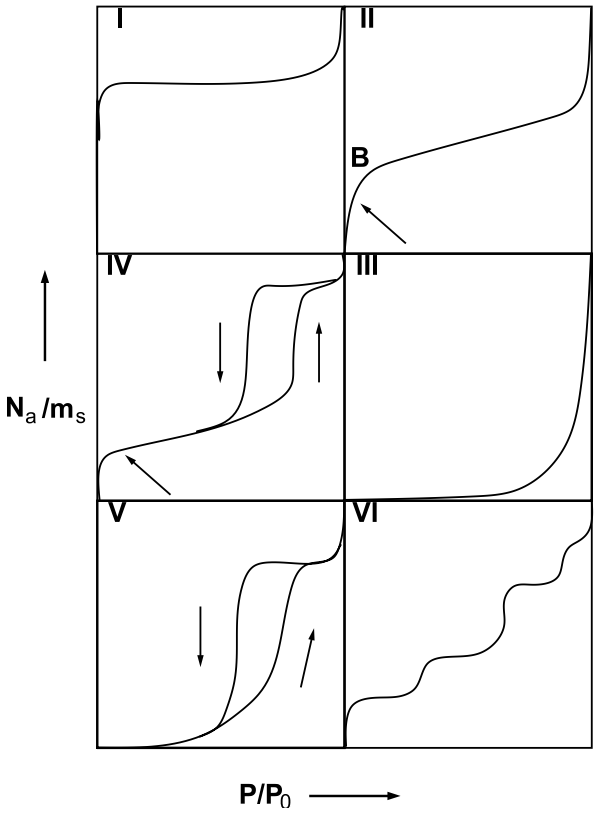

Figure 3.8. *Classification of adsorption isotherms according to IUPAC*

In the case of chemical adsorption, the attachment of the adsorbate results from a chemical reaction with the adsorbent. When all reaction sites have responded, the adsorption stops. Adsorption takes place on a single layer of adsorbate and the saturation of the adsorbent surface to increasing pressure does not translate into a horizontal asymptote. The isotherm shows shape I.

Physical adsorption on a non-porous solid (or porous macro) follows a type II isotherm. At growing pressure, the solid surface is gradually covered

7 The International Union of Pure and Applied Chemistry.

by the adsorbate (see Figure 3.9). For a particular value of pressure P_M, the solid is covered by a complete layer of adsorbate but, contrary to the chemical adsorption, the quantity adsorbed may increase further when the pressure is greater than P_M: we then have multilayer adsorption. The binding energy between an adsorbate particle and the adsorbent gradually decreases when the distance that separates them increases. Layers near the surface of the solid are more closely linked and, beyond a certain distance, the binding energy can be considered negligible. For example, we will show in Chapter 5 that the adsorption of water vapor on the surface of cement is limited to five layers.

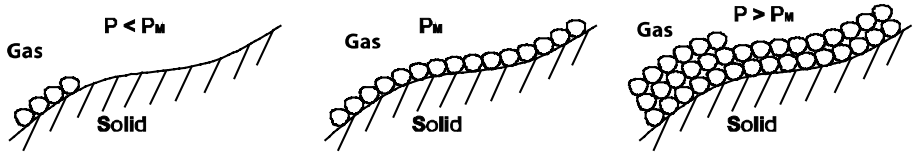

Figure 3.9. *Gradual recovery of the surface of a solid by an adsorbate at increasing pressure. For a particular value of pressure (P_M), the solid is covered by a complete monolayer of adsorbate*

The type IV isotherm appears to be a type II isotherm at relatively low pressures ($x = \frac{P}{P_0}$ <0.42 for adsorption of N_2 to 77 K). Beyond this we observe a rapid increase in the quantity of gas fixed by increasing pressure. This corresponds to another phenomenon – capillary condensation – which is discussed in Chapter 5. This type of isotherm is observed with microporous solids: from a certain pressure, which depends on the size of the pores, the gas condenses in the pores and the shape of the isotherm is modified. We can also observe a hysteresis between the isotherms obtained at increasing pressure (adsorption) and at decreasing pressure (desorption). We show in Chapter 5 that the hysteresis can be used to determine the size of the pores in the material.

The relation of isotherm IV is given by BET theory. This theory [BRU 38] considers that the maximum number of adsorbed layers is limited to a value N_c and the ratio $\frac{V_a}{V_M}$ depends on the pressure and on N_c. (V_a is the volume of adsorbed gas at relative pressure x and at temperature T. V_M is the

volume adsorbed on the solid in a complete monolayer.) When the adsorbed layers reaches infinity, the ratio of the isotherm is as follows:

$$\frac{V_a}{V_M} = \frac{Cx}{(1\text{-}x)[1+(C\text{-}1)x]}$$

where C is a constant.

If the number of layers adsorbed is limited, the $\frac{V_a}{V_M}$ ratio given by the BET theory is not the same. Figure 3.10 shows its progression for different values of N_c.

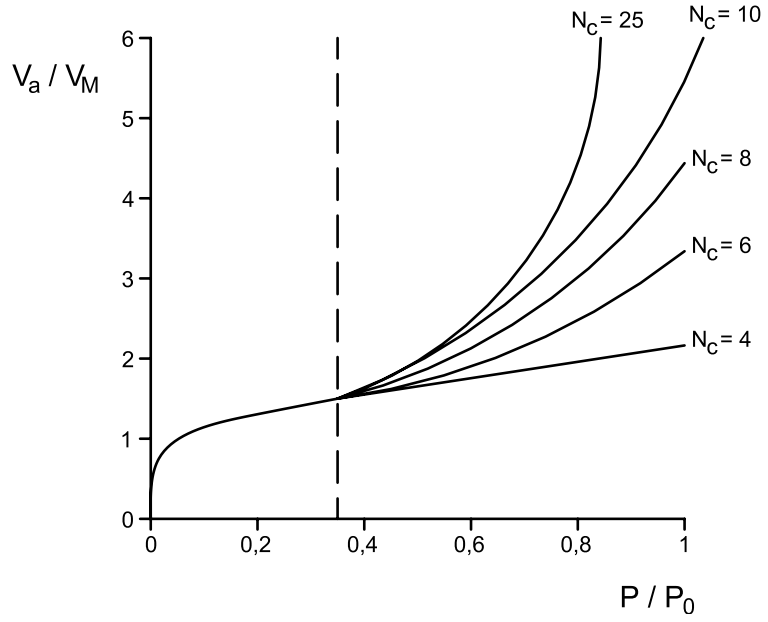

Figure 3.10. *Variation in the shape of the isotherm calculated according to the BET relation in relation to the maximum number N of adsorbable layers. According to the first part of the curve, N has no significant influence (according to [LLE 03])*

For x <0.35, the shape of the isotherm given by the BET relation is independent of the value of N_c used in the calculation. We can therefore

consider that the proposed ratio for an infinite value of N_c applies on the condition that the first part of the curve is considered (x <0.35).

3.4.3. *Determination of specific surface area from isotherm adsorption*

The relation giving the quantity of adsorbed gas shows that in order to facilitate the quantification of gas volume adsorbed on a solid (t_0 fixed), $\frac{Q_a}{RT}$ must be as large as possible. Measurements are therefore taken at a low temperature in a gas with a high adsorption heat. For instance, at 77 K (the temperature of liquid nitrogen), the retention time t of the nitrogen molecules or argon is equal to 10^{11} t_0 (Q_a in the order of 12–15 kJ/mole) instead of $2t_0$ with helium (Q_a in the order of 1.4 kJ/mole). The number of argon or nitrogen molecules adsorbed is therefore greater than that of helium molecules.

Measurement of V_a at different values of relative pressure x allows us to calculate the volume V_M of gas (per unit mass of solid) covering the solid in a monolayer. If we know the quantity of gas covering the solid in a complete monolayer, the surface of the solid and its specific surface area can be deduced. For this we must know the area σ occupied by an atom (or molecule) of adsorbed gas in a monolayer on the surface of the solid. This area depends on the geometry of the arrangement of adsorbate particles on the solid, the molar mass of the adsorbate and the density at liquid state. For example, for nitrogen this is equal to 0.162 nm^2 at 77 K.

The BET specific surface area can be calculated from the following relation:

$$S_{s,BET} = \sigma \frac{V_M N}{V}$$

where N is the Avogadro number (6.023×10^{23} mol^{-1}) and V is the molar volume of the adsorbate (m^3/mol). If σ is expressed in m^2, the specific surface area is obtained as m^2/kg.

$\frac{\sigma N}{V}$ represents the surface of the solid, which can be covered in a complete monolayer by a unit volume of gas. This is known as "steady recovery".

The isotherm adsorption operation of a gas by the BET model may therefore allow us to determine the specific surface area of a solid. This is called *BET specific surface area*. In practice, determination of the BET specific surface area begins with a plot of the isotherm. As an example, Figure 3.11 shows the isotherm adsorption of nitrogen produced on limestone filler at the temperature of liquid nitrogen. The adsorbed volume on the x-axis here refers to the unit mass of solid.

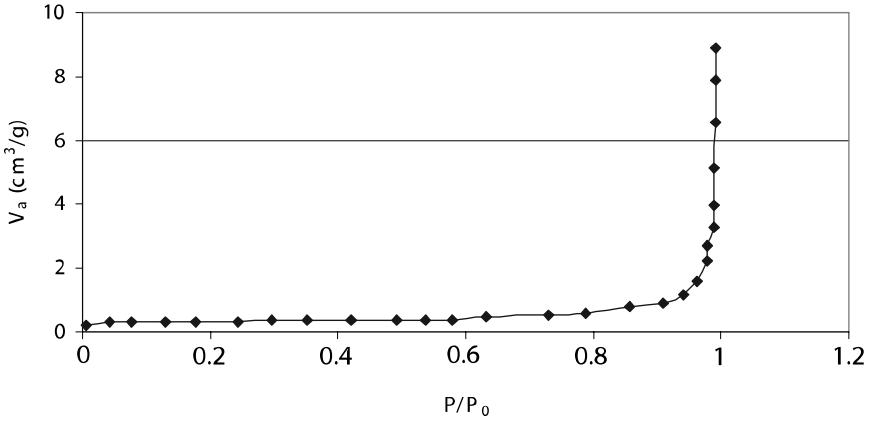

Figure 3.11. *Isotherm adsorption of nitrogen (77 K) on limestone filler, according to [MIC 06]*

To check the feasibility of applying the BET ratio to experimental data in order to determine the volume of gas adsorbed in a complete monolayer, the experimental points are shown in the $\left(\frac{x}{V_a(1\text{-}x)}, x\right)$ coordinates system.

If the BET relation is verified, we can in fact express it as:

$$\frac{V_a}{V_M} = \frac{Cx}{(1\text{-}x)[1+(C\text{-}1)x}$$

This can be converted as:

$$y = \frac{x}{V_a(1\text{-}x)} = \frac{1+(C\text{-}1)x}{CV_M} = \frac{C\text{-}1}{CV_M}x + \frac{1}{CV_M} = ax + b$$

Since C is a constant and V_M is the required value of the adsorbed gas volume in a complete monolayer, verification of the BET relation implies a linear relation between y and x. The values of the slope and ordinate allow us to calculate C and V_M. Figure 3.12 shows the results obtained by applying this conversion of the experimental points in Figure 3.11.

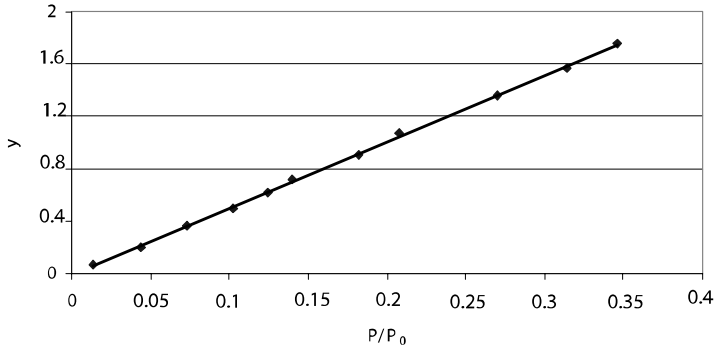

Figure 3.12. *Conversion of the isotherm adsorption in view of the exactitude of the BET ratio, according to [MIC 06]*

3.4.4. *Determination of the specific surface area from an isotherm point*

As Figure 3.12 shows, in the converted BET curve for high values of constant C, we can, from the first approximation, consider that the line passes through the origin and calculate volume V_M using the simplified ratio:

$$y = \frac{C\text{-}1}{CV_M}x + \frac{1}{CV_M} \approx \frac{1}{V_M}$$

The functioning of the BET apparatus using a single isotherm point is presented at the end of the chapter as Exercise 3.6.

3.4.5. *Comparison of techniques*

Measurements of specific surface area taken on filler using the Blaine permeameter and by BET [MIC 06] show that the values obtained can be very different. If the grains have a rough surface morphology or contain some clay particles, the BET specific surface area will be much larger than that obtained using the Blaine permeameter.

For cement, as standard NF EN 196-6 indicates, the Blaine permeameter measurement must be performed in comparison to a reference cement and is used primarily to monitor the manufacturing of fabric. In particular, it will not give very good results if the cement contains ultrafine particles, such as silica fumes.

3.5. Methylene blue test for the characterization of fine particles

The blue test (standard EN 933-9) is based on the adsorption of methylene blue on the fine particles of a fraction of 0/2 mm of an aggregate (blue value *MB*) or fraction 0/0.125 mm (blue value MB_F). It allows us to classify aggregates in accordance with their fine clay content.

The principle consists of a granular material in suspension in water to which successive doses of a solution of methylene blue are added. After each addition, the adsorption of methylene blue by the aggregate is tested by performing a spot check on filter paper to detect the presence of residual dye. When residual dye is detected, the adsorption capacity of the aggregate has been reached and the methylene blue value (*MB* or MB_F) is calculated and expressed in grams of dye adsorbed per kg of granular fraction tested.

There is no standard defining the compliance of aggregates (XP P18-345) limiting the value for *MB* or MB_F. In fact, as indicated by standard EN 12620 on “Concrete aggregates”, the limits depend on local feedback on the use of various aggregates. However, we can give orders of magnitude as the value $MB < 1$ and $MB_F < 10$ for the best sand.

3.6. Bibliography

[BEN 99] BENTZ D., GARBOCZI E., HAECKER C., JENSEN O., "Effects of cement particle size distribution on performance properties of Portland cement-based materials", *Cement and Concrete Research* vol. 29, pp. 1663-1671, 1999.

[BRU 38] BRUNAUER, S., EMMETT P. H., TELLER E., "Adsorption of gases in multimolecular layers", *J. Am. Chem. Soc.* vol. 60, pp. 309-319, 1938.

[MIC 06] MICHEL F., COURARD L., "Apport de la granulométrie LASER dans la caractérisation physique des fillers calcaires", *Septième Édition des Journées Scientifiques du Regroupement Francophone pour la Recherche et la Formation sur le Béton*, Toulouse, France, June 19-20, 2006.

[LLE 03] LLEWELLYN P., ROUQUEROL J., LUCIANI L., DENOYEL R., ROUQUEROL F., *Texture des Matériaux Pulvérulents ou Poreux*. Techniques de l'Ingénieur, Traité Analyse et Caractérisation, 2003.

3.7. Exercises

Exercise 3.1: *specific surface area of a grain (section 3.2.1)*

a) Show that $c = 6$ in the case of a spherical grain in choosing D that is equal to the diameter.

b) Calculate c for a cubic grain (in choosing D equal to the cube edge).

Exercise 3.2.

Let us consider a cement with a specific surface area that is equal to 3,500 cm^2/g.

a) We wish to calculate the order of magnitude of the average size of grains, d_{mean}.

b) Assuming they are all spherical and are the same size, calculate d_{mean}.

c) The grain density of cement is equal to 3.1 g/cm^3. Calculate the specific surface area in m^{-1}.

Exercise 3.3.

Cement has a granular curve shown in Figure 3.13

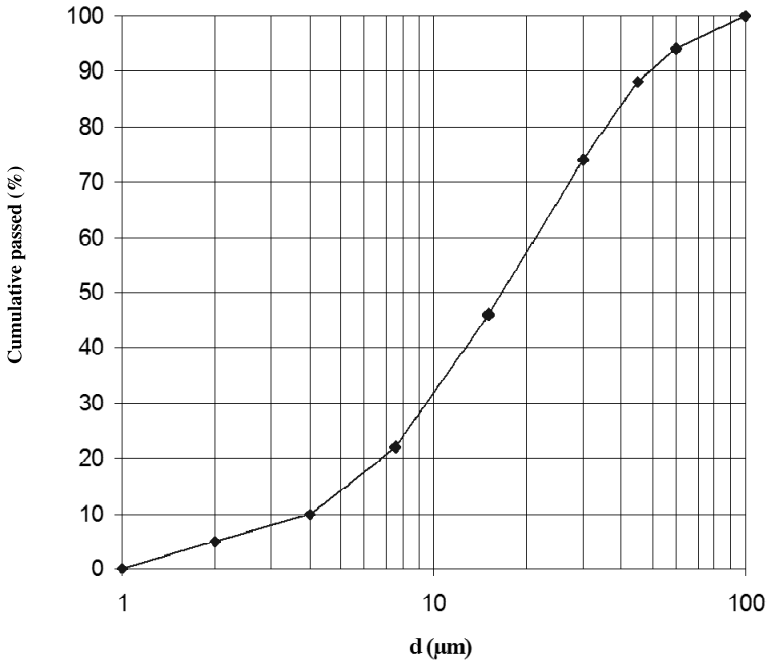

Figure 3.13. *Example of the granular curve of cement*

The grain density ρ_g is equal to 3.1 g/cm^3.

a) Calculate the order of magnitude of the specific surface area of cement, assuming that the particles are spherical and one-dimensional (diameter = D_{50}).

b) Calculate another more accurate order of magnitude of the specific surface area from the granular curve.

Exercise 3.4: ***the Poiseuille relation***

The Poiseuille relation for a channel with a circular cross section is:

$$Q_e = \frac{\pi r^4}{8\mu} \cdot \frac{\Delta P}{L_e}$$

Determine the value of the shape factor h_0.

Exercise 3.5.

a) We propose to measure the specific surface area of cement with density of ρ_g = 3.15 g/cm^3 using the Blaine apparatus. What is the dimension of the Blaine constant K_B?

b) The apparatus used has a constant K_B = 35,300 [SI]. In a permeability cell whose diameter is 2 cm, 5 g of cement is compacted to a height of 15 mm. The flow time of the manometric liquid between the two marks is equal to 20 s. What is the Blaine specific surface area of the cement?

Exercise 3.6: ***simplified apparatus using a single point of isotherm adsorption for measurement of the BET surface area***

The apparatus here consists of a cell C and a cylinder (volume V_d) swept by a piston (see Figure 3.14).

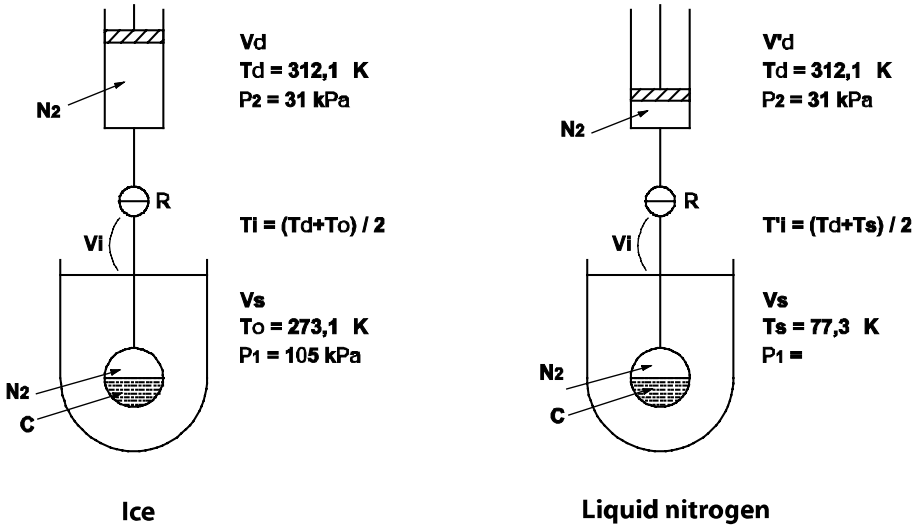

Figure 3.14. *Diagram of the principle of the BET apparatus*

Operation:

– We place the cell sample-holder C in melting ice (T_0 = 273.1 K) under pressure P_1 = 105 kPa. The temperature of the cylinder is regulated at 39°C (312.1 K) throughout the whole measurement.

– The valve R being closed, we lower the pressure in the cylinder to P_2= 31 kPa using a pump.

– For adsorption, the cell is immersed in liquid nitrogen (T_S = 77.3 K).

a) What is pressure P_1 in volume V_S in the absence of adsorption?

b) What happens at the opening of R?

c) If there is an adsorbent powder in the cell, the piston moves down to the bottom to maintain pressure P_2 after opening R: this displacement is directly linked to volume V_a of adsorbed gas. Complete the table below.

	CYLINDER			**CELL**			**TUBE**		
	P	V	T	P	V	T	P	V	T
State 1		V_d			V_S			V_i	
State 2		V'_d			V_S			V_i	
State 3 R open		V'_d			V_S			V_i	

d) Calculate the number of moles of gas in the system before and after adsorption. Deduce the number of moles adsorbed.

e) Knowing that the volume V_S of the cell is equal to 15 cm^3, what should the volume V_i be for the number of moles adsorbed to depend on the variation in the volume, $V_d - V'_d$, alone?

f) In the case of liquid nitrogen at -196°C, the constant of recovery is equal to 4.35 m^2/cm^3. According to the simplified BET obtained for high values of constant C, $\frac{V_M}{V_a(1-x)} = 1$, determine V_M as well as the specific surface area of the powder.

Exercise 3.7: *BET specific surface area*

The BET method consists of adsorbing the surface of a material to study a gas, usually nitrogen, at the normal temperature of liquefaction. For this, we have an adsorption cell containing the adsorbent. The gas is introduced into the cell and we measure the equilibrium pressure. The introduction of a series of gas doses therefore allows us to determine the isotherm adsorption point by point. This isotherm links volume V of adsorbed gas to the x ratio of gas pressure P and P_0, its saturated vapor pressure.

1) Adsorption in monomolecular layer (Langmuir). The assumptions used here are the following:

– there is only one type of adsorption site capable of binding a single adsorbate molecule; and

– there is no interaction between molecules adsorbed.

When a molecule from the gas phase hits an area that is free of adsorbate, S_0, it can settle there. However if it encounters an area that is already covered, S_1, it bounces elastically towards the gas phase. This is equivalent to assuming that the surface actions do not extend beyond the first layer.

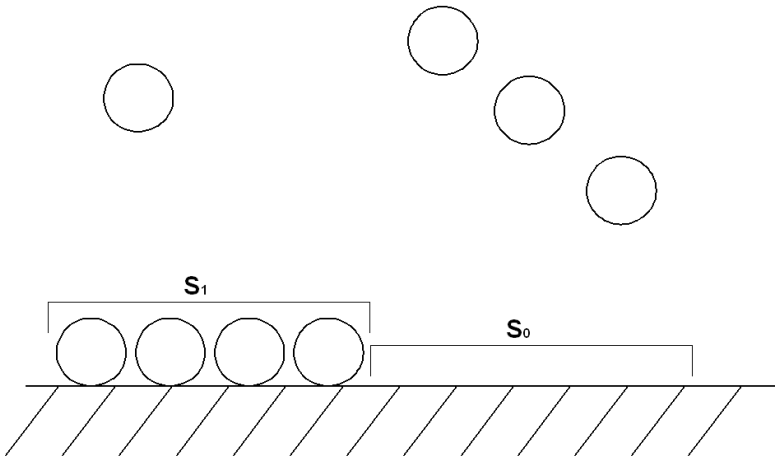

Figure 3.15. *Adsorption in a monomolecular layer*

Finally we assume that to reach equilibrium we obtain the following ratio: $S_1 = CxS_0$ where C is a constant.

a) Express then the ratio of the isotherm adsorption giving V/V_m as a function of C and x, where V_m is the volume of adsorbate required to cover a monomolecular layer. V_0 is the volume of adsorbate required to cover the monomolecular layer of the unit area of the adsorbent.

b) Draw the shape of the isotherm adsorption (known in this case as a type I or Langmuir isotherm) with $C = 100$.

2) Adsorption in a monomolecular layer (BET theory)

S_i is the surface covered by exactly i molecule layers (see Figure 3.16). The assumptions of this theory are the following:

– The rate of evaporation of the adsorbed molecules on a layer is equal to the rate of condensation of adsorbate on the previous layer (the evaporation balance is compensated for by the condensation for each layer).

– The first layer shows the effect of the surface, although the other layers are only linked by forces such as Van der Waals forces, as in a liquid. In all layers other than the first, the adsorption energy is equal to the liquefaction energy of the adsorbate ($E_i = E_L$ for i > 1 where E_i is the molar energy and adsorption of layer i and E_L the molar energy of liquefaction of the adsorbate).

– There is no capillary condensation.

a) Assuming that the rate of adsorption on the layer is proportional to pressure P and to the surface of the lower layer, and that the rate of desorption is proportional to the surface of the layer and a function of temperature T by means of an activation law expressing itself by $\exp(-E_i / R_{gp}T)$, show that the balance between both successive layers results in:

$$a_{i-1}PS_{i-1} = b_iS_i \exp(-E_i/R_{gp}T)$$

with a_{i-1} and b_i being proportionality coefficients. E_i is the molar energy of adsorption of the first layer and R_{gp} the constant of perfect gas here.

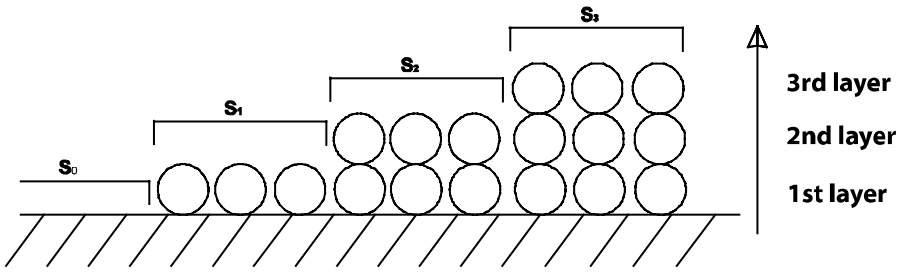

Figure 3.16. *Adsorption in multimolecular layers*

b) Assuming again that $S_1 = CxS_0$ and for $i > 1$, $S_i = xS_{i-1}$, i being the order of the layer, show that: $b_2/a_1 = b_3/a_2 = \ldots = b_i/a_{i-1} = g$ where g is a constant. Determine g in relation to P_0, E_L and T. C is known as the BET constant. Give the ratio of C in relation to a_0, b_1, g, E_1, E_L and T.

c) Summing up the surfaces covered by 0, 1, 2, . . . n layers, express the surface of the adsorbate in relation to S_0, C, x and n. Show that when n reaches infinity, the series converges. Give its ratio.

Hint: show that $x - x^{n+1} = (1 - x).(x + x^2 + \ldots + x^n)$

d) Give the ratio of volume V adsorbed under pressure P in relation to V_0, S_0, C, x and n. Show that when n reaches infinity the series converges. Give its expression.

Hint: use the fact that $i \,.\, x^{i-1}$ is the derivative of x^i.

e) We consider in the following that n reaches infinity. Express the ratio of the isotherm adsorption V/V_m in relation to C and x. Plot its variation shape with $C = 100$.

f) Calculation of surface mass: here we introduce the variable $y = 1/V.\ x/(1-x)$. Show that we can express $y = \alpha x + \beta$ and express V_m and C in relation to α and β. Give the ratio of the specific surface mass S_{MBET} in relation to V_m, the molar volume of the adsorbate v_m, the Avogadro number N and the area size of an adsorbed molecule in the monomolecular layer A_m.

g) Application: Figure 3.17 shows the result of a BET test on a limestone filler. Calculate the specific surface mass S_{MBET} for the limestone filler.

Assuming that the grains of the filler are spherical and all of them are the same height, deduce the radius of the grains.

Data:

- $\beta = 0.0098$ g.cm^{-3};
- for N_2 to $T = 77$K, N.$A_m/v_m = 4.35 \times 10^6$m^{-1}; and
- density of limestone filler: 2.74 g.cm^{-3}

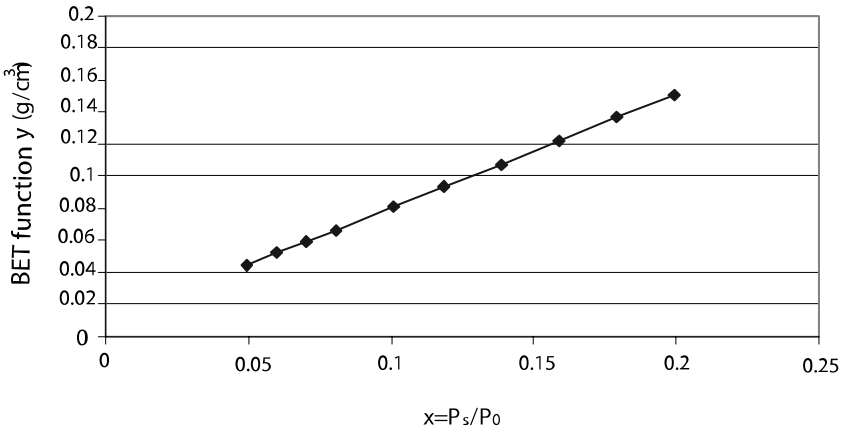

Figure 3.17. *Result of BET test for 1g of limestone filler*

Chapter 4

Voids in Granular Materials and the Arrangement of Grains

4.1. Introduction

The enhanced performance of concrete over the past decades is largely due to the improvement in the quality of its granular skeleton. The use of admixtures referred to under different names such as plasticizer, superplasticizer, water-reducer, etc., has enabled us to create increasingly dense granular skeletons as new generations of products progressively emerge. All of these admixtures can disperse (deflocculate) the smallest grains, which enables them to separate from each other to better fill the void while maintaining flow properties, or even enhancing them, in a fresh state.

This chapter discusses the physical bases for the formulation of a mixture of grains for a better understanding of the methods of composition. In Chapter 1 we showed that the shape of grains made their description difficult. In this chapter, where the interest is more focused on voids, complementary to that of the solid (grain), the analysis of grains filling voids faces the same problem: the complex shapes of grains are reflected by complicated intergranular voids shapes.

We will therefore proceed to the analysis of filling voids gradually by first considering identical spherical grains, then by studying the influence of the shapes of one-dimensional grains on the compactness obtained. We will finally consider grains of any form and any size. We will then focus on the

Physical Properties of Concrete and Concrete Constituents Jean-Pierre Ollivier, Jean-Michel Torrenti and Myriam Carcassès

influence of the implementation of compactness (achieved by vibration) of granular mixtures.

4.2. Sphere packing (one-dimensional: $\Phi = 2R$): theoretical approach and experimental data

In the plane, two types of compact arrangements exist (see Figure 4.1). In the square arrangement, the centers of the neighboring spheres are placed at the corners of a square and in the rhombic arrangement, also known as a compact arrangement, they are placed at the vertices of an equilateral triangle.

By overlaying the planes of the spheres, we can construct three-dimensional packing.

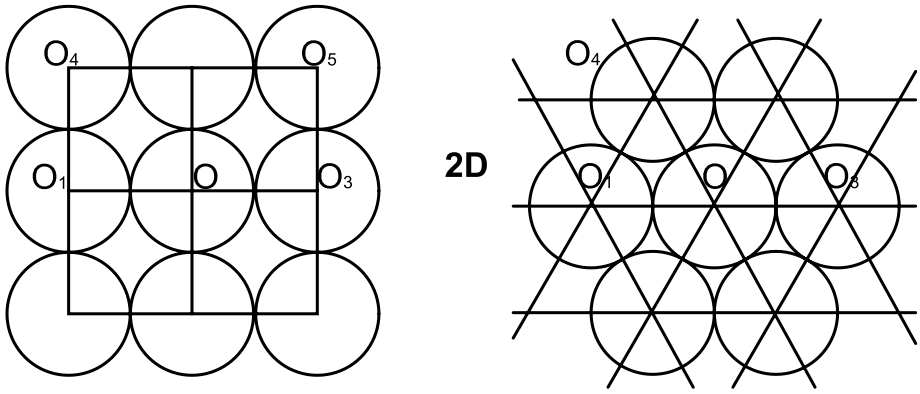

Figure 4.1. *In the plane, identical spheres can organize themselves according to square or rhombic arrangements*

4.2.1. *3D packing of square-based layers*

Consider the square-base layer shown in Figure 4.1 on which another square layer is overlaid. If the centers of the outer sphere are vertical to those

of the base sphere, the centers of the spheres are equal the corners of a cube and a cubic arrangement is obtained (see Figure 4.2a).

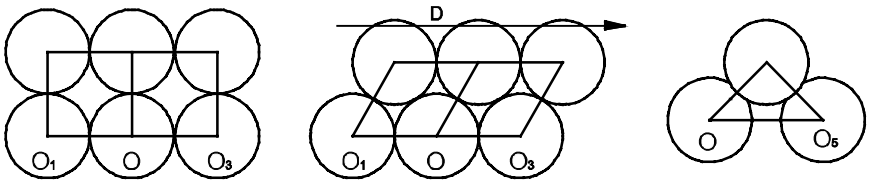

Cross-section O_1O_3 Cross-section O_1O_3 Cross-section O_5O

a) Cubic packing b) Orthorhombic packing c) Rhombohedral packing

Figure 4.2. *3D packing produced from square-based layer (seen as sections perpendicular to the plane in Figure 4.1)*

In cubic packing, the planes passing through the centers of two layers of neighboring spheres are distant from diameter D of the spheres. To increase the packing's level of compactness, these two planes must be brought together without modifying the 2D arrangements. For this, the sphere's plane can be dragged from above according to a direction Δ parallel to the right of O_1O_3 in Figure 4.2a. Each sphere in the upper plane will then be placed on the two spheres of the plane's base. The new packing is known orthorhombic packing (see Figure 4.2b).

To bring the two square planes closer (or layers), once again the spheres must be moved horizontally; this time according to a direction perpendicular to the precedent. Each center of the spheres of this plane is then vertical to the squares, such as $O_1O_2O_3O_4$. The packing obtained is rhombohedral (see Figure 4.2c). It is also called *closed-packed* when we further align the two planes' bases and increase their compactness.

In a square layer, each sphere is tangent to four other layers. In the cubic packing, each sphere is tangent to six spheres (four in its plane and one in the upper plane and one in the lower plane). This number of tangent spheres is also known as the *coordination number*. In orthorhombic packing, the coordination number is eight and it is twelve in rhombohedral packing.

4.2.2. *3D packing of rhombic-based layers*

In a rhombic layer, each sphere is tangent to six others. By overlaying a rhombic layer with another one, an orthorhombic packing is obtained. It is the same as the one obtained with square layers. According to the process described here, it is deducted from the previous format by a rotation of $\frac{\pi}{2}$. The coordination number is eight. To increase the compactness of the packing, the same method as that described for packing produced with square layers may be used. The base layers will be brought together, one against each other, by two relative orthogonal movements. We successively obtain a sphenoedric type of packing (coordination number ten) and a rhombic packing (coordination number twelve).

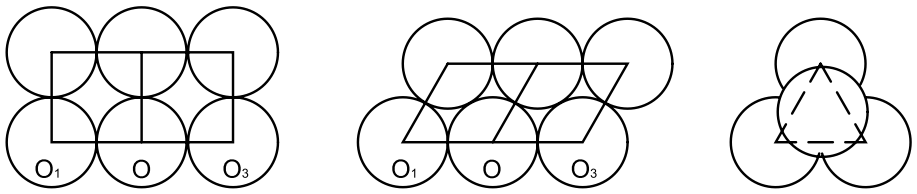

a) Orthorhombic packing b) Spherohedric packing c) Rhombic packing

Figure 4.3. *3D packing produced from rhombic layers (Figures a and b are sections perpendicular to the base of the plane in Figure 4.1, and c is a view from the top)*

4.2.3. *Porosity of identical spherical packing*

The porosity of identical 3D spherical packing can be calculated in two ways: by a direct method or by studying the variation in the void section.

4.2.3.1. *Calculation of the porosity using a direct method*

4.2.3.1.1. Packing from square layers

There are several different type of packing that can be found here:

– *Cubic packing*:

In a rectangular parallelepiped with sides *a*, *b* and *c* (multiple of the diameter $D = 2R$ of the spheres) we have $n = \frac{a.b.c}{(2R)^3}$ spheres with a radius *R*. These *n* spheres have a volume of $v_{solid} = \frac{a.b.c}{(2R)^3} \cdot \frac{4}{3}\pi R^3 = \pi \frac{a.b.c}{6}$.

The void volume is therefore $v = a.b.c(1-\frac{\pi}{6})$ and the porosity is:

$$p = \frac{v}{a.b.c} = 1 - \frac{\pi}{6} \approx 0.476$$

– *Orthorhombic packing*:

In the rectangle with sides *a* and *b*, we have $\frac{a.b}{(2R)^2}$ spheres and, at a height *c*, $\frac{c}{R\sqrt{3}}$ layers.

In the parallelepiped with sides *a*, *b* and *c*, we have $n = \frac{a.b.c}{4R^3\sqrt{3}}$ spheres, which have a volume of $v_{solid} = \frac{a.b.c}{4R^3\sqrt{3}} \cdot \frac{4}{3}\pi R^3 = \pi \frac{a.b.c}{3\sqrt{3}}$. The void volume is therefore $v = a.b.c(1-\frac{\pi}{3\sqrt{3}})$ and the porosity is $p = 1 - \frac{\pi}{3\sqrt{3}} \approx 0.395$

– *Rhombohedral packing*:

In a rectangle with sides *a* and *b*, there are always $\frac{a.b}{(2R)^2}$ spheres and, at a height of *c*, $\frac{c}{R\sqrt{2}}$ layers, whereby $n = \frac{a.b.c}{4R^3\sqrt{2}}$. These *n* spheres have a volume of $v_{solid} = \frac{a.b.c}{4R^3\sqrt{2}} \cdot \frac{4}{3}\pi R^3 = \pi \frac{a.b.c}{3\sqrt{2}}$.

The void volume is $v = a.b.c(1-\frac{\pi}{3\sqrt{2}})$ and the porosity is $p = 1-\frac{\pi}{3\sqrt{2}} \approx 0.26$.

4.2.3.1.2. Packing from rhombic layers

There are several different types of packing with rhombic layers:

– *Orthorhombic packing*:

In a rectangle with sides a and b, we have $\frac{a.b.c}{2R.R\sqrt{3}}$ spheres and at a height c we have $\frac{c}{2R}$ layers. We therefore have a parallelepiped a, b and c with a number $n = \frac{a.b.c}{4R^3\sqrt{3}}$ of spheres with a volume of $\frac{a.b.c}{4R^3\sqrt{3}}.\frac{4}{3}\pi R^3 = \pi\frac{a.b.c}{3\sqrt{3}}$. The void volume is therefore $v = a.b.c(1-\frac{\pi}{3\sqrt{3}})$ and the porosity is $p = 1-\frac{\pi}{3\sqrt{3}} \approx 0.395$.

– *Spherical packing*:

In a rectangle of sides a and b, there are always $\frac{a.b.c}{2R.R\sqrt{3}}$ spheres with a height of c where we have $\frac{c}{R\sqrt{3}}$ layers. We therefore have a parallelepiped a, b and c with a number $n = \frac{a.b.c}{2R^3 3}$ of spheres with a volume of $\frac{a.b.c}{6R^3}.\frac{4}{3}\pi R^3$. The void volume is therefore $v = a.b.c(1-\frac{2\pi}{9})$ and the porosity is $p = 1-\frac{2\pi}{9} \approx 0.30$.

– *Rhombohedral packing*:

In a rectangle with sides *a* and *b*, there are always $\frac{a.b.c}{2R.R\sqrt{3}}$ spheres with a height of *c* where we have $\frac{c}{2R\sqrt{\frac{2}{3}}}$ layers. We therefore have a parallelepiped *a, b* and *c* with a number $n=\frac{a.b.c}{4R^3\sqrt{2}}$ of spheres with a volume of $\frac{a.b.c}{4R^3\sqrt{2}}.\frac{4}{3}\pi R^3=\pi\frac{a.b.c}{3\sqrt{2}}$. The void volume is therefore $v=a.b.c(1-\frac{\pi}{3\sqrt{2}})$ and the porosity is $p=1-\frac{\pi}{3\sqrt{2}}\approx 0.26$.

4.2.3.2. *Calculation of porosity based on studying the variation in voids*

This method of calculation is more complex. The method is discussed here in the simplest way possible using cubic packing. O being the center of the sphere of the base layer, let us consider the reference plane to be (Ox, Oy), with the horizontal plane moving through the center of the spheres of the base layer. The axis Oz is vertically upwards moving through O. Let us isolate a pattern representative of the packing: a parallelepiped with a side measuring 2*R* and a height of *R*.

Place $z=RZ$ with $0\le Z\le 1$. The voids section of side z is worth:

$$A=4R^2-\pi R^2=4R^2-\pi(R^2-z^2)=R^2(4-\pi-\pi Z^2)$$

The pattern's porosity is:

$$p=\frac{v}{V_a}=\frac{\int_0^Z Adz}{4R^3}=\frac{\int_0^1 ARdZ}{4R^3}=\frac{1}{4}\int_0^1(4-\pi+\pi Z^2)dZ$$

That is:

$$p = \frac{1}{4}(4-\pi+\frac{\pi}{3}) = 1-\frac{\pi}{6}$$

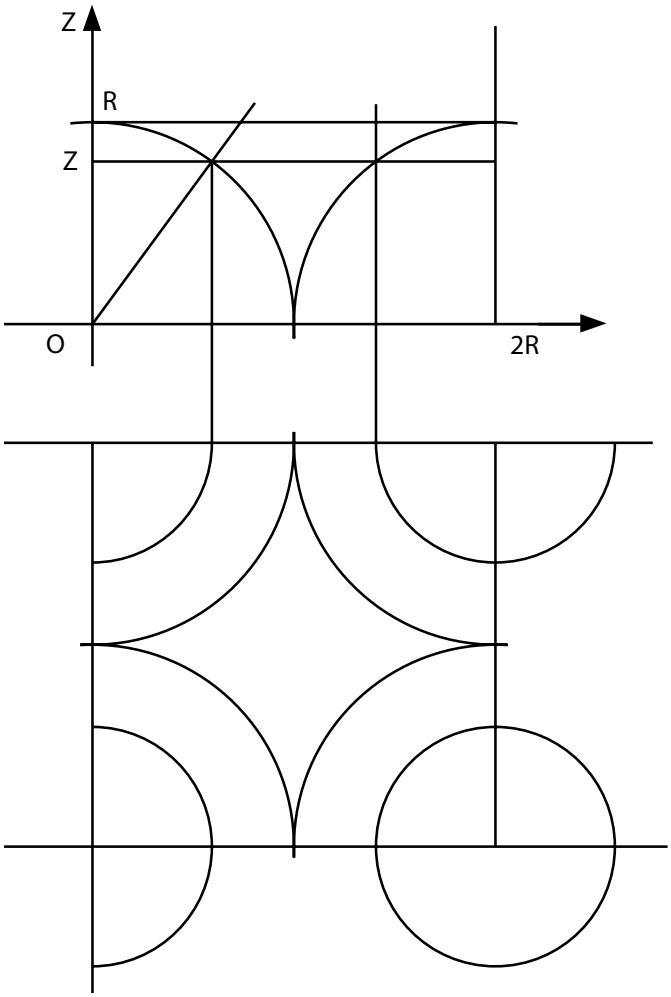

Figure 4.4. *Pattern representative of cubic packing*

4.2.3.3. *Assessment of results*

	From square layers			From rhombic layers		
Type of packing	Cubic	Ortho-rhombic	Rhombo-hedral	Ortho-rhombic	Spherical	Rhombo-hedral
Coordination number	6	8	12	8	10	12
Porosity	0.476	0.395	0.260	0.395	0.300	0.260

Table 4.1. *Porosity of different types of packing*

The minimum porosity of identical spherical packing is 26%. This is obtained for the rhombohedral packing.

The porosity of identical spherical packing is independent of the size of the spheres. However, the size of voids between the spheres depends on the diameter of the spheres: the bigger the spheres, the larger the voids between the spheres (see Exercise 4.1).

4.3. Experimental data

The porosity of a packing of spherical grains can be measured, for example, by filling a container with a known volume of glass beads of set diameter D. The number of beads in the container depends on the mode of implementation. Thus, by simply pouring we obtain porosity close to 0.40. Through a sufficiently long and energetic vibration, it is possible to decrease porosity to a minimum. This minimum porosity value obtained experimentally is still higher than the theoretical minimum (26%) and, moreover, for a given container it depends on the diameter of the beads.

Figure 4.5 shows that the minimum porosity of spherical packing depends on the relation between their diameter and the size of the container (the diameter of the container in the case of a cylindrical container).

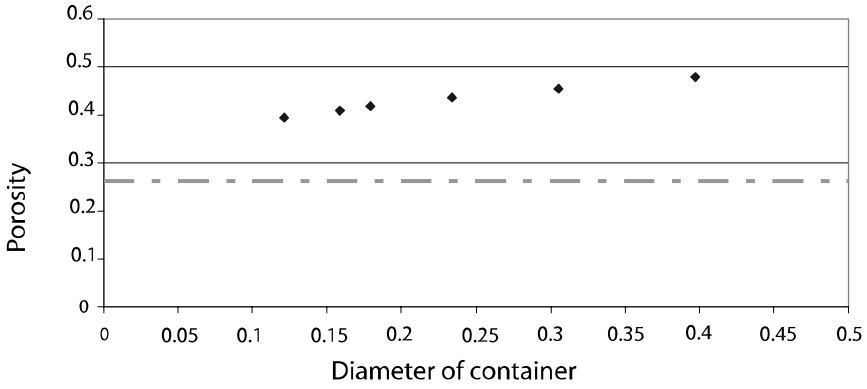

Figure 4.5. *The minimum porosity of an identical spherical packing depends on the relation between their diameter and the diameter of the container in which they are held*

This increase in porosity compared to that of the rhombohedral packing, is due to the *wall effect*. Near a wall, the spatial arrangements of the beads are disturbed. For example, if we consider a flat wall, at a distance that is infinitely close to it, the porosity is practically equal to 1, as a plane close to the wall only intercepts the beads locally (regularly along the wall). For planes parallel to the wall, porosity gradually decreases. In addition, we consider that the thickness of the area disturbed by a wall is in the order of five times the diameter of the spheres. Throughout this zone, porosity exceeds the minimum theoretical value and, the smaller the diameter of the sphere compared to the size of the container, the smaller the relative importance of the disturbed area, and the closer the porosity measured is to 26%. At the container's angles, another disturbance causes a further increase in porosity (see Figure 4.6).

This local increase in porosity in the vicinity of a wall can easily be viewed by considering an exposed concrete surface. Without special treatment, concrete appears uniformly gray as we only see hydrated cement. Water fills the empty voids between the sandy grains or gravel in concrete, which are organized in the vicinity of the formwork, just as the beads are shown in Figure 4.6. On exposure, only hydrated cement is visible. Thus, near the outer surface of concrete is an area of several centimeters with a higher cement content.

Hydrated cement constituting the porous part of concrete – this outer concrete, known as concrete skin – is concrete whose porosity is higher than core-concrete, which is less rich in cement. This can have adverse effects on the durability of concrete, as the outer area is that through which external aggressive agents penetrate.

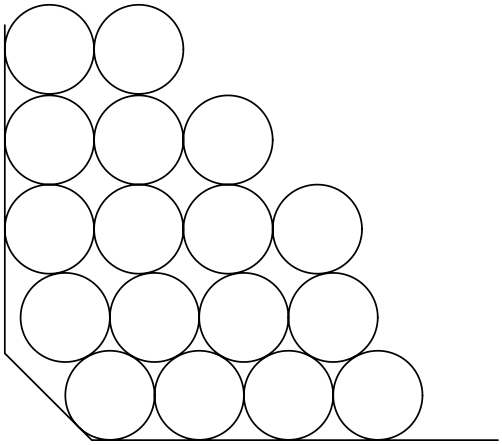

Figure 4.6. *Illustration of the wall effect responsible for the local increase in the porosity of a granular packing*

As we shall see later, these effects also exist when mixing grains of different sizes.

4.4. Influence of grain shape

Figure 4.7 illustrates the influence of a grain shape of minimal porosity obtained by packing. The grain shape is characterized by an angularity factor $1/\psi$ (see Chapter 2). The higher it is, the further the grain shape from that of a sphere and the higher the minimum porosity.

In the case of Figure 4.7, the minimum porosity of spherical packing in the container used is 42%. This value can reach 60% with very elongated grains.

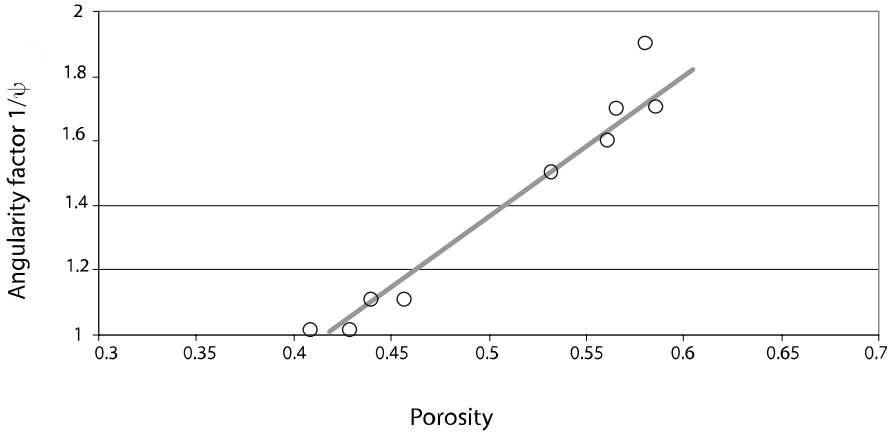

Figure 4.7. *Influence of grain shape on the minimum porosity of a packing*

The rest of this chapter will be devoted to the presentation of methods, which enable us to decrease porosity (increasing compactness) through the use of mixtures of grains of different sizes.

4.5. Search for maximum compactness

Unless we are using special prescriptions, such as those for porous asphalt in which we want to have an important porosity, when mixing the aggregate mixture to produce concrete we seek to optimize the compactness. This is for two reasons. The first is economic. Aggregates are components that are the least expensive element in concrete. The second reason is practical: the optimum compactness is also close to the optimum workability. It is therefore at this optimum that we will use less cement paste to obtain the desired workability.

Compactness can be increased by mixing grains of different granular classes. This is shown in Figure 4.8.

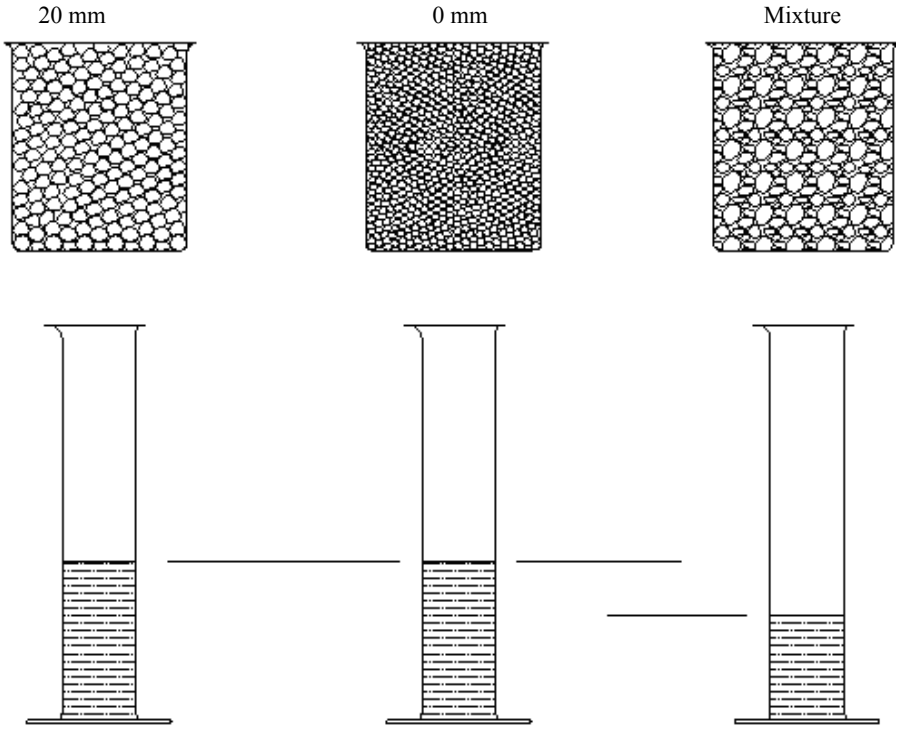

Figure 4.8. *The effect mixing two granular classes on porosity*

With a single granular class, porosity is almost independent of the size of grains and it is possible to decrease porosity (measured here by the volume of water filling the intergranular voids) by mixing two granular classes, with the small grains staying between the voids of large grains. The process of filling a granular skeleton can, theoretically, be pursued to infinity: the process is called the "Apollonian gasket".

We want to know the number and size of each grain allowing us to obtain a granular mixture of minimum porosity. In other words: what is the granular curve of the mixture leading to minimum porosity? To answer this question, we will proceed in stages through the following by successively considering the case of a binary mixture (constituted of two one-dimensional

aggregates), then a ternary mixture and finally a mixture containing an infinite number of elementary aggregates[1].

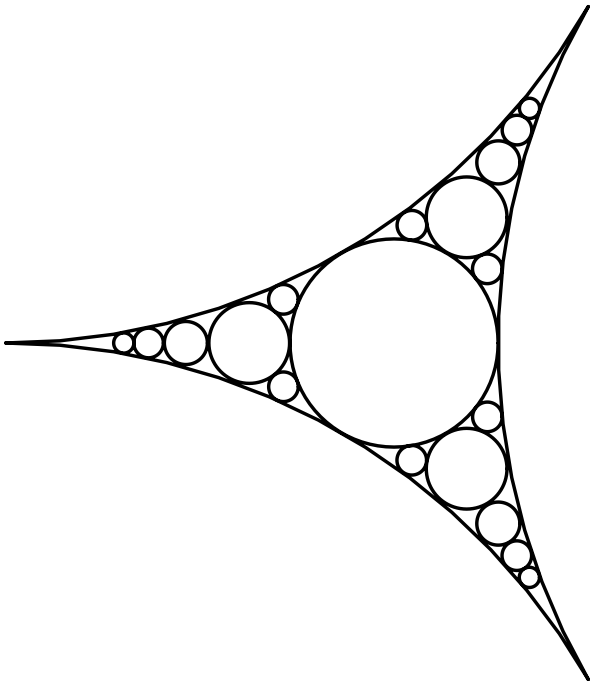

Figure 4.9. *Apollonian gasket: from an aggregate consisting of one-dimensional grains (the circles in the figure shown here are in two dimensions), it is possible to decrease porosity by inserting smaller grains that best fill the voids between the larger grains. Theoretically, this process can be pursued indefinitely*

4.5.1. *Mixture of two one-dimensional aggregates*

Figure 4.10 shows the variation in the void ratio of binary mixtures in relation to the volume fraction of large grains, n. This fraction n is defined by the relation:

$$n = \frac{g}{g + f}$$

1 An elementary aggregate is one whose grains have a size between two successive openings of the series of standard sieves.

where g is the volume of large grains (of diameter Φ_{max}) and f is the volume of the small grains (of diameter Φ_{min}). Different curves correspond to the increasing values of the size aspect of the two grain types.

Let us first consider the case of small grains ($n = 0$) and add large grains. The small grains have a void ratio of F. If we add large grains of volume g to this, the void ratio l is that which exists between the small grains fF and the volume of the grains is the sum of $f + g$.

$$e = \frac{fF}{f+g} = F\frac{f+g\text{-}g}{f+g} = F(1\text{-}n)$$

The void ratio of the mixture is a decreasing linear function of n.

Let us now consider large grains (with a void ratio G) to which we add some small grains of volume f. The small grains lodge themselves in the voids between the large grains and the void volume decreases. It becomes equal to $gG - f$. The void ratio of the mixture is:

$$e = \frac{gG\text{-f}}{f+g} = \frac{gG\text{-f}+\text{g-g}}{f+g} = n(G+1)\text{-}1$$

By adding increasing numbers of small grains to the large grains, the void ratio decreases linearly with the volume fraction of large n grains. The two ratios shown above are plotted graphically in Figure 4.10. The two right lines intercept at the point corresponding to proportion n of the most compact mixture. These laws of variation are theoretical laws in which various phenomena are neglected. (We shall revert to this later on.)

However, they show that, for a couple of given sizes, the voids ratio (and therefore the porosity) shows a minimum value for a given volume fraction n. The more different the grain size (the smaller $\frac{\varphi_{\min}}{\varphi_{\max}}$), the smaller the voids ratio. This result shows that in order to obtain a compact mixture, it is necessary that the difference in sizes between the small and large grains must be large and we must choose adequate proportions.

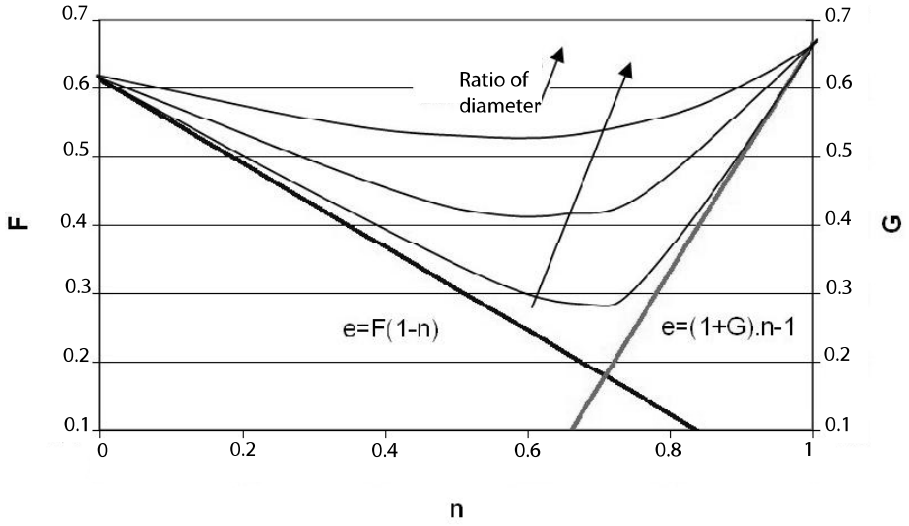

Figure 4.10. *Variation of the voids ratio of a binary mixture of one-dimensional grains in relation to the volume fraction of large grains for different values between the size of grains in two aggregates. G is the void ratio of large grains only and F that of small grains*

4.5.2. *Theoretical analysis of the variation of compactness with volume fractions of grains of different sizes [LAR 99]*

Initially, we will resume with the previous calculations by working with compactness. We are interested in the mixture of two one-dimensional granular classes of diameter d_i (as defined by sieves) and compactness c_i. We note ϕ_i the partial volume of class i in a unit volume. Compactness C of the packing is therefore equal to $C = \phi_1 + \phi_2$. We will finally note y_i, which is the volume proportion of class i: $y_i = \phi_i /(\phi_1 + \phi_2)$.

4.5.2.1. *In the case of large dominants: packing of large grains is not disturbed by the small grains*

We can express the compactness of mixture C_{m1} according to the proper compactness[2] C_1 of large grains and the proportion of small grains y_2:

$$C_{m1} = \phi_1 + \phi_2 = C_1 + y_2 (\phi_1 + \phi_2) = C_1 + y_2 C_{m1}$$

2 Compactness measured on grains of a single class.

whereby:

$$C_{m1} = C_1/(1 - y_2)$$

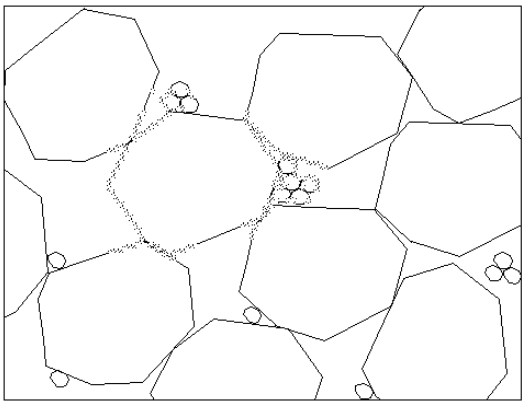

Figure 4.11. *Packing in the case of large dominants*

4.5.2.2. *In the case of small dominants: packing of small grains is not disturbed by the large grains*

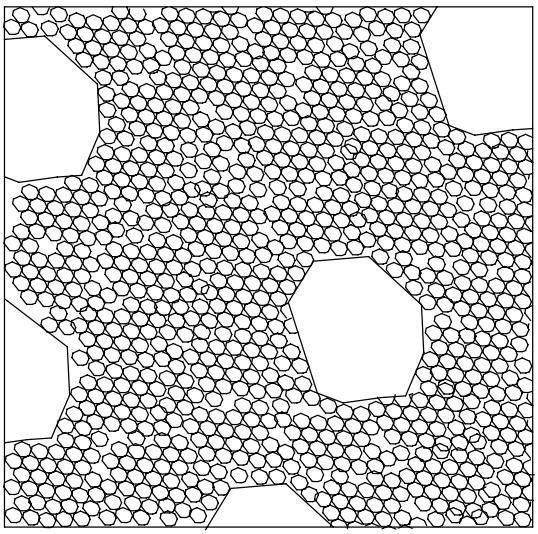

Figure 4.12. *Packing in the case of small dominants*

We can express the compactness of mixture C_{m2} according to the proper compactness C_2 of small grains and the proportion of small grains y_1:

$$C_{m2} = \phi_1 + \phi_2 = \phi_1 + C_2 (1 - \phi_1)$$

$$= C_2 + (1 - C_2)\ \phi_1$$

$$= C_2 + (1 - C_2)\ y_1\ C_{m2}$$

whereby:

$$C_{m2} = C_2 / (1 - (1 - C_2) y_1)$$

In this general case, we shall take $C_m = \inf(C_{m1}, C_{m2})$.

APPLICATION 4.1.– We will study the mixture of round Loire aggregate, screened to obtain two classes of unimodal characteristics in Table 4.2 (data taken from [LAR 99]).

	d_i (mm)	Compactness c_i
R8	8	0.628
R1	1	0.609

Table 4.2. *Size and compactness of aggregate classes*

Figure 4.13 allows us to compare the experimental compactness and that obtained using the linear model for the mixture R8R1. We note that if, qualitatively, variations are correct, the compactness tends to be overestimated. This comes from the interaction effects, which have been neglected in this first approach.

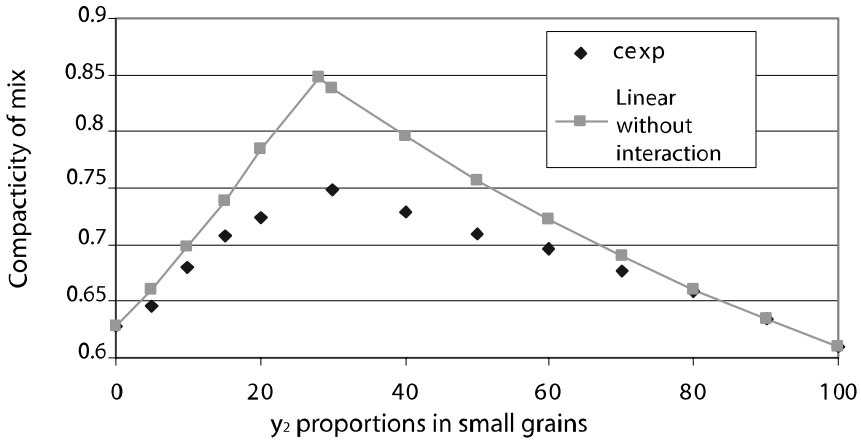

Figure 4.13. *Comparison between the experimental compactness (cexp) of the mixture and the linear model in relation to the proportion of small grains*

4.5.2.3. *Generalization of the linear model without interception*

We now consider a mixture of n grain class, such as $d_1 >> d_2 \ldots >> d_n$, with $n > 2$. Let us suppose that grain i is dominant. We then have:

$$\phi_i = C_i . (1 - \phi_1 - \phi_2 \ldots - \phi_{i-1}),$$

whereby:

$$C_{mi} = \sum_{j=1}^{n} \Phi_j$$

$$= (1 - C_i)(\phi_1 + \ldots + \phi_{i-1}) + C_i + \phi_{i+1} + \ldots + \phi_n$$

$$= C_i + C_{mi} \left[(1 - Ci) \sum_{j=1}^{i-1} yj + \sum_{j=i+1}^{n} yj \right]$$

whereby:

$$C_{mi} = \frac{Ci}{\left[1-(1-Ci)\sum_{j=1}^{i-1} yj + \sum_{j=i+1}^{n} yj\right]}$$

As previously, we finally have $Cm = \inf_{1 \le i \le n} Cmi$. Application to the case of n=3, i = 2 dominant class and $d_1 \geq d_2 \geq d_3$:

$$\phi_2 = C_2.\ (1 - \phi_1)$$

$$C_{m2} = \sum_{j=1}^{n=3} \varphi_j = \phi_1 + \phi_2 + \phi_3 = \phi_1 + C_2.\ (1 - \phi_1) + \phi_3$$

$$= C_2 + \phi_1 (1 - C_2) + \phi_3$$

$$= C_2 + y_1 C_{m2} (1 - C_2) + y_3\ C_{m2}$$

That is:

$$C_{m2}\ (1\text{-}(1 - C_2)\ y_1 + y_3) = C_2$$

whereby:

$$C_{m2} = \frac{C2}{\left(1-((1-C2)y1+y3)\right)}$$

4.5.3. *Model with interaction*

The hypotheses in the previous section are not actually valid. There are, in fact, interactions between grains.

4.5.3.1. *In the case of a small dominant*

The demonstration of the relation in the case of dominant small grains considers that each large grain added to the mixture brings matter to the

mixture without disrupting the spatial arrangement of the small grains. In fact, the surface of each large grain added to the mixture behaves like a wall around which small grains are unpacked (see Figure 4.14) as they are near the walls of the container. The greater the quantity of large grains and the greater the difference in their sizes from small grains, the greater the wall effect will be and the greater the deviation from theoretical law.

Packing of small grains is therefore locally disturbed by the large grains. This is what we call the wall effect. Assuming again that the effect is linear, we can express the compactness of mixture C_{m2} in relation to the levels of compactness of grains, C_1 and C_2, and in the proportion of large grains y_1. We take [LAR 99]:

$$\varphi_2 = C_2 \cdot \left(1-\varphi_1\right) \cdot \left(1 - \frac{\varphi_1 / C_1}{1-\varphi_1} \cdot b_{1,2} \right)$$

$$C_{m2} = \phi_1 + \phi_2 = \phi_1 + C_2 (1 - \phi_1) (1 - b_{1,2} (\phi_1/C_1)/(1 - \phi_1))$$

$$= C_2 + \phi_1 (1 - C_2 - b_{1,2} C_2/C_1) = C_2 + y_1 C_{m2} (1 - C_2 - b_{1,2} C_2/C_1)$$

whereby:

$$C_{m2} = C_2 /(1 - y_1(1 - C_2 - b_{1,2} C_2/C_1))$$

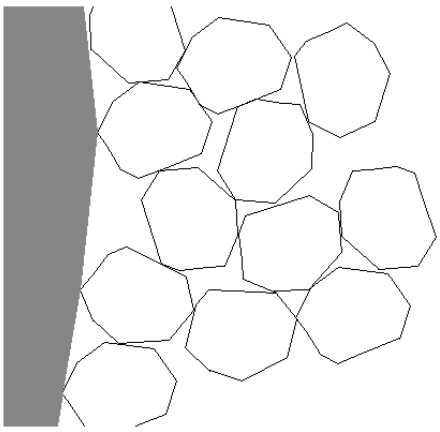

Figure 4.14. *Wall effect*

4.5.3.2. *In the case of a large dominant*

Another deviation is found between the theoretical law established with large grains and the experimental data. This deviation is explained by an effect known as interference or loosening (see Figure 4.15): small grains introduced to the large grains separate the later from their original position. We cannot therefore consider that the compactness of large grains remains unchanged when small grains are added. This separation of large grains from small grains is more important when the size of the small grains and their number increases, which corresponds well with experimental data in Figure 4.10.

Assuming that this effect is in relation to a linear function ϕ_2 on the compactness of large grains, we can express the compactness of mixture C_{m1} according to the respective levels of compactness C_1 and C_2 of grains and the proportion of small grains y_2.

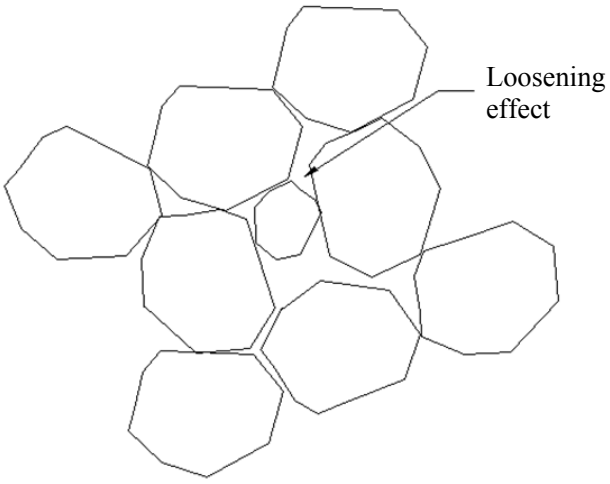

Figure 4.15. *The loosening effect of small grains on large grains*

We will take [LAR 99]:

$$\phi_1 = C_1.(1 - a_{1,2}\ \phi_2/C_2)$$

$$C_{m1} = \phi_1 + \phi_2 = C_1 (1 - a_{1,2}\, \phi_2/C_2) + \phi_2 = C_1 + (1 - a_{1,2}\, \phi_2\, C_1/C_2) + \phi_2 =$$

$$C_1 + (1 - a_{1,2}\, C_1/C_2)\, \phi_2 = C_1 + (1 - a_{1,2}\, C_1/C_2)\, y_2\, C_{m1}$$

whereby:

$$C_{m1} = C_1/(1 - (1 - a_{1,2}\, C_1/C_2)\, y_2)$$

APPLICATION 4.2.– we apply this model to the same aggregates as above. Figure 4.16 shows the comparison with experimental results. Taking into account the fact that interactions can approach the real compactness of mixtures, the compactness level is still overestimated.

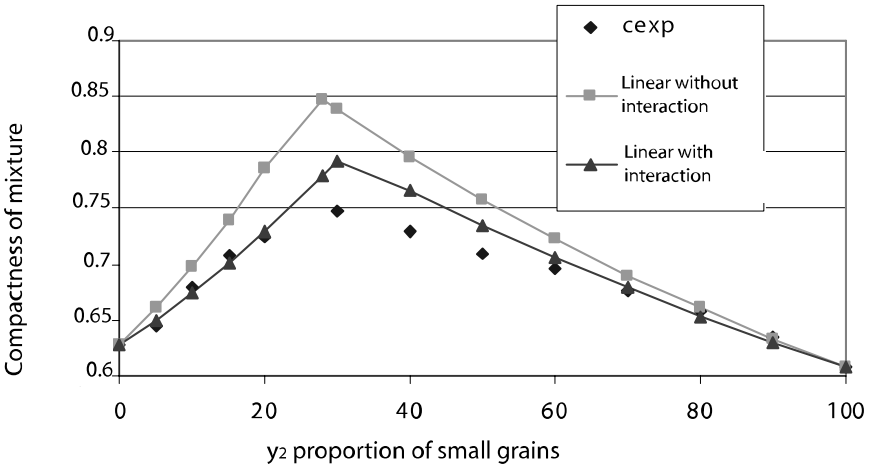

Figure 4.16. *Comparison between the experimental compactness (cexp) of mixture and linear models with and without interaction – Data: $a_{1,2} = 0.3$ and $b_{2,1} = 0.05$ (values calibrated based on experimental results [LAR 99])*

4.5.4. *Consideration of the vibration, compressible packing model [LAR 99]*

Let us introduce *K,* a scalar measurement representative of the energy of compactness and which we call the compaction index. We assume that this index is expressed in the following way:

$$K = \sum_i \frac{\varphi_i}{\varphi_i^* - \varphi_i} = \sum_i Ki$$

with ϕ_i^* being the maximum volume content of class i given the presence of other classes.

To start with, we study the case of one-dimensional grains ($i = 1$). For $i = 1$, $\phi_i^* = C_1$ and $K = \phi_1/(C_1 - \phi_1) = 1/(C_1/\phi_1 - 1)$.

We then see that if ϕ_1 reaches C_1 (here 0.74), K reaches infinity so in order to reach theoretical compactness it is necessary to provide aggregates with infinite energy.

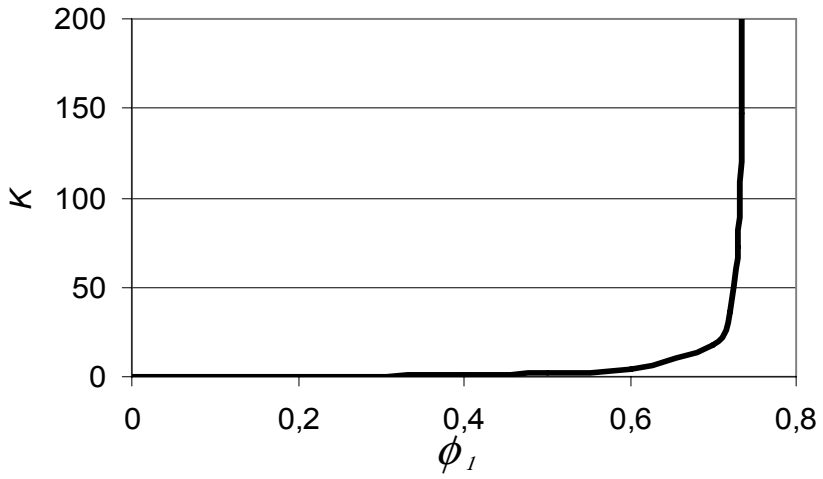

Figure 4.17. *Evolution of the compaction index with compactness*

We can calculate K for packing produced by a simple pouring with vibration. For spheres $C_1 = 0.74$ (in the case of maximum packing):

– pouring $\phi_1 = 0.58$, whereby $K = 3.6$; and

– vibration $\phi_1 = 0.64$, whereby $K = 6.4$.

We now study the case where $i = n$. Noting that the maximum volume content of a class is reached when it is dominant, ϕ_i^* according to its virtual

compactness c_i, volume content ϕ_j ($j \neq i$) and interaction coefficients $a_{i,j}$ and $b_{i,j}$, is:

$$\phi_i = \phi_i^* = Ci\left[1 - \sum_{j=1}^{i-1}(1+\frac{bij}{Cj}\varphi_j) - \sum_{j=i+1}^{n}\frac{aij}{Cj}\varphi_j\right]$$

wall effect loosening effect

$$= Ci\left[1 - \sum_{j=1}^{i-1}(1+\frac{bij}{Cj}yjCm) - \sum_{j=i+1}^{n}\frac{aij}{Cj}yjCm\right] =$$

$$CiCm\left[\frac{1}{Cm} - \sum_{j=1}^{i-1}(1+\frac{bij}{Cj})yj - \sum_{j=i+1}^{n}\frac{aij}{Cj}yj\right]$$

for the dominant class.

As $\phi_i = y_i\, C_m$, we have:

$$\phi_i^* - \phi_i = CiCm\left[\frac{1}{Cm} - \frac{yi}{Ci} - \sum_{j=1}^{i-1}(1+\frac{bij}{Cj})yj - \sum_{j=i+1}^{n}\frac{aij}{Cj}yj\right]$$

and:

$$K_i = \phi_i/(\phi_i^* - \phi_i) = \frac{yi\,/\,Ci}{\frac{1}{Cm} - \frac{yi}{Ci} - \sum_{j=1}^{i-1}(1+\frac{bij}{Cj})yj - \sum_{j=i+1}^{n}\frac{aij}{Cj}yj}$$

As:

$$y_i/C_i = \frac{1}{Ci}\left[1 - \sum_{j=1}^{i-1}yj - \sum_{j=i+1}^{n}yj\right]$$

whereby:

$$K_i = \frac{y_i / C_i}{\frac{1}{Cm} - \frac{1}{Cmi}}$$

4.5.4.1. *Application in mixture R8R1*

The previous relation can be developed in the case where $n = 2$:

$$K = \frac{y_1 / C_1}{\frac{1}{Cm} - \frac{1}{Cm1}} + \frac{y_2 / C_2}{\frac{1}{Cm} - \frac{1}{Cm2}}$$

or by developing:

$$C_m^2 (K + (1 - y_2) C_{m1}/C_1 + y_2 C_{m2}/C_2) + C_m (-K (C_{m1} + C_{m2}) - (1 - y_2) C_{m1} C_{m2}/C_1 - y_2 C_{m2} C_{m1}/C_2) + K C_{m1} C_{m2} = 0$$

Considering that aggregates R1 and R8 are made by vibration, we estimate the virtual compactness, c_1 and c_2, from the experimental compactness R8R1 when $y_2 = 1$ and $y_2 = 0$ and coefficient K is previously calculated for the case of a vibrated packing.

$$K = 6.4 = 1/(C_2/\phi_2 - 1) \text{ and } \phi_2 = 0.609$$

whereby:

$$C_2 = 0.704$$

For R8, $C_1 = 0.726$. This time we note that the estimated compactness is close to that measured.

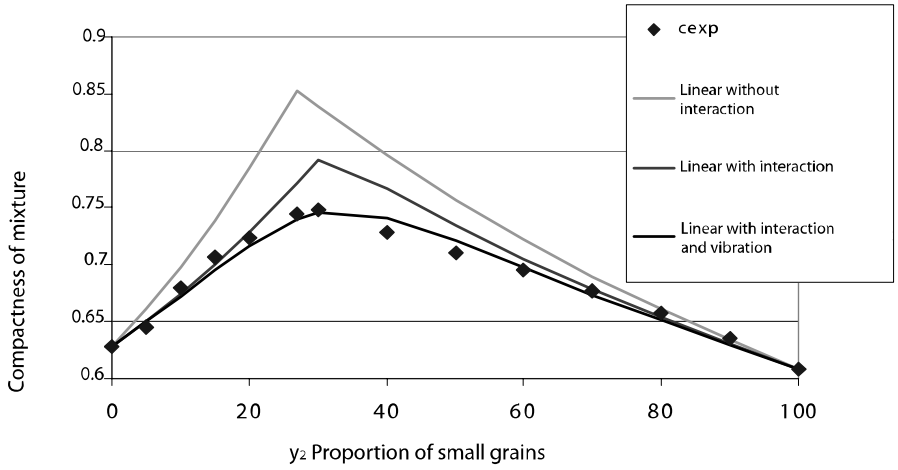

Figure 4.18. *Comparison between experimental compactness (cexp) of the mixture, linear models with and without interaction and compressible packing model*
Data: $a_{1,2} = 0.3$ *and* $b_{2,1} = 0.05$

4.5.5. *Mixture of three one-dimensional aggregates*

This section demonstrates the experimental works produced by Féret. The diagram in Figure 4.19 corresponds to mixtures of three aggregates in varying proportions:

– a sand whose grains are smaller than 500 μm;

– a medium sand whose grains are between 500 μm and 2 mm; and

– a large sand whose grains are between 2 and 5 mm.

The compactness of each mixture is measured and the triangular diagram shown thereafter shows lines of isocompactness.

Maximum compactness (63.8%) is obtained for a mixture containing 38% small grains and 62% large grains. We can notice that the optimum mixture is less "sharp" – the variation of the compactness near this optimum is low. Other experimental data provide an optimum consisting of a small proportion of medium grains.

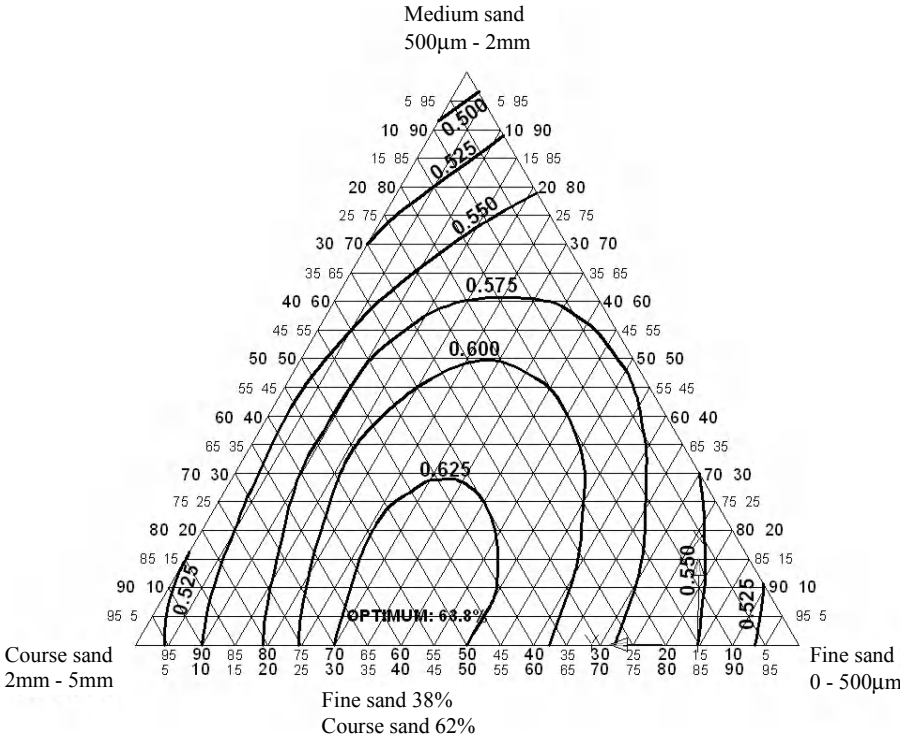

Figure 4.19. *Lines of isocompactness plotted on the triangular diagram of mixtures of three families of grains, based on Feret's works*

In terms of modeling, we can generalize the linear model with interaction where $n = 3$, $d_1 \geq d_2 \geq d_3$, and where class 2 is dominant:

$$C_{m2} = \phi_1 + \phi_2 + \phi_3$$

$$= \phi_1 + C_2 (1 - a_{3,2}\, \phi_3/((1 - \phi_1)C_3) - b_{1,2}\, \phi_1/((1 - \phi_1)C_1)) (1 - \phi_1) + \phi_3$$

$$= \phi_1 + C_2 (1 - \phi_1) - a_{3,2}\, \phi_3\, C_2/C_3 - b_{1,2}\, \phi_1\, C_2/C_1 + \phi_3$$

$$= C_2 + \phi_1 (1\text{-}C_2) - a_{3,2}\, \phi_3\, C_2/C_3 - b_{1,2}\, \phi_1\, C_2/C_1 + \phi_3$$

$$= C_2 + y_1 C_{m2} (1\text{-}C_2) - a_{3,2} y_3 C_{m2} C_2/C_3 - b_{1,2} y_1 C_{m2} C_2/C_1 + y_3 C_{m2}$$

$$= C_{2\,+} C_{m2} (1 - C_2 (1 + b_{1,2} C_2/C_1) y_1 + C_{m2} (1 - a_{3,2} C_2/C_3) y_3$$

whereby:

$$C_{m2} = C_2/(1 - (1 - C_2 (1 + b_{1,2} C_2/C_1) y_1 + C_{m2} (1 - a_{3,2} C_2/C_3) y_3)$$

4.5.5.1. *Mixtures of elementary aggregates: Caquot's results*

Minimum porosity can be determined by mixing elementary aggregates and optimizing the proportions of each. Caquot showed that the minimum porosity value, p_{min}, of such a mixture only depends on the size of larger grains, D, and the size of smaller grains, d, according to the relation:

$$p_{\min} = p_0 \sqrt[5]{\frac{d}{D}}$$

where p_0 is a constant without size.

To reduce the porosity of a mixture, it is necessary to increase the granular scope (d, D). Once d and D are determined, the amount of each aggregate must be optimized to obtain this minimum porosity. In the practice of producing concrete, this optimization is reached by adopting a reference curve for the mixture of grains.

In classic concrete, the smaller particles are cement grains. In the presence of water, these grains tend to form clusters (flocs), which increase the minimum porosity. To reduce it we must separate the cement grains, and even add smaller particles that could lodge themselves in the voids left in the assembly of cement plus sand plus gravel.

Granular arrangements studied consist of dry grains. The forces acting on the grains that allow them to find their place in the assembly are their own weight.

The results obtained could be different from those shown when the grains are very small as the mineral surfaces are electrically charged (often with negative charges) and the electrostatic repulsions may become predominant

and separate the grains from the positions they were in due to the effect of their own weight. For example, cement whose grain sizes are between 1 and 100 μm has a bulk porosity in the order of 66%. Silica fume, whose grains are even smaller (in the order of 0.2 μm), has a bulk porosity that can be as high as 98%! We can imagine that with such porosity grains no longer touch each other and, in particular for transport, we can understand the interest in densified silica fumes.

Finally, Caquot's law predicts that if *d/D* reaches 0, porosity reaches 0. This is only true in theory. De Larrard showed with the compressible packing model that when the number of granular classes increases, if the virtual porosity reaches 0 the mixture's porosity reaches a non-zero value (for a given value of *K*).

Exercise 4.3 shows an example of the application of the Caquot's formula in the mix design of concrete.

4.5.5.2. *Influence of water on the porosity of granular mixtures*

Aggregates often contain water, which is the origin of repulsive forces between capillary grains[3] resulting in an increase in the apparent volume of the aggregate. This is the expansion effect shown in Figure 4.20.

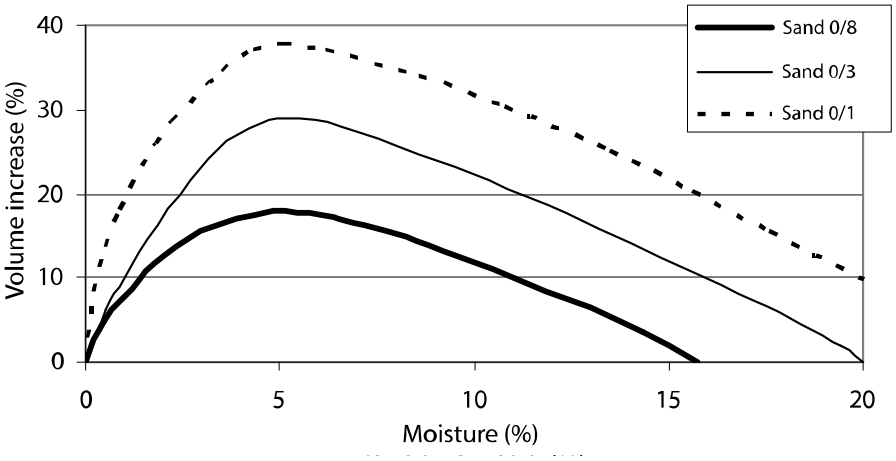

Figure 4.20. *Influence of moisture content and the size of grains on the expansion of sand (volume increase in relation to dry sand)*

3 See capillary forces in Chapter 5.

Expansion is more important when the grains are small. It is at a maximum for moisture content close to 5%. For higher moisture contents, it vanishes: water fills the intergranular voids and there are no longer capillary forces.

When grains are in water, other interactions can be produced between grains:

– *Repulsion forces due to adsorbed layers of water (disjoining pressure)*: in Chapter 3, we discussed the adsorption phenomenon. In water we can consider that five layers of water are fixed on the surface of grains and that their binding energy is even stronger when we consider the layers near the surface. To bring two grains close together, the water must be expelled from its binding sites and one should exert a greater force when the distance between grains is decreasing. If we think in terms of pressure, it is said to have overcome the disjoining pressure. Layers of water adsorbed oppose the reconciliation of grains.

– *Forces of electrostatic repulsion*: near the grain surfaces, electrically charged ions contained in the water are redistributed. According to Gouy-Chapman model, a double electric layer is formed (see Figure 4.21) based on a non-uniform distribution of the co-ions and counter ions for some distance, known as the Debye length. With certain assumptions (namely if the surface is flat and uniformly charged), the electrical potential exponentially decreases in a liquid according to a relation of type $\Psi_x - \Psi_\infty = (\Psi_0 - \Psi_\infty)e^{-\kappa x}$ – where $\frac{1}{\kappa}$ is the Debye length[4], which depends on the ionic force of the liquid, i.e. the nature and quantity of ions dissolved in water. If we consider two negatively-charged grains facing each other, each is surrounded by a double layer as shown in Figure 4.21. When the distance between the grains decreases, a repulsive electrostatic force resists the reconciliation when the double layers overlap.

– Van der Waals attractive forces.

Each of these interactions has decreasing intensity with increasing distance between grains. When we sum up the results in energy terms, two situations may arise. In the first, the energy in the system consisting of two

4 For common salt solutions, the Debye length is in the order of 1 to several tens of nanometers.

grains is decreasingly positive regardless of the distance separating the two grains (case 1, see Figure 4.22). In this case, the grains tend to move away from each other. This is known as a dispersed suspension.

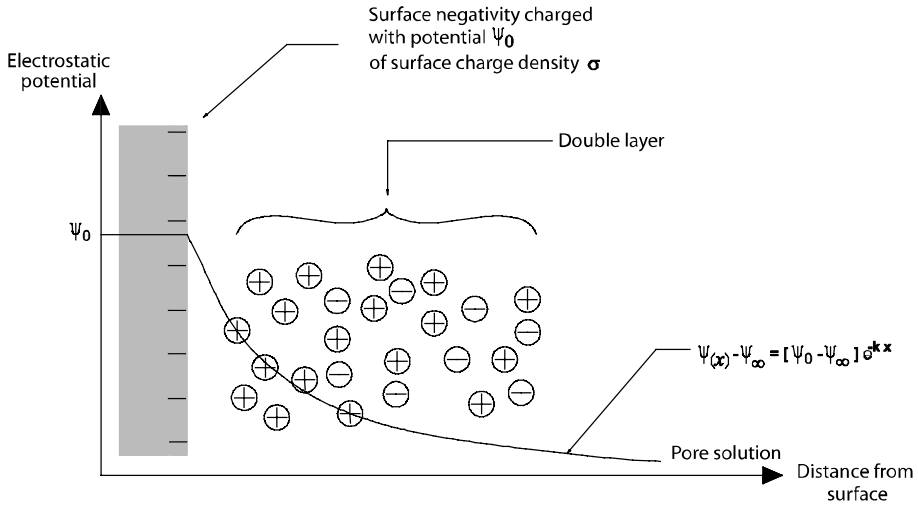

Figure 4.21. *Double electric layer formed in water close to the surface of a negatively charged solid*

In the second case (case 2, Figure 4.22), the energy of the system passes from a minimum value E_0, for a particular x_0 in between the spacing of the grains. At this minimum energy, the equilibrium position of the system is found. If we consider a set of grains in water with interactions that meet the second situation, the grains organize themselves in relation to each other and tend to form clusters (or flocs). It is said that the suspension is flocculated. Note that to distort the suspension (i.e. to move the grains against each other) we must provide energy greater than E_0, which we sometimes call the cohesive energy or binding energy. Cement grains in water (cement paste) behave this way. Strain energy can be introduced by vibration. From the rheological point of view, it is reflected in the yield stress.

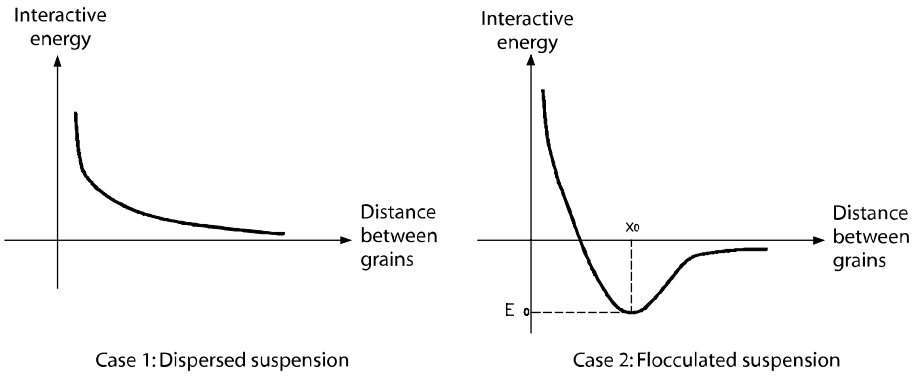

Figure 4.22. *Results of attractive and repulsive energy for two grains in water*

The type of suspension depends on the interactions between grains. For a flocculated suspension, E_0 also depends on the interactions. In modern concrete, the cement is in a flocculated state. To deflocculate grains, additives are used (plasticizer or superplasticizer). These are polymers made from hydrophilic macromolecular chains, which therefore tend to be deployed in the water. The ends of the chains are hydrophobic and bind to the grain surface. The presence of polymers between the grains creates osmotic water pressure, which separates the grains. The effects of the electrostatic charges and the effect of the steric hindrance of the superplasticizer seem to be secondary to this. We shall show the value of this grain deflocculation by applying the Caquot relation.

4.5.5.3. *Value of the deflocculation of cement grains in high and very high performance based concrete*

Let us consider a current concrete. The minimum porosity is given by the Caquot relation:

$$p_{\min} = p_0 \sqrt[5]{\frac{d}{D}}$$

Here D is the size of larger grains. It corresponds to gravel and depends on the geometry of the part to be produced, the coating and the characteristics of the reinforcement. For example, we can fix D at 20 mm.

d is the size of smaller grains. If the cement is flocculated, it is the size of flocs. For example, we can fix a value of 50 μm. The minimum porosity is therefore equal to:

$$p_{\min} = p_0 \sqrt[5]{\frac{50}{2.10^4}} \approx 0.30 p_0$$

If we deflocculate cement grains, we can consider that d is the average size of the cement grains, which is approximately 10 μm. The minimum porosity becomes:

$$p_{\min} = p_0 \sqrt[5]{\frac{10}{2.10^4}} \approx 0.22 p_0$$

We obtain a reduction of 27%.

High-performance concrete decreases the porosity by the effect of deflocculation of cement grains. The decrease in porosity allows us to decrease the water content, whereby the resistance is improved. The deflocculation is also reflected by a reduction in the binding energy E_0. It can be seen on a better workability of concrete.

It is possible to further decrease the porosity of concrete in its fresh state by using ultra small particles (for example silica fumes) to reduce the value of d. With silica fumes, the minimum porosity becomes:

$$p_{\min} = p_0 \sqrt[5]{\frac{0.2}{2.10^4}} \approx 0.11 p_0$$

which is a reduction of 63 % in relation to current concrete!

To effectively obtain this porosity, we must optimize the proportions of each family of grains. This leads to large quantity of silica fumes (in the order of 30–40% of cement by mass). In practice, in order to maintain a high pH level in concrete[5], lower quantities are used (in the order of 10%). We

5 Silica fumes react with lime released by hydrated cement (pozzolanic reaction). This reaction consumes OH^-, which has the effect of lowering the pH. In order to keep the steel reinforcement in a passive state (corrosion stopped), we limit the amount of silica fume to approximately 10% of the amount of cement, which leads to a small variation in pH.

therefore do not obtain porosities that are as low as those predicted by Caquot's law, but the improvements are significant (see Exercise 4.3). High-performance concretes are thus obtained. They contain silica fumes and a deflocculant admixture.

4.6. Bibliography

[LAR 99] DE LARRARD F., *Concrete Mixture Proportioning: A Scientific Approach*, Modern Concrete Technologies Series, N°9, E & FN Spon, London, 1999.

4.7. Exercises

Exercise 4.1.

Let us consider a sphere with a radius, r, tangent to the spheres with a radius, R, of the cubic packing. Give the expression of r according to R. What is your conclusion?

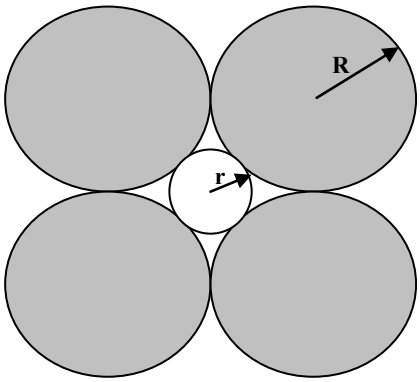

Figure 4.23. *Diagram of cubic packing*

Exercise 4.2.

This exercise shows an experimental method of formulating concrete based on research into the maximum compactness of a granular mixture.

Three granular mixtures are used: cement; crushed sand, S; and a round gravel, G. The grain density is equal to 3.1 g/cm^3 for the cement, 2.75 g/cm^3

for the sand and 2.6 g/cm^3 for the gravel. The bulk density of cement (γ_d) is 1 g/cm^3 and its surface area is equal to 3,425 cm^2/g.

Initially, the minimum porosity of the mixture of sand and gravel is experimentally researched. For this variable, the weight proportions of *S* and *G* are mixed. These mixtures are placed in a container with a volume equal to 10 liters. Table 4.3 shows the masses of each mixture filling the container.

Weight proportion of sand (%)	0	20	40	60	80	100
Mass of mixture in the container (kg)	14.85	16.32	17.89	18.29	17.10	15.08

Table 4.3. *Mass of mixtures filling the container*

1) Calculate the variation of the porosity according to the weight fraction of sand.

2) The bulk porosities of the three materials – sand, gravel and cement are not the same and are different from the theoretical value of the infinite close-packed spheres. Explain the differences.

3) One possible method of making concrete is to choose a volume of cement that is equal to the volume remaining between grains and the most compact granular assembly of sand plus gravel. What would the quantities of cement, sand and gravel be (in kg/m^3)? If the residual porosity was filled with water, what would the theoretical density of the fresh concrete be?

4) We actually measure porosity in the initial state p_o and find it equal to 26%. How do we explain the difference between this and the theoretical value deducted from the previous question, knowing that from the first approximation we can ignore the air in the mixture?

5) The minimum porosity of concrete in its fresh state is given by the following relation:

$$(p)_{\min} = p_0 \sqrt[5]{\frac{d}{D}}$$

where:

– p is the volume fraction of water in fresh concrete;

– d is the average size (expressed in mm) of a set of smaller grains, here the cement;

– D is the size of the larger grains in the aggregate (equally expressed in mm); and

– p_0 is a term that depends on the consistency of fresh concrete.

In a case where smaller grains are perfectly deflocculated, we define d according to the surface area using the following relation:

$$d = \frac{6}{\rho_S S_S}$$

What are the assumptions underlying this equation? Calculate d for the cement considered.

6) In current concrete, cement grains are not deflocculated and porosity is higher than that given in the equation in question 5. The smaller grains are in fact clusters of cement grains or flocs that have a size d_f that is larger than d. To deflocculate grains, we use a superplasticizer admixture.

For a given consistency of fresh concrete, the maximum reduction in porosity obtained by the superplasticizer is 20%. Calculate an order of magnitude d_f of flocs in current concrete.

Exercise 4.3. ***Influence of granular extent on the porosity of fresh concrete***

The porosity of materials is an important characteristic for various properties of use (mechanical, thermic or acoustic, sealing performances, etc.). The problem proposed deals with the porosity of concrete in its fresh state, which mainly determines the porosity of hardened concrete. Among the possible factors, here we show the influence of the granular extent (minimal and maximal grading).

In its fresh state, the porosity of concrete is the sum of the volume dose of water e and the proportional volume of air, v. Porosity ($e + v$) is based on the arrangement of solid grains and, consequently, the distribution of grains in different granular classes.

In his work published in 1953, Faury expresses a relation between the minimum value of porosity of fresh concrete and the size D of larger grains of concrete expressed in mm:

$$(e+v)_{\min} = \frac{K}{\sqrt[5]{D}} \qquad [4.1]$$

Here K is a constant, which depends on the consistency of concrete and the shape of grains in the aggregate. The minimum porosity is obtained by optimizing the proportions of grains in different granular classes. With round aggregates, experimental values of minimum porosity obtained by Faury for fluid concrete are recorded in Table 4.4.

D (mm)	2	4	8	20	60	120
$(e + v)_{min}$	0.36	0.31	0.27	0.23	0.18	0.16

Table 4.4. *Porosity of fresh concrete studied: the influence of D*

Later in this problem we will consider fluid concrete only.

1) Calculate the coefficient K of relation [4.1].

2) In Faury's experiments, the smaller part of grains are cement grains that, in all mixtures studied, were found in the flocculated state; therefore the cement grains were always assembled in clusters, known as flocs. In modern concrete, it is possible to deflocculate cement grains using a superplasticizer and the size of smaller grains, d, becomes a parameter on which it is possible to act. In order to highlight the influence of this parameter, relation [4.1] can be modified according to expression:

$$(e+v)_{\min} = \alpha \sqrt[5]{\frac{d}{D}} \qquad [4.2]$$

where α is a coefficient with no size.

To calculate its value, it is necessary to define *d*. We will adopt the following definition: *d* is the average size of the set of smaller grains. By the smaller set of grains, we denote:

– cement; or

– the assembly of cement and mineral additions of comparable thickness (fly ash, slag, limestone additions); or

– silica fumes.

The average size of the set of smaller grains can be measured conventionally by the relation:

$$d = \frac{6}{\rho S_S} \qquad [4.3]$$

where ρ is the density of the grain and S_s the specific surface of unit mass of the set of smaller grains considered.

What are the assumptions that allow us to establish equation [4.3]?

In practice, the specific surface S_s can be determined by the Blaine method for cement and mineral additions of comparable thickness and by the BET method for silica fumes.

3) Equation [4.2] can be applied in the cases of concrete implemented by Faury. In this case, *d* is the size of flocs of the cement grains whose value we are going to estimate. We consider that the cement has a specific surface equal to 3,175 cm^2/g and a density equal to 3,150 g/cm^3. With a high water-reducer plasticizer, it is possible to decrease the amount of water necessary to obtain the same consistency by 20%. If we consider that, with this admixture, cement grains are completely deflocculated, calculate the value of coefficient α, assuming that the reduction of the amount of water used is due exclusively to the increase in the granular extent.

4) What is the size of flocs of cement in fresh concrete without the admixture implemented by Faury with the cement in question 3?

5) Let us consider the case of concrete with silica fumes in which the amount of superplasticizer will be sufficient to deflocculate all grains and where the quantity of all components is optimized with a view to decreasing

the porosity of its fresh state by as much as possible. For silica fumes of a specific surface area equal to 15 m^2/g and a density of 2.65 g/cm^3, determine the minimum porosity of fresh concrete in the case where D is equal to 20 mm.

6) The quantity of silica fume necessary to optimize the granular distribution is in the order of 20–30% of the mass of cement. In practice, the quantities used are much lower, for reasons of cost. They are limited to approximately 10% of the mass of cement. In these conditions the porosity of fresh concrete is higher than the value calculated in question 5. If f is the volume dose of silica fumes, we can estimate a minimum porosity of fresh concrete by the relation:

$$(e+v)_{\min} + f = \alpha \sqrt[5]{\frac{d}{D}} \qquad [4.4]$$

where d is the average size of cement grains. Explain equation [4.4].

7) Let us consider fresh concrete prepared with the cement in question 3 and gravel whose D value is 20 mm. The cement content is given by the relation:

$$c_{(kg/m^3)} = \frac{700}{\sqrt[5]{D_{(mm)}}} \qquad [4.5]$$

and the silica fume content is 10% of the mass of the cement. Calculate the minimum porosity of fresh concrete.

8) The influence of the superplasticizer content and the addition of silica fumes has been studied with micro-concrete (D smaller than 10 mm) so as to limit the volumes of materials required. Figure 4.24 shows the variation in the porosity of fresh micro-concrete of a fluid consistency made with variable superplasticizer contents. Curve 1 is relative to a micro-concrete prepared with the cement discussed in question 3. Curve 2 has been obtained with the same cement to which silica fumes of 10% mass have been added. For the micro-concrete prepared without silica fumes, we observe that beyond a certain amount of superplasticizer porosity no longer decreases (it is said that we reach the saturation point). All grains therefore deflocculate.

Evaluate the maximum size, *D*, of the micro-concrete grains. Explain the differences between curves 1 and 2.

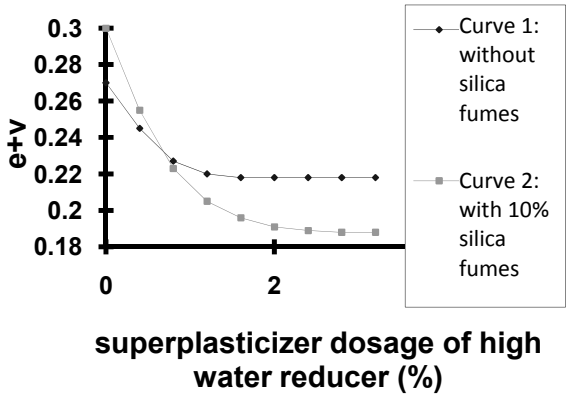

Figure 4.24. *Influence of superplasticizer on the porosity of micro-concrete of a given consistency*

Chapter 5

Voids in Concrete

5.1. Definitions

Concrete is a consolidated porous material, but what we will examine in this chapter concerns multiple natural (soil, wood, rock) and artificial (tile, brick) porous materials used in civil engineering. Pores are cavities that can manifest in very different forms. For example, cracks can be considered specific pores in which the elongation is much greater than the transverse dimension (opening).

The geometric characteristics of a porous solid make up what we call its texture. The volume of pores, their dimensions, and their spatial layout are characteristics of the porous structure. The description of a porous solid's microstructure contains information both about its porous structure and data regarding the composition and layout of its solid phases. In material science, the word "structure", when used alone, refers to the spatial organization of the atoms or molecules of a solid.

Many usage properties of porous materials depend on their porous structure (the volume and spatial layout of voids are of great importance). This is the case, for example, with mechanical performance; heat resistance; soundproofing; and air- and watertightness. Later on in this book we will show that the transfer of fluids in concrete depends not only on the volume of the voids in this material, but also on their interconnection or dimensions.

Physical Properties of Concrete and Concrete Constituents Jean-Pierre Ollivier, Jean-Michel Torrenti and Myriam Carcassès

All of these characteristics must be defined and measured, which is the principal objective of this chapter.

Let us consider a porous solid shown in cross-section in Figure 5.1.

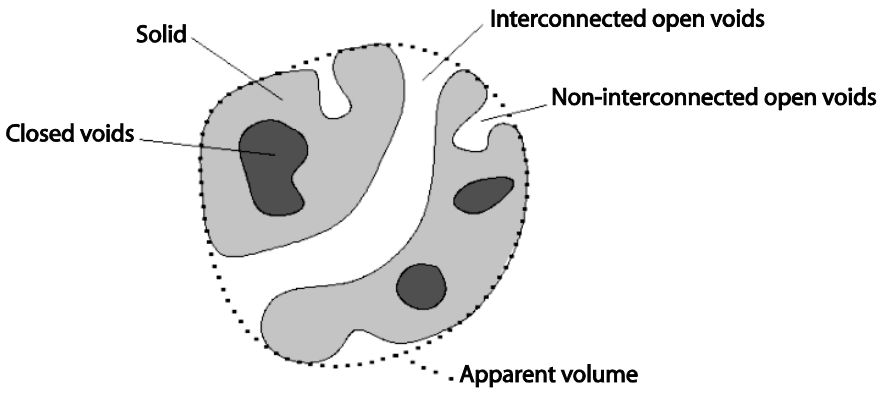

Figure 5.1. *Schematic representation of a porous solid*

We define the following volumes:

– V_a, the apparent volume contained in the material envelope;

– v_s, the volume of the solid part of the material;

– v, the volume of the pores (or voids);

– v_o, the volume of "open" pores (or voids); i.e. the pores connected to the outside;

– $v_{o,i}$, the volume of interconnected open pores (or voids) through which a fluid can travel throughout the material;

– $v_{o,ni}$, the volume of non-interconnected open pores (or voids). The term "obstructed" pores is also used;

– v_f, the volume of closed pores (or voids) that are not connected to the outside.

We can express the following relationships[1]:

$$\begin{aligned} V_a &= v_s + v \\ v &= v_o + v_f \\ v_o &= v_{o,i} + v_{o,ni} \end{aligned} \qquad [5.1]$$

Note that the cross-sectional view of the material does not give an objective perspective of the spatial organization of voids. Thus, voids that appear to be closed in the cross-sectional view can actually be open, because they are connected to the exterior at a point outside the cross-section. For the purposes of the following, we will consider that the cross-section view is representative of the structure in three dimensions.

We define porosities by relating the volumes of voids to the apparent volume:

– interconnected open porosity:

$$p_{o,i} = \frac{v_{o,i}}{V_a} \qquad [5.2]$$

– non-interconnected open porosity:

$$p_{o,ni} = \frac{v_{o,ni}}{V_a} a \qquad [5.3]$$

– open porosity:

$$p_o = \frac{v_o}{V_a} = p_{o,i} + p_{o,ni} \qquad [5.4]$$

– closed porosity:

$$p_f = \frac{v_f}{V_a} \qquad [5.5]$$

– total porosity:

$$p = \frac{v}{V_a} = p_o + p_f \qquad [5.6]$$

1 These notations and definitions are different from the ones given in Chapter 1, which have to do with granular materials made up of grains and intergranular spaces, with the grains being porous solids as defined in this chapter.

The open pores in materials contain air (and possibly water vapor) and/or water. As for the granular materials studied in Chapter 1, the quantity of water contained in a porous material can be characterized by two quantities: the degree of saturation and the water content (see Figure 5.2).

The degree of saturation, s, is the ratio between the volume of water, v_e, and the volume of open voids, v_o. It varies between 0 (dry material) and 1 (saturated material):

$$s = \frac{v_e}{v_o} \qquad [5.7]$$

Water content w is the relationship between the water mass, m_e, contained in the material and its dry mass[2], m_s:

$$w = \frac{m_e}{m_s} \qquad [5.8]$$

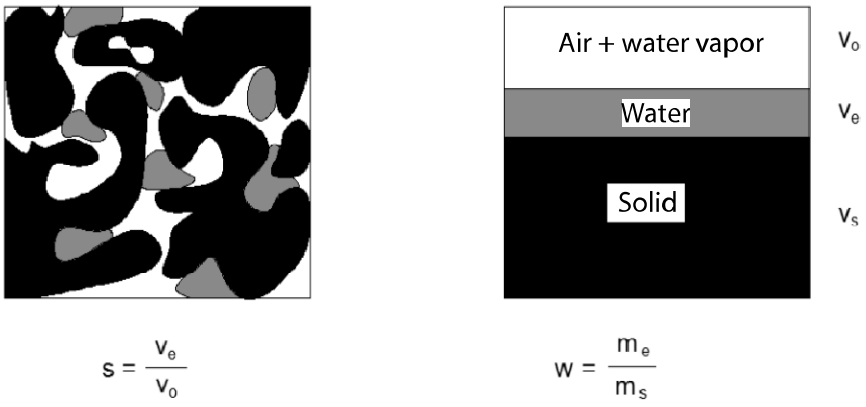

Figure 5.2. *Definitions of the degree of saturation and water content*

2 m_s is also the mass of the solid.

Two densities are also defined:

– The density of the solid:

$$\rho_S = \frac{m_S}{v_S} \qquad [5.9]$$

– The dry apparent density[3]:

$$\rho_a = \frac{m_S}{V_a} \qquad [5.10]$$

5.2. Characterization of heterogeneous materials

Porous materials are made up of a minimum of two phases: a solid phase, and voids. The solid phase is not always homogeneous.

Consider, for example, the case of hardened concrete. This is a mixture of aggregates (sand and gravel) and a paste of porous cement. The cement paste is not homogeneous either (see Figure 5.3); it is made up of anhydrous cement, different hydrates and porous spaces. We can describe the texture of the concrete using macroscopic quantities, such as porosity or specific surface area. These two characteristics mainly depend on the hardened cement paste, but it is a matter of relative quantities. The first characteristic, porosity, is the volume of voids (for most of the paste) related to the (apparent) volume of the concrete. The second characteristic is the external surface of the solid (for most hydrates) related to the mass of the concrete. In order to measure these quantities, we must take a sample of the concrete used in the construction, and it is important that this contain the same proportion of aggregate and paste as in the material being analyzed; i.e. the sample must be representative.

3 In Chapter 1, we also define a dry apparent density. For granular material, the apparent volume is that of the grains and the intergranular spaces. To avoid confusion, we will use the notation ρ_a here for this density.

Figure 5.3. *Microstructure of a hydrated cement paste (photograph courtesy of H. Hornain)*

Let us look at the measurement of porosity. To experimentally determine the representative volume, we can take samples of increasing volume, measure the porosity of each of these, and expect that the value obtained will not vary with the size measuring uncertainty being taken into account. As a general rule, we consider that the size of the measurement sample must be at least equal to five times the size of the largest defect in the material (here, five times the size of the largest aggregate).

To properly characterize a material using a macroscopic quantity, we must also understand its spatial distribution. For example, if we measure the porosity of concrete using a representative sample taken from the foot or the upper part of a column, it is possible that the values will be different due to the effects of settling. Another example of spatial variation in the properties of concrete is shown in Figure 5.4. Depending on the distance from the formwork, the proportions of cement paste and aggregate will vary; this is the wall effect, which was discussed in Chapter 2. The volume fraction of aggregate grains in concrete is heterogeneous in character. If we compare the porosity of the concrete near the formwork to the porosity at its heart, we will find higher values near the formwork, since there is more paste there

than at the heart. The wall effect is manifested here by a more porous "skin zone".

Now, considering the hardened cement paste in concrete on another scale, we can distinguish a more porous area surrounding the aggregates – the interfacial transition zone. The thickness of this zone is in the order of a few dozen microns. This is another level of heterogeneity.

To differentiate the porosity of these two zones (the skin zone and the interfacial transition zone), we must take measurements using adapted methods, applying them to representative samples from the concrete. Thus, a macroscopic quantity can have several values according to the region where it is measured. If we take a single measurement of a sample enveloping the two zones, the result is an average of the two porosities, weighted by their volume proportion.

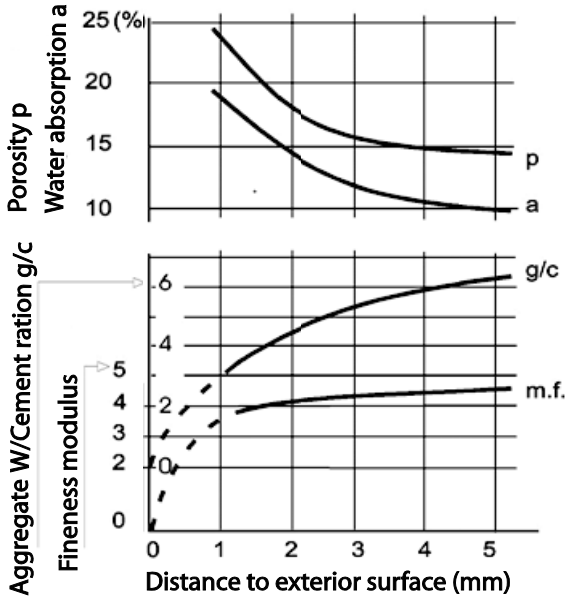

Figure 5.4. *Variation of the characteristics*[4] *of concrete in the area next to the side wall, according to [KRE 84]*

4 m.f. is the fineness modulus of the granular phase of concrete present at a given distance from the external surface.

The paste, as we have just noted, is a porous phase in which the voids are interconnected. The solid phase is not homogeneous; we can distinguish various hydrates and possibly non-hydrated grains of cement within it. Characterizing the volume proportions of components in the solid phase and/or their spatial localization in relation to the grains of aggregate, for example, can be one objective of material characterization. Likewise, pores are not all the same size. The larger ones are vestiges of spaces that contained mixing water in the fresh state; these are called capillary pores. Their dimension is greater than one hundredth of a nanometer. We will see in Chapters 6 and 7 that they play a particularly important role in the transfer properties of concrete. The smaller ones are pores contained in the hydration products. They are smaller than a few dozen nanometers. Pore size is another element in the texture of concrete. Cracks are other components of the microstructure. The voids that they make up can be accounted for in a measurement of porosity. The characterization of cracks can be an objective in itself. We may, for example, want to understand the effects of a mechanical load or pathology.

The extent of the cracks can be a strong indicator of the intensity of deterioration. Cracks can also present a preferential orientation under the effects of a mechanical load, for example. Knowledge of the orientation of cracks and fibers in fibrous concrete is useful for understanding material behavior. Generally, the anisotropy of a quantity, g, is represented by means of a polar diagram, $g(\theta)$, showing the evolution of the quantity in terms of orientation.

5.3. Specific surface area of porous solids

Specific surface area is defined in Chapter 3. The external surface of a porous solid is the site of exchange with the outside environment. The greater the specific surface area, the more possibilities there are for exchange. For example, an increase in specific surface area encourages the dissolution of a solid in its solvent, the binding of water molecules on the solid in humid air, etc.

The specific surface area of porous solids can be very high. In the case of cement pastes, for example, it is in the order of hundreds of m^2/g! Such values can only be explained by extreme surface roughness and by the presence of a porous structure made up of very fine, interconnected pores.

The concept of the roughness, R, of a surface is simple to grasp, but its definition lends itself to discussion. This is the relationship between the real surface area, S, and the apparent surface area, S_a.

$$R = \frac{S}{S_a}$$

Consider the layout of a material surface to be characterized. Figures 5.5a, 5.5b, and 5.5c contain three possible representations of the apparent surface. Three roughness values result from this. Now, imagine the measurement of the specific surface area of the corresponding material. The BET method, as we have shown, is used to determine the quantity of gas molecules that cover the surface of the solid in a complete monomolecular layer. The size of the molecules is taken into account when calculating the surface. We can consider that Figures 5.5a, 5.5b and 5.5c represent the results of three measurements carried out with molecules of increasing size. The smaller the gas molecules are, the more capable they are of entering ("seeing") small crevices in the solid. It is therefore not surprising to find different values for the specific surface areas of cement pastes when we use different types of gas.

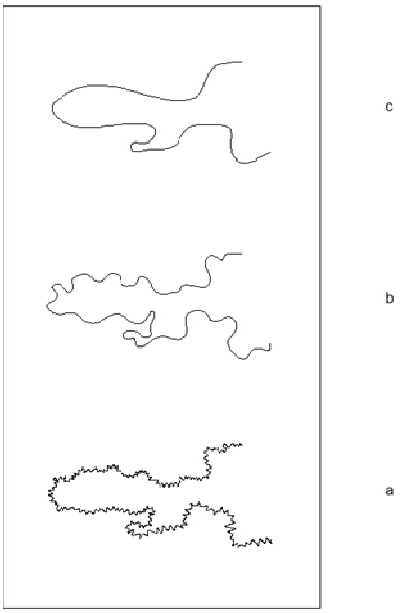

Figure 5.5. *Visible areas of a surface measured with gas molecules of different sizes*

More generally speaking, this analysis poses the issue of the meaning of the surface areas of porous solids. If we consider the surfaces of identical spheres with diameter ø, we can assimilate the area A of this surface into the product of the number of spheres used by the area of the square in which the sphere is inscribed. In the case of a flat surface, the result is independent of the diameter of the sphere. In the case of a surface like the one shown in Figure 5.5, the area calculated varies with the diameter of the spheres used to determine it, as indicated in Figure 5.6. In the domain of linearity of the figure, the area varies with the diameter of the measurement spheres according to the relationship:

$$A = k\Phi^{d-D} \text{ where } d<D. \qquad [5.11]$$

In this relationship, D is the dimension of space in which the measurement is taken (usually 3), and d is the fractal dimension of the object. Objects that present this characteristic are called fractal objects. Their fractal dimension is inferior to the dimension of space in which they are located. This is not the case with a flat surface, for example where $d = D$. These are called Euclidian objects.

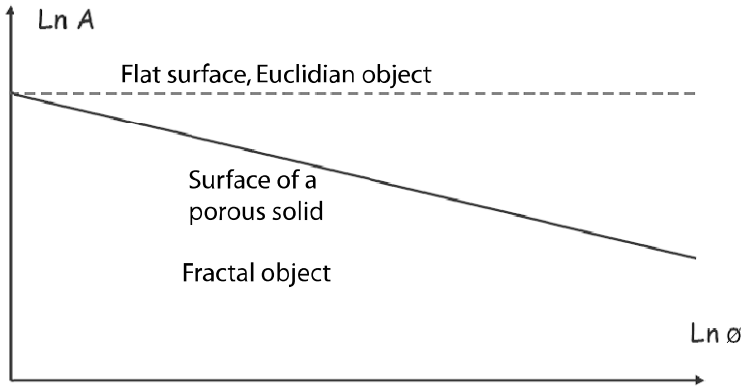

Figure 5.6. *Variation of area A of the external surface of a material with the diameter Φ of spheres used*

If the object has a fractal nature on any scale, the definition of the fractal dimension shows that its area tends toward infinity when the diameter of the

measurement spheres tends toward zero (or if magnification tends toward infinity). In practice, the value of the area tends toward a superior limit, which is that of the real surface.

We see, then, that in order to completely characterize the surface of a fractal solid, we must give the value of this limit, the fractal dimension, and the area value for a given magnification.

5.4. Measurements of the porosity of consolidated materials

5.4.1. *Measurement of total porosity*

5.4.1.1. *Method one: grinding*

We can write:

$$p = \frac{v}{V_a} = \frac{V_a - V_s}{V_a} = 1 - \frac{V_s}{V_a} \qquad [5.12]$$

Porosity may also be written as:

$$p = 1\text{-}\frac{\rho_a}{\rho_s} \qquad [5.13]$$

Porosity can be calculated from the measurement of the density of the solid and the apparent density. The latter is obtained by the hydrostatic weighing of a sample in any form, or by using a sample of simple geometric shape, usually a cylinder taken through core sampling (V_a is calculated from its dimensions). The mass of the solid is obtained by weighing after drying at 105°C until the mass is constant. The volume of the solid, which is necessary for the calculation of the density of the solid, is measured after a thorough grinding of the sample. In general, grinding is continued until 100% is reached when sieving at 80 μm, and we measure the volume of the grains using a pycnometer or a Le Chatelier volumenometer (thus disregarding the volume of residual closed voids in the grains by assimilating the volume of the grains into v_s).

5.4.1.2. *Method two: image analysis*

Images of the material obtained can be analyzed using optical or scanning electron microscopy (SEM). These images are digital images representing cross-sections of the material.

The first step of analysis consists of recognizing and isolating the objects to be quantified from the rest of the image. These may be voids, if we wish to determine the porosity of the material, but we can also seek to isolate the rest of the non-hydrated cement grains in order to quantify a degree of hydration of the cement in the concrete, or cracks in order to analyze a state of material damage. The quality of the result obtained depends greatly on this stage of recognition. To facilitate recognition, it is often useful to act on the material before observing it. For example, we can impregnate it with fluorescent resin and then observe it under ultraviolet light in order to better identify the larger pores and cracks.

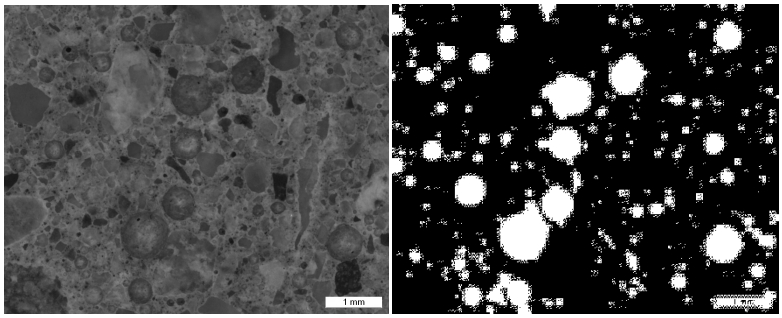

Figure 5.7. *A network of air bubbles trapped in concrete. Left: Original image; Right: binary image, with bubbles extracted*

Once the digital image is obtained, it must be treated so as to isolate the parts that are to be analyzed. For example, if we are measuring porosity, the objective is to obtain a binary image in which the voids on the one hand, and the solids on the other correspond to separate levels of gray. To conduct this operation without introducing a bias, we must use image processing tools designed to improve the quality of the images obtained (eliminate noise). They facilitate the localization of boundaries between the different phases present (filters). We then need to reconstruct a binary image that is as objective as possible (opening, closing, and thresholding tools). All of these complex operations are brought together in high-performance image

processing software. As an example, Figure 5.7 represents concrete containing trapped air, and the binary image obtained via extraction of the network of bubbles.

Once the image of the object to be analyzed is obtained, quantitative data must be assigned to it. The question of the correspondence of the 3D data measured to a 2D image then arises.

Let us look again at the binary image in Figure 5.7 (right). In this image, which is made up of black and white pixels, we can measure areas and lengths. For example, the area of the bubbles can be obtained by multiplying the number of white pixels by the size of the pixel. The distance between two bubbles can be obtained by multiplying the number of pixels separating the white walls by the dimension of the pixel in the direction under consideration.

By integrating the white spots into circles, we can measure their diameter in the same way on the binary image. Is this equal to the diameter of the corresponding bubble? The probability that the answer will be positive is virtually zero, as it would be necessary for the cross-section to pass through the median plane of the sphere. We say that the diameter of circles is not a stereological quantity: the data measured in two dimensions does not correspond to the data on the object[5].

Other quantities, called stereological quantities, allow the change from 2D to 3D. This is the case with surface fractions that, in cases of isotropic distribution, are equal to volume fractions. For example, the surface fraction of the white spots in Figure 5.7 is equal to the porosity of the trapped air bubbles.

Porosity is thus a quantity that can be measured through image analysis. We must, however, still be wary of the representativeness of the images analyzed, and of the choice of magnification. For example, in the images shown in Figure 5.7, taking into account the size of the pores, the magnification is sufficient to estimate the quantity of trapped air, but not to analyze the porosity of the cement paste.

---

5 According to certain theories, it is possible to know the distribution of the diameters of spheres from the distribution of the diameters of circles on the cross-section plan, but the two are not directly related.

5.4.2. *Measurement of open porosity*

Various methods based on different principles allow us to measure the open porosity of materials. The results provided by these methods are sometimes different, and when we state the result of a measurement, it is important that we always specify the method that was used to obtain it.

5.4.2.1. *Water impregnation method: water-accessible porosity*

This method consists of saturating the material with water and then drying it. The difference in mass between the two states is used to calculate the volume of water saturating the material. This volume is integrated into the volume of open voids. In the case of hardened concrete, this method is a standard operating procedure (NF P 18-459):

– Water saturation under vacuum[6] for 48 hours. The object being tested is placed in an airtight container and a vacuum is created in this container until pressure of 24 mbars is obtained. This vacuum is maintained for four hours. The object being tested is then covered with around 20 mm of water for 20 ± 1 hours, at reduced pressure and at 20 ± 2°C.

– The object being tested is weighed while submerged (hydrostatic weighing), and then weighed after being taken out of the container (cleaned of any surface film of water and water droplets on its exterior). M_{water} and M_{air} are the results of the two weighings.

– Drying in a ventilated oven at 105 ± 5°C until a constant mass is reached (between two successive weighings spaced 24 hours apart, with the results differing by no more than 0.05%). M_{dry} is the dry mass obtained.

Open porosity is expressed in per cent and is given by the relationship:

$$p_o(\%) = \frac{M_{air} - M_{dry}}{M_{air} - M_{water}} \cdot 100 \qquad [5.14]$$

5.4.2.2. *Gas pycnometer*

The porous solid, of known apparent volume V_a, is placed in a dry state in one of the compartments of the pycnometer shown in Figure 5.8.

6 This saturation procedure is analyzed in Exercise 5.2 at the end of this chapter.

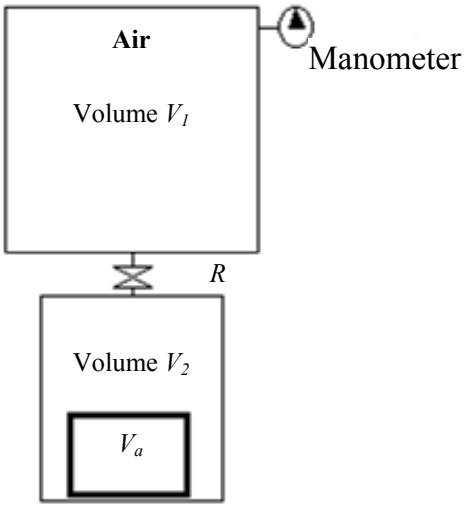

Figure 5.8. *Sketch of the measurement of open porosity using a gas pycnometer*

The volumes V_1 and V_2 of the two compartments (and the connecting channels to the communication valve, R) are known. At the initial time, air at atmospheric pressure P_a fills the upper compartment and the space not taken up by the porous sample being characterized in the lower compartment. The volume of air V in this compartment is equal to $V = V_2 - (V_a - v_o)$.

	State 1		**State 2**	
	Pressure	*Air volume*	*Pressure*	*Air volume*
Upper compartment	P_1	V_1	P_2	V_1
Lower compartment	P_a	$V = V_2 - (V_a - v_o)$	P_2	$V = V_2 - (V_a - v_o)$

Table 5.1. *The two states of the gas in the compartments of the pycnometer*

With the valve R closed, the pressure is adjusted to a value P_1 greater than the atmospheric pressure in the upper compartment. It is measured using the manometer. When the valve is opened, the air expands in the lower compartment and pressure is established in the device at a value P_2, as measured by the manometer. These two states are described in Table 5.1.

Supposing that the expansion is isothermal and that the air can be assimilated into a perfect gas, we can write $P_1V_1 + P_aV = P_2V_1 + P_2V$.

We can also write:

$$V_1(P_1\text{-}P_2) = V(P_2\text{-}P_a) = (V_2\text{-}(V_a - v_0))(P_2\text{-}P_a)$$

or:

$$v_o = V_a\text{-}V_2 + V_1\frac{P_1\text{-}P_2}{P_2\text{-}P_a}$$

and the open porosity can be calculated using the relationship:

$$p_o = \frac{v_o}{V_a} = 1\text{-}\frac{V_2 + V_1\dfrac{P_1\text{-}P_2}{P_2\text{-}P_a}}{V_a} \qquad [5.15]$$

A device based on a principle identical to that of the pycnometer is used on construction sites to measure the air content of fresh concrete. This is a concrete aerometer, the function of which is studied in Exercise 5.1 at the end of this chapter.

5.4.2.3. *Mercury penetration method*

This method consists of measuring the volume of open voids by the penetration of pressurized mercury. It is described in more detail in section 5.5.

5.4.3. *Determination of closed porosity*

Closed porosity is not measured directly. It is calculated using the difference between total porosity and open porosity.

5.5. Porometry

Porometry[7] is the measurement of the dimension of pores. Consider, for example, the microstructure of a hardened cement paste shown in Figure 5.3, which is an image obtained by SEM. In it, we can distinguish solid phases (in light gray levels) that are the hydrates in the cement, and – between these hydrates – porous spaces (the darker gray levels). We can reasonably imagine that the porous space is made up of pores of greater or lesser dimensions. Between the hydrates, we can see pores that are larger than those present inside the hydrates. We call these "capillary pores".[8]

If we attempt to go further into the characterization of the geometry of pores by assigning one dimension to each of them, we are confronted with the same difficulty that arises with the definition of the size of a solid grain. The characterization of the size of a pore is done using a measurement method based on a specific physical principle, and size is defined by adopting a specific convention. In the case of cement materials, the problem is a bit more complicated, since the porous spaces are totally interconnected, and thus constitute a continuum in the material. The measurement method must therefore also allow us to divide the void space conventionally into a group of individual pores.

The measurement of the size of the pores thus requires the modeling of their geometry as well as a measurement method.

5.5.1. *Mercury porosimetry (or Purcell porosimetry)*

With mercury porosimetry, voids are considered to be cylinders and we measure the distribution in volume of their diameter. The porosimeter device is based on capillarity, the part of physics that describes phenomena that take place at interfaces between phases (fluid and solid).

---

7 The term "porosimetry" is also used.

8 The terms "hydrate pores" and "capillary pores" are specific to the domain of cement materials. More generally, the IUPAC uses the following terminology for pores according to their diameter: macropores ($\varnothing > 50$ nm), mesopores ($50 > \varnothing > 2$ nm), and micropores ($\varnothing < 2$ nm) [ROU 94].

5.5.1.1. *The basis of capillarity*

Numerous natural phenomena can be explained by capillarity, and more precisely by the existence of forces that exist at the interfaces between phases. We can cite, for example:

– the formation of spherical soap bubbles (if they are not too large);

– the formation of water droplets that form on the leaves of trees or ducks' feathers;

– the absorption of ink by a blotter or water by a sponge;

– the curved shape of liquids in small tubes;

– the rising or the descent of these liquids in the tubes;

– etc.

These phenomena are in apparent contradiction to the statics of fluids, according to which the free surface of a liquid at rest is flat and horizontal. They can be explained by the existence of tension forces at the interfaces between fluids, notably at the separation interfaces between liquids and air. Note also that surface tension forces exist between solids[9] and air, as well as between solids and liquids.

Surface tension forces can easily be demonstrated by raising a glass off the surface of soapy water, as we form a swell of water. Place a thread onto this swell, holding the two ends on the sides of the glass. The thread can have any shape, but if we pierce the swell of liquid on one side of the thread, it takes on a circular shape, with the surface of the non-pierced film of water tending to reduce its area to the maximum[10].

Surface tension originates in the structure of the material near the interfaces. Molecules at the interface have altered surroundings in comparison to those which, within the phase being considered, are

9 This surface tension is taken into account when we calculate the energetic balance of the rupture of a solid: the deformation energy is reported on the two surfaces created by the rupture.

10 This experiment can be seen in the video located at: http://upload.wikimedia.org/wikipedia/commons/9/98/TensionSuperficielle_anneau-fil_240x180.gif (accessed 25.1.12).

surrounded by neighbors in all directions. In the area next to the surface, the result of interactions with other molecules is directed toward the interior of the phase being considered and, to reestablish equilibrium, interface tension results[11].

Let us consider an interface separation between two non-miscible phases, see Figure 5.9.

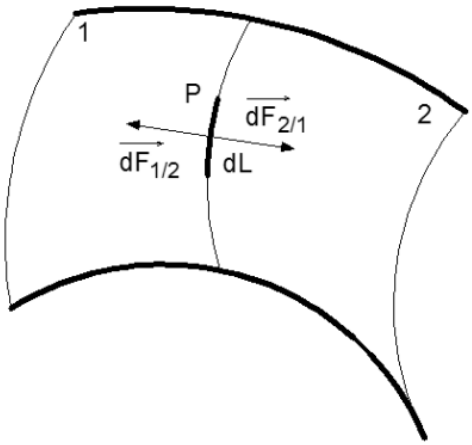

Figure 5.9. *Definition of surface tension*

A line of the interface splits it into two parts: 1 and 2. Consider a point *P* on this line and an elementary segment of length *dL* centered at *P*. The two semi-interfaces located on either side of the line of separation exercise tension forces $\overrightarrow{dF_{1/2}}$ and $\overrightarrow{dF_{2/1}}$ on *P*. These forces are perpendicular to the length of the component and tangent to the interface at *P*. At the balance point, these forces are opposing, and by definition they are given by the relationship:

$$dF = \left|\overrightarrow{dF_{1/2}}\right| = \left|\overrightarrow{dF_{2/1}}\right| = \sigma dL \qquad [5.16]$$

11 As in a pressurized reservoir.

where σ is the surface tension of the interface. It is expressed in N/m in the international system of units.

Some surface tension values at 20°C:

– air–water: 0.072 N/m;

– oil–water: 0.048 N/m;

– air–oil: 0.024 N/m; and

– air–mercury: 0.480 N/m.

We can also consider that the surface tension represents the energy content of the interface per unit of area. Imagine that part 1 of the interface is eliminated. At *P*, only the force $\overrightarrow{dF_{2/1}}$ remains. The interface area tends to diminish. Consider that the point *P* moves away from *dl*. The work of the surface tension force can be written as:

$$dW = \overrightarrow{dF_{2/1}}.\overrightarrow{dl} = \sigma dS \qquad [5.17]$$

where *dS* is the reduction of the interface area due to the movement of the elementary segment. According to this formulation, surface tension appears to be the interface energy per area unit.

5.5.1.2. *Laplace law*

The connecting meniscus of a liquid in a small-diameter vertical tube presents in the form of a spherical cap. We want to know the value of its radial curvature. To do this, in Figure 5.10 let us consider a vertical cross-section of the spherical cap passing through the center *C* of a sphere of radius *R*. It is limited at P and P', the points at which it connects to the vertical tube.

The interface separates the phases 1 and 2: phase 1 is located below, and phase 2 is located above. The cap rests on a base circle with a radius, ρ. At any point of the base circle, we may consider an elementary segment *dL*.

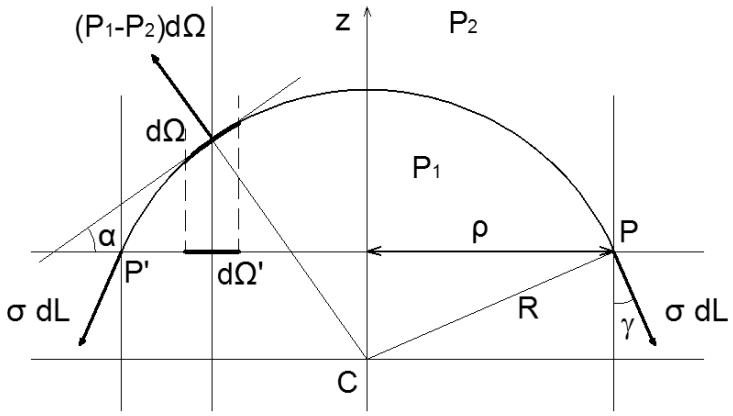

Figure 5.10. *Vertical cross-section of a connecting meniscus*

Now isolate the interface. So that its area is not diminished, at every point *P*, there is a force $dF = \sigma dL$ that is perpendicular at *P* to the elementary segment and oriented downward. The result of these forces is a vertical force oriented downward, with the horizontal components being eliminated two-by-two by considering the diametrically-opposed elementary segments. To balance this vertical result, a difference in pressure is created on both sides of the interface in the two phases. The pressure, P_1, in phase 1 is greater than the pressure, P_2, in phase 2. The resulting pressure force is therefore vertical and oriented upward, and equal to that of the resultant of the tension forces.

The vertical component of the resultant of the tension forces is given by:

$$\int_{Base\ circle} -\sigma dL\cos\gamma = \int -\sigma dL\cos\gamma = \frac{\sigma\rho}{R}\int_{Base\ circle} dL = -\frac{2\pi\rho^2\sigma}{R}$$

The vertical component of the resultant of the pressure forces is given by:

$$\int_{cap} (P_1 - P_2)\, d\Omega \cos\alpha = (P_1 - P_2)\int_{cap} d\Omega = (P_1 - P_2)\pi\rho^2$$

where $d\Omega$ is the area of the surface element of the spherical cap and $d\Omega'$ is its projection onto the horizontal base plane.

The equilibrium of the spherical cap leads to the relationship:

$$P_1 - P_2 = \frac{2\sigma}{R} \quad [5.18]$$

This relationship is the Laplace law. The smaller the radial curvature is, the greater is the difference in pressure between the two phases. Note that in the case of a flat interface (the free surface of a liquid contained in a large container, for example), the pressure difference is zero. If atmospheric pressure exists in the air above the liquid, we find this same atmospheric pressure in the liquid just below the interface.

The Laplace law can be generalized in the case of a curved interface. In this case, the difference in pressure is given by the relationship:

$$P_1 - P_2 = \sigma\left(\frac{1}{R_1} + \frac{1}{R_2}\right) \quad [5.19]$$

where R_1 and R_2 are the minimum and maximum radial curvatures of the interface.

5.5.1.3. *Equilibrium of a connecting edge: Young's law and surface wetting*

In Figure 5.10, the interface shown has a boundary that is represented by the base circle with radius ρ. To maintain the equilibrium of the interface, force must be exerted to compensate for the surface tension. Materially speaking, the interface boundary between phases 1 and 2 is composed of a third phase. For example, in the case of the interface in Figure 5.10, phases 1 and 2 can be a liquid and air, and the boundary is composed of their connection in a vertical cylindrical tube. Generally speaking, the connection between three phases occurs along a line called the connecting edge (see Figure 5.11). Let us consider a point P on this connecting edge and the elementary segment dl of this edge centered at P. The three phases are separated by three interfaces, the surface tensions of which are σ_{12}, σ_{13} and σ_{32}. Each interface exerts a tension force $\overrightarrow{\sigma_{ij} dl}$ in P directed toward the

interior of the interface, and the equilibrium condition of the elementary segment can be written as:

$$\overrightarrow{\sigma_{12}\,dl} + \overrightarrow{\sigma_{13}\,dl} + \overrightarrow{\sigma_{32}\,dl} = 0 \qquad [5.20]$$

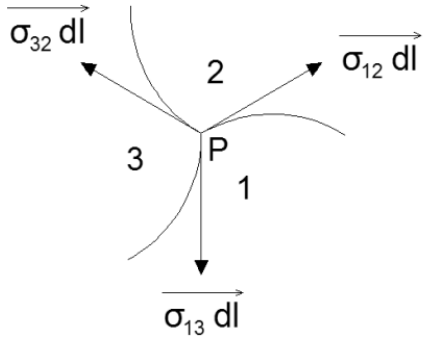

Figure 5.11. *Equilibrium at P of a connecting edge between three phases*

Let us consider the specific case of a drop of liquid deposited on the horizontal surface of a solid, see Figure 5.12.

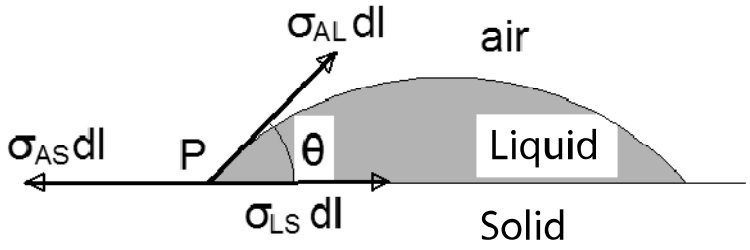

Figure 5.12. *Equilibrium of a drop of liquid on the horizontal surface of a solid*

The connecting edge is the base circle limiting the drop. At any point P of this edge, the drop's equilibrium is shown by the relationship[12]:

$$\sigma_{AS} = \sigma_{LS} + \sigma_{AL} \cos\theta \qquad [5.21]$$

where:

– θ is called the contact angle;

– σ_{AS} is the surface tension between the air and the solid;

– σ_{LS} is the tension between the liquid and the solid; and

– σ_{AL} is the tension between the air and the liquid.

The three surface tensions are scalars. The sign of $cos\theta$ is therefore that of the difference between the two surface tensions σ_{AS}-σ_{LS}. These surface tensions depend on the nature of the solid and the liquid present, and three cases may occur:

– that of Figure 5.12: the angle θ is inferior to $\frac{\pi}{2}$; we say that the liquid is a wetting liquid;

– that of Figure 5.13: the angle θ is superior to $\frac{\pi}{2}$; we say that the liquid is a non-wetting liquid;

– if the contact angle θ is equal to zero, the liquid wets the solid perfectly and stretches across it by forming puddles.

12 The relationship does not completely describe the equilibrium. The vertical component of force $\sigma_{AL} dl$ is compensated for by a force that deforms the solid. For ordinary solids, the surface displacement is negligible (on the order of 10^{-11} m; i.e. in the order of the atomic level [MOU 02]).

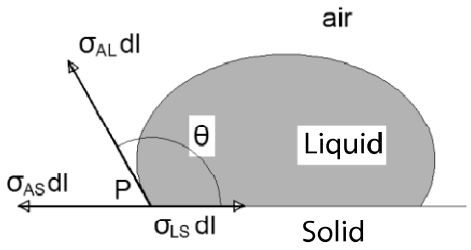

Figure 5.13. *Spreading of a non-wetting liquid on a solid*

The wetting of a solid by a liquid depends on the solid and the liquid, but mainly on the solid. Thus, solids with high surface energy (metal, ceramics and glass) are easily made wet by liquids if they are clean. Conversely, solids with low surface energy (organic solids) are less easily made wet. The case of mercury is a specific example, since it does not wet ordinary solids. Depending on the materials, its contact angle varies between 130 and 155°.

The case of water is important because of the large number of applications that involve it. In some cases, water is a wetting liquid (against glass, for example), while in others it is a non-wetting liquid (as in the case of Teflon or numerous plastic materials). The type of behavior depends largely on the aptitude (or lack thereof) of the solid to create hydrogen-type bonds with water molecules. If such bonds are possible, the solid is hydrophilic; in the opposite case, it is hydrophobic. In the hydrophobic case, the contact angle is greater than 90°. Its value depends on the nature of the solid. Its micro-roughness also influences the angle θ that can range from 120° for a flat surface to 170° for a rough surface [QUE 07]. A material can be made hydrophobic by applying a covering to it that destroys hydrogen bonds, or by creating microreliefs. This type of surface treatment is in development for car windshields, for example, in order to prevent the deposition of condensation and to facilitate the flow of raindrops. These cases are referred to as superhydrophobic surfaces.

5.5.1.4. *Capillary ascension and descent: Jurin laws*

5.5.1.4.1. Cases of wetting liquid

In a cylindrical tube of small dimensions (called a capillary tube), a wetting liquid connects itself to the wall through a meniscus in the shape of a spherical cap (see Figure 5.14a).

The Laplace law expresses the value of the pressure, P_2, that exists in the liquid just below the interface:

$$P_2 = P_1 - \frac{2\sigma}{R} = P_{atm} - \frac{2\sigma \cos\theta}{r} \quad [5.22]$$

where:

– R and r are the radii of the spherical cap and the tube;

– σ is the surface tension of the liquid; and

– θ is the contact angle.

The pressure, P_2, is lower than the atmospheric pressure. If the tube is plunged into a container, the level of the meniscus is higher than that of the liquid in a container. The capillary ascension, H, balances the difference in pressure between the liquid below the meniscus (P_2) and the atmospheric pressure that exists below the free (horizontal) surface of the liquid in the container. At equilibrium, we can write:

$$P_{atm} - P_2 = H\rho g = \frac{2\sigma cos\,\theta}{r}$$

where ρ is the density of the liquid.

Capillary ascension is given by the relationship:

$$H = \frac{2\sigma \cos\theta}{r\rho g} \quad [5.23]$$

It is inversely proportional to the radius of the cylinders. As an example, the ascension of water in a cylindrical tube with a 1 mm radius is around 15 mm if we suppose that the water is perfectly wetting; it is in the order of 15 m in a tube whose radius is equal to 1 μm[13] (see Exercise 5.5).

13 When the atmospheric pressure is in the order of 10 meter water column, the negative pressure of the water at the level of the meniscus should cause the formation of water vapor bubbles (cavitation). The small area of the bubbles in the tube will cause vapor pressure in the bubbles that is greater than the saturation pressure. The pressure is thus negative in these

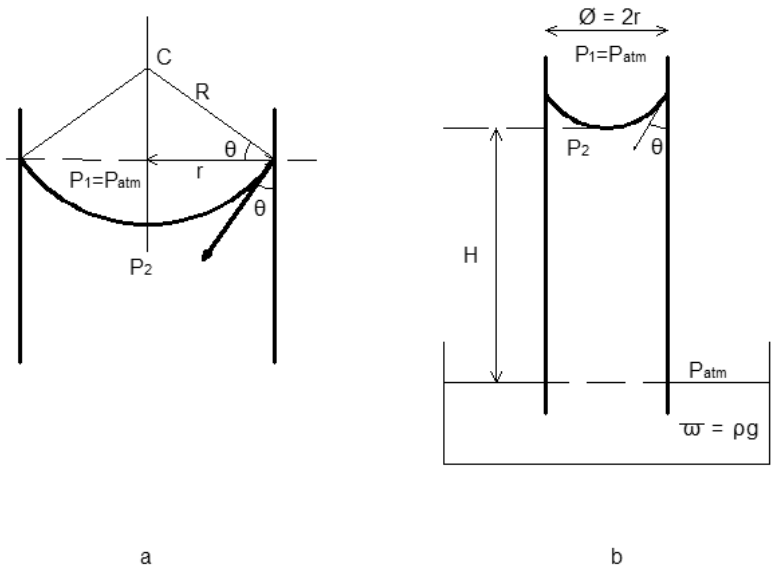

Figure 5.14. *Capillary ascension of a wetting liquid. (a) Zoom of the meniscus shown in (b)*

The difference at the interface between the air pressure and the pressure that exists in the liquid is called *capillary pressure* and is noted as P_c. In the case of a wetting liquid, P_c is positive: the lower pressure in the liquid causes a capillary depression that is the source of the phenomenon of capillary withdrawal. Hydrogen bonds allow water to support tensile stresses (they also allow us to drink water through a straw). If we assimilate the pores of a resting porous material into a wetting liquid in a group of vertical cylindrical tubes, capillary depression (the term capillary suction is also used) is manifested in a withdrawal of the liquid into the porous solid. If the porous solid is immersed in water, this water penetrates the pores under the effect of capillary suction (this is called imbibition).

If the capillary tube is closed at its upper end, the withdrawal of the wetting liquid is disturbed when air trapped above the meniscus is compressed. Likewise, when water penetrates an immersed porous solid, air can be trapped in interconnected open pores. This hinders underwater saturation and is the reason it is advised to saturate the material under

---

pores, and is responsible for the withdrawal phenomena that we observe in cement materials during the drying process.

vacuum when using the water-accessible porosity measurement method in order to evacuate the air contained in the pores.

5.5.1.4.2. Cases of non-wetting liquid

The connecting meniscus of a non-wetting liquid presents itself as indicated in Figure 5.15.

The pressure of the liquid near the interface is P_1, given by the Laplace law:

$$P_1 = P_2 + \frac{2\sigma}{R} = P_{atm} - \frac{2\sigma \cos\theta}{r}$$

If the tube is immersed in a container containing the non-wetting liquid, with the pressure of the liquid in the tube under the meniscus being greater than the atmospheric pressure, the level of the liquid in the tube will be below the level of the free surface of the liquid in the container. In this case, capillary descent occurs.

The height of capillary descent is calculated using the relationship[14]:

$$H = \frac{2\sigma cos\,\theta}{r\rho g}$$

Unlike the preceding case, if we place a porous solid on the free surface of a non-wetting liquid, the liquid will not penetrate the pores. The same is true if we immerse the solid in the liquid. In order to make the liquid penetrate the pores, we must exert a pressure upon it that opposes the capillary (drainage) pressure, or:

$$P = - P_c = - \frac{2\sigma \cos\theta}{r} \qquad [5.24]$$

This relationship, called the Washburn relationship, is the basis of the measurement of the dimension of pores using mercury porosimetry.

14 The calculated value of H is negative (capillary descent) due to the sign of $cos\,\theta$.

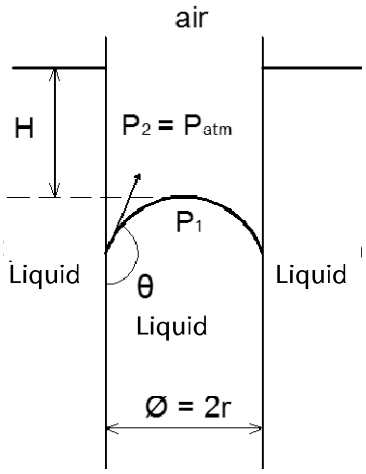

Figure 5.15. *Capillary descent of a non-anchoring liquid*

Water only penetrates into hydrophilic porous solids. As indicated previously, it is possible to make solids hydrophobic using surface treatments that inhibit capillary imbibitions. The products used in these treatments are called hydrofuges.

5.5.1.5. *Imbibition and drainage*

In the case of Figure 5.14, the liquid is wetting and the air can be considered a non-wetting fluid. In Figure 5.15, though the liquid is non-anchoring, air can be considered a wetting fluid. More generally speaking, if a porous material contains two non-miscible fluids, one is wetting and the other is non-wetting. Let us consider the drainage of a porous solid initially saturated with water (the wetting fluid) and then placed in air (the non-wetting fluid). The drainage curve represents the variation in the degree of saturation of the wetting phase, depending on the capillary pressure (applied on the air). As the air pressure increases, the water saturation diminishes and reaches the lower limit, s_{wi}, called *irreducible saturation*. In this situation, isolated water clusters are trapped in porous spaces and surrounded with air that presents itself as a continuous phase. The increase in air pressure no longer allows water to be drained.

In reducing air pressure, water penetrates the porous solid (imbibition). The imbibition curve shown in Figure 5.16 generally shows high hysteresis

in comparison to the drainage curve. When the air pressure regains its initial value water saturation remains lower than 1, since air remains trapped in the material. The saturation limit in the air (a non-wetting fluid) $s_{r,nm}$, which is the non-wetting fluid, is called *residual saturation*. Exercise 5.6 gives an example of this behavior in the case of non-saturated soil.

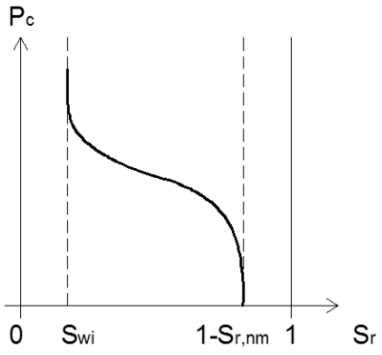

Figure 5.16. *Imbibition curves of a porous solid*

5.5.1.6. *Principle of mercury intrusion porosimetry*

A low-volume sample (of a few cm^3 at most) of the porous material being analyzed is placed in the cell of a penetrometer equipped with a calibrated pipe, see Figure 5.17. The penetrometer is then emptied of the air and mercury is introduced so as to fill the container and the calibrated pipe. Increased pressure is then exerted on the mercury. If the solid is not porous, the mercury level in the tube will not change (apart from the very low compressibility of mercury). If there are pores, however, these will progressively fill under increasing pressure (intrusion). The largest pores will be filled first. The pressure of the air contained in the pores is very low, and in this case the irreducible saturation is virtually zero.

If, between pressures P_c and $Pc+\Delta Pc$, the volume of the mercury in the tube varies from Δv, this means that the material contains a volume Δv of pores, the dimension of which falls between $r\text{-}\Delta r = \frac{-2\sigma \cos\theta}{P_c + \Delta P_c}$ and $r = \frac{-2\sigma \cos\theta}{P_c}$.

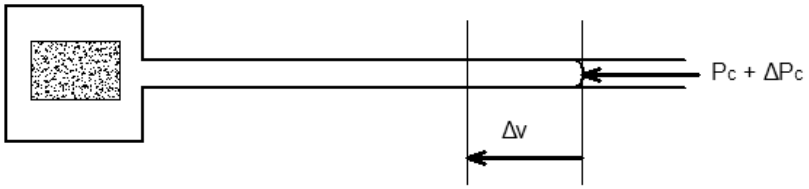

Figure 5.17. *Sketch of a mercury intrusion porosimeter*

Thus, it is possible to characterize the porous structure of a material by noting the volumes of mercury injected at each stage of pressure. The volumes measured are then compared to a unit of dry mass of the material being studied. As an example, Figure 5.18 shows the intrusion curve of mercury in a ceramic material. The scale of the abscissa is determined by applying relationship [5.24].

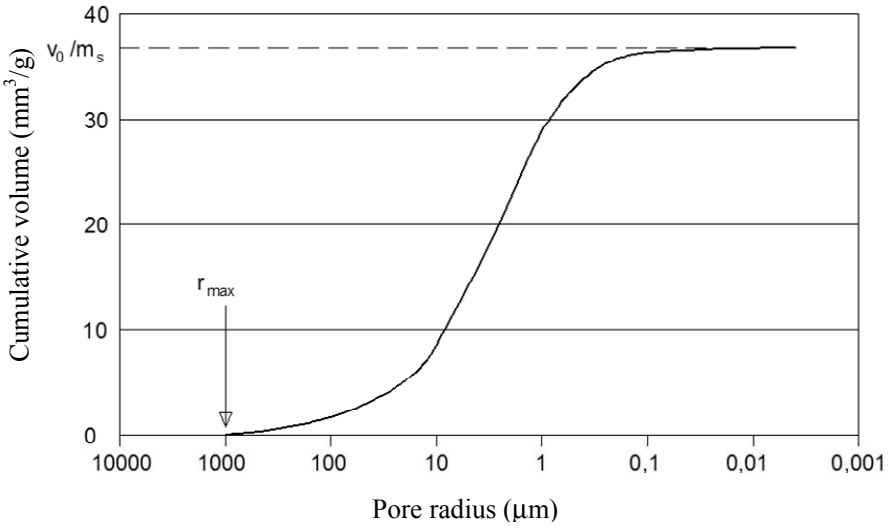

Figure 5.18. *Intrusion curve of mercury entering a ceramic*

The radius of the pores of the material in Figure 5.18 is between approximately 0.1 µm and 1,000 µm. Under increasing pressure (from left to right), the mercury begins to penetrate the material at pressure P_{min}, which corresponds to the radius of the largest pores (r_{max}). This radius is sometimes

called the *critical radius*. Under increasing pressure, the mercury progressively saturates the ceramic. Beyond a pressure corresponding to a pore radius of 0.1 μm, it no longer penetrates the porous material.

The maximum volume of mercury filling the material allows us to evaluate the open porosity by measuring the apparent density of the material:

$$p_o = \frac{v_o}{V_a} = \frac{v_o / m_s}{V_a / m_s} = (v_o / m_s).\rho_a$$

Figure 5.18 shows a cumulative curve.

The results of mercury porometry are sometimes shown in the form of a histogram or a pore size distribution curve. These are curves derived from preceding ones. For example, Figure 5.19 shows the microstructure of concrete with an average 28-day resistance of 25 MPa. Two groups of pores appear (the term bimodal distribution is used): small pores whose average radial dimension is in the order of 20 nm (200 Å); and larger pores, whose radius is around 150 nm (1,500 Å)[15].

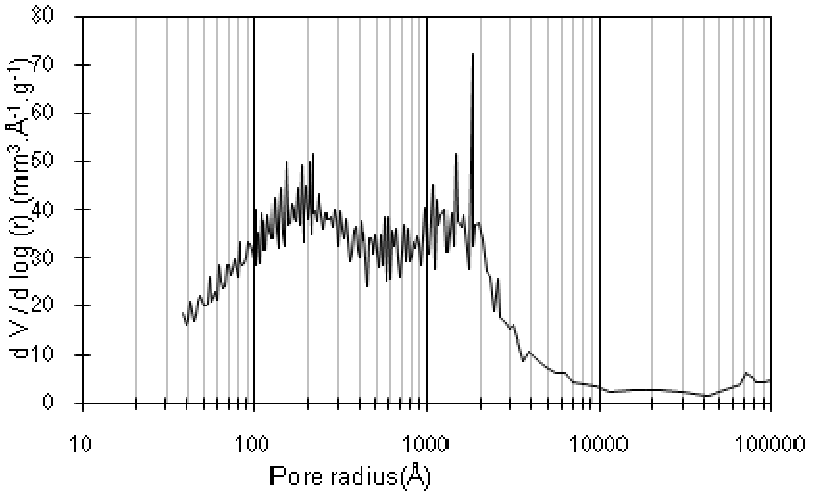

Figure 5.19. *Bimodal microstructure of concrete obtained by using mercury porometry [BAR 00]*

15 The formation of the microstructure of cement materials is studied in Exercises 5.3 and 5.4 at the end of this chapter.

The description of the microstructure using mercury intrusion is easy, which explains the relatively widespread use of this technique. Nevertheless, several things should be noted on the subject.

NOTE 5.1.– the size of the samples is small (of a few cm^3). For materials in which the larger heterogeneities are in the order of a few centimeters (and this is the case for concrete), this can pose a problem with representativeness and it is recommended that several measurements are taken.

NOTE 5.2.– the mercury penetrates the samples from the outside; therefore the spatial layout of the pores has an effect on the result. This is illustrated in Figure 5.20:

– In case (a), where the mercury penetrates the larger pores with radius r_1 at pressure P_1, the volume v_1 is correctly measured. Mercury fills the small pores with radius r_2 at pressure P_2. The measurement of volume v_2 is correct.

– In case (b), where the mercury cannot access the pores with radius r_1 until after it fills the smaller pores with radius r_2 at pressure P_2. At this pressure, all of the pores are filled by the mercury and the corresponding volume is accounted for as the volume of pores with radius r_2, since they are filled at pressure P_2. The volume of the small pores is therefore measured by excess. It is said that mercury porosimetry gives information about the dimension of access to pores and not their dimensions.

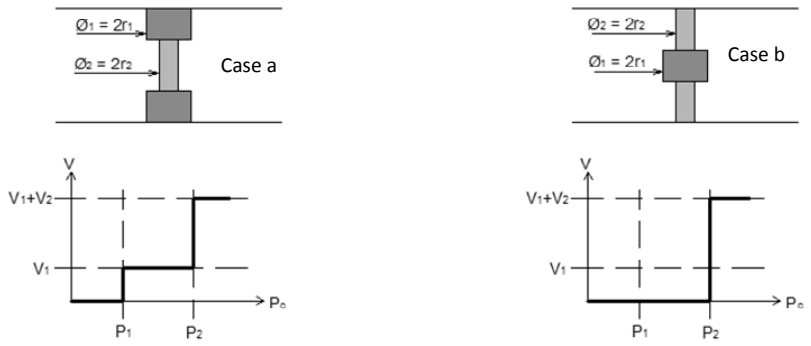

Figure 5.20. *Theoretical schema of the filling of pores with mercury at increasing pressure*

NOTE 5.3.– the mercury penetrates materials tested at increasing pressure. In practice, the minimum pore dimension measured is limited by the maximum pressure supported by the apparatus. High-performance devices can support a pressure of 400 MPa, which corresponds to radii in the order of 2 nm. Such pressures might well damage the materials being tested, and it is reasonable to wonder whether the variation in the volume of mercury measured corresponds to crushing of the solid rather than the intrusion of mercury into the pores.

NOTE 5.4.– materials such as cement pastes possess smaller pores than mercury can access. For this reason, the open porosity calculated by mercury porometry is generally lower than the porosity accessible to water, which gives access to the smallest pores. As an example, Figure 5.21 shows the porosity values obtained with cement materials (W/C = 0.32) prepared with varying proportions of cementitious paste (concrete, mortar and pure paste). The greater the proportion of paste, the more elevated the porosity and the greater the difference between water porosity and mercury porosity. The very small pores, which are more abundant in materials containing more paste, are not detected by mercury intrusion.

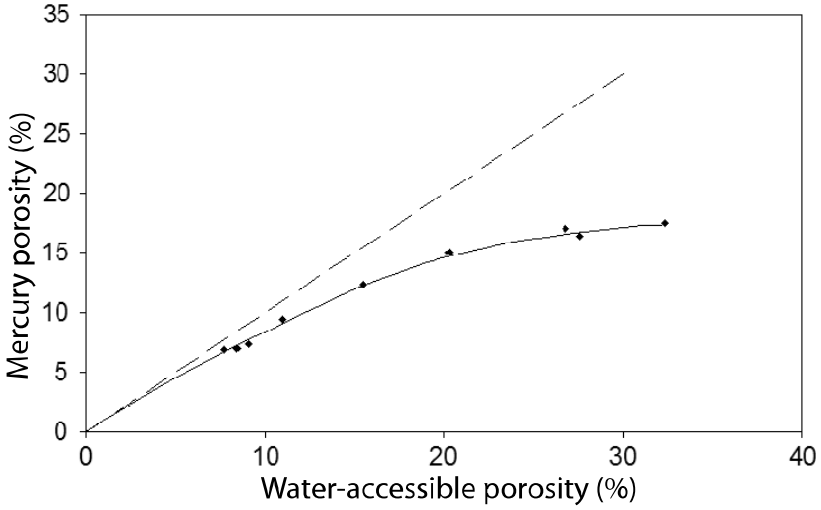

Figure 5.21. *Differences between mercury porosity and water porosity in the case of cementitious materials with a W/C ratio of 0.32 [LOB 03]*

NOTE 5.5.– mercury porometry is used to calculate the specific surface area of porous solids. Working from the hypothesis of the cylindrical geometry of pores, it is possible to determine the area of their developed surface. With n cylindrical pores with a length of h and a radius of r, the total porous volume is:

$$V = n\pi r^2 h$$

and the developed surface of the pores is:

$$S = 2\pi rnh = \frac{2V}{r}.$$

The mechanical work done by the outside pressure to cause the mercury to penetrate to a depth of dl in a pore of radius r is given by $dW = \sigma \cos\theta \, dS$, where dS is the unit of the pore's area covered by mercury.

This work, carried out by outside pressure P causing penetration of a volume dv, can also be written as: $dW = -pdv$. From this, we get the total surface covered by the mercury during the test:

$$S = -\frac{1}{\sigma \cos\theta} \int_0^{v_Q} P dv \qquad [5.25]$$

To obtain the specific surface area, we must relate S to the unit of mass of the material, which can be done by directly using the data generated in ordinates of the intrusion curve (the volumes injected being related to the unit of mass of the solid)[16].

16 Very small pores contribute in a significant manner to the specific surface area of porous materials since for a given volume of pores the outside surfaces are greater. Porosimetry that does not give access to pores with radii below certain limit depends on the device used; the specific surface area calculated by the mercury porosimetry of material that contains pores inferior to this limit is inferior to that given by a BET measurement, for example.

NOTE 5.6.– the mercury intrusion curve, see Figure 5.18, is a drainage curve. Its derived curve, see Figure 5.19, gives the distribution of the dimension of access to pores. After mercury intrusion, the pressure can be reduced. The so-called imbibition curve presents a hysteresis with the drainage curve. The larger the ratio between the dimension of the pores and that of their access, the larger is the hysteresis and the greater is the residual mercury saturation.

NOTE 5.7.– before taking a measurement for concrete (this will also be the case for clay), as much of the water contained in the pores must be evacuated as possible. This can be done using various techniques, but the result is not always the same and the microstructure may be damaged (for example, after drying concrete at 105°C). Quenching the sample in liquid nitrogen (which traps the water in ice without increasing the volume, since the water molecules do not have the time to rearrange themselves) and then sublimating the ice is the technique that seems to cause the least disruption to the microstructure.

5.5.2. *Image analysis*

Image analysis is sometimes used to measure the dimension of pores despite the non-stereological character of this scale (see footnote 5 in section 5.4.1.2). Morphological treatments carried out on 2D images are intended to ensure the correspondence of the pores observed with circles, the diameters of which are determined. The hypothesis is made that these diameters are the "dimensions" of the 3D pores. This method is most often used to analyze the largest pores of materials (with diameters greater than 1 μm). Conversely, the smaller pores are difficult to measure, because their observation requires significant magnification of the images (and resolution is limited by pixel size).

Figure 5.22 gives a comparison of two pore size analysis, with one done using image analysis, and the other using mercury intrusion. The image analysis reveals numerous pores that are larger than 1 μm, while they do not appear with mercury porosimetry. This result can be explained by the fact that, since these larger pores are not interconnected, mercury porosimetry does not identify them. Their volume is accounted for when the mercury fills them at a higher pressure, corresponding to the dimension of the access routes. This figure shows the importance of the choice of measurement method and the corresponding hypotheses of physical analysis.

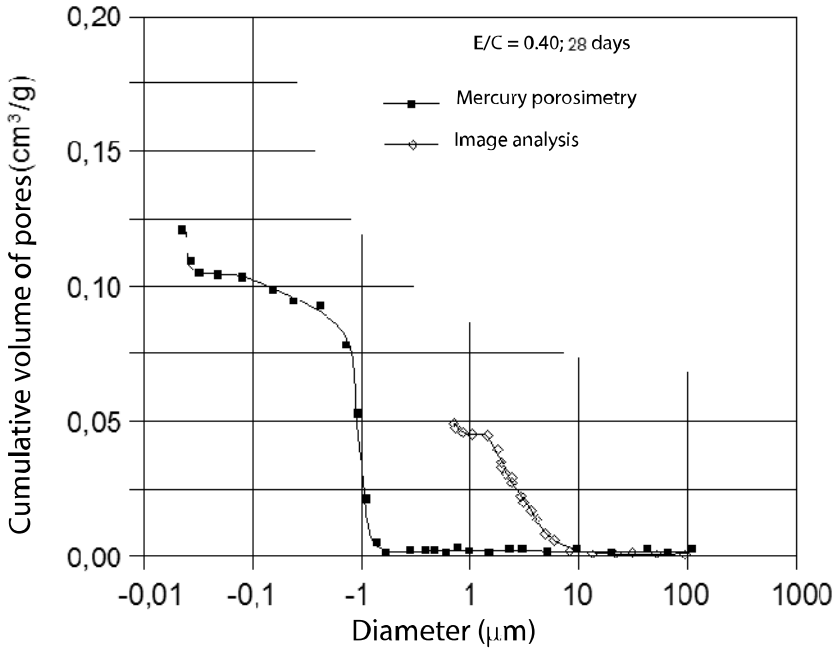

Figure 5.22. *Comparison of porometry results for cement paste obtained using image analysis and mercury intrusion [DIA 94]*

5.5.3. *Method based on the adsorption of a gas*

As described in Chapter 3, the adsorption of a gas corresponds to its binding to the surface of a solid. At increasing pressure, the number of layers of molecules adsorbed increases. The adsorption of a gas on a solid at increasing pressure allows us to trace the adsorption isotherm and to deduce the specific BET area of the adsorbent from it. This is done by means of the BJH (Barret, Joyner, and Halenda) method, which is based on the Kelvin and Kelvin-Laplace laws, which we will now discuss.

5.5.3.1. *Kelvin law*

Though the Kelvin law is more generally applicable, we have chosen to demonstrate it in the case of water. Here, we will use the case of a porous material whose pores can contain liquid water and a gas composed of air and

water vapor. The pressure in the liquid will be called p_l and that of the gas p_g. We will operate from the hypothesis that the porosity is connected to the outside. We will also assume that the transformations are isothermic.

Free enthalpy is expressed by the relationship $G = n\ \mu$, where n is the number of moles and μ is the chemical potential. In addition, we have the Gibbs-Duhem identity:

$$SdT+nd\mu - VdP = 0$$

where:

– S is entropy;

– T is temperature;

– V is volume; and

– P is pressure.

If we suppose that liquid water is incompressible, that M is the molar mass and that (μ_{l0}, p_{l0}) describes a reference state, with the number of moles n being equal to $V\ \rho_l/M$, the Gibbs-Duhem identity in an isotherm transformation is written as:

$$n.d\mu_l = V.dp_l,$$

that is to say:

$$d\mu_l = M.\ dp_l/\rho_l$$

By intergration, we have the chemical potential of liquid water:

$$\mu - \mu_{l0} \frac{M}{\rho_l} \cdot (p_l - p_{l0})$$

Likewise, supposing that water vapor follows the perfect gases law $PV = nRT$, where R is the gas constant and (μ_{v0}, p_{v0}) describes a reference state, the Gibbs-Duhem identity will be written as:

$$n.d\mu_v = V\ dp_v \text{ or } d\mu_v = RT\ dp_v/p_v.$$

By integration, we obtain the chemical potential of water vapor:

$$\mu_v - \mu_{v0} = RT \ln(p_v/p_{v0})$$

We choose $p_{l0} = p_g$ (the pressure of the vapor + air mixture) = p_{atm} as the reference state for liquid water and $p_{v0} = p_{vs}$ (the pressure of saturating vapor) for the vapor. At atmospheric pressure, if the water vapor pressure is equal to the saturating vapor pressure, equilibrium exists, thus there is equality of the chemical potentials. Finally:

$$\mu_{l0} = \mu_{v0}$$

At equilibrium, $\mu_l = \mu_v$. Then, by introducing relative humidity, ψ, the ratio between the vapor pressure and saturating vapor pressure at the same temperature, we get:

$$\frac{M}{\rho_l} \cdot (pl - pg) = RT\, ln(\psi)$$

By having $p_c = p_g - p_l$, we get:

$$-p_c = \frac{RT\rho_l\, ln(\psi)}{M}$$

ψ being <1, we have a depression.

5.5.3.2. *Kelvin-Laplace law*

In the case of porous solids, gas can condense in the pores at a vapor pressure lower than its saturating vapor pressure. This is the phenomenon of *capillary condensation*. Supposing that the pores are cylindrical with radius r, the pressure P of the gas (vapor) at which condensation occurs is given by the Kelvin-Laplace law, which combines the Kelvin law and Laplace equation:

$$\ln \frac{P}{P_{sat,T}} = -\frac{2\sigma M \cos\theta}{rRT\rho_l} \qquad [5.26]$$

In this relationship, $P_{sat,T}$ is the saturation pressure of the gas at atmospheric temperature T. σ, ρ_l and M, respectively, are the surface tension

of the liquid, its density, and its molar mass. θ is the contact angle of the liquid on the solid, and R is the gas constant.

In the case of a porous solid at equilibrium in humid air, water vapor will condense in the pores with a radius below the limit value given by the Kelvin-Laplace relationship. By introducing relative humidity, ψ, the limit radius of the largest pores filled with liquid water is given by:

$$r_{\text{lim}} = -\frac{2\sigma M\cos\theta}{RT\rho_l \ln\psi} \qquad [5.27]$$

Figure 5.23 illustrates the Kelvin-Laplace relationship in the case of water at 20°C and gives the radius of the largest pores filled with liquid water, depending on the relative humidity of the air. As an example, in air at 60% relative humidity, all pores with radii below 2 nm are filled with water. This law allows us to take into account a physical reality that is well-known elsewhere; i.e. that porous materials in equilibrium with air can contain liquid water, and even more so when they contain numerous very small pores and as the air increases in humidity.

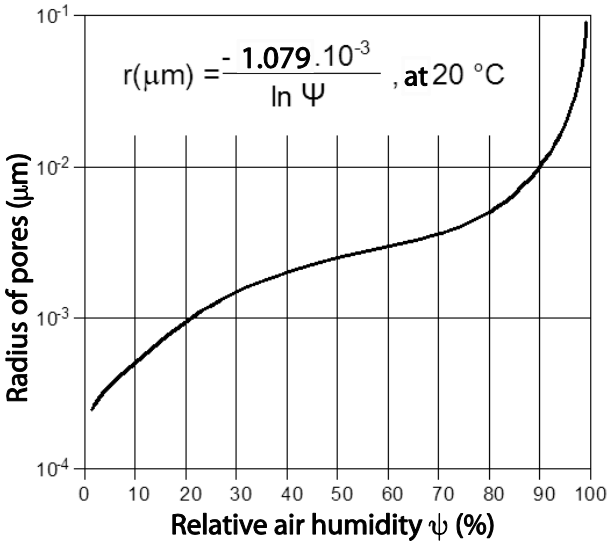

Figure 5.23. *Maximum radius of pores filled with water at 20°C, depending on relative humidity [DAI 93]*

5.5.3.3. *BJH (Barret, Joyner and Halenda) method*

The nitrogen adsorption–desorption isotherm measured at the temperature of liquid nitrogen (77 K) is of type IV[17] in the case of materials presenting mesoporosity (50 nm > ø > 2 nm). As an example, Figure 5.24 shows the isotherm of aluminum oxide.

The BJH method [ROU 03] is based on the following considerations:

– The saturation level observed on the desorption curve corresponds to the presence of mesopores. At the corresponding saturation pressure, all of the mesopores are saturated with nitrogen.

– When the pressure is lowered beyond this saturation pressure, the pores with a radius of $radius_1$ empty at pressure P_1 given by the Kelvin-Laplace law (equation [5.27]). Below pressure P_1, nitrogen remains adsorbed on the walls of pores with a radius of $radius_1$. The pores remain covered with a layer of adsorbed gas, the thickness t_1 of which depends on the pressure. The value of t_1 can be expressed in terms of P.

– When the pressure diminishes to a value P_2, pores of radius r_2 given by relationship [5.25] desaturate in turn. The of evaporated gas comes from the desaturation of pores with radius r_2 and the reduction in the thickness of gas adsorbed on the pores of radius r_1. When the pressure P_2 is known, the new thickness of the layer adsorbed on r_1 pores can be calculated.

– By progressively desorbing the material and measuring the volumes of gas evaporated at each stage of pressure, we can calculate the distribution of pore sizes[18]. Figure 5.24 shows the pore size distribution curve of aluminum oxide, the isotherm of which has been traced on the same figure.

---

17 See Figure 3.8.

18 In this figure, n_a, m_s and V_{pn} represent the quantity of gas adsorbed, the mass of the solid, and the cumulative volume of pores with a radius corresponding to the n first pressure stages,

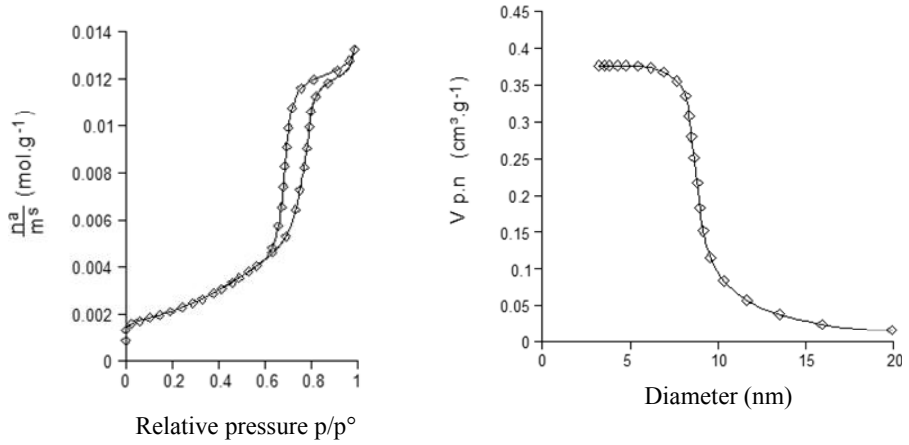

Figure 5.24. *Nitrogen adsorption isotherm (left) on aluminum oxide at 77 K and pore size distribution (right) calculated using the BJH method [ROU 03]*

The BJH method can also be used to determine porometry from water desorption isotherm curves. This method is particularly well adapted to cementitious materials because it does not require prior drying and can be applied to larger samples than those used in nitrogen sorption tests. The isotherms are obtained by monitoring the losses of mass until the stabilization of samples of concrete placed in containers filled with saturated saline solutions that maintain constant relative humidity. An example of this, Table 5.2 shows the relative humidity levels obtained using different salt solutions at 20°C.

This method is used to reach pores smaller than those reached by mercury porometry (for concrete, this allows us to characterize hydrated cement pores down to the nanometer) [BAR 94]. Thus, it supplements this technique well (see Exercise 5.7).

---

respectively. For a more detailed examination of this method of calculation, the reader may wish to consult [ROU 03].

Salts	Chemical formula	Relative humidity (%)
Lithium chloride	$LiCl, nH_2O$	*12*
Magnesium chloride	$MgCl_2, 6H_2O$	*33*
Potassium carbonate	$K_2CO_3, 2H_2O$	*44*
Magnesium nitrate	$Mg(NO_3), 6H_2O$	*55*
Sodium nitrate	$NaNO_2$	*66*
Sodium chloride	$NaCl$	*76*
Ammonium sulfate	$(NH_4)SO_4$	*81*
Potassium nitrate	KNO_3	*93*
Potassium sulfate	K_2SO_4	*97*

Table 5.2. *Relative humidity obtained at 20°C for different saturated saline solutions, adapted from norm NF X 15-014*

Figure 5.25 shows an example of a water sorption isotherm on high-performance concrete and the porometric structure deduced from it by applying the BJH method.

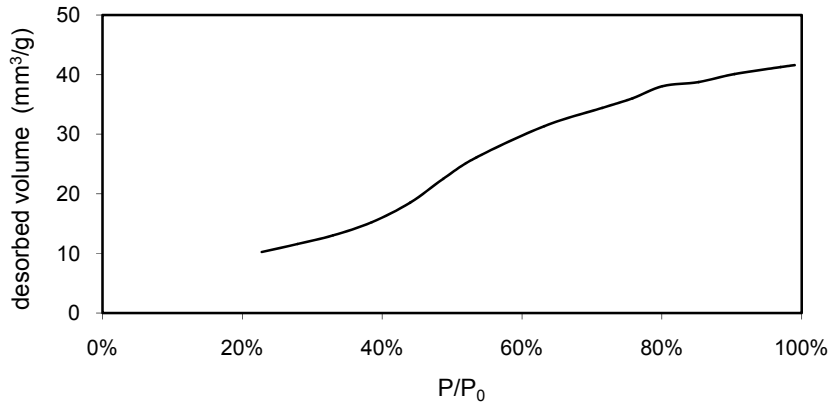

Figure 5.25. *Water sorption isotherm of concrete at 23°C and corresponding pore size distribution [BAR 94]*

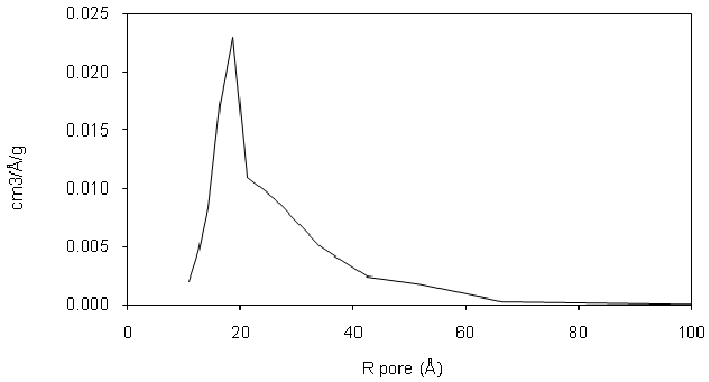

Figure 5.25. (continued) *Water sorption isotherm of concrete at 23°C and corresponding pore size distribution [BAR 94]*

5.5.4. *Dynamic porosimeter: the Brémond porosimeter*

The determination of porous structure using a Brémond porosimeter is done in two stages. The material being analyzed is first saturated with water, and then the outflow of air in the material at growing pressure is measured.

Air begins to flow when the air pressure is sufficient to open the largest pores. The corresponding pressure is called *breakthrough pressure*. It is a characteristic of a porous material that indicates the continuous porous path with the largest dimension. If we use the hypothesis of a cylindrical pore structure, relationship [5.24] allows us to calculate the corresponding pore radius (see Exercise 7.4). When the pressure increases, the outflow from these pores increases, and other smaller pores progressively contribute to the flow.

5.5.5. *Thermoporometry*

Thermoporometry utilizes the fact that the temperature of fusion (or solidification) of water in a porous medium depends on the radius of the pores; the smaller the pores, the lower this temperature is[19].

19 This is one of the reasons why very high-performance concretes with fine porosities do not break down during freezing/thawing cycles; the other reason being that they contain little water.

The Gibbs-Thompson law gives the relationship between pore radius and temperature. It is expressed by writing that the difference in pressure between ice and liquid water, $p_c - p_l$, is equal to the product of the entropy of fusion, ΔS, by the temperature difference $T - T_m$, where T_m is the fusion temperature of unconfined ice. Since $p_c - p_l$ is equal to $2\sigma_{cl}/r$ where σ_{cl} is the surface tension, we get:

$$r = 2\sigma_{cl}/(\Delta S\,(T - T_m))$$

Where ΔS = 1.2 MPa °C^{-1} and σ_{cl} = 0.0409 J m^{-2} [COU 08], we have:

$$\Delta T = 0.0682/r \text{ with } r \text{ in } \mu\text{m}.$$

Thus pores in hydrated cementitious materials, the fusion temperature of ice is lowered by around 50°K, see Figure 5.26. This technique is generally applicable for pore radii between 2 and 50 nm.

During the phase change, the latent heat of fusion (or solidification) can be detected by differential calorimetry (differential scanning calorimetry, DSC). DSC is a technique that measures the flow of heat absorbed or released by a material depending on the temperature when it is subjected to a controlled temperature program. The quantity of heat for a given temperature corresponds to the porous volume and the temperature to the radius of the pore.

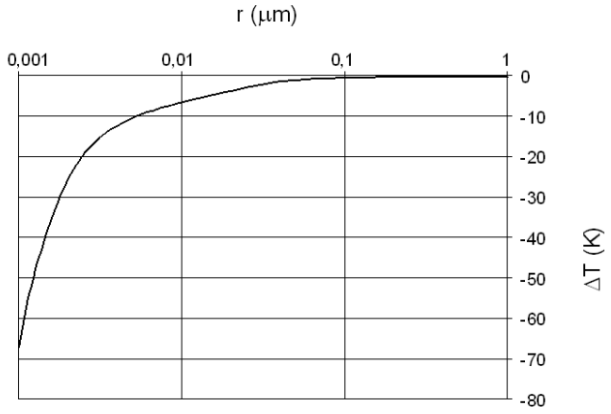

Figure 5.26. *Evolution of the difference in the fusion temperature of ice compared to that of unconfined ice depending on pore radius*

For concrete, as for other porous materials containing water, thermoporometry has the benefit of not requiring the material to be dried beforehand. Figure 5.27 gives an example of the porosimetric distribution obtained for a hardened cement paste compared with that obtained using the BJH method (see Exercise 5.7) [BAR 94].

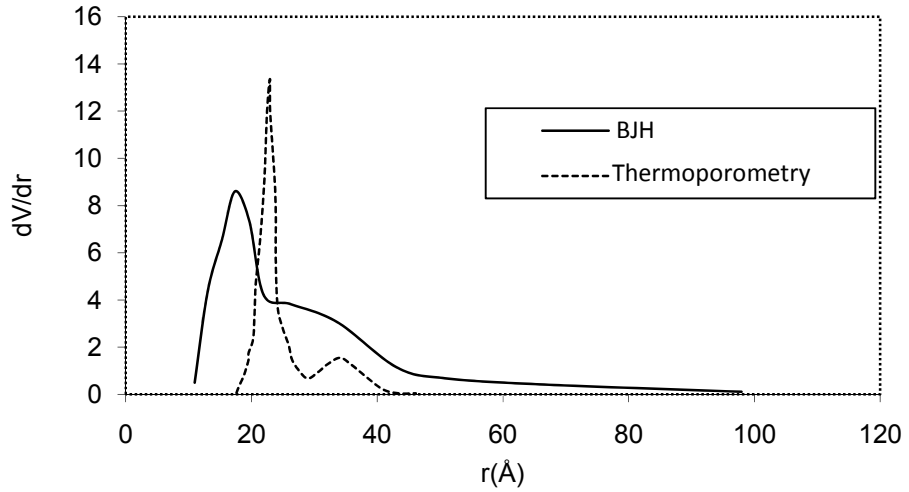

Figure 5.27. *Comparison of pore size distributions of cement paste obtained by thermoporometry and by the BJH method [BAR 94]*

5.5.6. *Small angle X-ray scattering and small angle neutron scattering*

The techniques of small angle X-ray scattering (SAXS) and small angle neutron scattering (SANS) utilize the fact that water in the pores has an electronic density (SAXS) or nucleus density (SANS) that is different from that of the solid phase, which causes a difference in the refraction indices between the two phases. This difference causes the scattering of part of the beam incident with a small angle in comparison to the straight line. The measurement of the intensity of this diffused fraction with respect to the diffusion angle gives us information about the shape, average size and volumetric fraction of pores. This measurement also provides information about the fractal dimension of the solid [ADE 92, ALL 07, WIN 85].

These techniques are applicable for pore sizes between 0.5 nm and 30.0 nm, without the need for the material to be dried; thus, they provide

access to information about the nanoporosity of the material [JEN 07]. However, the difficulty of interpreting the results and the material mean that they are still difficult to access.

5.5.7. *Innovative techniques in development*

Other techniques can also provide information about porosity. Nuclear magnetic resonance (NMR) and X-microtomography are among the promising techniques already in use.

NMR consists of forcing an increase in the level of the magnetic moment of protons by means of external magnetization, and monitoring their return to equilibrium[20]. The time of relaxation, T_1 (i.e. the time taken to return to magnetic equilibrium) is then measured, as is T_2 (return to a magnetic time phasing that had been dephased during excitation). The interpretation of these times provides information on the pore size distribution (T_2) and on the evolution of the microstructure (T_1) [KOR 08].

X-microtomography is used to reconstitute a 3D image using 2D views of a sample subjected to X-rays[21]. It can attain a resolution of 0.7 µm for one pixel. Image analysis techniques are used to directly reconstruct the capillary porosity of material in 3D, and to deduce morphological (volume, specific surface area and pore size distribution) and topological (tortuosity and connectivity) parameters from it [GAL 08]. This technique has been used, for example, to monitor the evolution of the porosity of cementitious materials subjected to leaching [BUR 06]. It is non-destructive and requires no particular preparation of the sample. It is currently, however, only used for on relatively small samples (600 µm in diameter for [GAL 08] and 8 mm for [BUR 06]).

5.6. Bibliography

[NOR] Norm NF P 18-459: Porosity and density test.

---

20 We will not discuss NMR imaging here. This technique is not currently applicable for the issue of porosity, as its resolution is fairly poor (40 μm^3).

21 For concrete, in order to attain sufficient resolution it is necessary to use “hard” X-rays generated with the aid of a synchrotron.

[ADE 92] ADENOT F., Durabilité du béton: caractérisation et modélisation des processus physiques et chimiques de dégradation du ciment, thesis, University of Orléans, France 1992.

[ALL 07] ALLEN A.J., THOMAS J.J., "Analysis of C-S-H gel and cement paste by small-angle neutron scattering", *Cement and Concrete Research*, vol. 37, pp. 319-324, 2007.

[ARL 07] ARLIGUIE G., HORNAIN H., *GranDuBé - Grandeurs Associées à la Durabilité des Bétons*, Presses de L'ENPC, 2007.

[AUD 87] AUDIGUIER-MARCEL M., DELAGE P., "Etude microscopique et porométrique de sols fins naturels dans une perspective géotechnique", *VII*^{ème} *Réunion Internationale de Micromorphologie des Sols*, Paris, France, pp. 493-500, 1985.

[BAR 93] BAROGHEL-BOUNY V., CHAUSSADENT T., "Caractérisation de la texture d'un béton durci à partir des isothermes de sorption de vapeur d'eau". *Bulletin de Liaison des Ponts et Chaussées*, vol. 187, pp. 69-75, 1993.

[BAR 94] BAROGHEL-BOUNY V., *Caractérisation des Pâtes de Ciment et des Bétons – Méthodes, Analyse, Interprétations*, LCPC, 1994.

[BAR 00] BAROGHEL-BOUNY V, AMMOUCHE A., HORNAIN H., GAWSEVITCH J., "Vieillissement des bétons en milieu naturel: une expérimentation pour le XXème siècle: caractérisation microstructurale sur éprouvettes de bétons de résistance 25 à 120 MPa", *Bulletin des Laboratoires des Ponts et Chaussées*, vol. 225, 2000.

[BUR 06] BURLION N., BERNARD D., CHEN D., "X-Ray microtomography: application to microstructure analysis of a cementitious material during leaching process", *Cement and Concrete Research*, vol. 36, pp. 346-357, 2006.

[COU 08] COUSSY O., "Poromécanique et changement de phases en milieu confiné. Application aux matériaux cimentaires", *Ecole Thématique Physique, Chimie et Mécanique des Matériaux Cimentaires*, La Colle sur Loup, 2008.

[DAÏ 93] DAÏAN J.-F., LAURENT J.-P., "Structure poreuse et transport d'humidité dans les roches", in: LEFEBVRE R.A. (ed.), *Cours Européen Sciences et Matériaux du Patrimoine Culturel, 1*^{ère} *Session*, Ravello/Rome, Istuto Poligraphico e Zecca dello Stato, Libreria delle Stato, Rome, Italy, pp. 83-112, 1993.

[DIA 94] DIAMOND S., LEEMAN M.E., "Pore size distributions in hardened cement paste by SEM image analysis". *Mat. Res. Soc. Symp. Proc*., vol. 370, pp. 217–226, 1994.

[GAL 08] GALLUCCI E. Caractérisation du milieu poreux par imagerie 2D/3D, Ecole Thématique Physique, Chimie et Mécanique des Matériaux Cimentaires, La Colle sur Loup, 2008.

[JEN 07] JENNINGS H.M., THOMAS J.J., GEVRENOV J.S., CONTANTANIDES G., ULM F.J., "A multi technique investigation of the nanoporosity of cement paste", *Cement and Concrete Research*, vol. 37, pp. 329-336, 2007.

[KOR 08] KORB J.P., Exploration du milieu poreux par RMN, Ecole Thématique Physique, Chimie et Mécanique des Matériaux Cimentaires, La Colle sur Loup, 2008.

[KRE 84] KREIJGER P.C., "The skin of concrete. Composition and properties", *Matér. Constr. RILEM*, 17, 100, p. 275-283, 1984.

[LOB 03] LOBET A., Influence des paramètres de composition des matériaux cimentaires sur les propriétés de transfert des bétons, thesis, INSA Toulouse, France, 2003.

[MOU 02] MOUETTE J., "Physique des Surfaces et des Interfaces", from the course by CHARLAIX E., (Available at: http://malsain.org/~joss/ surfaces/, accessed 25.1.12).

[QUE 07] QUERE D., "Les surfaces super-hydrophobes", *Images de la Physique*, pp. 239-244, 2007.

[ROU 94] ROUQUEROL J., "Recommendations for the characterization of porous solids", *Pure & Appl. Chem*, vol. 66, no. 8, pp. 1739–1758, 1994.

[ROU 03] ROUQUEROL F., LUCIANI L., LLEWELLYN P., DENOYEL R., ROUQUEROL J., *Texture des Matériaux Pulvérulents et Poreux*, Publication P1 050, Techniques de l'Ingénieur, 2003.

[WIN 85] WINSLOW D.N., "The fractal nature of the surface of cement paste", *Cement and Concrete Research*, vol. 15, 1985.

5.7. Exercises

Exercise 5.1: *Principles of the concrete aerometer*

This equipment is used to measure the air content of concrete in its fresh state (concrete in which hydration reactions have not yet begun). The air content, t, is defined as the ratio between the volume of air bubbles in the concrete and its apparent volume. To find this, we use a concrete aerometer, the function of which we will examine here.

The concrete aerometer is composed of two compartments. In the upper part, the volume compartment V_0 is filled with air; in the lower part, the volume compartment V_1 is filled with fresh concrete. In the initial state, the air pressure in the upper compartment and in the air bubbles (of volume v) in the concrete is equal to the atmospheric pressure, H. The two compartments are separated, and a pressure P greater than H is established in the upper compartment. Communication is then reestablished between the two compartments. An isotherm expansion is used to equalize the air pressures in the two compartments, since water transmits the pressure into the voids in the concrete. The air pressure is thus equal to P', falling between P and H. In the air volume, v, of the concrete, the pressure changes from H in the initial state to P' in the final state. The pressures P and P' are measured by a manometer connected to the upper compartment.

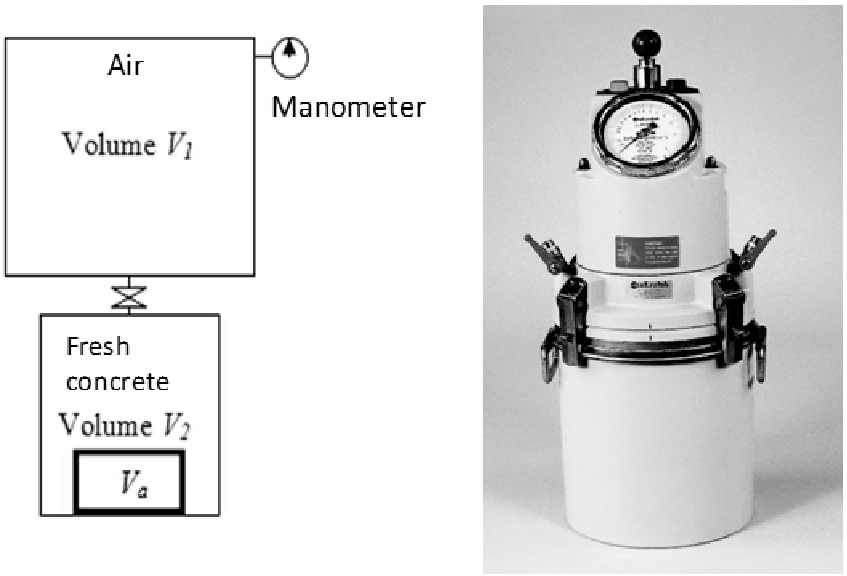

Figure 5.28. *Sketch and photo of a concrete aerometer (CONTROLAB)*

1) Express the relationship between v and the problem data.

2) The apparent volume of the fresh concrete being equal to V_1 (the concrete fills the lower compartment), express the value of the air content t of the fresh concrete.

3) The volumes of the two compartments being fixed, the air content depends only on the pressures. We want to graduate the manometer directly in air content values. How can we do this?

Exercise 5.2: *Saturation of porous materials and the importance of creating a vacuum*

Imagine a horizontal cylindrical capillary tube ($\varnothing = 2r$) that is open at both ends and located at the level of the free surface of a reservoir of water that feeds it.

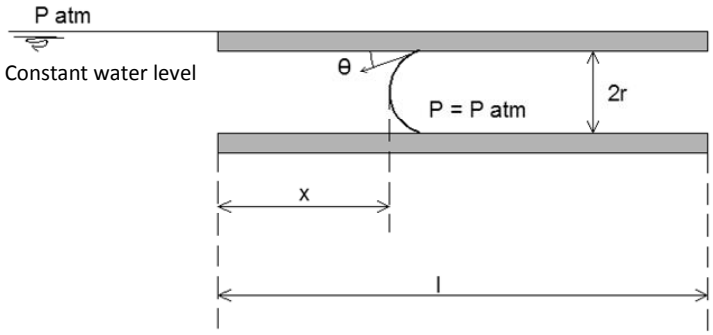

Figure 5.29. *Schematic drawing of the capilliary penetration*

The water – with a viscosity of μ, a density of ρ, and surface tension σ – wets the walls of the capillary and is connected to it by a spherical cap with an angle θ. The diameter of the capillary being very small, we assume that the pressure is constant in the cross-section in contact with the reservoir and equal to the atmospheric pressure.

1) Express the relationship *x(t)* causing the advancement of the meniscus in the capillary ($x < l$ = capillary length), supposing a viscous flow of water under the influence of the sole forces of surface tension.

In viscous flow, the volume outflow of water, Q, under driving pressure, ΔP, is given by the Poiseuille relationship (see Chapter 6 for more details).

$$Q = \frac{\pi r^4}{8\mu}\frac{\Delta P}{l}$$

2) Give the expression of the volume outflow $Q(t)$ of water in the capillary ($x < l$).

3) The capillary is now closed at the end located at a distance l from the reservoir. If we suppose that at the initial time the capillary is filled with air (a gas assumed to be perfect) at atmospheric pressure, the forward movement of the water is opposed by the compression of the air at the bottom of the capillary. If the flow regime is viscous, give the expression of the filling rate of the capillary $\frac{dx}{dt} = f(x)$. We will suppose that air compresses in an isothermal manner and that the meniscus is a flat surface perpendicular to the axis of the capillary.

4) At what distance x_0 will the water stabilize?

5) Calculate the ratio $\frac{x_0}{l}$ for a tube with a radius of $r_1 = 10$ μm and for a tube with a radius of $r_2 = 1$ μm where we have σ (water) = 0.074 N/m, $\theta = 0$ degrees and $P_{atm} = 10^5$ Pa.

6)

a) If $l = 1$ cm, what is the maximum mass of water, m_1, penetrating the capillary with radius r_1 initially filled with water at atmospheric pressure?

b) We have 100 capillaries with radius r_2. Their total volume is the same as that of a capillary with radius r_1. What is the total mass m_2 of water penetrating the 100 capillaries?

c) What can we conclude with regard to the measurement of the volume of open voids by water absorption at atmospheric pressure?

Exercise 5.3: ***Formation of the porous structure of cement paste: the Powers model***

In this exercise, we will anticipate the evolution of the porous structure of a cement paste in terms of its composition (*W/C* ratio) and its state of hydration.

1) The fresh cement paste being considered here is a mixture of anhydrous cement grains (volume v_c and density ρ_c = 3.15 g/cm^3) and water (volume v_e and density ρ_e = 1 g/cm^3). The mixture is characterized by the *W/C* ratio of the masses of water [*W*] and cement [*C*].

a) Calculate the initial porosity $p_0 = \dfrac{v_e}{v_e + v_c}$ of the cement paste with respect to the *W/C* ratio.

b) Give its numerical value for the paste prepared with a *W/C* ratio of 0.60.

2) As time passes, the hydration reaction progresses and the hydates progressively fill the intergranular spaces of the pores. Porosity becomes inferior to the initial porosity p_o, since 1 cm^3 of anhydrous cement when hydrated produces 2.13 cm^3 of hydrates. In the following, we will assume that the quantity of water is sufficient to hydrate all of the cement.

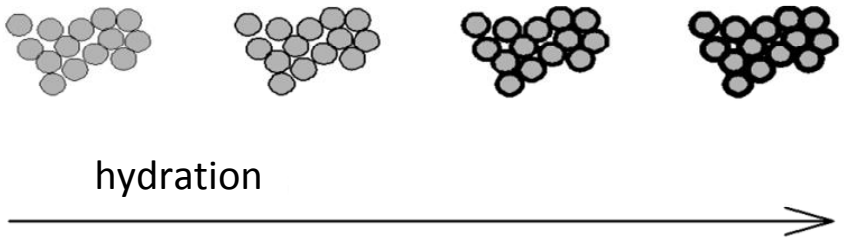

Figure 5.30. *Schematic representation of cement grains hydration*

The progression of hydration reactions in the cement at time *t* is characterized by a "degree of hydration", noted α, which is equal to the ratio between the mass of the cement that has become hydrated up to the time *t* and the initial mass of the anhydrous cement.

Figure 5.31 presents the volumes of the different phases in the initial state (left) and for a degree of hydration α (right). We will assume that hydration occurs at a constant apparent volume.

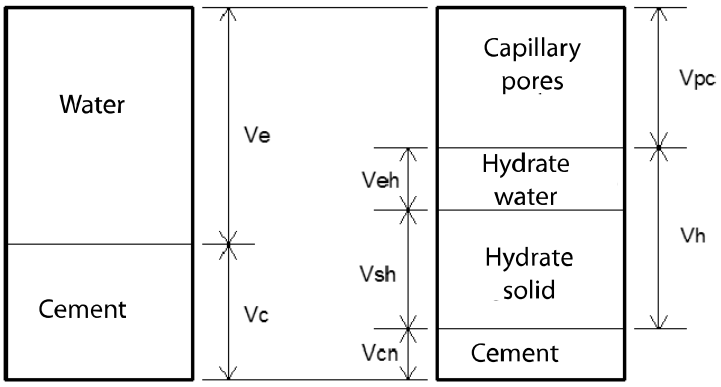

Figure 5.31. *Volume change during hydration*

The part of the initial volume of water that is not filled in by hydrates is referred to as "capillary pores". Its volume is called v_{cap} and capillary porosity p_{cap} is the relationship $\frac{v_{cap}}{v_{tot}} = \frac{v_{cap}}{v_e + v_c}$ between the volume of capillary pores and the apparent volume.

At time t, v_h is the volume of hydrates and v_{cn} is the volume of cement that has not yet been hydrated.

When hydration occurs in a closed milieu (no exchanges with the outside environment), some of the capillary pores are not filled with water. The situation described here is different; it corresponds to a case where outside water can keep the capillary pores saturated.

a) Express the capillary porosity p_{cap} of the cement paste with respect to α and p_o.

b) Trace the graph $p_{cap} = f(\alpha)$ for the paste being considered.

3) Hydrates are porous compounds; they include a solid phase of volume v_{sh} and water-filled pores of volume v_{eh}. Their porosity $\frac{v_{eh}}{v_h}$ is equal to 28%.

a) Express the total porosity p_{tot} ($p_{tot} = \frac{v_{cap} + v_{eh}}{v_{tot}}$) of the cement paste with respect to α and p_o.

b) Draw the graph $p_{tot} = f(\alpha)$ for the paste being considered.

c) If the degree of hydration is equal to 70% at the 28-day mark, what is the total porosity for the paste with a *W/C* ratio of 0.60?

Exercise 5.4: *Porous structure of hardened cement*

In its initial state, the cement paste is a mixture of cement grains and water. It is characterized by the *W/C* ratio of the weight quantities of water and cement.

As time passes, the cement reacts with the water and forms hydrates that progressively fill the intergranular spaces, which are initially filled with water. Spaces not filled by hydrates at a given time are called capillary pores. The hydrates also have their own porosity, made up of pores that are much smaller than the capillary pores.

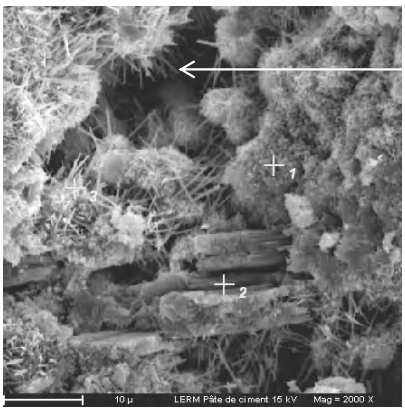

Figure 5.32. *Microscopic view of hardened cement paste (W/C = 0.50) after 28 days*

Figure 5.33 shows the influence of the *W/C* ratio on the pore structure of cement pastes. The results are obtained using mercury intrusion porosimetry. The values of the volumes given in the ordinates are related to the unit of mass of the solid of cement paste and are expressed in cm^3/g.

Note the following terms:

– "capillary porosity": the open porosity of capillary pores with dimensions larger than around 100 nm.

– "total open porosity": the open porosity of all pores ($\Phi > 4.5$ nm).

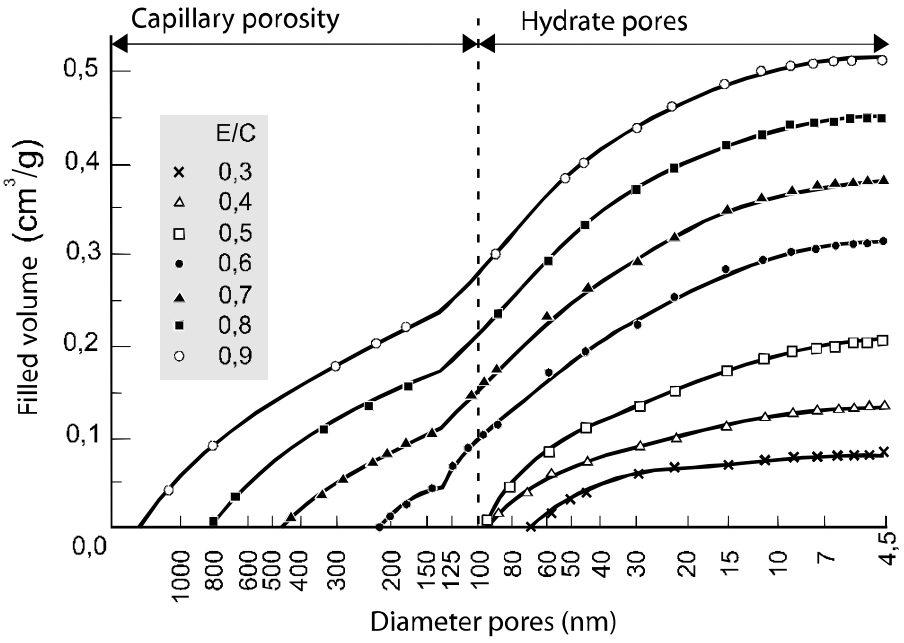

Figure 5.33. *Pore size distribution of the of 28 day-cement pastes prepared with different W/C ratio*

The apparent densities of pastes vary at 28 days depending on the *W/C* ratio. They are given in Table 5.3.

W/C **ratio**	0.3	0.4	0.5	0.6	0.7	0.8	0.9
Apparent density (g/cm^3)	1.89	1.65	1.50	1.26	1.18	1.09	0.91

Table 5.3. *28 day-apparent densities of the cement pastes*

The cumulative curves show:

– the reduction in open porosity with the *W/C* ratio (given by the ordinate of the horizontal asymptote); and

– the reduction in the maximum size of the pores with the *W/C* ratio (given by the origin abscissa).

Show the evolution curves of capillary porosity and of total open porosity with respect to the *W/C* ratio.

Exercise 5.5: *Tree sap (inspired by ", P. Cruiziat, M.T. Tyree,"La montée de sève dans les arbres La Recherche, vol. 21, April 1990)*

1) Plants use their roots to draw up the water and nutritive mineral salts they need from the soil. The liquid that results is sap, which travels through the conductor tubes that run through the roots, stems, branches, and leaves. Explain, using the phenomena described in this chapter, how the sap can be transported to the upper parts of trees, while gravity exercises an opposing effect.

2) Numerical application: using the hypotheses necessary, give the radius of the vessels necessary for sap to reach the top of a tall tree (a 120 m-high sequoia) and calculate the corresponding capillary depression.

Data: water surface tension $\sigma_{water} = 0.073$ N/m and $\theta = 0$.

3) The capillary depression measured is actually much larger, and reaches 50 MPa[22]! Deduce the radius of the vessels from this.

Exercise 5.6: ***Capillary phenomena in non-saturated soil***

1) In geotechnics, capillary depression is called suction. If we take clay in which the average pore radius is around 0.2 μm, calculate the corresponding suction. From this, deduce the theoretical height of capillary withdrawal above the layer.

2) Water retention curve: it is usual in soil mechanics to introduce a suction potential *pF*:

$$pF = log_{10}(\frac{-pc}{\rho l \cdot g}) + 2$$

where the suction p_c is expressed in kPa and ($\rho_l.g$) in kN/m^3.

Suppose that the pores of the soil being considered are all cylindrical and parallel. Starting from a state of 100% saturation, draw the evolution of *E pF* with respect to saturation, *Sr*, when the soil is desaturated. Assume that the pores are distributed as shown in Table 5.4.

If we begin a cycle of drying/wetting, we will see that there is a difference in behavior between the curves. By discussing the hypotheses used in the previous modeling, show that they may be the source for this difference.

---

22 This means that the water is in a state of tension. The bonds, called covalent bonds, between the oxygen atom and the two hydrogen atoms produce a stable molecule. The atoms are arranged in a chevron, with the oxygen atom making the peak of an angle of around 105°. This asymmetrical configuration explains several of water's characteristics. The hydrogen part of the molecule carries a positive electric charge, and the oxygen part carries a negative charge. Each molecule is thus a dipole, which is the electrical equivalent of a tiny magnet. The water molecule is thus the simultaneous recipient and generator of an electrostatic connection, called hydrogen bonds. The reason that water can support tension is due to the hydrogen bonds between water molecules. These tensions are easy to show; for example, when we drink through a straw.

Pore radius (nm)	Cumulative porous volume (mm^3/g)
5	0
10	7
50	27
100	45
200	115
300	140
500	155
1,000	175
10,000	190
100,000	200

Table 5.4. *Results of mercury porosimetry on clayey sand [AUD 87]*

Exercise 5.7: *Characterization of porosity using the BJH method (exercise adapted for the use of a spreadsheet)*

The BJH method (which was first developed by Barrett, Joyner and Halenda) uses water desorption isotherms to describe the pore size distribution in cement materials. It is applicable for pore sizes between approximately 2 and 50 nm.

Its principal hypotheses are as follows:

– an adsorbed phase and a capillary phase coexist in pores that are assumed to be cylindrical (see Figure 5.34);

– a multi-molecular layer of water of an average statistical thickness, t, depending on relative humidity, RH, is adsorbed to the surface of the pores. Table 5.5 gives the thickness, t, in relation to RH;

– the desorption isotherm represents the balance of capillary condensation;

– the radius of the meniscus is given by the Kelvin-Laplace equation.

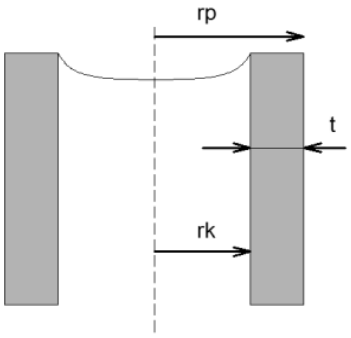

Figure 5.34. *The BJH model*

RH	t (Å)
0.99	18.18
0.97	13.529
0.904	10.735
0.8525	9.4608
0.801	8.52
0.758	7.7157
0.715	7.1569
0.632	6.299
0.535	5.4902
0.4875	5.0735
0.44	4.6324
0.385	4.1667
0.33	3.7255
0.279	3.3824
0.228	3.0098

Table 5.5. *Thickness of the adsorbed water film for different relative humidities*

1) Show that when we move from relative humidity h_{n-1} to h_n, the porous volume Vp_n of the pores with average radius of rp_n drained from their condensation RH is written as:

$$Vp_n = \frac{rp_n^2}{\left(rk_n + \Delta t_n\right)^2}\left[\Delta V_{desn} - \Delta t_n \sum_{j=1}^{n-1} Ap_j\right]$$

where:

– rk is the Kelvin radius;

– rp is the porous radius such as $rp = rk+t$;

– Ap is the internal surface of the pores supposed to be cylindrical ($Ap = 2\ Vp/rp$); and

– V_{des} is the adsorbed volume of liquid water determined from the experimental desorption isotherm.

NOTE 5.8.– for *rp, rk* and *t*, we will consider average values between h_{n-1} and h_n. Likewise, the variation Δx is calculated by $\Delta x_n = x_{n-1} - x_n$.

Deduce from this the cumulative area of the pores and the cumulative porous volume.

2) Using a spreadsheet, calculate the pore size distribution using the data from the desorption isotherm (Table 5.6).

NOTE 5.9.– the distribution is obtained by calculating the porous volume corresponding to a given pore size, or $Vp_n / \Delta rp_n = f(rp_n)$.

NOTE 5.10.– data taken from reference [BAR 93].

R	V mm^3/g
0.990	41.61
0.970	41.25
0.904	40.06
0.8525	38.75
0.801	38.03
0.758	36.00
0.715	34.42
0.632	31.37
0.535	26.10
0.4875	22.50
0.440	18.50
0.385	15.20
0.330	13.01
0.279	11.56
0.228	10.25

Table 5.6. *Desorption isotherm of concrete*

Exercise 5.8: *hydration: the prediction of concrete resistance*

Using cement hydration modeling, we will seek to find the relationship between concrete's resistance and its porosity. First, we will consider the hydration of cement paste.

1) Hydration

Here, we will examine the prediction of the porosity of Portland cement paste after hydration. For this, we will consider a sample of cement paste of a given composition (*W/C* ratio) and kept in air.

In this instance, p_o is the initial porosity of the cement paste in the fresh state, the ratio between the volume of voids and the apparent volume. Neglecting any air that may be trapped in the paste, express p_o with respect to the weight ratio, *W/C*, of mixture of water and cement.

2) During hydration of the cement, the volume fractions of cement, hydrates and residual voids (capillary pores) change. We will determine the evolution with hydration of these volume fractions.

Hypotheses:

– 1 cm^3 of anhydrous cement and 1.34 cm^3 of water produce 2.13 cm^3 of hydrates (the Le Chatelier contraction);

– the hydration of cement can occur as long as there is water;

– the degree of hydration, the relationship of the mass of hydrated cement at a given time to the initial mass of anhydrous cement, is called α; and

– we consider that there is no desiccation of the paste, since it is protected (treated).

a) Give the expressions of the volume fraction of hydrates (f_{hyd}) and the volume fraction of anhydrous cement (f_{anh}) with respect to p_o and α. Deduce the fraction of capillary pores (P_{cap}) from this.

b) Calculate the maximum degree of hydration, taking into account the hypotheses with respect to W/C.

c) Justify the value W/C = 0.42 leading to complete hydration without any anhydrates or water remaining.

d) Using the expressions of capillary porosity P_{cap} and initial porosity p_o, and assuming maximal hydration, find a relation giving the W/C ratio with respect to P_{cap}. Consider the two cases $W/C \geq 0.42$ and $W/C \leq 0.42$.

3) Resistance

Remember the Féret law, which is used to estimate the compression resistance of concrete:

$$f_{cm} = K\frac{R_C}{\left(1+\frac{V_e+V_v}{V_c}\right)^2} = K\frac{R_c}{\left(1+(\frac{\rho_c}{\rho_e})\frac{E}{C}\right)^2}$$

where:

– V_e : water volume per liter;

– $\frac{\rho_c}{\rho_e}$: ratio of densities of cement and water = 3.15;

– K : granular coefficient = 6;

– R_c : true strength class of cement = 65 MPa; and

– f_{cm} : average resistance of concrete.

a) Express the resistance with respect to capillary porosity, P_{cap}, still assuming maximum hydration.

b) We have experimental results on four types of concrete made up of the same basic materials, and for which the *W/C* ratio is varied. These experimental results are reported in Figures 5.35 and 5.36. Report the curves corresponding to Féret law and to the expression of resistance with respect to capillary porosity in Figures 5.35 and 5.36. Explain them.

c) The Balshin model is used to estimate the relationship between the resistance and porosity of a porous material. This model is expressed by the following relationship:

$$f_{cm} = f_{c0}(1 - p)^n$$

where:

– p is the porosity (that we assume to be equal to capillary porosity),

– f_{c0} represents the limit of resistance when p tends toward 0; and

– n is an adjustment coefficient.

Place the curve corresponding to this expression on Figure 5.35, using the values f_{c0} = 120 MPa and n = 3. Explain the curve you have drawn.

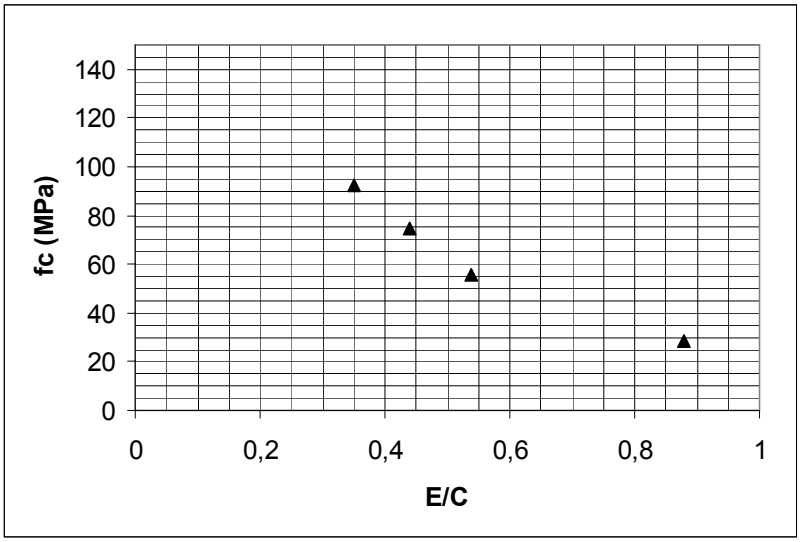

Figure 5.35. *Resistance determined by the W/C ratio*

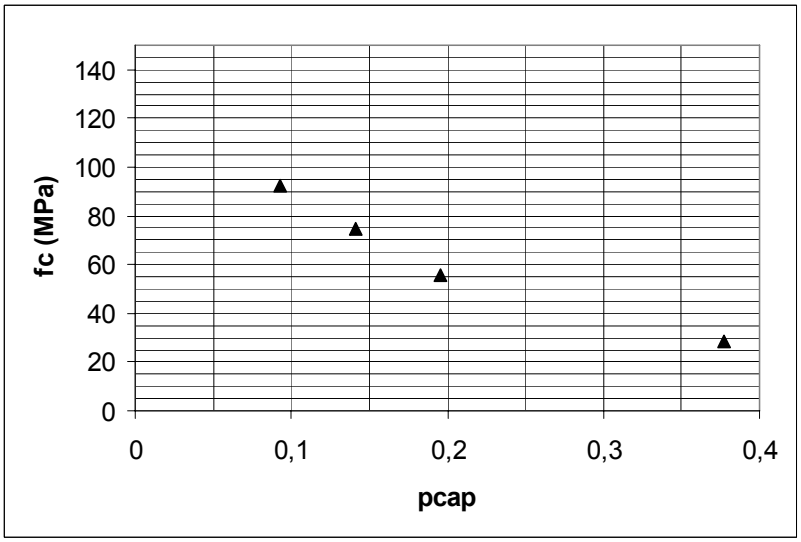

Figure 5.36. *Resistance determined by capillary porosity*

Exercise 5.9: ***Water adsorption study in hydrated plaster***

Plaster in the anhydrous state is an anhydrite (calcium sulfate, $CaSO_4$). When water is present, it hydrates to form gypsum according to the reaction:

$$CaSO_4 + 2\ H_2O \rightarrow CaSO_4,\ 2H_2O$$

In the mixing stage, a mass of water *W* is added to a mass of anhydrite *A*. A mixture whose proportions correspond exactly to the reaction above is called a stoichiometric mixture.

1) Calculate the *W/A* ratio of the stoichiometric mixture. Determine its theoretical initial porosity and final porosity when the hydration reaction is complete.

2) If we prepare this stoichiometric mixture, the placing of plaster is very difficult and the initial porosity is much greater than the theoretical value. To facilitate placing, we use a larger quantity of water than is strictly necessary for the hydration of the anhydrite.

Consider a mixture with *W/A* ratio of 0.50. Determine its theoretical initial porosity and the final porosity at complete hydration.

3) This completely hydrated mixture (*W/A* = 0.50) is analyzed with mercury porosimetry. The porosity found is equal to the theoretical final porosity and shows a single group of pores corresponding to a mercury pressure equal to 0.67 MPa. What is the diameter of this group of pores?

Problem data:

– *molar masses*: Ca = 40 g, S = 32 g, O = 16g and H = 1g;

– *densities*: anhydrite = 2.61 g/cm^3, gypsum = 2.32 g/cm^3 and water = 1 g/cm^3;

– *surface tension*: mercury = 0.474 N/m; and

– *contact angle*: mercury/plaster = 130°.

Chapter 6

The Fundamentals of Diffusion

6.1. The basics of diffusion

Diffusion is a process that occurs at the atomic level and which can lead, under certain conditions, to the transport of matter on a macroscopic scale. It occurs in many situations, and this chapter is particularly concerned with the diffusion of the particles of a solute dispersed in a fluid (solvent), and with gaseous diffusion, which will be introduced in the latter part of the chapter.

In fluids, the particles of a solute are subject to *Brownian movement* under the effect of thermal agitation. This movement was described in 1827 by the botanist R. Brown, who observed the displacement of pollen grains in water. It results from the successive impacts that a particle undergoes with the molecules of the fluid in which it is located. This displacement of particles by a succession of jumps occurring at random in different directions is the phenomenon of diffusion.

Before considering the macroscopic transport of matter by diffusion, we will define the diffusion coefficient in the following section by considering a microscopic approach to this phenomenon.

6.1.1. *Microscopic approach to diffusion*

Figure 6.1 illustrates a random progression due to Brownian movement.

Physical Properties of Concrete and Concrete Constituents Jean-Pierre Ollivier, Jean-Michel Torrenti and Myriam Carcassès

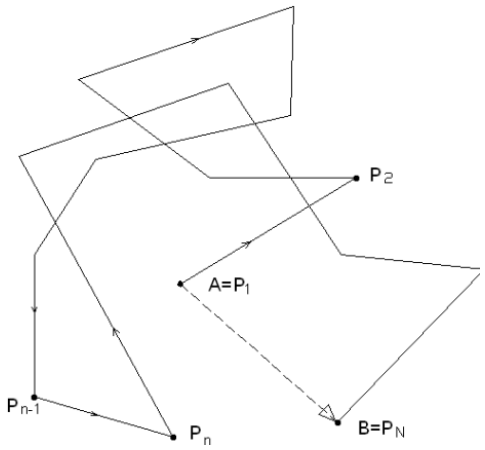

Figure 6.1. *The Brownian movement of a particle. It shows random forward movement under the influence of successive impacts [TOU 05]*

6.1.1.1. *The case of fluids*

Imagine the displacement of a particle via the random movement described in Figure 6.1, and consider the approach proposed by Tourrenc [TOU 05].

A solute particle starting from position A reaches position B after N impacts, including the first impact at position A. The trajectory between two collisions at points P_{n-1} and P_n is rectilinear, and can be characterized by the vector $\overrightarrow{l_n} = \overrightarrow{P_{n-1}P_n}$.

Its length, l, and its orientation at each point, P, have the same laws of probability (homogeneity hypothesis), and the orientations of $\overrightarrow{l_n}$ are equiprobable (isotropy hypotheses).

Let us take $\vec{\delta} = \overrightarrow{AB}$. The hypotheses of homogeneity and isotropy imply that the average value of $\vec{\delta}$ is zero, and that it can be written as: $\langle \vec{\delta} \rangle = \vec{0}$.

For the impact n, we can write: $\overrightarrow{AP_n} = \overrightarrow{AP_{n-1}} + \overrightarrow{l_n}$ and $\overline{AP}_n^2 = \overline{AP}_{n-1}^2 + \vec{l}_n^2 + 2 l_n AP_{n-1} \cos\theta_{n-1}$, where l_n and AP_{n-1} are the modules

of the vectors $\overrightarrow{l_n}$ and $\overrightarrow{AP}_{n-1}$, and where θ_{n-1} designates the angle of vectors $\overrightarrow{l_n}$ and $\overrightarrow{AP}_{n-1}$.

The average $\left\langle \overrightarrow{AP}_n^2 \right\rangle$ can be expressed by the relationship:

$$\left\langle \overrightarrow{AP}_n^2 \right\rangle = \left\langle \overrightarrow{AP}_{n-1}^2 \right\rangle + \left\langle \vec{l}_n^2 \right\rangle + \left\langle 2 l_n AP_{n-1} \cos\theta_{n-1} \right\rangle$$

The variables l_n and θ_{n-1} are independent. Taking isotropy into account, $\langle \cos\theta_{n-1} \rangle = 0$ and $\langle 2 l_n AP_{n-1} \cos\theta_{n-1} \rangle = 0$. The average $\left\langle \vec{l}_n^2 \right\rangle = \left\langle l_n^2 \right\rangle$ is independent of *n*.

Let us take $\left\langle l_n^2 \right\rangle = 3\bar{l}^2$. $\left\langle \overrightarrow{AP}_n^2 \right\rangle = \left\langle \overrightarrow{AP}_{n-1}^2 \right\rangle + 3\bar{l}^2$ and *N* being the total number of impacts (including the first at A), then:

$$\left\langle \overrightarrow{AP}_N^2 \right\rangle = \left\langle \overrightarrow{AP}_{N-1}^2 \right\rangle + 3\bar{l}^2 = \left\langle \overrightarrow{AP}_{N-2}^2 \right\rangle + 2.3\bar{l}^2 = \cdots = (N-1).3\bar{l}^2$$

Now take:

$$\left\langle \bar{\delta}^2 \right\rangle = \left\langle \overrightarrow{AB}^2 \right\rangle = \left\langle \overrightarrow{AP}_N^2 \right\rangle = 3(N-1)\bar{l}^2$$

where t_c is the "collision time" that represents the average time between two successive impacts, which is a characteristic of the environment.

The time elapsed between the departure from A and the arrival at B being *t*, we have:

$$N - 1 = t/t_c \ .$$

From this we deduce that:

$$\bar{\delta}^2 = 3t/t_c \bar{l}^2$$

If x, y and z are displacements of the particle during time t and along the three orthogonal axes, we can write:

$$\bar{\delta}^2 = x^2 + y^2 + z^2$$

Taking isotropy into account,

$$\langle x \rangle = \langle y \rangle = \langle z \rangle = 0$$

and:

$$\left\langle x^2 \right\rangle = \left\langle y^2 \right\rangle = \left\langle z^2 \right\rangle = \frac{1}{3}\bar{\delta}^2 = \frac{t}{t_c}\bar{l}^2 = 2Dt \qquad [6.1]$$

where D is the *diffusion coefficient* defined by the relationship:

$$D = \frac{\bar{l}^2}{2t_c} \qquad [6.2]$$

In the case of the diffusion of a solute in a liquid, Einstein supposes that the Stockes relationship (equation [2.5]) applies to particles subject to Brownian movement and to a force of viscosity in the fluid in which they are moving. By linking the diffusion of particles and viscous dissipation, he establishes the relationship:

$$D = \frac{k_B T}{6\pi\mu r v} \qquad [6.3]$$

where:

– μ is the dynamic viscosity of the fluid;

– r is the radius of the diffusing particle;

– T is the absolute temperature (K); and

– k_B is the Boltzmann constant ($1.380 \times 10^{-0s}\,\mathrm{J.K^{-1}}$).

This relationship is used, for example, to estimate the self-diffusion coefficient of water (the diffusion of water in water). By assimilating water molecules into spheres 28 nm in diameter and taking the value of the dynamic viscosity of water at 20°C as 10^{-3} Pa.s, relationship [6.3] leads to a diffusion coefficient of 1.5×10^{-9} m^2/s, a value fairly close to the measured value (2×10^{-9} m^2/s).

In the case of gases, it is possible to estimate the diffusion coefficient. $\bar{l}$ is the average distance traveled by a molecule (or an atom)[1] of gas between two successive impacts. This is called the "mean free path"[2] and is often written as $\bar{\lambda}$. According to calculation hypotheses, different expressions are proposed, but the orders of magnitude remain similar. For example, relationship [6.4] can be demonstrated as part of the kinetic theory of gases for molecules that are supposed to be rigid and spherical. At pressure P and temperature T:

$$\bar{\lambda} = \frac{RT}{\sqrt{2}\pi d^2 N_A P} = \frac{k_B T}{\sqrt{2}\pi d^2 P} \qquad [6.4]$$

In this relationship:

– N_A is Avogadro's number (6×10^{23} mol^{-1});

– d is the "diameter" of the molecules;

– k_B is the Boltzmann constant; and

– R is the gas constant.

For example, in the case of oxygen ($d = 4 \times 10^{-10}$ m) under normal conditions of temperature and pressure, the mean free path is in the order of 60 nm.[3]

---

1 We are still generally referring to "particles" here.

2 In liquids, the mean free path is estimated to be around 0.1 nm.

3 The kinetic theory of gases allows us to introduce the viscosity μ of a gas in the expression of the mean free path, which is then expressed as $\bar{\lambda} = \frac{\mu}{P}\sqrt{\frac{\pi RT}{2M}}$, where M is the molar mass of the gas being considered.

The kinetic theory of gases allows us to express t_c at pressure P and temperature T:

$$t_c = \frac{\sqrt{mk_B \frac{T}{3}}}{P\sigma} \ .$$

In this relationship, m is the mass of the gas molecule and σ is the effective collision cross-section[4].

For oxygen ($m = 5.3 \times 10^{-26}$ kg, $r = 0.2$ nm), the collision time is equal to 1.6×10^{-10} s. The diffusion coefficient D, estimated according to relationship [6.2], is thus equal to 1.5×10^{-5} m^2/s, a value close to that measured.

6.1.1.2. *The case of metals*

In metals, diffusion occurs in successive jumps by atoms from an initial position to another free position in the lattice (lacuna or interstitial site). These jumps require activation energy, Q_a. It can be shown that diffusion depends on the relationship between this activation energy and the thermal agitation, k_BT, and the diffusion coefficient is given by the relationship:

$$D = D_0 \cdot \exp\left(-\frac{Q_a}{k_BT}\right) \qquad [6.5]$$

Diffusion coefficients in gases, liquids and solids have very different orders of magnitude (10^{-5} m^2/s, 10^{-9} m^2/s and 10^{-30} m^2/, respectively). Tables 6.1 and 6.2 give some values.

4 In order for there to be a collision between two molecules a and b, the center of molecule b must be inside the effective area of collision of the molecule. For example, for the collision of two identical spherical molecules of radius r, the effective collision cross-section is $\sigma = 4r^2$

Type of gas	Temperature (°C)	D (m^2/s)
Hydrogen	0	6.34×10^{-5}
Water vapor	8	2.39×10^{-5}
Oxygen	0	1.78×10^{-5}
Alcohol vapor	40	1.37×10^{-5}

Table 6.1. *Diffusion coefficient of the different gases in air [TOU 05]*

Diffusing species	Molar mass (g)	Radius (nm)	D (m^2/s)
Water	18	0.15	2.0×10^{-9}
Oxygen	32	0.2	1.0×10^{-9}
Glucose	180	0.5	6.7×10^{-10}
Hemoglobin	68,000	3.1	6.9×10^{-11}
Tobacco mosaic	5×10^7		3.9×10^{-10}

Table 6.2. *Diffusion coefficients in water at 15°C [TOU 05]*

6.1.2. *Diffusion and transport of matter at the macroscopic level: Fick's first law*

Imagine the particles of species A dispersed homogeneously in a fluid B at an initial time (see Figure 6.2). Under the effect of Brownian movement, each particle of A is displaced by diffusion. These displacements occur in all directions and if we observe any type of vertical plan, on average as many particles of A cross the plane per unit of time from left to right as from right to left. At the macroscopic level, the diffusion of particles does not result in the transport of species A into B.

On the other hand, if there is a concentration gradient at the initial state, diffusion results in transport at the macroscopic level, see Figure 6.3. This transport occurs in the sense of decreasing concentrations, and ends by homogenizing particles of A within fluid B.

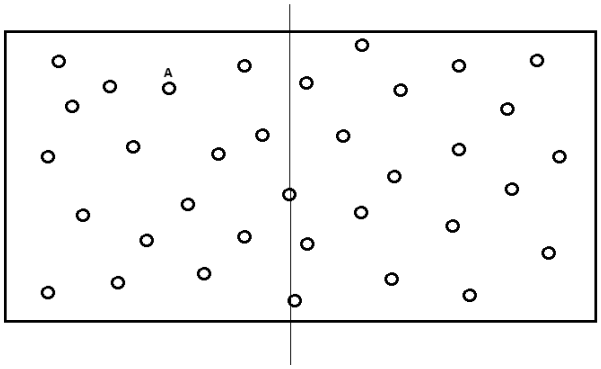

Figure 6.2. *Diffusion in a homogeneous environment: the displacement of particles does not result in the transport of matter at the macroscopic level*

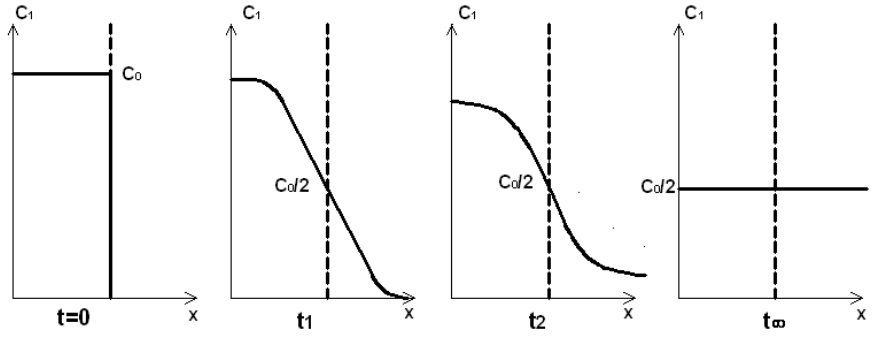

Figure 6.3. *Under the effect of a concentration gradient, the macroscopic transport of matter occurs, which tends to homogenize the concentrations of particles in the fluid*

In Figure 6.3, the overall transport of particles of A can be analyzed in the following manner: impacts and changes in direction due to Brownian movement are more numerous in the more concentrated area. Overall transport toward the less concentrated area can be explained by the displacement of matter toward an area where the lower number of impacts reduces the possibilities of change in direction and of a return toward the more concentrated area.

Transport under a concentration gradient is described by a phenomenological law ascribed to Fick and generally referred to as *Fick's first law*:

$$\vec{J} = -D \cdot \overrightarrow{grad\, c} \qquad [6.6]$$

Here:

– $\vec{J}$ represents the flow of the diffusing species;

– c is its concentration; and,

– by definition, D is the diffusion coefficient.

This law was established experimentally in 1855 by Adolph Fick, who showed the proportionality relationship between the flux of sodium chloride in a solution in water, and the concentration in solute [FIC 55].

More generally speaking, in addition to the concentration gradient, the displacement of matter in direction x can also be due to the action of an exterior transport force. Under the effect of this external force, particles are displaced at an average speed $\langle v \rangle$, which causes a flow equal to $\langle v \rangle c$.

Fick's first law can thus be written as:

$$J = -D\frac{\partial c}{\partial x} + \langle v \rangle c \qquad [6.7]$$

6.1.3. *A thermodynamic approach to molecular diffusion*

Molecular diffusion can be analyzed using thermodynamic considerations, as it has been demonstrated that we can apply perfect gas kinetics to molecules in solution. The chemical potential μ_i of a molecular species i in solution, equal to Gibbs free energy, can be written as follows [BOC 70]:

$$\mu_i = \left(\frac{\partial G}{\partial n_i}\right) = \mu_{i0} + RT \ln\left(a_i\right) \qquad [6.8]$$

where:

– μ_{i0} is the standard chemical potential of species i – i.e. the chemical potential in an infinitely diluted solution;

– R is the gas constant;

– T is the temperature;

– a_i is the ionic activity equal to $\gamma_i c_i$ where c_i is the concentration of species i in solution; and

– γ_i is the activity coefficient of the solution.

For an ideal solution, as in the case of an infinitely diluted solution, the activity coefficient of the solution is equal to 1 and equation [6.8] becomes:

$$\mu_i = \mu_{i0} + RT \ln(c_i) \qquad [6.9]$$

If a concentration gradient exists in direction x, it is possible to define a chemical potential force F_i at the source of the displacement of the molecules:

$$F_i = -\left(\frac{\partial \mu_i}{\partial x}\right)_{P,T} = -\frac{RT}{c_i}\left(\frac{\partial c_i}{\partial x}\right)_{P,T} \qquad [6.10]$$

The second principle of thermodynamics involves the existence of a flow of matter, proportional to force F_i, which helps to re-establish equilibrium:

$$J_i = \frac{D_i c_i}{RT} F_i \qquad [6.11]$$

Placing equation [6.10] into [6.11], we get:

$$J_i = -D_i \frac{\partial c_i}{\partial x} \qquad [6.12]$$

This expression is Fick's first law, which is valid in the case of an infinitely diluted solution. It is applicable in the case of molecular diffusion[5]. More generally, we can express flow as follows:

$$\vec{J}_i = -D_i \cdot \overrightarrow{grad\, c_i} \qquad [6.13]$$

6.1.4. *The diffusion of ions in solution*

6.1.4.1. *The Nernst-Planck relationship*

The diffusion of ions in a solution is frequently described by Fick's first law, which was established experimentally by studying the transport of solute under a concentration gradient.

In a solution, however, an ionic species is never alone. There are always at least the counter-ions of the salt that establish the electroneutrality of the solution. For example, in the experiments carried out by Adolph Fick, Na^+ and Cl^- ions are associated, and the measurement of ionic flows concerned the two ions at once, which were displaced simultaneously in the solution. Since the diffusion coefficient of the Na^+ ion in water is smaller than that of the Cl^- ion, if we base our reasoning on Fick's law, a gradient in sodium chloride should result in a smaller transport of Na^+ ions. This is impossible, because the electroneutrality must be satisfied at all points of the solution. We must consider that in their displacement, in addition to the force of chemical potential, ions that are electrically charged undergo an electric potential force that, in this case, accelerates the sodium ions and slows down the Cl^- ions. The schema in Figure 6.4 takes into account the coupling between ionic species: we say that a *liquid junction potential* ensures coupling between ions.

To describe ionic diffusion, it is useful to introduce a potential different to the one defined in relationship [6.2]. We use an electrochemical potential that is the sum of a chemical potential and an electric potential [BOC 70]:

---

5 To characterize the properties of diffusion in cementitious materials, some laboratories measure the diffusion coefficient of tritiated water. Tritiated water is water in which the hydrogen is replaced by the radioactive isotope tritium, which allows its movement to be observed. The measurements consist of following the diffusion of the radioactive water molecules in the water. This is molecular diffusion.

$$\mu_{EC,i} = \mu_i + z_i F \Psi \qquad [6.14]$$

where:

– μ_i is the chemical potential defined by relationship [6.7];

– z_i is the valency of the ion;

– F is Faraday's constant; and

– Ψ is the local electric potential (liquid junction potential).

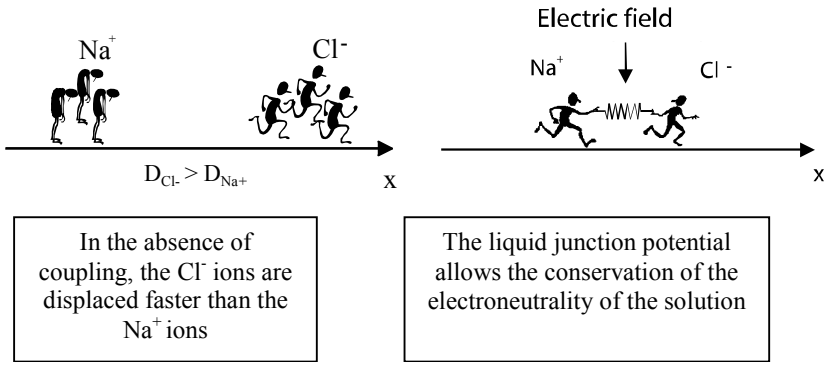

Figure 6.4. *Schematic representation of coupling between ions and counter-ions in their diffusion [TRU 00]*

The flow of species *i* can be described as the result of the action of a force derived from the electrochemical potential of species *i*. In fact, flow calculation is more complex. It depends not only on the electrochemical potential of species *i*, but also on the electrochemical potentials of the other species present in the solution. For standard solutions with a concentration lower than 3,000 mol.l^{-1}, the expression of *i* ion flow can be described by the following simplified equation:

$$J_i = -\frac{D_i c_i}{RT} grad\, \mu_{EC,i} = -D_i c_i grad(\ln a_i) - \frac{z_i F D_i c_i}{RT} grad \Psi \qquad [6.15]$$

In the case of an ideal solution, activity a_i is equal to concentration c_i and the preceding equation becomes:

$$J_i = -D_i grad c_i - \frac{z_i F D_i c_i}{RT} grad\Psi \qquad [6.16]$$

This expression is the *Nernst-Planck relationship*. Its analytical solution is not simple, since it requires knowledge of the local electric potential, which depends on the concentration of all of the different species present.

In order to be able to solve this equation, a numerical approach is necessary, since it allows us to address all of the species present simultaneously. This numerical method is developed in a so-called "multi-species" approach, which we will not explore in detail here, but which can be consulted in various references ([TRU 00] and [NGU 07], for example). This approach is illustrated in Figure 6.5, which again uses the case of the diffusion of sodium chloride previously shown. In this example, a solution of 500 moles of NaCl per m^3 is placed at the edge of a water blade. The two outside curves represent the profiles of chloride and sodium in solution in the water after five days of exposure, supposing that Fick's law describes diffusion[6]. As indicated above, in this hypothesis, the Cl^- ions penetrate the solution more rapidly. The middle curve is calculated on the basis of the multi-species approach, supposing that the Nernst-Planck law is applicable. This description is the best one since, in fact, the two species are simultaneously displaced.

In his original experiments, Fick defined the diffusion coefficient of sodium chloride, and consequently the law he proposed is perfectly justified. The description of the flow of chloride is, however, related to the junction potential due to the presence of counter-ions; in this case sodium. In the presence of potassium, for example, Cl^- ions are displaced more rapidly because the diffusion coefficient of potassium is higher than that of sodium.

In general, the description of the transport of an ionic species using the multi-species approach requires us to solve a system of n equations, with n being the number of ionic species present in the solution, and knowledge of the diffusion coefficients of these n species. This is no simple matter,

6 The method of calculation of the profile is explored in section 6.1.6.

especially when we are addressing the case of diffusion in a porous medium, since the determination of the various effective diffusion coefficients is very complicated. In practice, the description of ionic diffusion continues to be done using Fick's law. This involves disregarding the electric contribution in the Nernst-Planck relationship [6.16]. Exercise 6.1 illustrates the joint diffusion of Cl^- and Na^+ ions.

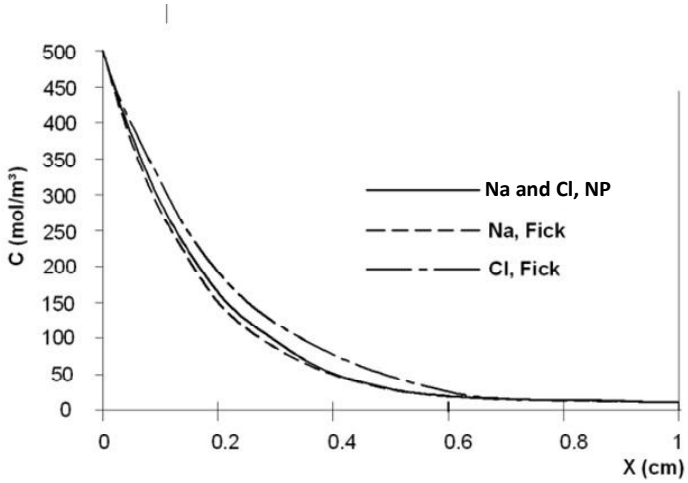

Figure 6.5. *Profiles of Cl^- and Na^+ ions in solution calculated using a multi-species approach (the curve labeled NP is the Nernst-Planck curve) or assuming that Fick's law is applicable*

6.1.4.2. *The Nernst-Einstein relationship*

According to the general expression of Fick's first law (equation [6.7]), the flow of matter can stop if the external transport force is such that the two flows become equal and opposite. If we consider, in a unidirectional approach, that the transport force f is derived from a potential: $f = -\frac{d\Psi}{dx}$, the concentration profile of the species considered must follow a Boltzmann distribution law at thermodynamic equilibrium:

$$c_i = A \cdot \exp - \frac{\Psi(x)}{kT} \qquad [6.17]$$

This relationship must be the solution of equation [6.7]. Deriving expression [6.17] from this, we get:

$$\frac{dc_i}{dx} = -\frac{c_i}{kT} \cdot \frac{d\Psi}{dx} = \frac{c_i f}{kT} \qquad [6.18]$$

Combining this with equation [6.7] for a resulting flow of zero, we can write the *Nernst-Einstein relationship:*

$$\frac{\langle v \rangle}{D_i} = \frac{f}{kT} \qquad [6.19]$$

Fick's first law must therefore be written in the general form:

$$J_i = -D_i \frac{dc_i}{dx} + \frac{D_i f c_i}{kT} \qquad [6.20]$$

In the case of an electrical field, E, applied to ionic species of valency, z_i, the force applied to ions of charge, q_i, is:

$$f = q_i E = z_i e E = z_i \frac{F}{N_A} E = z_i \frac{Fk}{R} E$$

from which we get the new expression of relationship [6.20]:

$$J_i = -D_i \frac{dc_i}{dx} + \frac{z_i F D_i c_i}{RT} E = -D_i \frac{dc_i}{dx} + \frac{z_i F D_i c_i}{RT} \frac{d\Psi}{dx} \qquad [6.21]$$

Thus, we obtain the Nernst-Planck relationship once more.

6.1.5. *Fick's second law*

Fick's second law is a balance equation. It states that an increase in the quantity of species considered in the unit of volume is due to flows entering

and leaving by surfaces limiting this volume, and to sources (or losses) of existing matter in this volume.

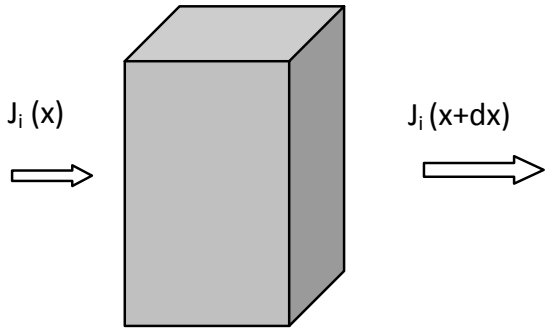

The balance equation (also called the continuity equation) applied to a volume of solution located at abscissa x with thickness dx in which there is production of matter, P_v[7], per unit of time and per unit of volume, is written as:

$$\frac{\partial c_i}{\partial t} = -\frac{\partial J_{ix}}{\partial dt} + P_v \qquad [6.22]$$

If we express the flow using Fick's first law, if there is no production of matter, and if D is independent of x (a homogeneous medium), we obtain *Fick's second law*:

$$\frac{\partial c_i}{\partial t} = D\frac{\partial^2 c_i}{\partial x^2} \qquad [6.23]$$

More generally, the continuity equation can be written as:

$$\frac{\partial c_i}{\partial t} - D \cdot div\vec{J}_i = P_v \qquad [6.24]$$

7 The term 'production' can be positive (for source) or negative (for consumption).

6.1.6. *The concentration profile of diffusing species*

To understand the spatial distribution of diffusing species, Fick's second law must be solved. The solution depends on the initial conditions and on the boundary conditions of the problem being addressed. A brief explanation is provided here for some simple cases. In general, the solution to Fick's second law can be written in the form of a series of error functions or as a trigonometric series.

For more complicated cases and a more in-depth description, the reader may refer to Crank's book [CRA 75], which inspired the following demonstrations.

Three methods can be used to integrate Fick's second law:

– the reflection and superposition method;

– the method of separation of variables; and

– the Laplace transformation method.

In the following, we will illustrate these three methods using a simple example, and then we will give the solution to Fick's second law in some practical cases of diffusion problems encountered in civil engineering.

6.1.6.1. *Reflection and superposition method*

First, let us imagine the case of an instantaneous flat source: at the initial time, the diffusing species is concentrated along the length of a plane at abscissa $x = 0$ and then diffuses throughout the plane. We can verify by differentiation that the function:

$$c = \frac{A}{\sqrt{t}} \exp - \frac{x^2}{4Dt} \qquad [6.25]$$

In this relation, A is an arbitrary constant that c is the solution to Fick's second law without the production of matter.

The quantity of matter, M, being diffused in a cylinder of infinite length, and of section equal to the unit, is given by the relationship:

$$M = \int_{-\infty}^{+\infty} c\,dx \qquad [6.26]$$

writing:

$$x^2/4Dt = \xi^2 ,$$

$$dx = 2\sqrt{Dt}\,d\xi$$

and:

$$M = 2A\sqrt{D}\int_{-\infty}^{+\infty} \exp(-\xi^2)d\xi = 2A\sqrt{\pi D} \qquad [6.27]$$

Expression [6.26] shows that the quantity of diffusing matter remains constant and equal to that initially present in the plane (x = 0). By substituting this value in equation [6.26], we get the solution to Fick's second law, which describes the dispersion by diffusion of a quantity M, of species present at time t = 0 in a plane (x = 0):

$$c = \frac{M}{\sqrt{4\pi Dt}}\exp(-\frac{x^2}{4Dt}) \qquad [6.28]$$

Figure 6.6 illustrates this result.

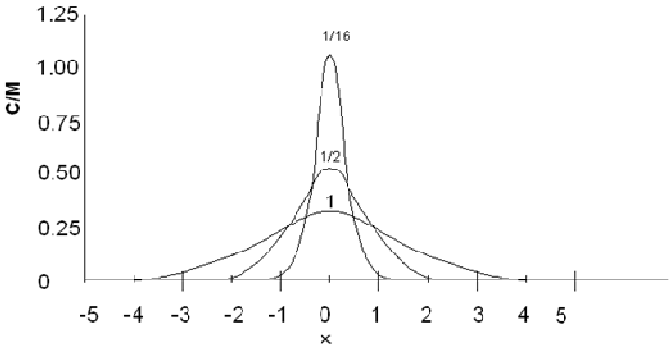

Figure 6.6. *Instantaneous flat source: variation of concentration depending on distance. The numbers opposite the curves are the values of product Dt*

To illustrate this reflection superposition method, now imagine that, in the preceding case, the species diffuses only on the positive side of x. We can imagine that the part that diffuses from the negative side of x is reflected on the plane $x = 0$ and superimposed on the part that diffuses in the positive side of x. Since the concentration distribution was symmetrical compared to $x = 0$ in the initial case, the concentration for the semi-infinite case is given by the relationship:

$$c = \frac{M}{\sqrt{\pi Dt}} \exp(-\frac{x^2}{4Dt}) \qquad [6.29]$$

6.1.6.2. *Method of separation of variables*

A classic method of solving an equation with partial derivatives consists of assuming that the variables can be separated. This leads us to seek a solution to Fick's second law in the form:

$$c = X(x).T(t) \qquad [6.30]$$

Applying this to [6.26], we get:

$$X\frac{dT}{dt} = DT\frac{d^2X}{dx^2} \ ,$$

which can be written as:

$$\frac{1}{T}\frac{dT}{dt} = \frac{D}{X}\frac{d^2X}{dx^2} \qquad [6.31]$$

The two parts of the equation must be equal to the same constant, which can be written as $-\lambda^2 D$. Thus we get:

$$\frac{1}{T}\frac{dT}{dt} = -\lambda^2 D \qquad [6.32]$$

and

$$\frac{1}{X}\frac{d^2X}{dx^2} = -\lambda^2 \qquad [6.33]$$

the solutions to which are:

$$T = e^{-\lambda^2 Dt} \qquad [6.34]$$

and

$$X = A\sin\lambda x + B\cos\lambda x \qquad [6.35]$$

which leads to the solution of [6.26]:

$$c = (A\sin\lambda x + B\cos\lambda x)\exp(-\lambda^2 Dt) \qquad [6.36]$$

where A and B are integration constants.

Equation [6.23] being linear, the most general solution is obtained by adding together the solutions of type [6.36], or:

$$c = \sum_{m=1}^{\infty}(A_m \sin\lambda_m x + B_m \cos\lambda_m x)\exp(-\lambda_m^2 Dt) \qquad [6.37]$$

where A_m and B_m are determined by the initial and boundary conditions.

Let us consider diffusion across a parallel blade of thickness L in which the solute is uniformly concentrated ($c = c_0$) at the initial time, and the surfaces of which are maintained at zero concentration. The initial and boundary conditions can be written as:

$$t = 0, \quad 0 < x < L, \quad c = c_0$$
$$t > 0, c = 0 \quad \text{for} \quad x = 0 \quad \text{and} \quad x = L$$

The boundary condition implies that:

$$B_m = 0 \quad \text{and} \quad \lambda_m = \frac{m\pi}{L}$$

The initial condition becomes:

$$c_0 = \sum_{m=1}^{\infty}(A_m \sin\frac{m\pi x}{L}), 0 < x < L \qquad [6.38]$$

By multiplying the two parts of equation [6.38] by $sin(p\pi x/L)$ and integrating from 0 to L using the following expressions:

$$\int_0^L sin\frac{p\pi x}{L} sin\frac{m\pi x}{L} dx = \begin{cases} 0 si\, m \neq p \\ L/2 si\, m = p \end{cases},$$

the final solution, substituting m by $2n+1$ so that the successive values of n are 0, 1, 2, etc., can be written as:

$$c = \frac{4c_0}{\pi} \sum_1^\infty \frac{1}{2n+1} \exp\left[-D(2n+1)^2 \frac{\pi^2 t^2}{L^2}\right] \sin\frac{(2n+1)\pi x}{L} \qquad [6.39]$$

6.1.6.3. *The Laplace transformation method*

Take $f(t)$, a known function of t for $t>0$. The Laplace transform $\overline{f}(p)$ of $f(t)$ is defined by:

$$\overline{f}(p) = \int_0^\infty e^{-pt} f(t)\, dt \qquad [6.40]$$

where p is sufficiently large for the integral [6.40] to converge. In the following, we will simply consider it to be a real positive. For example, if $f(t) = e^{2t}$, p must be larger than 2. The Laplace transforms of standard functions are obtained by integrating [6.40] as in the following examples:

$$f(t) = 1, \quad \overline{f}(p) = \int_0^\infty e^{-pt} dt = \frac{1}{p} \qquad [6.41]$$

$$f(t) = e^{at}, \qquad \overline{f}(p) = \int_0^\infty e^{-pt} e^{at} dt = \int_0^\infty e^{-(p-a)t} dt = \frac{1}{p-a} \qquad [6.42]$$

$$f(t) = \sin \omega t, \qquad \overline{f}(p) = \int_0^\infty e^{-pt} \sin \omega t\, dt = \frac{\omega}{\omega + p} \qquad [6.43]$$

Lists of Laplace transforms can be found in mathematics books.

We will illustrate this method with an important case, that of the semi-infinite medium. This case corresponds to the penetration of a species by diffusion into a material that it is in contact with via a flat face. The term "semi-infinite" means in a practical sense that during the time considered, the diffusing species does not reach the face opposite the entry face. In this problem, we will consider that the concentration is kept constant on the entry face and is initially zero in the material being considered.

We will therefore seek a solution to Fick's second law [6.23], respecting the following boundary conditions:

$$c = c_0 \quad \text{where} \quad x = 0 \ \text{ and } \ t > 0 \qquad [6.44]$$

and the initial condition:

$$c = 0 \quad \text{where} \quad x > 0 \ \text{ and } \ t = 0 \qquad [6.45]$$

By multiplying the two terms of relationship [6.23] by e^{-pt} and integrating with respect to t from 0 to infinity, we get:

$$\int_0^\infty e^{-pt} \frac{\partial^2 c}{\partial x^2} dt - \frac{1}{D} \int_0^\infty e^{-pt} \frac{\partial c}{\partial t} dt = 0 \qquad [6.46]$$

For the functions considered here, we can suppose that the order of differentiation and integration can be inverted. Therefore, we can write:

$$\int_0^\infty e^{-pt} \frac{\partial^2 c}{\partial x^2} dt = \frac{\partial^2}{\partial x^2} \int_0^\infty c e^{-pt} dt = \frac{\partial^2 \bar{c}}{\partial x^2} \qquad [6.47]$$

Integrating by parts, we get:

$$\int_0^\infty e^{-pt} \frac{\partial^2 c}{\partial x^2} dt = \left[c e^{-pt} \right]_0^\infty + p \int_0^\infty c e^{-pt} dt = p\bar{c} \qquad [6.48]$$

since the term between square brackets is zero at $t = 0$ due to the initial condition [6.45] and at $t = \infty$ due to the exponential term. Consequently, Fick's second law is reduced to:

$$D\frac{\partial^2 c}{\partial x^2} = p\bar{c} \qquad [6.49]$$

Treating boundary condition [6.44] in an analogous manner, we get:

$$\bar{c} = \int_0^\infty e^{-pt}dt = \frac{c_0}{p}, \quad x = 0 \qquad [6.50]$$

The solution to equation [6.49] that satisfies [6.50], and for which $\bar{c}$ remains finite when x approaches infinity, is:

$$\bar{c} = \frac{c_0}{p}e^{-\sqrt{\frac{p}{D}}x} = \frac{c_0}{p}e^{-qx} \qquad [6.51]$$

Referring to the Laplace transforms tables, the function for which the transformed curve is given by relationship [6.51] is:

$$c = c_o erfc\frac{x}{2\sqrt{Dt}} \qquad [6.52]$$

where:

$$erfc\, z = 1 - erf\, z \quad \text{and} \quad erf\, z = \frac{2}{\sqrt{\pi}}\int_0^z e^{-\eta}d\eta \qquad [6.53]$$

It is easy to verify that [6.53] verifies [6.23], [6.44] and [6.45]. This is the solution to the problem of diffusion in a semi-infinite medium.

NOTE 6.1.– the use of the Boltzmann transformation.

The Boltzmann transformation presented below is also used to solve Fick's second law. In equation:

$$K\left(\frac{\partial^2 c}{\partial x^2}\right)=\frac{\partial c}{\partial t} \qquad [6.54]$$

the Boltzmann transformation consists of putting:

$$\alpha=\frac{x}{2\sqrt{t}}. \qquad [6.55]$$

We can write:

$$\frac{\partial c}{\partial x}=\frac{\partial c}{\partial \alpha}\frac{\partial \alpha}{\partial x}=\frac{1}{2\sqrt{t}}\frac{\partial c}{\partial \alpha}$$

and

$$\frac{\partial^2 c}{\partial x^2}=\frac{\partial}{\partial x}\left(\frac{\partial c}{\partial x}\right)=\frac{1}{2\sqrt{t}}\frac{\partial}{\partial x}\left(\frac{\partial c}{\partial \alpha}\right)=\frac{1}{2\sqrt{t}}\frac{\partial \alpha}{\partial x}\frac{\partial^2 c}{\partial \alpha^2}=\frac{1}{4t}\frac{\partial^2 c}{\partial \alpha^2}$$

$$\frac{\partial c}{\partial t}=\frac{\partial c}{\partial \alpha}\frac{\partial \alpha}{\partial t}=\frac{-x}{4t\sqrt{t}}\frac{\partial c}{\partial \alpha}=\frac{-\alpha}{2t}\frac{\partial c}{\partial \alpha}$$

by replacing:

$$K\left(\frac{1}{4t}\frac{\partial^2 c}{\partial \alpha^2}\right)=\frac{-\alpha}{2t}\frac{\partial c}{\partial \alpha}$$

in equation [6.54], from which we get:

$$K\frac{\partial^2 c}{\partial \alpha^2}=-2\alpha\frac{\partial c}{\partial \alpha} \qquad [6.56]$$

Equation [6.56] is independent of x and of t, which means that for a given value of x, c varies in $\sqrt{t}$ in a semi-infinite medium.

6.2. Diffusion in porous media

In the domain of civil engineering, transport by diffusion occurs principally via porous materials. We can cite, for example:

– the penetration of chlorides into concrete immersed in seawater;

– the penetration of CO_2 into concrete; and

– the diffusion of water vapor into the walls of buildings.

Concrete is a heterogeneous material made up of solids (aggregates and hardened cement paste), liquid (interstitial water) and humid air (if the concrete is not saturated). *A priori*, the transport of gases such as CO_2 can occur in these three parts, while ions can be displaced in the liquid and solid phases. The difference between diffusion coefficients in liquids and solids being of 11 orders of magnitude, and there being four orders of magnitude between gases and liquids, the flows are very different. In practice, we can consider that ions diffuse in the water contained in pores, and that CO_2 penetrates through empty pores or in water, if the concrete is saturated.

In this chapter, we are considering molecular diffusion and ionic diffusion in porous media in which the pores contain a liquid phase. Gas diffusion in porous media is presented at the end of the chapter.

6.2.1. *Molecular diffusion*

In an infinite environment (liquid, gas, solution and solid), the process is characterized by the diffusion coefficient D defined by *Fick's first law*:

$$J_i = -D_i \frac{\partial c_i}{\partial x} \qquad [6.57]$$

where J_i is the flow of the constituent i in direction x and $\frac{\partial c_i}{\partial x}$ is its concentration gradient in this direction. The diffusion coefficient is characteristic of the diffusing species, the medium in which it is diffused and temperature.

In a pore, particles can collide with the walls. This disturbs transport in the direction of the concentration gradient. The flow, written as J_i^*, is still expressed by Fick's first law, but the diffusion coefficient D_i^* is smaller than the diffusion coefficient in the infinite environment D_i :

$$J_i^* = -D_i^* \frac{\partial c_i}{\partial x} \qquad [6.58]$$

In a porous medium, transport is described with the help of the effective flow $J_{e,i}$, which represents the quantity of the constituent that traverses the porous medium per unit of time and per unit of cross section of the matter in direction x. This flow remains proportional to the concentration gradient of the species in the support phase in which it diffuses (the liquid contained in the pores) and the proportionality coefficient is given by Fick's first law applied to a porous material:

$$J_{e,i} = -D_{e,i} \frac{\partial c_i}{\partial x} \qquad [6.59]$$

$D_{e,i}$ is called the *effective diffusion coefficient* and depends on the diffusing species, the support phase, the porous structure of the material, and the temperature. It also depends on the degree of saturation. Next, we will initially consider that the porous medium is saturated by the support phase.

Diffusion coefficients are expressed in m^2/s.

Physical models link the effective diffusion coefficient, $D_{e,i}$, of a given constituent i to the diffusion coefficient D_i of this same constituent in the phase filling the pores. The following relationship is sometimes used:

$$D_{e,i} = \frac{\tau\, p_0}{T} D_i \qquad [6.60]$$

In this relationship:

– the constrictivity parameter τ takes into account the effects of the section variation of pores;

– p_0 is the open porosity; and

– T is tortuosity.

This relationship is analogous to the one that defines the formation factor, F. This is relationship [5.12]:

$$F = \frac{\sigma}{\sigma_e} = \frac{D}{D_e}$$

This model shows that, unlike the case of permeability studied in the next chapter, pore size in itself has no influence on the properties of transport by diffusion.

NOTE 6.2.– in general, tortuosity is defined by relationship [5.11]:

$$T = \left(\frac{L_e}{L}\right)^2$$

In the case of diffusion, another definition is sometimes adopted:

$$T = \frac{D_e}{D}$$

This is, therefore, the inverse of the formation factor. This latter definition leads to lower unit tortuosity values, unlike the definition given in [5.11]. Moreover, it involves two measurable quantities.

6.2.2. *Ionic diffusion*

The relationship giving the effective flow of an ionic species *i* in a porous medium is established in a manner analogous to the Nernst-Planck law:

$$J_{e,i} = -D_{e,i}\frac{\partial c_i}{\partial x} - \frac{z_i F}{RT} D_{e,i} c_i \frac{\partial \Psi}{\partial x} \qquad [6.61]$$

In the following, we will describe ionic diffusion using Fick's law instead of Nernst-Planck's law (see section 6.1.4). The errors that result from this are not very important, but certain results obtained which may appear abnormal are unexplainable without considering that Fick's law is only a simplification. We will return to this subject later in section 6.3, which is dedicated to the measurement of the effective diffusion coefficient.

6.2.3. *The penetration kinetic of a species by diffusion: Fick's second law*

If the volume element considered is a volume of porous material saturated by the support phase. The continuity equation is written as[8]:

$$\frac{\partial C}{\partial t} = -\frac{\partial J_e}{\partial x} \qquad [6.62]$$

where C represents the concentration of the diffusing species per unit of volume of the porous material. The latter being saturated, we can write $C = p_0 c$ if the entire diffusing constituent is contained in the support phase. This hypothesis corresponds to the case where the constituent being considered is inert with regard to the solid phase. Expressing the effective flow by Fick's first law, we obtain *Fick's second law applied to non-reactive porous material*:

$$\frac{\partial c}{\partial t} = \frac{D_e}{p_0}\frac{\partial^2 c}{\partial x^2} = D_a \frac{\partial^2 c}{\partial x^2} \qquad [6.63a]$$

where D_a is the apparent diffusion coefficient of the porous material.

8 In the measurement wherein we no longer use the multi-species description (in the following), no further confusion is possible with regard to the ion being considered, and we will no longer indicate index "*i*" in the expressions.

In relationships [6.12] and [6.23], which express Fick's two laws in the case of an infinite medium, the proportionality coefficients are the same. In the case of a porous medium, this is not so. The effective diffusion coefficient is used in Fick's first law and the apparent diffusion coefficient in Fick's second law.

Diffusing species sometimes react with the solid. Thus, in the case of concrete, CO_2 reacts with certain hydrates; this is carbonation. Likewise, the hydrates in cement can react with the ionic species present in its environment, such as the Cl^- ions present in seawater, for example. In the latter case, hydrated calcium chloroaluminates are formed. These reactions delay the penetration of species into the concrete, and the preceding laws must be modified in consequence.

In the following, we will consider the specific case of the diffusion of chlorides in concrete. Equation [6.62] can be rewritten considering that the total concentration in diffusing species C is a quantity of total chlorides, C_t. C_t is the sum of two terms, C_l and C_f. C_l is the concentration of free chlorides contained in the interstitial liquid and C_f, the concentrations of the bound chlorides, those which have reacted with the solid.

Concentrations are generally related to the quantities of matter that contain them. Thus, concentrations of free chlorides are expressed in moles (or kg) per m^3 of solution (notation c) and concentrations of bound chlorides are expressed in moles (or kg) per kg of solid (notation $c_{m,f}$). Equation [6.63a] is thus written as:

$$\frac{\partial c}{\partial t} = \frac{D_e}{p_0 + (1-p_0)\rho_s \dfrac{\partial c_{m,f}}{\partial c}} \frac{\partial^2 c}{\partial x^2} = D_a \frac{\partial^2 c}{\partial x^2} \qquad [6.63b]$$

This relationship is *Fick's second law applied to reactive porous matter*. The apparent diffusion coefficient D_a of reactive porous matters depends on the effective coefficient, on the open porosity p_0, and on interactions expressed as the quantity $\dfrac{\partial c_{m,f}}{\partial c}$, called the *binding capacity*, which is the slope of the curve $c_{m,f} = f(c)$, called the *binding isotherm*.

In the case of chlorides, this isotherm is determined by measuring the quantities of chlorides bound by concrete in solutions at different concentrations [ARL 07]. Figure 6.7 shows that this isotherm is not linear, and consequently the apparent diffusion coefficient D_a depends on the concentration.

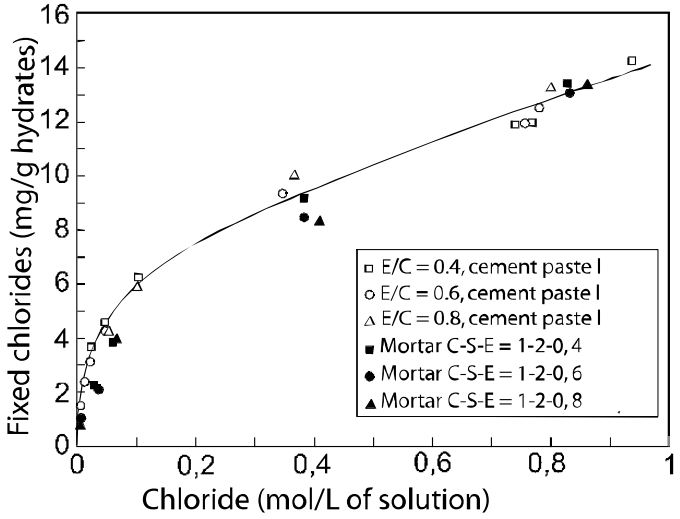

Figure 6.7. *Binding isotherm of chlorides*[9] *[TAN 93]*

An important practical case is that of the penetration of chlorides in seawater into an immersed reinforced concrete structure. The corrosion of the reinforcements in these structures occurs when the chloride concentration against the steel bars reaches a value higher than a certain critical value, c_{cr}, called the initiating corrosion threshold. The prediction of the duration for initiating corrosion is done by determining the time, t_{cr}, at the end of which concentration attains the threshold value, c_{cr}, at a depth, x_p, corresponding to the cover of the reinforcement bars (see Figure 6.8).

9 C, S, and E are the proportions of cement, sand, and water in mortar by weight.

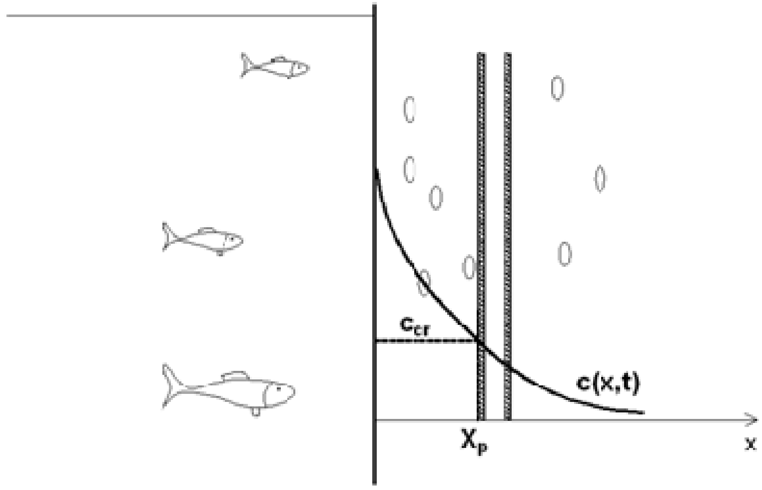

Figure 6.8. *Chloride concentration profile in a reinforced concrete structure immersed in seawater*

Fick's second law, expressed as [6.63], is used to describe the penetration of chlorides in concrete, and its solution $c(x,t)$ allows us to predict the initiating time for initiating the corrosion process. We can consider that the reinforced concrete structure is a semi-infinite wall on the surface of which the chloride concentration of the seawater is constant and equal to c_0. Unlike the case described in section 6.1.6, here diffusion occurs in the interstitial liquid of the concrete.

The diffusion coefficient that is used in Fick's second law is the apparent diffusion coefficient, D_a, rather than the diffusion coefficient, D. If the apparent diffusion coefficient is constant, the resolution method described in section 6.1.6 can be applied identically, and the chloride concentration in the interstitial liquid varies according to the function:

$$c = c_0 erfc \frac{x}{2\sqrt{D_a t}} \qquad [6.64]$$

If the concrete contains chlorides prior to its immersion (at a concentration of c_{in}), relationship [6.64] becomes:

$$c = c_{in} + (c_{in} - c_0)erfc\frac{x}{2\sqrt{D_a t}} \qquad [6.65]$$

This classic relationship is based on a number of hypotheses:

– The penetration of chlorides is described by Fick's second law, which leads us to consider that Cl^- ions are not electrically charged particles.

– The apparent diffusion coefficient given by the relationship $D_a = \frac{D_e}{p_0 + (1-p_0)\rho_s \frac{\partial c_{m,f}}{\partial c}}$. For D_a to be constant, it is necessary for the effective diffusion coefficient, open porosity and density of the solid to be constant (a homogeneous material that is also stable in time), and for the interactions to be zero or linear.

We may consider that these hypotheses are not very realistic, but taking into account the reality of all phenomena is very complex, and the approach proposed above is usually retained. To apply this method, we have to know the apparent diffusion coefficient. In the following section, we will describe the methods used to measure it, as well as those used to obtain the effective diffusion coefficient.

NOTE 6.3.– As we have previously indicated, the chlorides in concrete are present in the interstitial solution (these are referred to as free chlorides) or bound by the solid phases. The sum of these two types of chlorides constitutes what we refer to as the "total chlorides".

Relationship [6.65] pertains to concentrations of free chlorides.

In practice, chloride concentrations in concrete are measured in a sample reduced to powder and then dried. The chlorides are then extracted from the powder by dissolution in water. These are normally representative of the free chlorides contained in the interstitial solution (also referred to as water-

soluble chlorides). The chlorides can also be extracted with an acid attack to determine total chlorides. They are then chemically dosed. Methods of measurement are recommended in France [ARL 07]. The results of the measurements are related to the unit of mass of dry powder; and thus of dry concrete. For example, the total chloride concentration, written as $c_{m,t}$, is related to the concentration C expressed per unit of volume of concrete by the relationship:

$$C = (1 - p_0)\rho_s c_{m,t} \qquad [6.66]$$

In general, initiating corrosion thresholds are expressed in total chlorides. This may seem strange because the corrosion is induced by free chlorides contained in the pore solution. In fact, two reasons can explain this choice. The first is that bound ions are not irreversibly bound, and so they can re-enter solution under the effect of carbonation, for example. The second, practically speaking, is that the measurement of total chloride concentrations is considered more reliable than the measurement of water-soluble chlorides.

In relationship [6.65], which expresses the free chloride concentration profile, all of the concentrations are expressed in the same unit. We can also relate the quantities of free chlorides to the unit of mass of the concrete. To apply this relationship to total chlorides, the concentrations of total chlorides must be proportional to the concentrations of free chlorides. The curve in Figure 6.7 shows that this is not the case. Nevertheless, to obtain relationship [6.65] by integration of Fick's second law, we must suppose that the apparent diffusion coefficient is constant, which implies a linear binding isotherm (or no interactions). We can thus remain consistent with this demonstration by writing relationship [6.65] as:

$$c_{m,t} = c_{m,t,in+}(c_{m,t,in} - c_{m,t,0})erfc\frac{x}{2\sqrt{D_a t}} \qquad [6.67]$$

In this relationship, all of the concentrations are the concentrations of total chlorides, and are expressed in kg (or moles) of chloride per kg of dry concrete. This is natural, since these units correspond to the measurement method being used. This unit must also be that of the chloride concentration of the seawater, which is less usual, since this is generally expressed in kg (or moles) of chloride per m^3 of water.

6.3. Measurement of the effective diffusion coefficient in porous matter

6.3.1. *Diffusion cell method*

The effective diffusion coefficient of ionic species in porous matter is classically measured by means of a diffusion cell, see Figure 6.9. A cylindrical disk of the thickness L of the material to be tested is trapped between two compartments containing a liquid (solvent). The solute is placed in one of the compartments (called the upstream compartment) at concentration c_0 at an initial time. The porous matter is saturated with the solvent, and under the effect of the concentration gradient the solute diffuses toward the downstream compartment. This test is sometimes called a *pure diffusion (or simple diffusion) test* – which is wrong, as we will see later – as opposed to the electric field diffusion test, which will be discussed next.

The initial and boundary conditions of the test are as follows:

$$\forall t, c = c_0 \quad \text{for} \quad x \leq 0 \left(\text{upstream compartment}\right);$$

$$\text{if} \quad t = 0, \quad c = 0 \quad \text{for} \quad x > 0;$$

$$\forall t, \, c = 0 \quad \text{for} \quad x \geq L \left(\text{downstream compartment}\right)$$

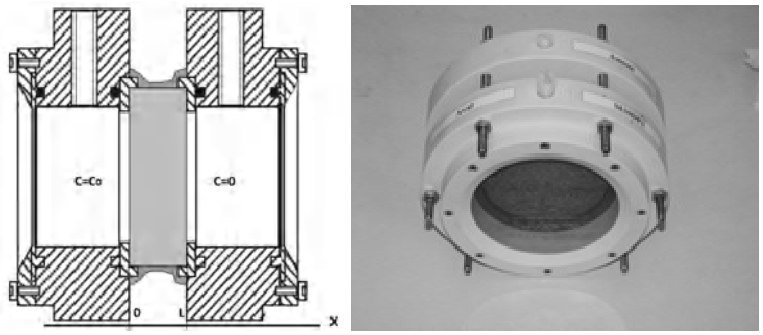

Figure 6.9. *Device for the measurement of the diffusion coefficient: simple diffusion test*

To maintain the boundary conditions, the upstream and downstream solutions are regularly refreshed, and the downstream concentration is measured each time. This device was developed for the measurement of the diffusion coefficient of tritiated water in concrete, and then adapted for the

measurement of the diffusion coefficient of chlorides in concrete [BIG 94, RIC 92].

If we suppose that the binding isotherm between the diffusing species and the material being tested is linear, the binding capacity is a constant called the *distribution coefficient*, written as K_d. By introducing the term $\alpha = p_0 + (1-p_0)\rho_s K_d$, Fick's second law [6.63] can be written as:

$$\frac{\partial c}{\partial t} = \frac{D_e}{p_0 + (1-p_0)\rho_s \dfrac{\partial c_{m,f}}{\partial c}} \frac{\partial^2 c}{\partial x^2} = \frac{D_e}{p_0 + (1-p_0)\rho_s K_d} \frac{\partial^2 c}{\partial x^2}$$
$$\frac{\partial c}{\partial t} = \frac{D_e}{\alpha} \frac{\partial^2 c}{\partial x^2} = D_a \frac{\partial^2 c}{\partial x^2} \qquad [6.68]$$

With the boundary and initial conditions of the cell diffusion test, this differential equation gives the following solution:

$$c(x,t) = c_0 \left[1 - \frac{x}{L} - \frac{2}{\pi} \sum_{n=1}^{\infty} \frac{1}{n} \sin\left(\frac{n\pi x}{L}\right) \cdot \exp\left(-D_e \frac{n^2 \pi^2 t}{\alpha^2}\right) \right] \qquad [6.69]$$

From this, we can deduce the quantity $Q(t)$ of species being diffused in the downstream compartment per unit of area of the disk (see Exercise 6.2). $Q(t)$ tends asymptotically toward the value:

$$Q(t) = \frac{c_0}{L} \left(D_e t - \alpha \frac{L^2}{6} \right) \qquad [6.70]$$

Considering the variation of quantity $\dfrac{QL}{c_0}$ with respect to time, we get a result such as the one in Figure 6.10, relative to the diffusion of chlorides in a cement paste with a *W/C* ratio of 0.3. The curve tends toward an asymptotic regime, the slope of which is equal to the effective diffusion coefficient of the material being tested. The asymptotic limit of the curve

cuts the axis of the abscissa at time $t_r = \frac{\alpha L^2}{6D_e}$, called the *delay time*. The delay time increases with binding between the diffusing species and the material. Having determined the effective diffusion coefficient, it is possible to determine the term K_d from the value of the delay time.

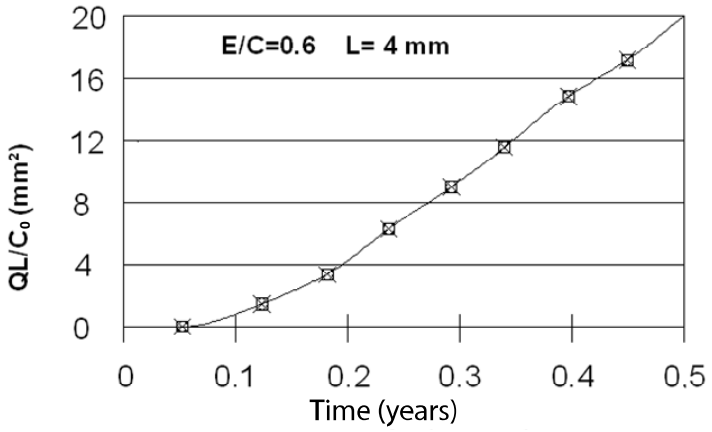

Figure 6.10. *Evolution with time of cumulative quantities of chlorides traversing a disk of cement paste 4 mm in thickness*

The interpretation of this test is based on Fick's second law. The result obtained is a characteristic of the material and of the diffusing species. This is verified, for example, in the case of the diffusion of tritiated water, since the diffusing species is electrically neutral and the binding isotherm with cementitious materials is linear.

The case of chlorides is different. A first illustration of this non-Fickian behavior is given in Figure 6.11. The cumulative quantities of ionic species traversing a disk of cement paste are indicated with respect to time for two types of solutes placed at the same concentration in the upstream compartment: sodium chloride and potassium chloride. The quantity of chlorides traversing the material is higher if potassium chloride is used instead of sodium chloride. By applying relationship [6.70], we find a higher diffusion coefficient of Cl^- ions with potassium chloride, which is incorrect since effective diffusion coefficients are intrinsic values for a given material and species.

Using the analysis from section 6.4.1.1, the diffusion coefficient of potassium being larger than that of sodium, potassium ions traverse the material in larger quantities. On the other hand, they slow the Cl^- ions down less, and the effective diffusion coefficient of chlorides calculated by applying Fick's first law in the case of potassium chloride is higher than that obtained with sodium chloride. This is incorrect, and this result can be explained by the unjustified use of Fick's law to calculate D_e.

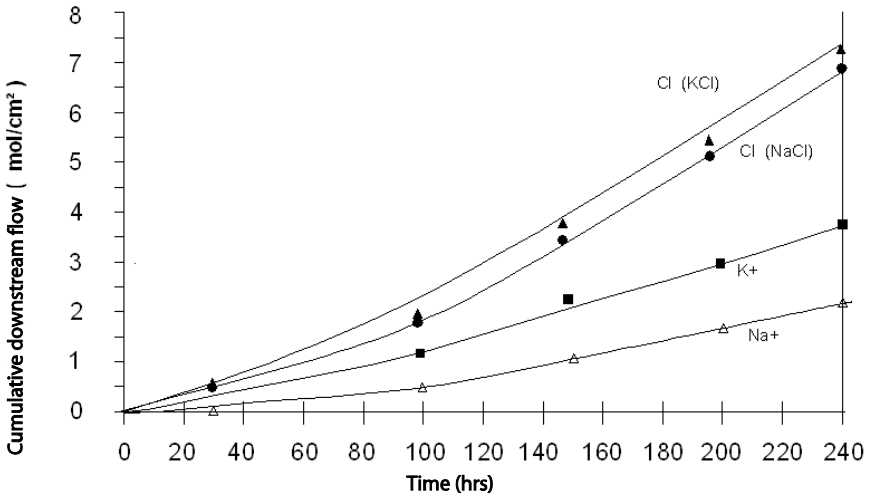

Figure 6.11. *Cumulative quantities of ionic species traversing cement paste with potassium chloride or sodium chloride in the upstream compartment [USH 74]*

A second illustration of the insufficiency of Fick's law is given by tests carried out with sodium chloride dosed at different concentrations in the upstream compartment. According to Fick's law, the effective diffusion coefficient is independent of concentration. If we apply relationship [6.70] to calculate the effective diffusion coefficient in a steady-state system, the effective diffusion coefficient calculated varies with concentration, as shown in Figure 6.12. To calculate the effective diffusion coefficient, it would be necessary to use Nernst-Planck's law and the multi-species approach presented in section 6.1.4.1. Using the hypothesis that the effective diffusion coefficient has an intrinsic value independent of concentration, the multi-species approach allows us to simulate the "pure diffusion" test and to calculate the flow traversing the samples for each concentration. Thus, by

applying relationship [6.70], we can find the "effective diffusion coefficients" that result from the application of Fick's law.

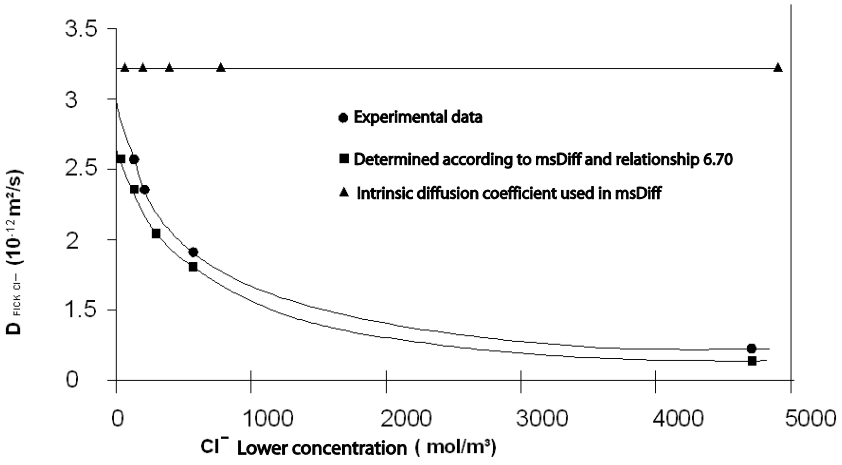

Figure 6.12. *Apparent variation of the effective diffusion coefficient calculated by applying Fick's law. By applying the multi-species approach, it is possible to simulate the test and to find the inexact values given by Fick's law [TRU 00]*

NOTE 6.4.–

– During the test, the material tested is in prolonged contact with the upstream and downstream solutions. In the case of a cementitious material (paste, mortar or concrete), precautions must be taken against leaching by using highly alkaline solutions.

– The interpretation of the simple diffusion test supposes that interactions between the diffusing species and the solid are linear. We showed in Figure 6.7 that this is not the case for chlorides in cementitious materials.

– The use of this method for concrete, for reasons of representativeness, requires a disk that is thicker than the aggregates, which leads to an experimentation time of several years to measure the effective diffusion coefficient. As an example, Figure 6.13 represents the variation of Cl^- ion flow with time during a simple diffusion test carried out with a disk of concrete 15 mm thick. In this case, it would be necessary to wait around two years for the flow to stabilize and to obtain the value of the effective

diffusion coefficient. Methods have been developed to obtain the diffusion coefficient value more rapidly; they are presented below.

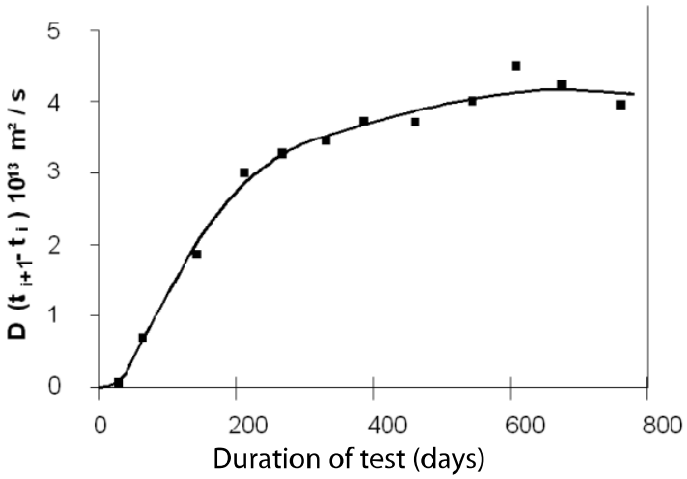

Figure 6.13. *Variation of chloride flow in a concrete disk 15 mm thick subjected to a simple diffusion test [NUG 02]*

6.3.2. *Electric field migration tests*

The flow of an ionic species is given by the Nernst-Planck relationship, as indicated in relationship [6.61], which we will reiterate here:

$$J_{e,i} = -D_{e,i}\frac{\partial c_i}{\partial x} - \frac{z_i F}{RT} D_{e,i} c_i \Psi = -D_{e,i}\frac{\partial c_i}{\partial x} - \frac{z_i F}{RT} D_{e,i} c_i E \qquad [6.71]$$

The density of the current traversing a sample of section A is $j = \frac{I}{A}$, where I is the intensity of the electric current. This current density can be related to the flows of ionic species i by the relationship:

$$j = F\sum_{i=1}^{n} z_i J_{e,i} \qquad [6.72]$$

This term is zero in the case of a simple diffusion test, since the electric circuit made up by the disk of material is an open circuit. By replacing the flows with their value given by relationship [6.71], the electrical field is given by the relationship:

$$E = -\frac{RT}{F}\frac{\frac{j}{F}+\sum_{i=1}^{n} z_i D_{e,i}\frac{\partial c_i}{\partial x}}{\sum_{i=1}^{n} z_i^2 c_i D_{e,i}} \qquad [6.73]$$

In a simple diffusion test, the current density term is zero. However, the difference in potential (*pd*) measured at the edges of the disk is not zero. We obtain a value in the order of several dozen mV for disks of centimetric thickness [ARS 99]. The electrical field corresponding to this difference in potential can be expressed by relationship [6.73]. In the usual practice of the simple diffusion test, this term is disregarded.

Generally speaking, the flow of a given species can be expressed as being the sum of two terms: a purely diffusive part that corresponds to the first term of the Nernst-Planck relationship; and an electric part corresponding to the second term. In the case of chlorides ($z = -1$), we can therefore write the relationship [6.71], giving the ionic flow in the following simplified form, omitting the index *i* and showing the diffusive ($J_{e,diff}$) and electric ($J_{e,elec}$) contributions of the flow and putting $a = \frac{FE}{RT}$:

$$J_e = J_{e,diff} + J_{e,elec} = -D_e\frac{\partial c}{\partial x} + \frac{F}{RT}D_e cE = -D_e\left(\frac{\partial c}{\partial x} - ac\right) \qquad [6.74]$$

In steady state, we can write:

$$-\frac{J_e}{D_e} = k = \frac{dc}{dx} - ac$$

That is:

$$\frac{dc}{dx} = k + ac \Rightarrow \int_{c_0}^{c_1=0} \frac{dc}{k+ac} = \int_0^L dx$$

By integrating this expression, we get:

$$k = \frac{ac_0 e^{aL}}{1 - e^{aL}} \qquad [6.75]$$

In the simple diffusion test, the electric field is negligible and we find the expression of flow given by Fick's first law:

$$a \to 0, \quad e^{aL} \approx 1 + aL, \quad D_e = \frac{J_e L}{c_0} \qquad [6.76]$$

One way to accelerate the transfer of ions consists of increasing the flow that is electric in origin, $J_{e,elec}$, by applying a potential difference to the edges of the strip. If the potential difference is much higher than that measured at the edges of the strip in the simple diffusion test, the flow that is electric in origin is principally influenced by this exterior *pd*. If, on the other hand, this *pd* is such that the flow diffusive in origin is much lower than that created by the electrical field, we can write:

$$e^{aL} >> 1, \quad J_e \approx 1 + e^{aL}, \quad D_e \approx \frac{J_e}{ac_0} = \frac{J_e RT}{FEc_0} = \frac{J_e RTL}{FUc_0} \qquad [6.77]$$

where U is the potential difference applied to the edges of the strip on parallel faces. The measurement of the chloride flow in steady state regime is then used to calculate the effective diffusion coefficient. This approach is implemented in the *migration test* device shown in Figure 6.14.

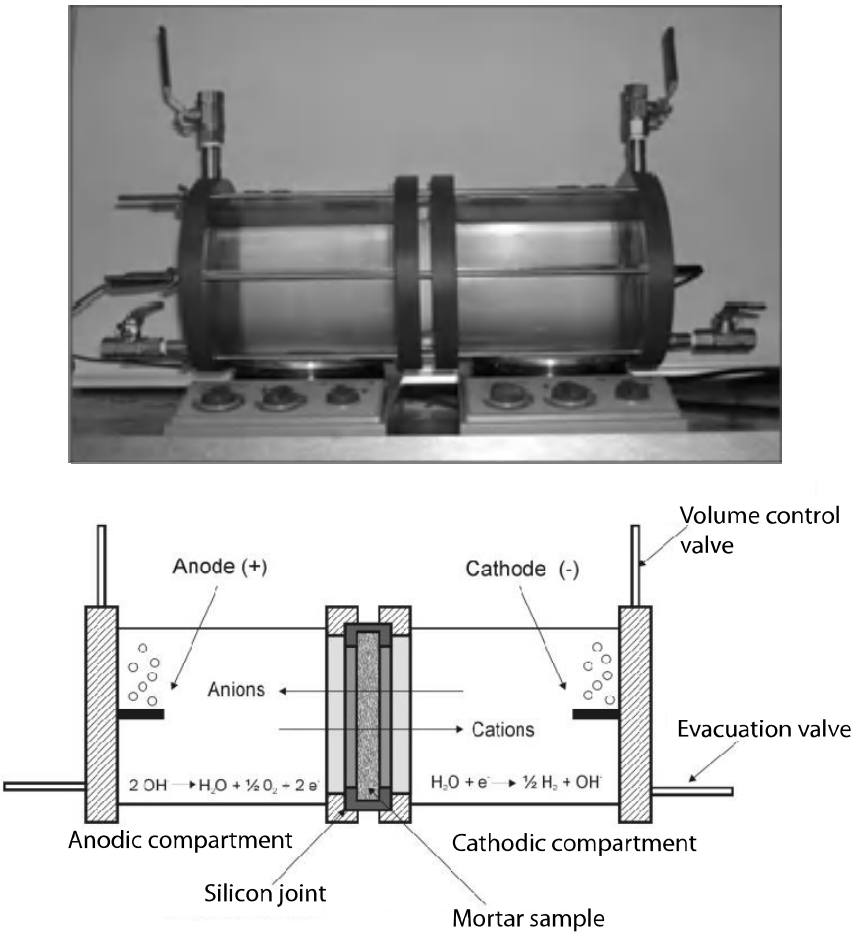

Figure 6.14. *Electric field diffusion cell and principle diagram [FRI 03]*

A cathode placed in the compartment containing chlorides at concentration c_0 accelerates their transfer toward the anodic compartment. The potential difference applied to the edges of samples of centimetric thickness is in the order of 12 V, which creates an electrical field much stronger than that which exists in the simple diffusion test (this has a *pd* in the order of 12 mV). The electrical field thus created causes movement in all of the charged particles in the anodic and cathodic solutions, as well as those in the interstitial solution of the material being tested.

To determine the chloride effective diffusion coefficient, we only measure the quantities of chlorides that arrive in the anodic compartment. As an example, Figure 6.15 represents the evolution of the cumulative quantities of chlorides arriving in the anodic compartment during a test conducted under a *pd* of 10 V with a 3 cm thick sample of high-performance concrete (*W/C* = 0.32). The steady-state regime is obtained after several days instead of several years in a simple diffusion cell test.

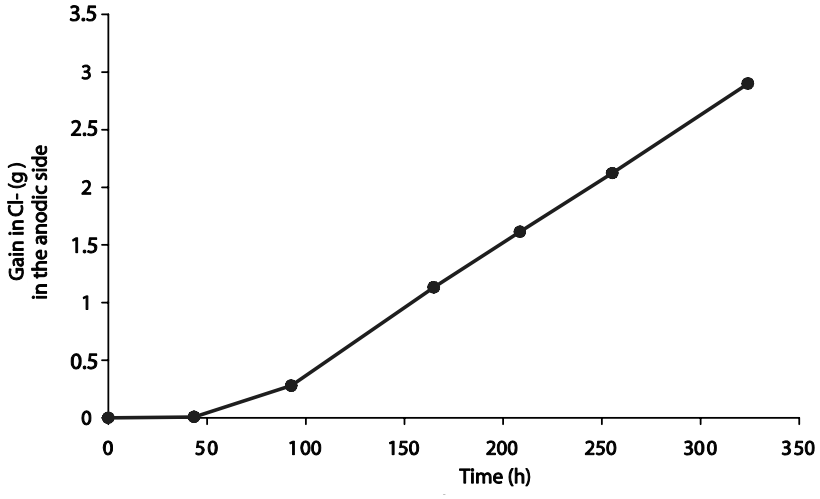

Figure 6.15. *Migration test of high-performance concrete: the steady-state regime is obtained after only a few days [TRU 00]*

In the migration cell diagram in Figure 6.14, reactions to electrodes are represented. According to the experimental conditions, these reactions can lead to the transformation of chlorides from the anodic compartment into hypochlorite, which will falsify the measurement of chloride quantities. In practice, it is useful to take precautions to avoid such reactions to electrodes [BOC 82], particularly by limiting the electrical tension to a 12 V and by using alkaline solutions.

In the migration test, insofar as the electrical field applied is sufficient, the diffusive term is negligible and relationship [6.74] can be simplified as:

$$J_e \approx J_{e,elec} = \frac{F}{RT} D_e c E \qquad [6.78]$$

This flow only varies with the value of the chloride concentration. On the cathodic face, concentration is constant and equal to c_0. The flow of chlorides is thus also constant. We can therefore modify the cell test by measuring the quantities of chlorides that leave the cathodic compartment instead of those arriving from the anodic compartment. The measurement of the effective diffusion coefficient is thus more rapid. This principle is implemented in the LMDC (Laboratoire Matériaux et Durabilité des Constructions) test, shown in Figure 6.16. We can thus create very simple migration cells that allow rapid measurement.

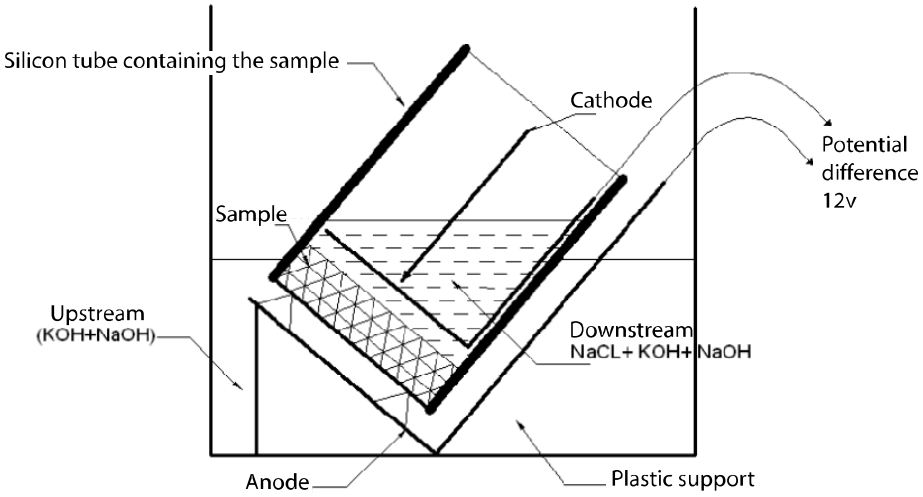

Figure 6.16. *LMDC diffusion test. The cathodic compartment is made up of a cylindrical silicon reservoir containing chlorides in alkaline solution. The large volume of this compartment allows us to avoid renewing the solution. The chloride concentration there is regularly measured so as to calculate the flow of chlorides used in relationship [6.77] and determine the effective diffusion coefficient [LOB 03]*

As time passes, the chlorides penetrate the sample tested. If the flow is solely due to the electrical contribution, the chloride profile is a penetration front, the shape and progression of which are related to the effective diffusion coefficient, as well as to interactions with the material. If there are no interactions with the solid, the penetration front is a step. If there are interactions, the shape of the front is modified and the chlorides penetrate more slowly [AMI 97]. Figure 6.17 experimentally confirms the form of this type of relatively "steep" profile, measured here in total chlorides.

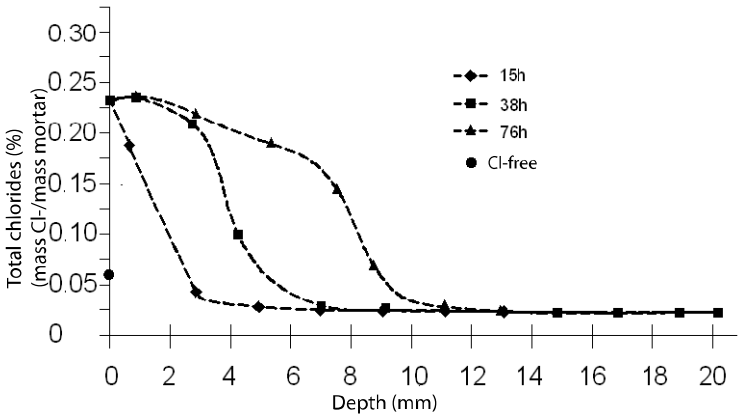

Figure 6.17. *Penetration of chlorides into mortar (D_e = 0.78 10^{-12} m^2/s) during a migration test [LOB 03]*

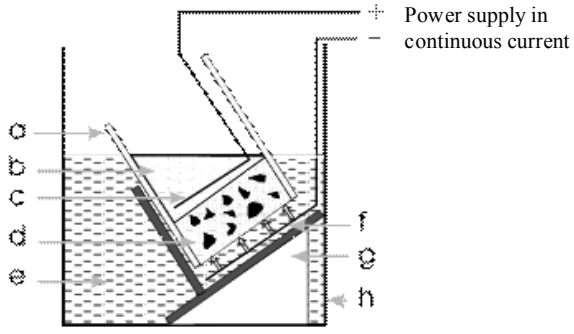

a: Rubber cylinder
b: Anodic compartment
c: Anode
d: Sample
e: Cathodic compartment
f: Cathode
g: Support
h: Plastic matter container

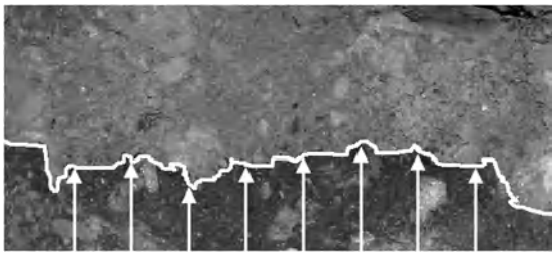

Figure 6.18. *Hypothetical CTH NT Build 492 test sketch and view of chloride penetration front in the sample at the end of the test [TAN 96]*

This type of profile allows us to simply characterize the penetration of chlorides, for example by the position of the inflection point. We can thus define a "penetration depth" that can be localized experimentally, for example by pulverizing a color indicator (a solution of silver nitrate) on a cross-section of the sample taken by splitting. This principle is used in the CTH NT Build 492 method shown in Figure 6.18. In this test, the potential difference applied is chosen so that at the end of the test, which lasts 24 hours, the penetration front does not reach the cathodic face of the sample. The regulation of tension is effected on the basis of the measurement of the current traversing the sample at the start of the test. The apparent diffusion coefficient is calculated using an empirical formula.

6.3.3. *Measurement of the apparent diffusion coefficient by immersion*

Equation [6.67] expresses the solution to Fick's second law in the form of the variation in the concentration of total chlorides with time and depth through a sample immersed in a chloride solution where the concentration is fixed and known. In this equation, the material is characterized by its initial chloride concentration (which is generally very low or even zero) and by its apparent diffusion coefficient, D_a:

$$c_{m,t} = c_{m,t,in+}(c_{m,t,in} - c_{m,t,0})erfc\frac{x}{2\sqrt{D_a t}} \qquad [6.67]$$

The immersion test (NT Build 443) is based on the application of this equation to concrete. It is a non-steady state test; the samples to be tested are immersed for 35 days at 23°C in a solution containing 165 g/L of sodium chloride (see Figure 6.19). The concentration chosen is elevated so as to encourage the penetration of chlorides into the concrete for a reasonable experimental duration. At the end of the test, the total chloride profile is determined by measuring the quantities of chlorides in samples of powder collected by the erosion of concrete at variable depths. The experimental curve of the profile obtained is then adjusted by a complementary error function. The adjustment coefficient is the apparent coefficient sought.

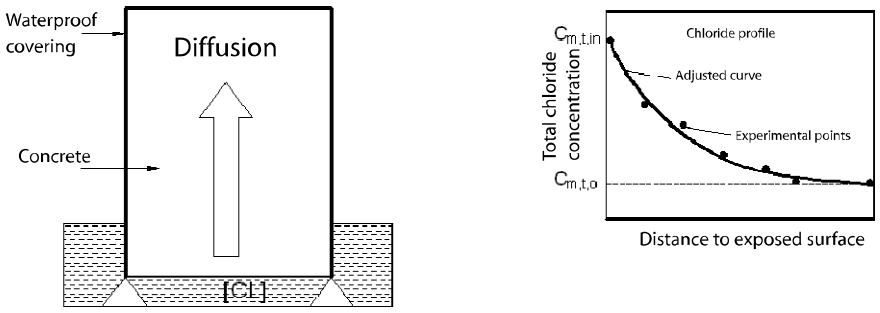

Figure 6.19. *Sketch of the NT Build 443 immersion test used in measuring the apparent diffusion coefficient of concrete*

6.3.4. *Principle of methods of measuring the effective diffusion coefficient based on measurements of conductivity*

We have shown that the Nernst-Einstein law can be written as:

$$\frac{\langle v \rangle}{D_i} = \frac{f}{kT} \qquad [6.19]$$

If we consider an ionic species i of valency z_i, in solution under an electrical field $E = \frac{d\Psi}{dx}$, it sustains a Coulomb force $\vec{f} = z_i e\vec{E}$ where e is the elementary charge (-1.06 × 10^{-19} C).

The Nernst-Einstein law becomes:

$$\langle v \rangle = \frac{D_i z_i e}{kT} \frac{d\Psi}{dx} \qquad [6.79]$$

If the concentration of ions considered is c_i (expressed in number of particles per unit of volume), the flow of charges j_i, also called the electric current density, is equal to:

$$j = z_i e c_i \langle v \rangle \qquad [6.80]$$

By replacing velocity by its value given in equation [6.79], we can write:

$$j_i = \frac{D_i z_i^2 e^2 c_i}{kT} \frac{d\Psi}{dx} \qquad [6.81]$$

Ohm's law relates this density of electric current to the electrical field:

$$j_i = \sigma_i \frac{d\Psi}{dx} \qquad [6.82]$$

σ_i being electrical conductivity. Thus we get:

$$\sigma_i = \frac{D_i z_i^2 e^2 c_i}{kT} \qquad [6.83]$$

NOTE 6.5.–

– To obtain the current density in the SI unit system, the second term of equation [6.83] must be multiplied by Avogadro's number.

– The current density given in [6.81] is that which results from the transport of charges *i;* likewise for conductivity σ_i. If there are several species in solution, the current density transported by a species *i* is given by the transport number $t = \frac{j_i}{j_{tot}}$ where j_{tot} is the total current density transported by all of the ions. Experimental methods are used to determine these transport numbers and the diffusion coefficient.

– Relationship [6.83], which is one of the many expressions of the Nernst-Einstein relationship, is transposable in the case of porous materials. The diffusion coefficient becomes the effective diffusion coefficient and the solution conductivity becomes the conductivity of the solid saturated by this

solution. The other terms of the relationship remain unchanged, and we can rewrite relationship [5.12], which defines the formation factor, as:

$$F = \frac{\sigma}{\sigma_e} = \frac{D}{D_e} \qquad [6.84]$$

6.3.5. *Orders of magnitude of the diffusion coefficient in concrete*

The methods of measuring diffusion coefficients presented in the preceding sections are varied and based on different hypotheses. Strictly speaking, to determine the effective diffusion coefficient for ionic species like chlorides, it would be necessary to interpret the experimental results with the Nernst-Planck law according to the multi-species approach previously described. The amount of knowledge we have does not allow this, and we must be contented with the approximations presented.

The "diffusion coefficients" obtained are therefore not intrinsic values, but depend on the type of test implemented as well as the experimental conditions used. The values obtained for various materials must, therefore, be compared with caution. Moreover, prediction of the penetration of chlorides into concretes is difficult, since we do not know how to describe the phenomena with precision, nor can we determine the intrinsic characteristics of the different types of material. Different models are in the process of being developed, but the one based on the more or less direct application of the solution to Fick's second law is currently the most frequently used.

Table 6.3 gives some orders of magnitude. The effective diffusion coefficients are measured for tritiated water using a simple diffusion test. This test conducted with this species has the strictest interpretation, since the diffusion of the tritiated water is part of molecular diffusion and not ionic diffusion. The values of the effective diffusion coefficients measured with chlorides have comparable orders of magnitude.

Property	*Method used*	*Standard concrete*	*High-performance concrete*	*Very high-performance concrete*	*Ultra high-performance fibrous concrete*
Water porosity (%)	AFREM (Association Française d'étude et de recherche sur les matériaux)-AFGC (Association Française de génie civil)	14–20	10–13	6–9	1.5–5.0
Effective diffusion coefficient to tritiated water (m^2/s)	Simple diffusion in steady state regime	2.10^{-11}	2.10^{-12}	2.10^{-13}	2.10^{-14}

Table 6.3. *Orders of magnitude of porosity and of the effective diffusion coefficient of concrete [BFU 02]*

NOTE 6.6.– the diffusion of ionic species occurs in the liquid phase contained in the porosity of porous matters. The state of saturation has influenced ionic transfers. The direct measurement of the effective diffusion coefficient in a partially saturated environment is not easy, but relationship [6.87] allows us to know the influence of the state of saturation on ionic diffusion thanks to measurements of electrical conductivity. Figure 6.20 represents the variation of electrical conductivity of mortar, and consequently that of the effective diffusion coefficient, with respect to the degree of saturation [FRA 01]. A threshold effect is observed above 60% saturation; the liquid phase in the matter is no longer continuous and the diffusion of ions is impossible.

This variation becomes very important when we consider the tidal area at marine sites. In this area, structures undergo immersion–drying cycles due to tide swells and the change in tides. The degree of saturation thus varies regularly, as does the diffusion coefficient of concrete. When we know that it is in this tidal area that the corrosion of reinforcements is heaviest, the

variation of the diffusion coefficient with water saturation must be carefully considered.

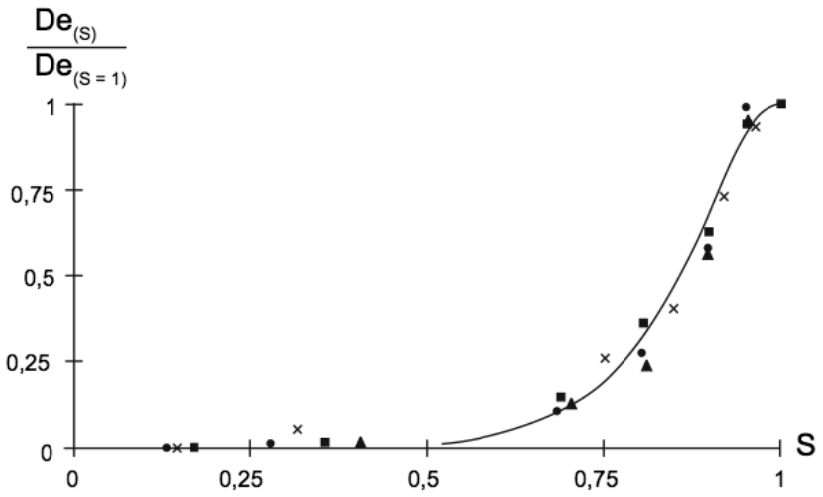

Figure 6.20. *Influence of the degree of saturation on the effective diffusion coefficient of ions [FRA 01]*

6.4. The relationship between the effective diffusion coefficient and porous structure

Various experimental data on the influence of the porous structure of concrete may be consulted in [OLL 08]. In this section, we will present some models used to quantify this influence.

There are two categories of models: empirical models and polyphasic models.

In the empirical type, the effective diffusion coefficient is expressed with respect to the characteristics of the porous structure. As indicated in relationship [6.60], the effective diffusion coefficient of a material depends on the characteristics of its porous structure. To develop a matter that has a given set of diffusion properties, this porous structure must be worked on, but in relationship [6.60] tortuosity and constrictivity are not easy quantities to measure. The models presented below aim to relate the effective diffusion coefficient to the measurable quantities characterizing the porous structure.

In the case of concrete, the porous structure depends on the cement paste, but also on the granular phase. The second models presented here consider concrete to be a polyphasic porous matter, and the diffusion coefficient of the composite is sought with respect to:

– the diffusion coefficients of the different phases;

– the content of these phases; and

– possibly other geometric characteristics.

These models are more directly related to formulation data.

NOTE 6.7.– For certain models, it is not diffusion that is modeled, but electric conductivity. This is also true if we seek to understand diffusion in a saturated medium, since the effective diffusion coefficient, D_e, of a saturated material can be related to electrical conductivity by the Nernst-Einstein relationship [6.84].

6.4.1. *Empirical models*

The basic principle of empirical models consists of relating the effective diffusion coefficient to the characteristics of the microstructure using a function by which the constants and exponents are adjusted in order to obtain the best correlation possible with a series of experimental data. The characteristics of the porous structure can be porosity and the critical or average radius (or diameter) of pores[10]. Among all of the models proposed, we will first present those classically identified as stemming from Archie's law. These models express the proportionality between the effective diffusion coefficient and a power function of porosity.

6.4.1.1 *Archie's law*

Archie's law [ARC 42] empirically relates the porosity and conductivity of a matter. This expression was initially suggested for rocks.

$$\sigma_e = A\sigma_0 p_0^n \Leftrightarrow \frac{\sigma_0}{\sigma_e} = F = \frac{p_0^{-n}}{A} \qquad [6.85]$$

10 See section 5.5.1.6 for the definitions of these terms.

where:

– p_0 is open porosity;

– n is a constant that varies between 1.3 and 2.5 for rocks;

– A is a factor between 1 and 5. Its value is usually 1.

According to Guégen *et al.* [GUE 94], the application of Archie's law remains limited to materials in which the porosity falls within a certain interval, for example $0.05 < p_0 < 0.40$ for the case of rocks. Figure 6.21 shows an example of the application of Archie's law.

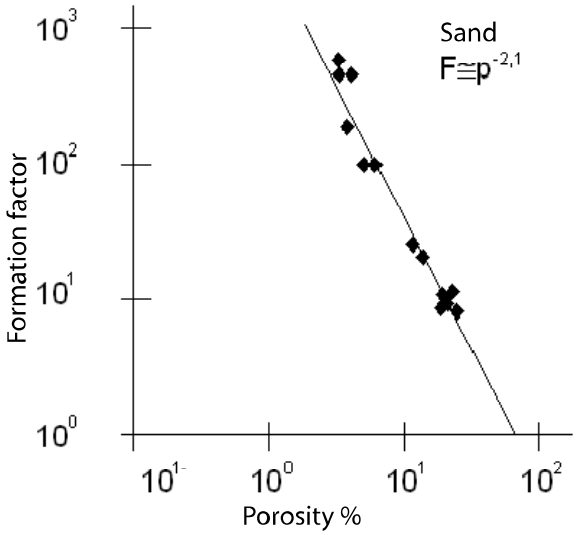

Figure 6.21. *The empirical relationship between the formation factor and porosity (Archie's law) for Vosges and Fontainbleau sandstone (from Ruffet et al, 1994 [GUE 94])*

In the case of cementitious materials, the results are not clear. Many authors conclude that Archie's law is not valid [ATK 84, CHR 94, [GAR 90], but some work gives more encouraging results. Archie's law does, in fact, appear to be applicable for well-hydrated cement pastes (see Figure 6.22) and satisfying results have also been obtained for mortar with a *W/C* ratio of 0.35 prepared with different sand contents [TUM 96].

This same Figure 6.21 shows the limits of this type of model, as insofar as the coefficients of Archie's law vary from one material to another. This means that other characteristics of the porous structure influence diffusion.

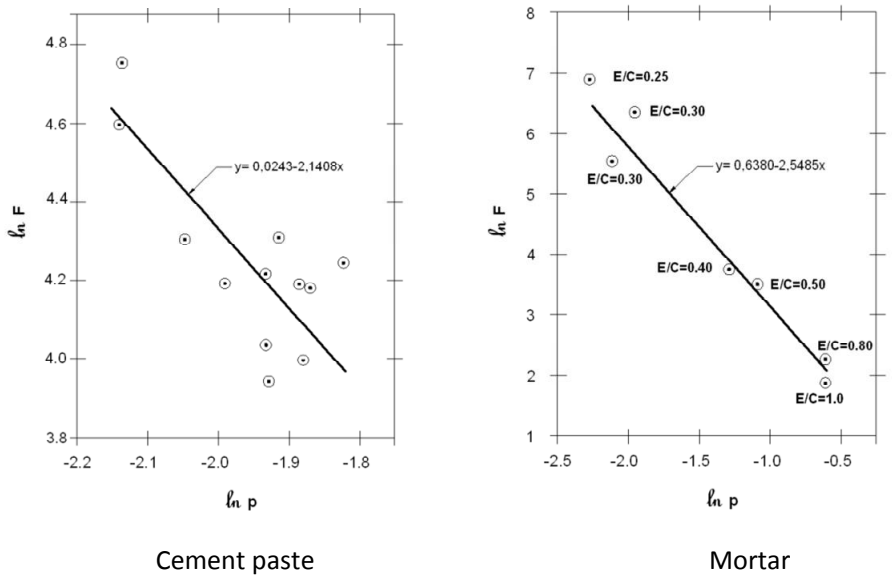

Figure 6.22. *Application of Archie's law for cement paste and mortar [TUM 96]*

6.4.1.2. *Other relationships*

Several researchers [KAM 03, NUM 90, TER 76, TOG 98] have established simple empirical relationships between the effective diffusion coefficient of tritiated water (or chlorides) and the porosity evaluated, generally using a mercury porosimetry test. Other researchers propose a correlation of the diffusion coefficient of a cementitious material with the critical radius of pores [HAL 95] or the average radius of pores [KUM 86]. These relationships are summarized in Table 6.4.

Another approach for predicting the properties of mortar or concrete consists of considering materials as composites, and calculating the diffusion coefficient with respect to the diffusion coefficients of each of the phases. This approach is described below.

Relationships	Limit of validity: Tracer – material	Authors
$D_e = 2.3 \cdot 10^{-13}\ exp^{9.95 p_0}$	Tritiated water – Cement paste (CEM I)	[TOG 98]
$D_e = 10^{-10.25}\ p_0^{1.067}$	Tritiated water – Paste, mortar, and concrete	[TER 76]
$D_e = 10^{-10.45}\ p_0^{0.947}$	Tritiated water – Paste and mortar W/C of 0.4 to 0.5 (CEM I)	[NUM 90]
$D_e = (1.692 p_0 - 0.356)10^{-10}$ if $p_0 \le 0.37$ $D_e = \left(4.464 p_0^2 - 3.156 p_0 + 0.57\right)10^{-9}$ if $p_0 > 0.37$	Tritiated water – Cement paste	[KAM 03]
$D_e = -4.3 \cdot 10^{-12} + 6.5 \cdot 10^{-13} d_c$	Chlorides – Cement paste and mortar **W/C** = 0.5 (ASTM type I)	[HAL 95]

Table 6.4. *Empirical models relating the effective diffusion coefficient to characteristics of the porous structure (mercury porosity p_0 or critical pore diameter d_c) [LOB 03]*

6.4.2. *Polyphasic models*

In this type of model, cementitious material is considered to be compositive with *n* different phases, each one possessing its own properties of porosity, diffusion coefficient, and electric conductivity or resistivity. We will first present the simple polyphasic models: series and parallel models, and models resulting from the homogenization technique. Then we will present the more complex models developed using the theory of effective media.

6.4.2.1. *Series and parallel models*

Due to the similarity between the Ohm's and Fick's laws, in this model the constituents of the composite material are assimilated into layers placed either in parallel or in a series, like the resistances of an electric circuit (see Figure 6.23).

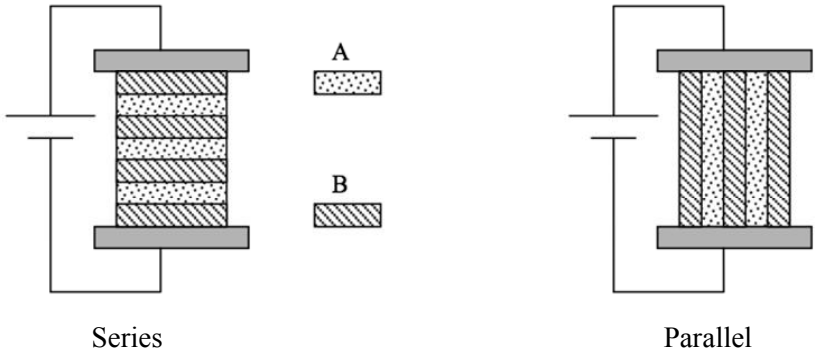

Figure 6.23. *Biphasic model in series and in parallel*

For example, we can consider that concrete is composed of two (cement paste and aggregate) or three (cement paste, aggregate, and transition zones) phases. Each of these phases is considered a homogeneous phase laid out in series or in parallel, see Figure 6.24.

In the biphasic model, paste with a diffusion coefficient D_p is associated with aggregates with diffusion coefficient D_g, the volume fractions of the components being v_p and v_g, respectively.

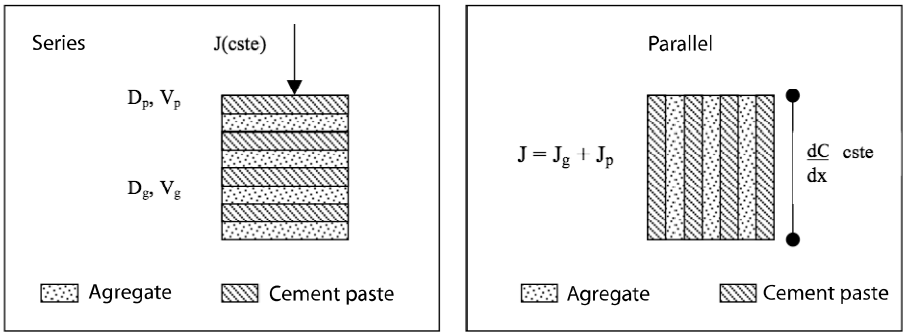

Figure 6.24. *Diffusion model in series and in parallel*

In the series model, the effective diffusion coefficient of concrete is given by:

$$\frac{1}{D_e} = \frac{v_p}{D_p} + \frac{v_g}{D_g} = \frac{1 - v_g}{D_p} + \frac{v_g}{D_g} \qquad [6.86]$$

In the parallel model, the effective diffusion coefficient of concrete is:

$$D_e = v_p D_p + v_g D_g = (1 - v_g) D_p + v_g D_g \qquad [6.87]$$

In practice, we consider that the diffusion coefficient of aggregates is significantly smaller than that of paste. The coefficient thus calculated with the parallel model shows the effect of dilution.

Concrete is sometimes considered a triphasic medium containing aggregates, cement paste and an interfacial zone called the interfacial transition zone (ITZ). The diffusion coefficient can be estimated using a *triphasic model*. With D_{ITZ} and v_{ITZ} being diffusion coefficient and the volume fraction of the transition zones, adopting the parallel model the effective diffusion coefficient of the matter is obtained by the following relationship:

$$D_e = (v_p - vITZ) D_p + v_{ITZ} D_{ITZ} + v_g D_g \qquad [6.88]$$

6.4.2.2. *Homogenization technique (three-phase model)*

This model was proposed by Caré and Hervé [CAR 95]. The idea is to use homogenization techniques to predict the diffusion coefficient of cementitious materials.

In the case of cementitious materials, we consider three phases: aggregate, ITZ, and the cement matrix. The hypotheses of the model are:

– one phase corresponds to aggregates (gravel and sand) of volume v_g, the diffusion coefficient of which is zero;

– one continuous phase corresponds to the cement matrix (diffusivity D_p); and

– a last phase, the ITZ, presents a properties gradient (with a volume V_{ITZ} and diffusivity D_{ITZ}).

The following expression is used to calculate the effective diffusion coefficient of concrete:

$$D_e = D_p \frac{3D_p(1-v_g)(2v_g+2v_{ITZ})+2v_{ITZ}(D_{ITZ}-D_p)(1+2v_g+2v_{ITZ})}{3D_p(3v_g+2v_{ITZ})+(1-v_g-v_{ITZ})\left[2v_{ITZ}(D_{ITZ}-D_p)-3v_gD_p\right]}$$

[6.89]

The volume fraction of the transition zones, v_{ITZ}, is estimated using the composition parameters by means of the following expression:

$$v_{ITZ} = (1-v_g)-(1-v_g)e_v e_{ITZ} \qquad [6.90]$$

where e_v is a function of the size distribution of the aggregates and the thickness of the ITZ. This expression takes into account the superposition of the transition zones.

6.4.2.3. *Models based on the effective environment theory*

Models based on the effective media theory have been developed with the aim of determining the effective conduction properties of a continuum containing randomly placed spherical or ellipsoidal inclusions. An effective medium designates a homogeneous medium that is topologically equivalent to the heterogeneous and multi-phasic environment (paste and aggregate, for example) for which we wish to determine the transport or conductivity properties.

For porous matters, relationships have been established between material transfer properties (diffusivity, electrical conductivity and permeability), the transfer properties of the conductor phase (e.g. the cement matrix in mortar or concrete), and the volume fraction of zero conductivity inclusions (or diffusivity) (aggregates in cementitious matters).

If we consider a biphasic cementitious material composed of a cement paste and grains, it is possible to determine the diffusion coefficient of the material if we know the diffusion coefficient of the paste and the volume fraction of the aggregates (v_g) by only considering the dilution phenomenon caused by the introduction of inclusions (the grains). Thus we get the equation:

$$D_e = (1-v_g)D_p + v_g D_g = (1-v_g)D_p \quad [6.91]$$

To take into account the combined effect of dilution and tortuosity associated with the addition of aggregates, Bruggeman [BRU 35] has proposed a law to resolve the problem of the homogenization of the conductive properties of a heterogeneous environment. This is based on the effective medium theory, still considering a biphasic medium (paste and aggregate):

$$D_e = D_p(1-v_g)^{1.5} \quad [6.92]$$

This relationship constitutes one of the simplest approaches for determining the conductivity or diffusivity of a porous material. Applied to mortar, relationship [6.92] predicts values lower than the experimental values [XU 00]. These differences can possibly be explained by the influence of transition zones, since the differences detected become more pronounced as the volume percentage of aggregate increases.

Maxwell has proposed a relationship of the same type [MCL 90]:

$$D_e = D_p(1-1.5v_g) \quad [6.93]$$

In order to take into account the influence of transition zones, the work carried out by Yang and Su [YAN 02] has led to a relationship modified from Bruggemann's law:

$$D_e = D_p(1-v_g)^{1.5} + D_p(\alpha-1)\beta v_g \quad [6.94]$$

where αD_p is the diffusion coefficient of the transition zone and βv_g is its volume fraction. The diffusion coefficient of the transition zones is considered constant.

The volume fraction of the transition zone, v_{ITZ}, is calculated from the following expression:

$$v_{ITZ} = \beta v_g = v_g \sum \frac{R_i}{d_i^3}\left[(d_i + h^3) - d_i^3\right] \quad [6.95]$$

where:

– v_{ITZ} is the volume fraction of the transition zone;

– R_i is the individual proportion retained in the sieve i;

– d_i is the average size of the fine aggregate in the sieve i; and

– h is the thickness of the ITZ.

Maxwell-Wagner, cited in [BAR 01], proposes a relationship between the diffusion coefficient of the material D_e and that of the paste D_p. Aggregates are considered as inclusions with zero diffusivity, with spherical form where the volume content is theoretically below 10% [CAM 02]. The following expression is used to calculate the effective diffusion coefficient of the matter:

$$D_e = D_p(1-v_g)\frac{2}{2+v_g} \qquad [6.96]$$

6.4.2.4. *The Garboczi model*

Garboczi and Bentz [GAR 92] have simulated diffusion in cement pastes, considering that species can diffuse in both capillary and in hydrates pores (C-S-H). This simulation is based on the Nernst-Einstein relationship, which allows us to make an electrical analogy of diffusion, and on a three-dimensional model of the development of the microstructure during hydration. The following relationship is proposed:

$$\frac{D_e}{D_0} = 0.001 + 0.07\,p_{cap}^2 + 1.8H_{(p_{cap}-0.18)}(p_{cap}-0.18)^2 \qquad [6.97]$$

where:

– D_e is the effective diffusion coefficient of the cement paste;

– D_o is the diffusion coefficient in water;

– p_{cap} is the capillary porosity of the cement paste; and

– H is the Heaviside function:

$$H_{(p_{cap}-0.18)} = 0 \quad \text{if} \quad (p_{cap} - 0.18) \leq 0$$

and

$$H_{(p_{cap}-0.18)} = 1 \quad \text{if} \quad (p_{cap} - 0.18) > 0$$

This function manifests a threshold effect[11] overlooked by the preceding models. If capillary porosity is below 18%, the capillary pores are no longer interconnected (see [OLL 08]) and diffusion occurs solely through the pores of hydrates, which provides the first term of equation [6.98]. The second term is analogous to the aforementioned Archie's law, in which the exponent is taken as equal to 2.

This expression is used to determine a diffusivity ratio (in the case of chlorides, for example, it is the ratio between the diffusion coefficient of the chlorides in pure cement paste and that of the chlorides in free water) from capillary porosity. This is calculated with respect to the *W/C* ratio and to the degree of hydration of the cement (α) using the Powers model:

$$p_{cap} = 1 - \frac{1 + 1.13\alpha}{1 + 3.2\frac{E}{C}} \qquad [6.98]$$

where 3.2 is the density of the cement and 1.13 represents the relative increase in volume of the solid due to the hydration reaction.

Mills [MIL 89] gives the value of $D_o = 2.10^{-9}$ m^2/s at 25°C in the case of the diffusion of chlorides. The ratio between the diffusivity of the cement paste and the water can be calculated according to relationship [6.98]. If we assume a porosity of the transition zone, we can calculate D_{ITZ}/D_o. To obtain the effective diffusion coefficient of mortar, these diffusivity values are used in a model that provides the values of D_{mortar}/D_p with respect to D_{ITZ}/D_p and to the proportion of sand (see Figure 6.24). In fact, the figure presents the conductivity values, but it is directly transposable to the effective diffusion coefficients thanks to relationship [6.84].

11 The threshold effect noted here will be developed in Chapter 7 relative to permeability via the description of percolation theory.

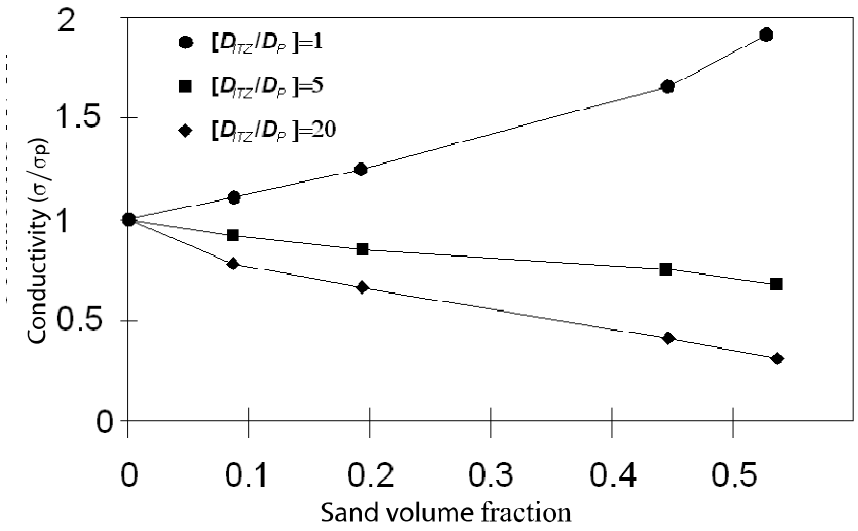

Figure 6.25. *Variation of the ratio between the conductivities of mortar and cement paste with the same W/C ratio and the same degree of hydration with respect to the sand volume fraction for different relationships between the diffusivity of the translation zone and the paste [GAR 94]*

6.5. Gaseous diffusion

Gaseous diffusion in concrete is a process that occurs in various situations: humidity transfer, carbonation, gaseous transfer in waste containers, etc. This process can occur alone or be associated with transfers in the liquid phase, or coupled with chemical reactions.

6.5.1. *The diffusion of a gas in an infinite medium*

The diffusion of a gas, i, in another gas is presented in section 6.1. This diffusion is characterized by a diffusion coefficient D_i given by relationship [6.2]:

$$D_i = \frac{\bar{l}^2}{2t_c}$$

By replacing the average distance traveled between two successive impacts with the value of mean free path $\bar{\lambda}$ given in [6.4] and the time, t_c, separating two collisions by the expression also given in section 6.1, the diffusion coefficient of gas *i* with a molar mass *M*, the molecules of which have a diameter *d*, can be written as follows[12] at total pressure *P* and at temperature *T*:

$$D_i = \frac{0.137}{d^2}\frac{k_B T}{P}\cdot\sqrt{\frac{RT}{M}} \qquad [6.99]$$

The macroscopic transport of a gas by diffusion is described by Fick's first law (relationship [6.100]), which expresses the value of the flow of gas transported under the effect of a unidirectional concentration gradient.

$$J_i = -D_i\frac{\partial c_i}{\partial x} \qquad [6.100]$$

In the international unit system, flow is expressed in mole/m^2.s, concentration in mole/m^3, and the diffusion coefficient in m^2/s. By applying the perfect gas relationship:

$$c_i = \frac{n_i}{V} = \frac{p_i}{RT},$$

we get:

$$J_i = -\frac{D_i}{RT}\frac{\partial p_i}{\partial x} \qquad [6.101]$$

In this expression, p_i is the partial pressure of the gas. The concentration gradient thus corresponds to a partial pressure gradient (not a total pressure gradient). This gradient is the motor of the transfer. Under a total pressure difference, the process of gas transport would be convection and therefore governed by Darcy's law, which is studied in Chapter 7. The diffusion coefficient depends on the gas, *i*, but also on the other gas in which it is diffusing. Equation [6.99] shows that it also depends on the temperature and average pressure of the gas.

12 Analogous relationships using a multiplying coefficient slightly different from 0.137 can also be found in the literature.

We also find several empirical relationships in the literature. For example, relationship [6.102] is used to calculate the diffusion coefficient of water vapor at atmospheric pressure [FAR 73]:

$$D_{(m^2/s)} = 2.74 \cdot 10^{-4} \left(\frac{T_{(°C)} + 273}{293} \right)^{2.3} \qquad [6.102]$$

6.5.2. *The diffusion of a gas in a pore*

In a rectilinear pore parallel to the partial pressure gradient far from the walls, diffusion is of the same type previously described. We can refer to this as *free diffusion*. On the other hand, impacts between gas molecules and walls can also occur, and diffusion is disturbed. This is called Knudsen diffusion, or sliding along walls. This phenomenon becomes greater as the pore diameter becomes smaller with regard to the mean free path of gas molecules. This type of diffusion corresponds to a flow system governed by Knudsen's law, which, in the case of a cylindrical capillary with radius r, is expressed according to [BLO 46]:

$$\frac{dm}{dt} = -\frac{8r^3}{3} \sqrt{\frac{\pi M}{2RT}} \cdot \frac{dP}{dx} \qquad [6.103]$$

in which $\frac{dP}{dx}$ is the partial pressure gradient in the capillary tube. The mass flow can be written as:

$$\frac{1}{\pi r^2} \frac{dm}{dt} = -\frac{8r}{3\pi} \sqrt{\frac{\pi M}{2RT}} \cdot \frac{dP}{dx}$$

and the molar flow as:

$$J = -\frac{8r}{3\pi} \sqrt{\frac{\pi}{2MRT}} \cdot \frac{dP}{dx} = -\frac{8r}{3\pi} \sqrt{\frac{\pi RT}{2M}} \cdot \frac{dc}{dx} = -D_K \frac{dc}{dx} \qquad [6.104]$$

This relationship is similar to Fick's law, but the coefficient of proportionality between the flow and the concentration gradient is different.

We can write this as D_K, and designate it as the Knudsen diffusion coefficient.

From which relationship between mean free path and the diameter ϕ of a pore can we consider that the flow is not disturbed by the wall? To answer this question, we introduce the Knudsen number, $K_n = \frac{\overline{\lambda}}{\phi}$. For a Knudsen number lower than 0.1, the free diffusion system prevails. If K_n is higher than 10, the flow is governed by Knudsen's law. For values of K_n falling between these two limits, flow is a combination of the two mechanisms.

In each capillary, we can consider that under the same concentration gradient (i.e. of partial pressure), free diffusion far from the walls and Knudsen diffusion near the walls combine in parallel. The resulting flow remains proportional to the concentration gradient and the proportionality coefficient is homogeneous to a diffusion coefficient. We can therefore write:

$$J_{pore} = -D_{pore} \frac{\partial c}{\partial x} \qquad [6.105]$$

In this relationship, the proportionality coefficient D_{pore} depends on each type of flow, and thus on the diameter of the pore and the mean free path of molecules; and therefore, on total pressure.

6.5.3. *The diffusion of a gas in a porous material*

In the case of a porous matter, gaseous diffusion can again be described, as in the case of solutes in a saturated porous medium, by a proportionality relationship designated by Fick's law applied to dry porous material. This law relates the effective parameters:

$$J_{e,dry} = -D_{e,dry} \frac{\partial c}{\partial x} \qquad [6.106]$$

The proportionality coefficient $D_{e,dry}$ is called the effective diffusion coefficient. It depends on the diffusion coefficient of the gas and on the characteristics of the porous structure accessible to the transport of gas.

We showed in section 6.1 that the mean free path of oxygen at atmospheric pressure is in the order of 60 nm. In cementitious materials, the diameters of many pores are of this order of magnitude or below this value. If we consider the diffusion of this gas in the porous structure of cementitious materials, Knudsen diffusion is significant. The effective diffusion coefficient $D_{e,dry}$ takes into account the two modes of diffusion (free and Knudsen) in an overall manner. The "response" of the material to a partial pressure gradient can be characterized by the tortuosity that is defined here by the relationship between the effective diffusion coefficient and the diffusion coefficient of the same gas in an infinite medium[13].

In the case of ionic diffusion in a saturated porous medium, transport occurs in the liquid phase contained in the interconnected open porosity. If the state of saturation diminishes, transport is maintained as long as there is still a continuous liquid route in the porous environment. In the case of gases, diffusion still occurs through interconnected open porosity, but in the gaseous phase.[14] It is therefore highest in dry porous materials. However, it does not necessarily involve all of the interconnected open porosity. In fact, gas molecules can adsorb on the walls of pores and limit the area of passage.

One specific and important case is that of the diffusion of a gas in a porous solid containing atmospheric humid air. This situation occurs in many practical cases, particularly in numerous applications related to the storage of volatile matters. For example, this type of diffusion occurs in concrete barriers or rocks that can let gases that are formed by radiolysis escape from radioactive waste at storage sites. In a porous material in the dry state, gas can diffuse throughout the interconnected open porosity. When the relative humidity of the air increases, water molecules adsorb on the pore walls. The available passage area for the diffusion of gas decreases, and the effective diffusion coefficient, is reduced. As a first approximation, we can express the effective diffusion coefficient $D_{e,v}$ of the gas in the partially saturated porous material with respect to open porosity and the degree of saturation by the relationship [DAÏ 93]:

$$D_{e,v} = p_0(1-s)D_{e,dry} \qquad [6.107]$$

13 See note 6.2.

14 The diffusion coefficient of a gas in a liquid phase is lower than that of the diffusion coefficient in a gaseous phase by around four orders of magnitude.

When the relative humidity of atmospheric air increases, the degree of saturation of the porous environment increases and liquid water can condense. The Kelvin-Laplace law (relationship [5.26] presented in Chapter 5) expresses the relationship between relative humidity and the radius of the largest pores filled with water. At increasing humidity, the area of the passage available for the diffusing gas diminishes and, when the continuity of the gaseous phase is interrupted, the effective diffusion coefficient drops considerably, as Figure 6.26 shows.

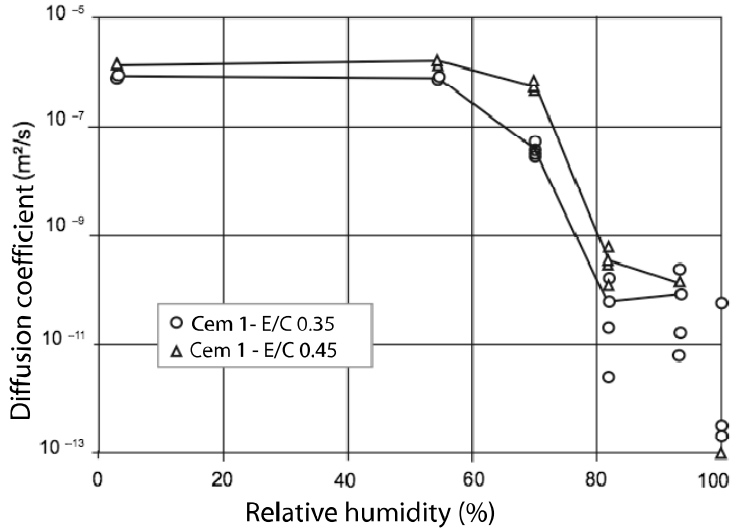

Figure 6.26. *Influence of the state of saturation of concrete on an effective diffusion coefficient of hydrogen [SER 06]*

Drying (isothermal transport of humidity) of walls is an important problem in the domain of construction. We will present this specific case in Chapter 7, since this transport results from two components: one governed by permeability, which will be at the heart of Chapter 7; and the other governed by the diffusion of water vapor.

6.5.4. *The diffusion of a gas in a reactive porous environment*

A specific and important case of gaseous diffusion in a reactive porous solid is that of the diffusion of atmospheric CO_2 in concrete. The term

"carbonation" designates chemical reactions between CO_2 and cement hydrates. This carbonation, which is manifested by a reduction in the pH of the interstitial solution of concrete, is of great practical consequence, since it is the principal cause of the initiation of corrosion of reinforcements in reinforced concrete.

The description of the phenomenon of carbonation is extremely complex, as it generally occurs in a partially saturated environment (concrete in the exterior atmosphere) and chemical reactions lead to the production of liquid water in the material. From a phenomenological point of view, the phenomena are described fairly simply by the progression of a carbonation front that corresponds to the transition of pH from around 13 to 9, with the latter value corresponding to that for which the steel in the reinforcements loses its immunity. As for other diffusion phenomena, carbonation penetrates into the concrete according to a law of type:

$$x = k\sqrt{t}$$

Factor k of proportionality depends on numerous factors, such as the concentration of CO_2, the formulation of the concrete, the composition of the cement, the relative humidity of the atmosphere, etc. It is thus difficult to predict, even more so since the humidity of the conservation atmosphere varies, which is the case in natural environments. In addition, the chemical reactions of carbonation cause a reduction in the porosity of the cement paste, which has positive effects on the progression of CO_2 in the material.

Due to its importance, this subject needed to be mentioned here, but its solution has not yet been achieved. We refer interested readers to two references that discuss the studies in progress: [HYV 09] and [THI 05].

6.6. Bibliography

[AMI 97] AMIRI O., AIT-MKHTAR K., SEIGNEURIN A., "A complement to the discussion of A. Xu and S. Chandra about the paper 'Calculation of chloride coefficient diffusion in concrete from ionic migration measurements' by C. Andrade", *Cement and Concrete Research*, vol. 26, pp. 951-957, 1997.

[ARC 42] ARCHIE G.E., "The electrical resistivity log as an aid in determining some reservoir characteristics", *Trans. AIME*, vol. 146, pp. 54–67, 1942.

[ARL 07] ARLIGUIE G., HORNAIN H., *GranDuBé – Grandeurs Associées à la Durabilité des Bétons*, Presses de L'ENPC, 6, 1997.

[ARS 99] ARSENAULT J., Étude des mécanismes de transport des ions chlore dans le béton en vue de la mise au point d'un essai de migration. Doctoral thesis, University of Laval, Québec and INSA of Toulouse, France, 1999.

[ATK 84] ATKINSON A.,NICKERSON A., "The diffusion of ions through water-satured cement", *J. Mat. Sci.*, vol. 19, pp. 3068-3078, 1984.

[BAR 01] BAROGHEL-BOUNY V., "Transferts dans les bétons et durabilité", *Revue Française de Génie Civil*, vol. 5, no. 2-3, pp. 149-177, 2001.

[BES 84] BESSON J., *Précis de thermodynamique et cinétique électrochimiques*, Imprimeries Aubin, 1984.

[BFU 02] Bétons Fibrés à Ultra Hautes Performances (BFUP) – Recommandations Provisoires, 2002. Downloadable at: http://www.afgc.asso.fr/images/stories /pub/Betons_fibres.pdf.

[BIG 94] BIGAS J.P., La diffusion des ions chlores dans les mortiers, Doctoral thesis, INSA Toulouse, France, 1994.

[BLO 46] BLOCH E. *Théorie Cinétique des Gaz*, Armand Colin, 1946. Available at: www.archive.org/stream/thoriecintiqued00blocgoog/thoriecintiqued00blocgoog_ djvu.txt, accessed 27.1.12.)

[BOC 70] BOCKRIS J. M., REDDY A.K.N., *Modern Electrochemistry*, Plenum Press, New York, 1970.

[BOC 82] BOCKRIS J.M., CONWAY B.E., *Modern Aspects of Electrochemistry*, Plenum, New York, 1982.

[BRU 35] BRUGGEMAN V.D.A.G., "Berechnung verschiedener physikalischer konstanten von heterogenen substanzen", *Annalen der Physisk*, vol.24, pp. 636-679, 1935.

[CAM 02] CAMPO M.A., WOO L.Y., MASON T.O., GARBOCZI E.J., "Frequency-dependent electrical mixing law behavior in spherical particle composites", *Journal of Electroceramics*, vol. 9, no. 1, pp. 49-56, 2002.

[CAR 95] CARE S., HERVE E., "Prediction of the chloride diffusion coefficient in concrete using the homogenization technique", *Testing and Modelling the Chloride Ingress into Concrete, 2nd International RILEM Workshop*, Saint-Rémy-lès-Chevreuse, France, October 1995.

[CHR 94] CHRISTENSEN B.J., COVERDALE R.T., OLSON R.A., FORD S.J., GARBOCZI E.J., JENNINGS H.M., MASON T.O., "Impedance spectroscopy of hydrating cement-based matters: measurement, interpretation, and application", *Journal American Ceramic Society*, vol. 77, no. 11, pp. 2789-2804, 1994.

[CRA 75] CRANCK J., *The Mathematics of Diffusion*, Clarendon Press, Oxford, 1975.

[DAÏ 93] DAÏAN J.-F., LAURENT J.-P. "Structure poreuse et transport d'humidité dans les roches", in : LEFEBVRE R.A. (Ed.), *Cours Européen Sciences et Matériaux du Patrimoine Culturel,* first session, Ravello/Rome, Istituto Poligrafico e Zecca dello Stato, Libreria dello Stato, Rome, Italy, pp. 83-112, 1993.

[FAR 73] FARDADE H., Évolution du profil hydrique dans le sol en présence d'un gradient thermique, Doctoral thesis, Faculté des sciences agronomiques, Gembloux, 1973.

[FRA 01] FRANCY O., FRANCOIS, R., "Modélisation du transfert couplé ion chlore-humidité dans les matériaux cimentaires", *Revue Française de Génie Civil*, vol. 5, no. 2-3, pp. 377-396, 2001.

[FIC 55] FICK A., "Concerns diffusion and concentration gradient", *Ann. Phys. Lpz*., vol. 170, no. 59, 1855.

[FRI 03] FRIZON F., Décontamination électrocinétique des milieux poreux. Etude expérimentale et modélisation appliquées au césium dans les matériaux cimentaires, Doctoral thesis, INSA Toulouse, France, 2003.

[GAR 90] GARBOCZI E.J., "Permeability, diffusivity and microstructural parameters: a critical review", *Cement and Concrete Research*, vol. 20, no. 4, pp. 591-601, 1990.

[GAR 92] GARBOCZI E.J., BENTZ D.P., "Computer simulation of the diffusivity of cement-based matters", *J. Mat. Sci*., vol. 27, pp. 2083-2092, 1992.

[GAR 94] GARBOCKI E.J., SCHWARTZ L.M., BENTZ D.P., "Modelling the DC electrical conductivity of mortar", *Microstructure of Cement-Based Systems/Bonding and Interfaces in Cementitious Matters*, MRS Symposia, Vol. 370, pp. 429-436, 1994.

[GUE 94] GUEGEN Y., PALCIAUSKAS V., *Introduction to the Physics of Rocks*, Princeton University Press, 1994.

[HAL 95] HALAMICKOVA P., DETWILER R.J., BENTZ D.P., GARBOCZI E.J., "Water permeability and chloride ion diffusion in Portland cement mortars: relationship to sand content and critical pore diameter", *Cement and Concrete Research*, vol. 25, no. 4, pp. 790-802, 1995.

[HYV 09] HYVERT N., Application de l'approche probabiliste à la durabilité des produits préfabriqués en béton, Doctoral thesis, University of Toulouse, France, 2009.

[KAM 03] KAMALI S., Comportement et simulation des matériaux cimentaires en environnements agressifs: lixiviation et température, Doctoral thesis, Ecole Normale Supérieure de Cachan, 2003.

[KUM 86] KUMAR A., ROY D.M., "Pore structure and ionic diffusion in admixture blended Portland cement systems", *Eighth International Congress on the Chemistry of Cement*, Rio de Janeiro, Brazil, vol. V, no. 4, pp. 73-79, 1986.

[LOB 03] LOBET A., Influence des paramètres de composition des matériaux cimentaires sur les propriétés de transfert, Doctoral thesis, INSA de Toulouse, France, 2003.

[MCL 90] MCLACHLAN D.S., BLASZKIEWICZ M., NEWNHAM R.E., "Electrical resistivity of composites", *Journal American Ceramic Society*, vol. 73, no. 8, pp. 2187-2203, 1990.

[MIL 89] MILLS R., LOBO V.M., *Self-Diffusion in Electrolyte Solutions*, Elsevier Press, Amsterdam, Netherlands, 1989.

[NGU 07] NGUYEN T.Q., Modélisations physico-chimiques de la pénétration des ions chlorure dans les matériaux cimentaires, Doctoral thesis, Ecole Nationale des Ponts et Chaussées Paris, France, 2007.

[NUM 90] NUMATA S., AMANO H., MINAMI K., "Diffusion of tritiated water in cement matters', *Journal of Nuclear Matters*, vol. 171, pp. 373-380, 1990.

[NUG 02] NUGUE F., Recherche d'une méthode rapide de détermination du coefficient de diffusion en milieu cimentaire saturé, Doctoral thesis, INSA de Toulouse, France, 2002.

[OLL 08] OLLIVIER J.P., TORRENTI, J.M., "La structure poreuse des bétons", in: OLLIVIER J.P., VICHOT A. (eds.), *La Durabilité des Bétons*, Presses de l'ENPC, Paris, France pp. 51-135, 2008.

[RIC 92] RICHET C., Etude de la migration des radioéléments dans les liants hydrauliques – Influence du vieillissement des liants sur les mécanismes et la cinétique des transferts, Doctoral thesis, Paris XI, Orsay, France, 1992.

[SER 06] SERCOMBE J., VIDAL R., ADENOT F. "Diffusion des gaz dans les ciments, mécanismes et paramètres principaux", *Transfert 2006*, 1-2 February, Lille, France, 2006.

[TAN 93] TANG L., NILSSON L.O., "Chloride binding capacity and binding isotherm of OPC pastes and mortars", *Cement and Concrete Research*, vol. 23, pp. 247-253, 1993.

[TAN 96] TANG L., "Electrocally accelerated methods for determining chloride diffusivity in concrete – current development", *Mag. Concr. Res*., vol. 48, no. 176, pp. 173-179, 1996.

[TER 76] TERASHIMA Y., KUYAMI T., *Proc. Jpn. Soc. Civ. Eng*, vol. 256, pp. 91, 1976.

[THI 05] THIERY M., Modélisation de la carbonatation atmosphérique des bétons – Prise en compte des effets cinétiques et de l'état hydrique, Doctoral thesis, Ecole Nationale des Ponts et Chaussées, 2005.

[TOG 98] TOGNAZZI C., Couplage fissuration-dégradation chimique dans les matériaux cimentaires: caractérisation et modélisation, Doctoral thesis, INSA de Toulouse, France, 1998.

[TOU 05] TOURRENC P., Thermodynamique et Applications Biologiques, University Pierre and Marie Curie, 2005.

[TRU 00] TRUC O., Prediction of chloride penetration into concrete – Multi-species approach, Doctoral thesis, INSA de Toulouse, France, 2000.

[TUM 96] TUMIDAJSKI P.J., SCHUMACHER A.S., PERRON S., GU P., BEAUDOIN J.J., "On the relationship between porosity and electrical resistivity in cementitious systems", *Cement and Concrete Research*, vol. 26, no. 4, pp. 539-544, 1996.

[USH 74] USHIYAMA H., GOTO S., "Diffusion of various ions in hardened Portland cement pastes", *The VI International Congress on the Chemistry of Cement*, 21-28 September, Moscow, 1974.

[XU 00] XU G., BEAUDOIN J.J., JOLICOEUR C., PAGE M., "The effect of a polynaphthalene sulfonate superplasticizer on the contribution of the interfacial transition zone to the electrical resistivity of mortars containing silica and limestone fine aggregate", *Cement and Concrete Research*, vol. 30, no. 5, pp. 683-691, 2000.

6.7. Exercises

Exercise 6.1: *Application of Nernst-Planck's law in the case of two ions*

Let us examine a case where the concentrations in solution remain low (thus, activity = concentration). The equation that governs the transport of an ion, *i*, in the presence of an electrical field is the Nernst-Planck equation:

$$J_i = -D_i^0 \left[\nabla c_i + z_i c_i \frac{F}{RT} \nabla \varphi \right]$$

where:

– J_i is the unitary flow of the ion *I*;

– c_i is its concentration;

– z_i is its valency; and

– F is the Faraday constant.

Let us look at the specific case wherein only two ions are present: Cl^- and Na^+. In the case of a diffusion test, there is electroneutrality, from which:

$$\sum_{i=1}^{n} z_i c_i = 0$$

In our case, since the valence of the two ions is equal to 1, this means that their concentrations are equal to *c*. In a diffusion test, there is no current, which results in:

$$j = 0 = F\sum_{i=1}^{n} z_i J_i \ .$$

a) Replacing J_i with its expression in this equation, if we call D^0_1 the coefficient of sodium and D^0_2 that of chlorides, show that we can express the potential φ by:

$$\nabla\varphi = -\frac{RT}{F}\frac{\left(D_1^0 - D_2^0\right)}{\left(D_1^0 + D_2^0\right)}\frac{\nabla c}{c}$$

This relationship shows that the potential gradient is proportional to the concentration gradient, and inversely proportional to concentration. We can also note that if the diffusion coefficients are equal, the potential gradient disappears. In other words, this means that when we apply Fick's law, we suppose that the diffusion coefficients of species are equal, which is not the case.

b) By introducing this value of potential gradient in the Nernst-Planck law, show that we then obtain:

$$J_1 = J_2 = -\frac{2D_1^0 D_2^0}{D_1^0 + D_2^0}\nabla c\ .$$

In the end, everything occurs as if we used Fick's law with an average diffusion coefficient such as:

$$D_m^0 = \frac{2D_1^0 D_2^0}{D_1^0 + D_2^0}$$

This relationship shows the interaction between ions during diffusion.

Exercise 6.2.

The goal of this exercise is to study a way of predicting the lifespan of structures in reinforced concrete, in a simplified manner, with the criterion being the corrosion of reinforcements in sea environments; i.e. in the presence of chlorides.

We will limit ourselves in this problem to cases of saturated concrete in which the penetration of chlorides occurs by diffusion.

1) *The diffusion of ions in solution*

We will suppose that there is no interaction between the chlorides and the hydrates in the concrete.

We will examine the porosity of concrete and consider in this part the diffusion of chlorides in the interstitial liquid. The flow of ions J^* traversing a single area of interstitial solution contained in a pore is given by Fick's first law:

$$\overrightarrow{J^*} = -D^* \overrightarrow{gradc}$$

or, uniaxially:

$$J^* = -D^* \frac{\partial c}{\partial x}$$

where:

– c is the concentration of Cl^- ions in solution in kg/m^3 of solution;

– J^* is the flow in kg/m^2.s of interstitial solution; and

– D^* is the diffusion coefficient of chlorides in solution of pores in m^2/s, which we will suppose to be constant for a given matter and ionic species.

Writing the conservation of the mass of ions in a elementary volume (see Figure 6.27), show that we obtain Fick's second law (uniaxially):

$$\frac{\partial c}{\partial t} = D^* \frac{\partial^2 c}{\partial x^2}$$

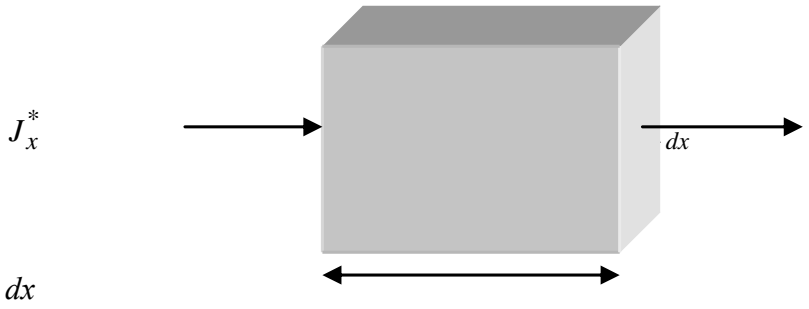

Figure 6.27. *Elementary volume*

2) *Diffusion in a porous medium*

Concrete is a porous medium with a porosity of p_0 . We will suppose that if we take a cross-section, the surface porosity (ratio of pore surface to total surface) is equal to p. We write the flow J_e of chloride ions passing through a single concrete surface in the following manner:

$$\vec{J}_e = -D_e \overrightarrow{gradc}$$

where D_e is the effective diffusion coefficient in m^2/s and c is the concentration of Cl^- ions in solution in kg/m^3 of solution.

Show that we get:

$$D_e = p_0 D^*$$

3) *Interaction with the solid*

In reality, a portion of the Cl^- ions are bound by the solid. We will suppose that the binding is linear; i.e. that the relationship linking concentrations of fixed chlorides C_s (in kg of Cl^-/kg of solid) to the concentrations of free chlorides c in solution is given by: $C_s = K_d \,.\, c$, where K_d is the distribution coefficient in m^3/kg.

Writing the conservation of mass, taking this interaction into account, show that Fick's second law can be written monoaxially as:

$$\frac{\partial c}{\partial t} = D_a \cdot \frac{\partial^2 c}{\partial x^2}$$

with

$$D_a = \frac{D_e}{p_0 + (1 - p_0) \cdot \rho_s \cdot K_d}$$

where D_a is the apparent diffusion coefficient and ρ_s is the density of concrete. We will then put $\alpha = p_0 + (1 - p_0) \cdot \rho_s \cdot K_d$.

4) *Measurement of the diffusion coefficient*

The measurement of the diffusion coefficient can be done with the help of a diffusion cell, see Figure 6.28.

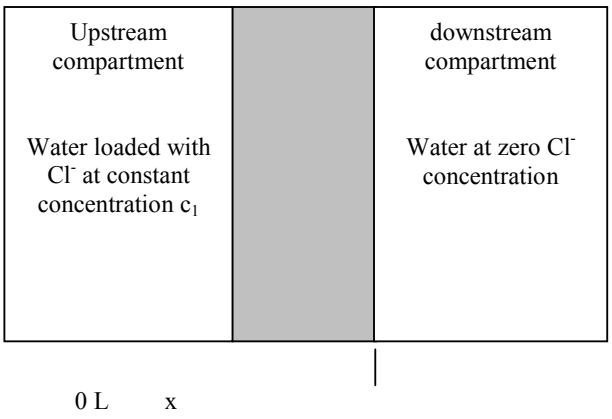

Figure 6.28. *Diffusion test*

Show that the following expression is the solution to Fick's second law and verifies the experimental boundary conditions in Figure 6.28:

$$c(x,t) = c_1\left[1 - \frac{x}{L} - \frac{2}{\pi}\sum_{n=1}^{\infty}\frac{1}{n}sin(\frac{n\pi x}{L}).exp(-D_e.\frac{n^2\pi^2 t}{\alpha L^2})\right]$$

We can show that the cumulative quantity of ions, $Q(t)$, being diffused in the lower compartment per unit of area during time, t, tend asymptotically toward a relationship such as:

$$\frac{L\cdot Q(t)}{c_1} = D_e\cdot t - \alpha.\frac{L^2}{6}$$

Experimental data can be inserted into the system of coordinates:

$$\frac{L.Q(t)}{c_1} = f(t)$$

a) To what does the effective diffusion coefficient correspond in this system of coordinates?

b) Using Figure 6.29, determine the effective diffusion coefficient (in mm^2/year) of concrete with a *W/C* ratio of 0.60 and a porosity of 0.18. Deduce from this the diffusion coefficient in the solution of pores, D^*.

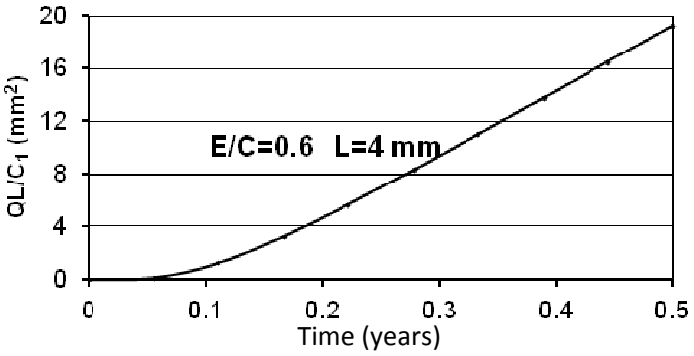

Figure 6.29. *Result of the diffusion test on concrete with W/C 0.60 and L = 4mm*

c) Knowing that the theoretical diffusion coefficient of the chloride ion in water D_0 is equal to 63.10^3 mm^2/year, we can define the coefficient f so that $D^* = f \cdot D_0$. Calculate f for concrete. What is the physical meaning of this parameter?

5) *Size of the covering of reinforcements*

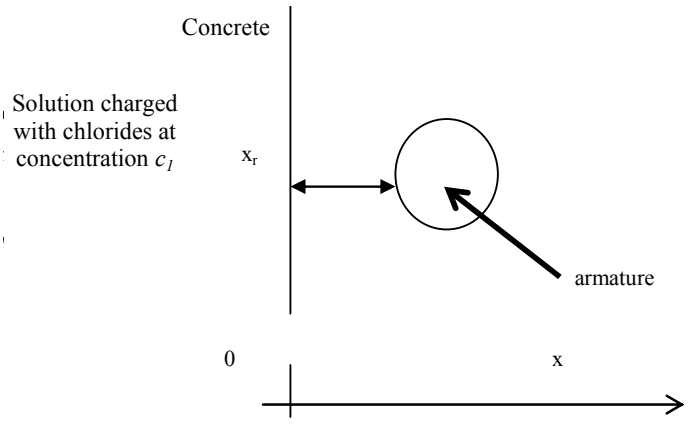

Figure 6.30. *Positioning of the arm in the reinforced concrete*

Now let us consider the problem of a semi-infinite reinforced concrete structure in contact with a chloride-charged solution, see Figure 6.230.

The analytical solution of Fick's second law is written for such a problem as:

$$c(x,t) = c_1 \cdot erfc(\frac{x}{\sqrt{4D_a \cdot t}})$$

where:

$$erfc(y) = \frac{2}{\sqrt{\pi}} \cdot \int_y^{\infty} e^{-\xi^2} d\xi$$

Trace the analytical solution obtained for concrete at t = 100 years.

Givens: *c1*= 2 % per kg of cement (we will use the unit proposed by standard EN V 206 "Performances, production, implementation, and compliance criteria" of concrete here). *Kd* = 10–3 m^3/kg and ρ_as = 2,400 kg/m^3 for concrete.

Table 6.4 gives the values of function *erfc (y)* for some values of *y*.

y	***erfc(y)***	***y***	***erfc(y)***
0	1	0.8	0.2579
0.05	0.9436	0.9	0.2030
0.1	0.8875	1.0	0.1572
0.15	0.8320	1.1	0.1198
0.2	0.7773	1.2	0.0897
0.25	0.7237	1.3	0.0660
0.3	0.6713	1.4	0.0477
0.35	0.6206	1.5	0.0338
0.4	0.5716	1.7	0.0162
0.45	0.5245	2.0	0.0046
0.5	0.4795	2.3	0.0011
0.6	0.3961	2.6	0.0002
0.7	0.3221	3.0	0.00002

Table 6.4. *Table of functions erf(y) and erfc(y)*

For size, we seek the covering x_r so that at the end of time t_{dv} the chloride concentration will be less than a critical value, c_{cr}.

a) With $c_0 = erfc^{-1}(c_{cr}/c_1)$, show that $x_r = 2c_0\sqrt{D_a \cdot t_{dv}}$

b) Give the covering necessary to guarantee a life span t_{dv} of 100 years with the concrete considered.

Given: c_{cr} = 0.4% per kg of cement.

Exercise 6.3: ***hydration of cement and diffusion of chlorides***

1) *Hydration*

In this section, we will look at the evolution of the porosity of Portland cement paste during its hydration. To do this, we will consider a sample of cement paste with a given composition (*W/C* ratio) and conserved in air.

Take p_o as the initial porosity of the cement paste in the fresh condition, the ratio between the volume of voids and the apparent volume. Disregarding occluded air that may be in the paste:

– express p_o with respect to the weighted *W/C* ratio of the masses of mixing water and cement,

– determine the values of p_o for the *W/C* values in Table 6.5.

W/C	0.1	0.2	0.3	0.4	0.5	0.6	0.7	0.8	0.9	1.0

Table 6.5. *Values of E/C ration*

Additional data: we will take ρ_s = 3.12 g/cm^{3}as the absolute density of the cement.

During the hydration of cement, the volume fractions of the cement, hydrates and residual voids (capillary pores) change. We will determine the evolution with the hydration of these volume fractions.

Hypotheses:

– 1 cm^3 of anhydrous cement and 1.34 cm^3 of water produce 2.13 cm^3 of hydrates (the Le Chatelier contraction);

– the hydration of cement can continue as long as there is water;

– the degree of hydration, the ratio of the mass of hydrated cement at a given time to the initial anhydrous cement mass, is called α;

– initially, we will consider that there is no desiccation of the paste, since it is protected (cured).

a) Give the expressions of the volume fraction of hydrates (f_{hyd}) and of the volume fraction of anhydrous cement (f_{anh}) in terms of p_o and α. Deduce from this the fraction of capillary pores (P_{cap}).

b) Calculate the maximum degree of hydration taking into account the hypotheses pertaining to *W/C*. Justify the *W/C* value of 0.42 leading to complete hydration without any remaining anhydrates or water.

c) Figure 6.31 represents the evolution of the volume fractions f_{hyd}, f_{anh} and P_{cap} for a maximum degree of hydration with respect to the *W/C* ratio. We will now consider that the cement paste is not protected from premature desiccation. Show on Figure 6.31 the evolution of the volume fractions f_{hyd}, f_{anh} and P_{cap} for a degree of hydration equal to half of the maximum degree of hydration.

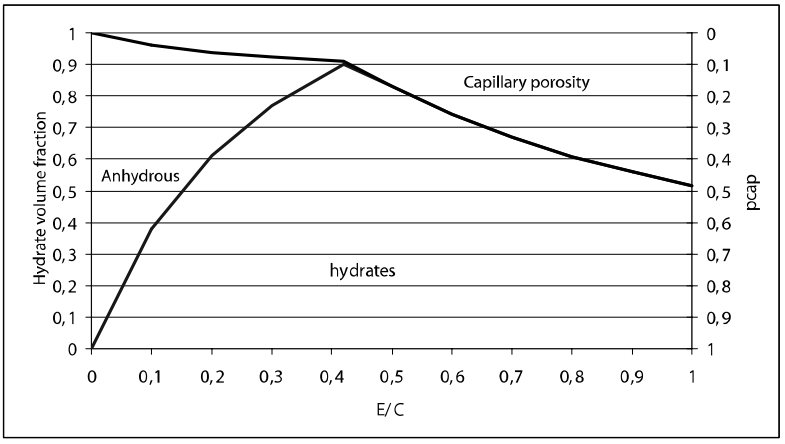

Figure 6.31. *Volume fractions of components of hydrated cement*

2) *Diffusion*

Now let us look at the diffusivity of ions through cement paste. We will suppose that we have only steady state diffusion without the sorption of ions, and that the degree of hydration is maximal.

a) If capillary porosity is below 18%, we will suppose that diffusion occurs in series across the three phases, as indicated in Figure 6.30. Using Fick's first law $J = -D\frac{\partial C}{\partial x}$ show that the equivalent diffusion coefficient D_{eq} of the cement paste is such that:

$$\frac{1}{Deq} = \frac{fanh}{Danh} + \frac{fhyd}{Dhyd} + \frac{pcap}{Dcap}$$

b) If capillary porosity is higher than 18%, diffusion occurs in part through capillary porosity. The hypothetical schema is that of Figure 6.32.

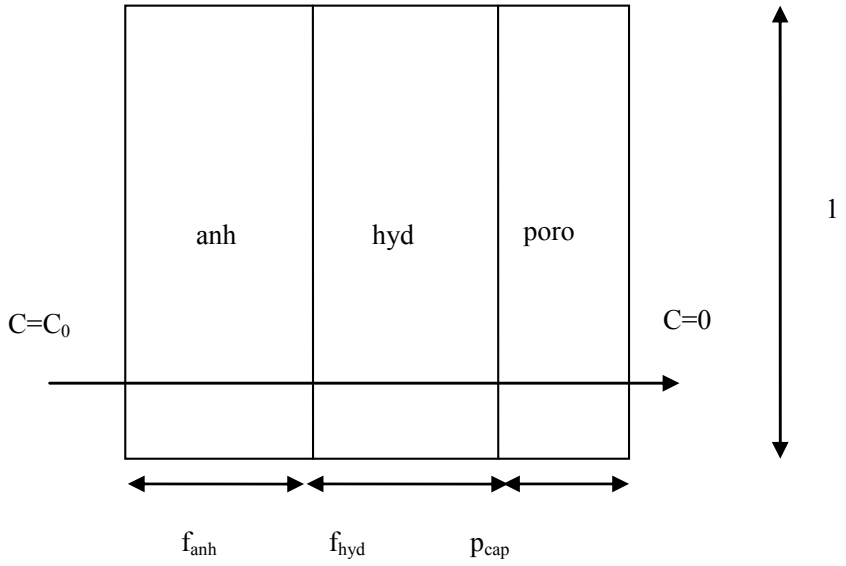

Figure 6.32. *Hypothetical schema of diffusion in in steady state regime for* $p_{cap} > 0.18$

Express the equivalent diffusion coefficient D_{eq} of the cement paste by writing that the total flow passing through the cement paste is the sum of the flows passing through the two parts.

c) *Numerical applications*

The diffusion coefficients of the various phases are as follows:

– porosity $D = 9 \times 10^{-11}$ m^2/s;

– anhydrous $D = 2 \times 10^{-13}$ m^2/s; and

– hydrates $D = 1 \times 10^{-11}$ m^2/s.

Calculate the diffusion coefficients corresponding to cement pastes of *W/C* 0.3, 0.5 and 0.6. Place these points on Figure 6.33.

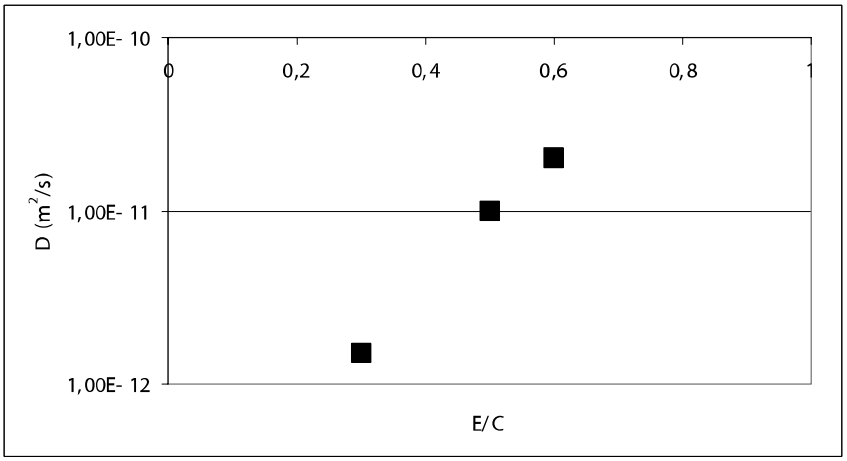

Figure 6.33. *Diffusion coefficients – experimental values*

W/C	0.3	0.5	0.6
D (m^2/s)	1.5×10^{-12}	1×10^{-11}	2×10^{-11}

Table 6.6. *Experimental data for Figure 6.33*

Chapter 7

Permeability

7.1. Introduction

The permeability of a material is defined as its ability to be traversed by a fluid under the effect of a pressure gradient. This physical magnitude can be a property of use, as in the case of a dam or a pressurized gas reservoir. For concrete structures, it can also act as an indicator of durability like other parameters, such as porosity or diffusion coefficient.

In Chapter 6, the physical phenomenon studied was diffusion and its associated parameter, the diffusion coefficient. The term "permeability" is sometimes associated as much with the physical phenomenon as with the physical parameter that characterizes it. Others use the term "permeability coefficient" to designate the parameter, but we will see that this term has another meaning entirely in the domain of soil hydraulics. To avoid any risk of confusion, we will use the following terminology here: the physical phenomenon of transfer under pressure gradient is called "permeation" and the physical parameter associated with it is called "permeability".

The flow of a fluid through a porous material under the effect of a pressure gradient is the result of flows that occur through interconnected open pores. The permeability of a material is thus linked to its porous structure. In this chapter, after defining permeability and the methods of

Physical Properties of Concrete and Concrete Constituents Jean-Pierre Ollivier, Jean-Michel Torrenti and Myriam Carcassès

measurement used to characterize consolidated materials[1], we will look in more detail at flows in pores under pressure gradients, and we will then present the relationships between permeability and porous structure. To conclude, we will examine the drying of concrete; indeed, we will see that drying and transfer by permeation are closely related.

7.2. Definition of the permeability of a material

Consider a slice of a material with a primary thickness dx and a visible area A. The two parallel faces of the material are in contact with a fluid of viscosity, μ. A pressure difference, dP, exists between the two faces. If the material is permeable, a volume flow, q, of fluid occurs. The expression of this flow by Darcy's law[2] is used to define the permeability k of the material:

$$q = -\frac{k}{\mu} A \frac{dP}{dx} \qquad [7.1]$$

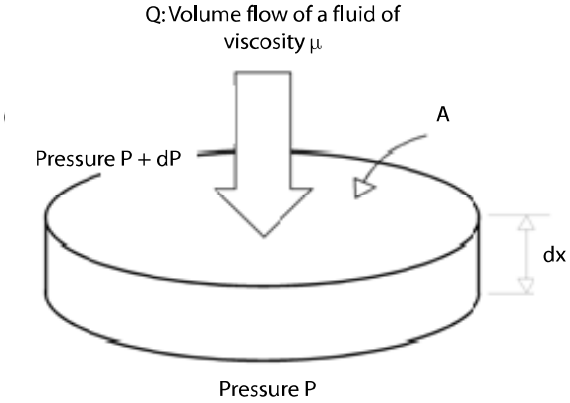

Figure 7.1. *Diagram of transport by permeation*

1 The permeability of granular materials, such as soils, belongs more to the domain of soil hydraulics; we will not discuss this here.

2 If the pressure gradient presents components in the three directions x, y and z, Darcy's law can be generalized by defining a permeability tensor of which the components in the three directions are only identical if the material is homogeneous. Here, In Chapter 7, we will only consider homogeneous materials with unidirectional pressure gradients. Relationship [7.1] will therefore define the permeability of the material.

The permeability thus defined is homogeneous in an area and is thus expressed in m^2 in the international system (SI) of units[3].

Darcy's relationship [7.1] is only applicable if the flow system is laminary and if the fluid is inert with regard to the material. If these hypotheses are verified, it appears that permeability is an intrinsic magnitude. This means in particular that its value is independent of the (inert) fluid used and the pressure gradient.

In the domain of soil hydraulics, a coefficient designated by the term "permeability" is sometimes defined, which is expressed in m/s in the SI unit system, and is thus homogeneous with speed. It is therefore not the same parameter. This parameter, k_e, which we will call the "permeability coefficient" here to distinguish it from permeability, is defined by the following relationship:

$$v = \frac{q_e}{A} = -k_e i \qquad [7.2]$$

Where v is the apparent speed[4] of the water in the material, defined as the relationship between the volume flow of water, q_e, and the apparent section, A. The flow occurs under the effect of the hydraulic gradient i, defined as the relationship between the difference in the driving charge of water and the length of water flow in the material. Taking the permeability definition schema, the hydraulic gradient can be written as:

$$i = \frac{dh}{dx} = \frac{dP}{\varpi_e dx} \qquad [7.3]$$

where ϖ_e is the volume weight of the water. By replacing this value in equations [7.1] and [7.2], the permeability coefficient can be expressed in terms of the permeability and the viscosity, μ_e, of water:

---

3 A "darcy" is a practical unit of permeability. A material has permeability of 1 darcy if it lets flow 1 cm^3/s of a fluid with a viscosity of 1 centipoise (1cP) through a section of 1 cm^2 under a pressure gradient of 1 atm/cm. 1 darcy is equal to 10^{-12} m^2.

4 Also called the filtration speed.

$$k_e = \frac{k\varpi_e}{\mu_e} \qquad [7.4]$$

Relationships [7.2] and [7.4] show that the permeability coefficient is comparable to speed. Unlike permeability, the permeability coefficient is not an intrinsic magnitude, since it is dependent on the fluid. This is not a problem in the domain of soil hydraulics, insofar as the fluid considered is always water, but in other cases of application in which we are interested in the permeation of another fluid this coefficient is no longer pertinent.

7.3. Measurement of permeability

The permeability of porous materials can be measured using permeameters with constant head (the difference in pressure is fixed during the measurement) or variable head.

7.3.1. *Constant head permeameters*

The material to be analyzed presents classically a cylinder with constant transversal section A and length L. Between the two ends, we apply a constant pressure difference, ΔP, and measure the flow when it becomes permanent. In the case of permeable materials (granular materials, for example), the measurement fluid is a liquid; generally water. In the case of low-permeability consolidated materials, we use gases in order to be able to measure flows more easily, since their viscosity is around a 1,000 times lower than that of liquids.

In the case of liquids, permeability can be deduced very simply using Darcy's law (equation [7.1]):

$$v = \frac{q}{A} = -\frac{k}{\mu}.\frac{\Delta P}{L} \qquad [7.5]$$

In the case of gases, compressibility must be taken into account, since if the pressure difference is constant between the ends of the material in a permanent system, the volume flow at the entry is different from that at the

exit. The permeameter used for mortar and concrete is shown in Figures 7.2 and 7.3.

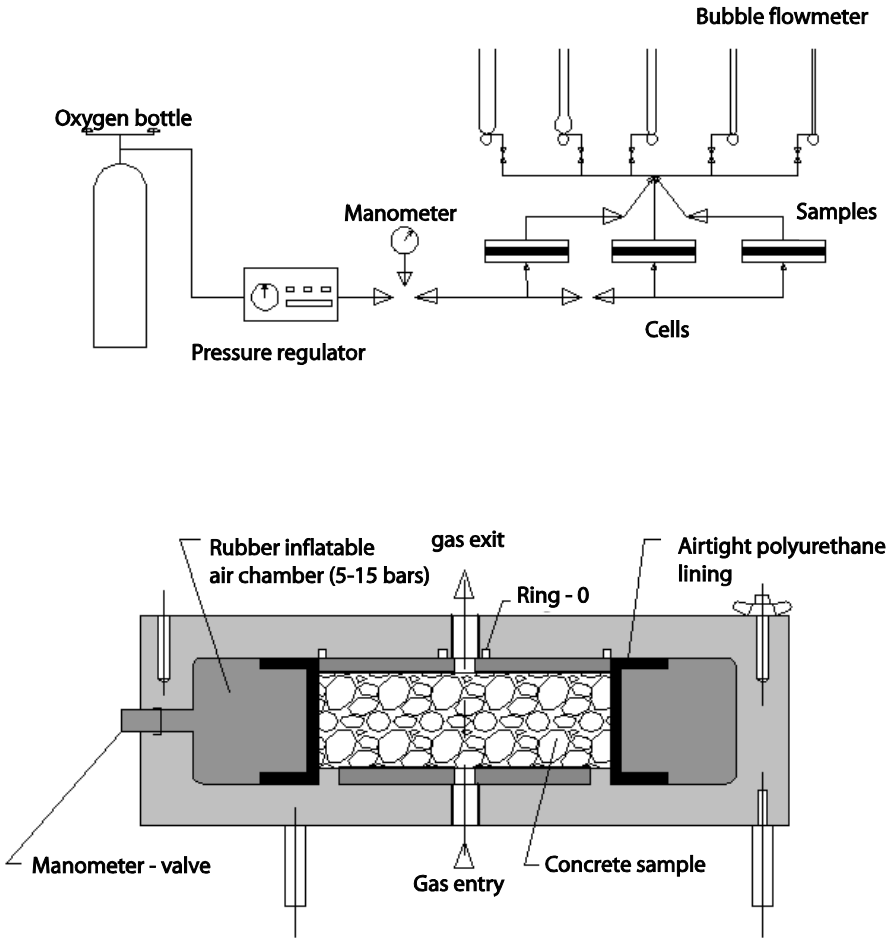

Figure 7.2. *Hypothetical diagram of the CEMBUREAU permeameter used for mortar and concrete*

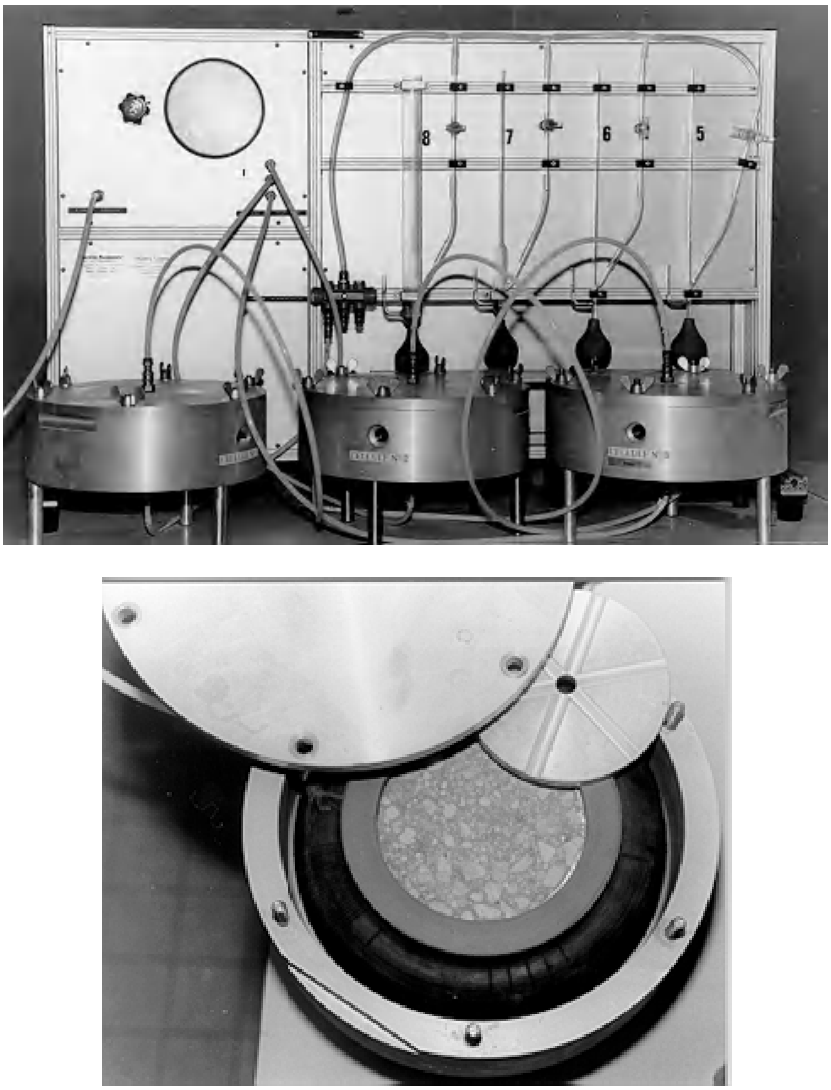

Figure 7.3. *CEMBUREAU permeameter used for mortar and concrete*

The cylindrical sample is schematized in Figure 7.4. In a stationary system, the mass flow of gas $\dot{m}$ is constant in the sample. This flow can be expressed equally on the entry face, in the material, or on the exit face: $\dot{m}_e = \dot{m} = \dot{m}_s$. By introducing the density of gas ρ_e to entry pressure P_e, ρ to

pressure p and ρ_s to exit pressure P_s, we can express the three volume flows at entry, in the material, and at exit as:

$$\rho_e Q_e = \rho q = \rho_s Q_s$$

It is usually the exit flow that is measured. We can express it with respect to the flow within the sample:

$$Q_s = q \frac{\rho}{\rho_s}$$

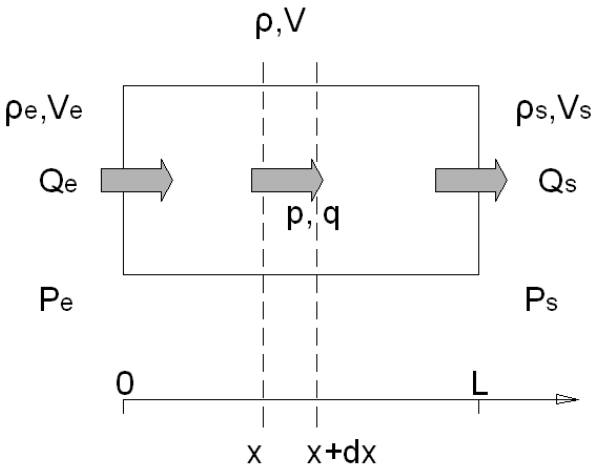

Figure 7.4. *Diagram of a sample in the gas permeameter at constant load*

Supposing that the gas is perfect, the density can be written as:

$$\rho = \frac{PM}{RT}$$

and we get:

$$Q_s = q \frac{P}{P_s}$$

By expressing the flow, q, according to Darcy's law, we get:

$$Q_s = q\frac{P}{P_s} = -\frac{k}{\mu}A\frac{PdP}{P_s dx}.$$

By integrating this equation, we get the permeability value:

$$k = \frac{2\mu Q_s P_s L}{A(P_e^2 - P_s^2)} \qquad [7.6]$$

7.3.2. *Analysis of results: validity of Darcy's law*

The permeability defined thanks to Darcy's law is an intrinsic coefficient, and thus independent of the type of fluid used as well as of the experimental conditions. It is again useful for the fluid used not to react with the study material. For example, in the case of cement materials, water can dissolve certain phases and cause the reprecipitation of new phases. Certain gases, like carbon dioxide, are also discouraged for the measurement of permeability since they react with cement hydrates.

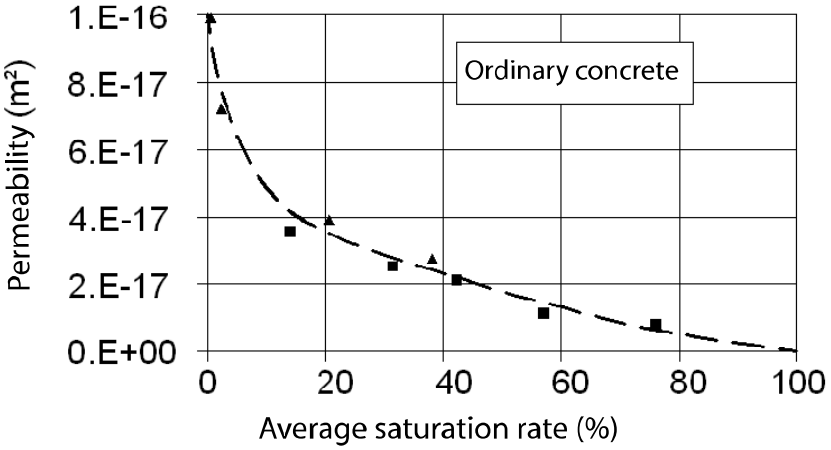

Figure 7.5. *Variation of the permeability of concrete measured for gas with respect to the degree of saturation [VIL 01]*

To measure the permeability of a porous material, it is necessary for all of the communicating porosity to be accessible to the measurement fluid. As an illustration, Figure 7.5 indicates the variation in permeability with the degree of saturation in concrete. We see that the permeability measured varies enormously, particularly near the dry state.

Finally, Darcy's law is only valid if the flow of fluid in the pores is laminary. Taking into account the shape of the pores and the different sizes they can assume in a material, this condition is very difficult to understand *a priori*. On the other hand, by varying the test conditions, it is possible to ensure the validity of Darcy's law *a posteriori* by verifying that the permeability calculated by relationship [7.6] does not change when the experimental conditions are modified.

Experiments show that, in the case of consolidated materials, this is not always the case. The permeability calculated is no longer intrinsic, since its value depends on the experimental conditions and, moreover, the values calculated are higher than that obtained with a liquid. This means that relationship [7.6] cannot be used to calculate the (intrinsic) permeability of a material when measured with a gas. This relationship can be rewritten as follows, noting with P_M the average pressure of the gas in the sample:

$$\begin{aligned} k &= \frac{2\mu Q_s P_s L}{A(P_e^2 - P_s^2)} \\ &= \frac{2\mu Q_s P_s L}{A(P_e + P_s).(P_e - P_s)} \\ &= \frac{\mu Q_s P_s L}{A P_M (P_e - P_s)} \end{aligned} \qquad [7.7]$$

Figure 7.6 represents the variation of permeability of concrete calculated according to relationship [7.7] with respect to the inverse of the average pressure. If Darcy's law has been verified, the permeability calculated must be independent of the test pressure.

Figure 7.6 shows that this is not the case. A classic explanation of this difference is based on the experiments carried out Kundt and Warburg [KUN 75], who showed that if the pressure of a gas flowing in a capillary is reduced until its mean free path becomes of the order of magnitude of the

diameter of the capillary, the flow speed becomes higher than that calculated by Poiseuille's law.

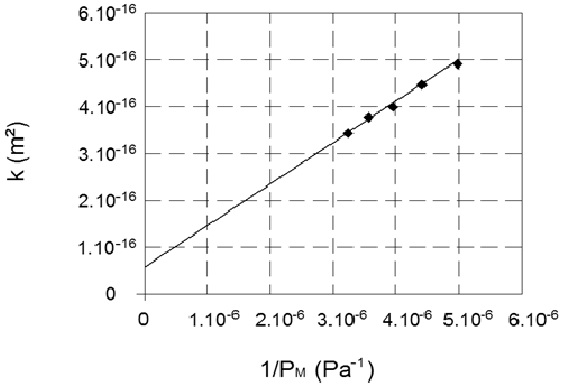

Figure 7.6. *Variation of the permeability, k, with respect to the average pressure in the concrete sample (CEM I – W/C=0.58) [ROZ 07]*

This law expresses the volume flow, Q, of an incompressible fluid flowing in a cylindrical tube of radius r (see Figure 7.7) when the flow is laminary:

$$Q = \frac{\pi r^4}{8\mu} \cdot \frac{\Delta P - Z\rho g}{L_e}$$

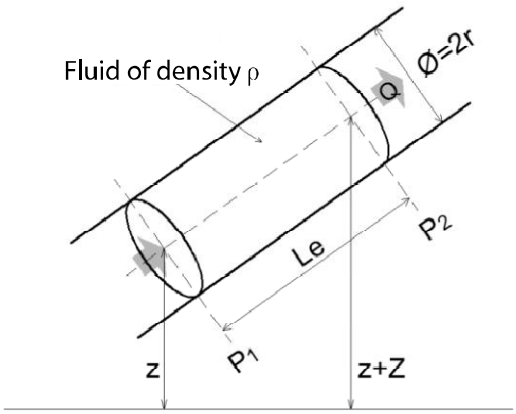

Figure 7.7. *Diagram of a flow governed by Poiseuille's law in a capillary tube*

If the fluid is compressible and disregarding the term $Z\rho g$, the flow is given by relationship:

$$Q = \frac{\pi r^4}{8\mu} \cdot \frac{P_e^2 - P_s^2}{2.P_s.L_e}$$

To analyze the consequences of the phenomenon described by Kundt and Warburg, consider that the flow that occurs by permeation in the material is the sum of the flows that occur in the pores that we suppose to be cylindrical. If the flow is laminary, Poiseuille's law applies, and the exit volume flow can be written as:

$$q_S = \frac{\pi r^4}{8\mu} \cdot \frac{P_s^2 - P_e^2}{2P_s L} = \frac{\pi r^4}{8\mu} \cdot \frac{(P_s - P_e)P_M}{4P_s L}$$

If the entry pressure changes at constant exit pressure, the quantity:

$$\frac{q_s P_s}{P_M (P_s - P_e)} = \frac{\pi r^4}{32 P_s L}$$

is constant and independent of the average pressure. This is the same type of result as the one previously described for permeability when Darcy's law is applicable.

In Chapter 6, the mean free path of a gas molecule of diameter d under pressure P is expressed by relationship [6.4]:

$$\bar{\lambda} = \frac{RT}{\sqrt{2}\pi d^2 N_A P} = \frac{k_B T}{\sqrt{2}\pi d^2 P}$$

The order of magnitude of the mean free path of oxygen in normal conditions of temperature and pressure is 60 nm. This value is of the same order as the dimension of numerous pores in cement materials, and therefore it is not surprising that Poiseuille's law does not correctly represent the

gaseous flows in these pores at pressures close to those used in measurements of the permeability of oxygen reported in Figure 7.6.

When the mean free path of gas molecules is in the order of the diameter of the pores, the flow is governed by Knudsen's law (introduced in Chapter 6, equation [6.106]):

$$J = -\frac{8r}{3\pi}\sqrt{\frac{\pi}{2MRT}}.\frac{dP}{dx}$$

J being molecular flow, we can express the volume flow supposing that the gas is perfect as:

$$q = \frac{8r^3}{3P}\sqrt{\frac{\pi RT}{2M}}.\frac{dP}{dx}$$

From which we can determine the exit flow:

$$q_S = \frac{8r^3}{3P_S}\sqrt{\frac{\pi RT}{2M}}.\frac{(P_S - P_e)}{L}$$

As in the case of a laminary system, we can calculate:

$$\frac{q_S P_S}{P_M (P_S - P_e)} = \frac{8r^3}{3P_M L}\sqrt{\frac{\pi RT}{2M}}$$

Unlike the case of the laminary system, this quantity depends on the average pressure of the gas and varies proportionally to its inverse. This can explain the experimental result in Figure 7.6. The gas flow through the porous material is the sum of a laminary flow independent of the value of the average pressure and of a molecular flow governed by Knudsen's law, which varies proportionally to the inverse of the average pressure. The value of the ordinate at the origin corresponds to the one that would be obtained if the flow were purely laminary: we call this intrinsic permeability, k_v. For the

zero value of $\frac{1}{P_M}$, the pressure is infinite; the mean free path would be zero, and the molecular flow nonexistent. This analysis is consistent with the empirical analysis model proposed by Klinkenberg [KLI 41], which gives an intrinsic permeability value, k_v, depending on the average pressure and apparent permeability, k_a, calculated by Darcy's relationship according to:

$$k_a = k_v(1+\frac{\beta}{P_M}) \qquad [7.8]$$

This conduction of measurements using the calculation of apparent permeabilities calculated for different test pressures is quite classical. It gives a permeability value referred to as intrinsic, as we can see in Figure 7.8. Note that the apparent permeabilities calculated are variable, and in the order of four to five times greater than those of intrinsic permeability. This is also the difference noted with permeability measured with an inert liquid, the value of which will therefore display a more intrinsic character [SKO 05].

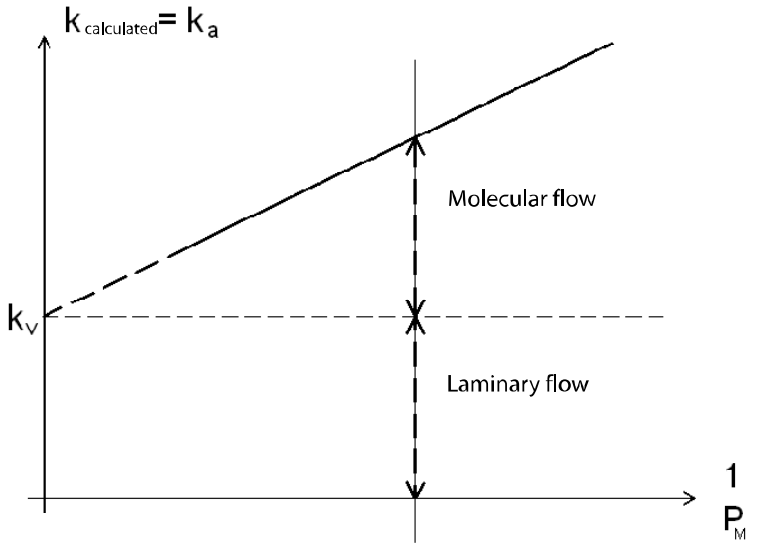

Figure 7.8. *Graph of the variation in the calculated permeability of apparent permeability with respect to the inverse of average pressure*

Taking into account the influence of the state of saturation of the material and the test pressure leads, in some cases, to the expression of the apparent permeability k_a for a given state of saturation, s, by the following expression: $k_a = k_v.k_r(s)$ in which k_v is the intrinsic permeability and $k_r(s)$ is the relative permeability. Relative permeability (which can be calculated whatever the percolating fluid used) is the relationship between the apparent permeability measured in a sample with a given degree of saturation, s, supposed to be uniform in the interior of the material, and the apparent permeability measured on dry material. Relative permeability marks the reduction of the porous space accessible to fluid when the liquid saturation increases, and vice versa.

The differences between the experimental data and Darcy's law are sometimes explained using another approach. The apparent speed of the gas in the sample submitted to the gas permeability test can be deduced from equation [7.6]:

$$v_s = \frac{k}{\mu}\frac{(P_e^2 - P_s^2)}{2P_s L} \qquad [7.9]$$

Figure 7.9 presents the results of the measurements of permeability in air of a porous ceramic [MUR 00]. The terms $\frac{P_e - P_s}{L}$ and $\frac{P_e^2 - P_s^2}{2P_s L}$ are expressed with respect to the apparent speed obtained in various test conditions (for different entry pressures). Relationship [7.5] shows a significant difference from the experimental data with a correlation coefficient of $r^2 = 0.9328$. With relationship [7.9], the adjustment is improved ($r^2 = 0.9915$). The permeability values obtained by these two methods are 1.32×10^{-15} m^2 and 3.96×10^{-16} m^2 respectively, which shows that disregarding the compressibility of air leads to the overestimation of permeability by a factor of 3.3.

The taking into account of the compressibility of air should, however, lead to a linear relationship in the system of coordinates in Figure 7.9. This is not the case; the points move away from a straight line as speed increases. This effect was described by Forchheimer.

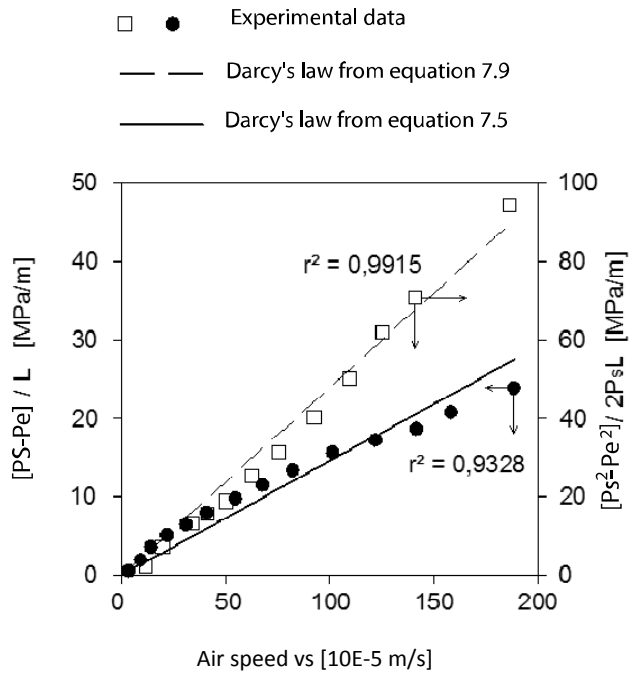

Figure 7.9. *Results of permeability in air expressed according to relationships [7.5]and [7.9], from [MUR 00], for a porous ceramic*

In Darcy's law, only viscous effects are taken into account. As speed increases, the effects of inertia and turbulence become greater, and law [7.9] must be modified:

$$\frac{P_e^2 - P_s^2}{2P_s L} = \frac{\mu}{k} v_s + \frac{\rho}{k'} v_s^2 \qquad [7.10]$$

The experimental points included in the system of coordinates $\frac{P_e^2 - P_s^2}{2P_s L} = f(v_s)$ can be approximated by a function of type [7.10] with a closer approximation than law [7.9].

For the coefficients $k = 4.84 \times 10^{-16} m^2$ and $k' = 1.65 \times 10^{-5} m$, the correlation coefficient becomes $r^2 = 0.9996$. We can thus consider that

Forchheimer's law expressed by relationship [7.10] correctly characterizes gaseous flow in the material being considered. This proper agreement with the experimental data has been verified [MUR 00] in wide ranges of variation of the magnitudes k (from 10^{-13} to 10^{-17} m^2) and k' (from 10^{-9} to 10^{-15} m).

One interpretation of the permeability test according to Forchheimer's law leads to the characterization of the material using the two magnitudes k and k'. This approach is not usual in the case of cement materials.

Note that the two approaches allow us to characterize material either with intrinsic permeability k_v and the Klinkenberg coefficient β, or with permeability k and k', sometimes called the inertial permeability. Like the Klinkenberg coefficient β, the term k' depends on the nature of the gas used for the measurement. In both cases, these magnitudes can only be known by an adjustment of experimental data in a model. It is then possible to predict the gas flow occurring through a given section of the material in given conditions of service fixed either by reporting the value of apparent permeability calculated by relationship [7.9] in relationship [7.6], or by using relationship [7.9].

7.3.3. *Methods of measuring gas permeability*

These experimental studies have led to the development of a method of measuring the gas permeability of concrete that takes into account both the state of saturation of the material and the test pressure. Two possibilities exist regarding the state of saturation of the material.

The simpler one involves completely drying the material and measuring its permeability in the dry state. We can also measure the permeability for different states of saturation of the material in order to obtain a description of permeability depending on the state of saturation.

This second solution is recommended in the AFGC-AFREM method, with three states of saturation attained by increasing durations of drying until complete drying is achieved. To take into account the Klinkenberg effect, there are two options: either a single test pressure is fixed (the AFGC-AFREM method), or we measure the apparent permeabilities for at least

three test pressures and deduce the intrinsic permeability from them, as shown in Figure 7.8.

7.3.4. *Variable head permeameters*

The gas permeability of cement materials can be measured using a variable head permeameter; that is, in a non-permanent flow system. In general, a disk of section A and thickness L is subjected to driving air suction created by a column of manometric liquid in communication with the base of the sample, as shown in Figure 7.10. Lateral airtightness is ensured by resin, and the air flow is displaced along the axis of the disk. In the lower part, a glass tube plunges into a container at a constant level containing a manometric liquid of density ρ_l (usually water). The driving suction is obtained by connecting the permeameter to a vacuum pump. The opening of the faucet causes the rising of liquid in the tube. At level h_0 the faucet is turned off. Air at atmospheric pressure flows through the sample under the effect of driving pressure, which is equal to $h_0\rho_l g$. The pressure of the air trapped under the disk of concrete increases, and the level of manometric liquid in the tube drops. Two marks are made on the tube and we measure the time of passage, t, of the liquid between these two marks.

Disregarding the compressibility of the air between the two pressures existing in the two parts of the sample, we can apply Darcy's relationship [7.1] to the whole thickness L. The air flow, q, occurring for a difference in level h in the manometric tube is written as:

$$q = -\frac{k.A}{\mu}.\frac{\rho_l g h}{L}$$

The flow, q, is also equal to $s.\frac{dh}{dt}$ if s is the calibrated section of the tube. By measuring the time, t, of the flow of liquid between two points, h_0 and h, we can deduce the permeability of the material:

$$k = \frac{\mu.s.L}{\rho_l.A.g.t}\ln(\frac{h_0}{h})$$

This test is similar in function to the Blaine device used to measure the specific surface of powders (see section 3.3.3). Indeed, it is an adaptation of Blaine device for the measurement of the gas permeability of consolidated materials.

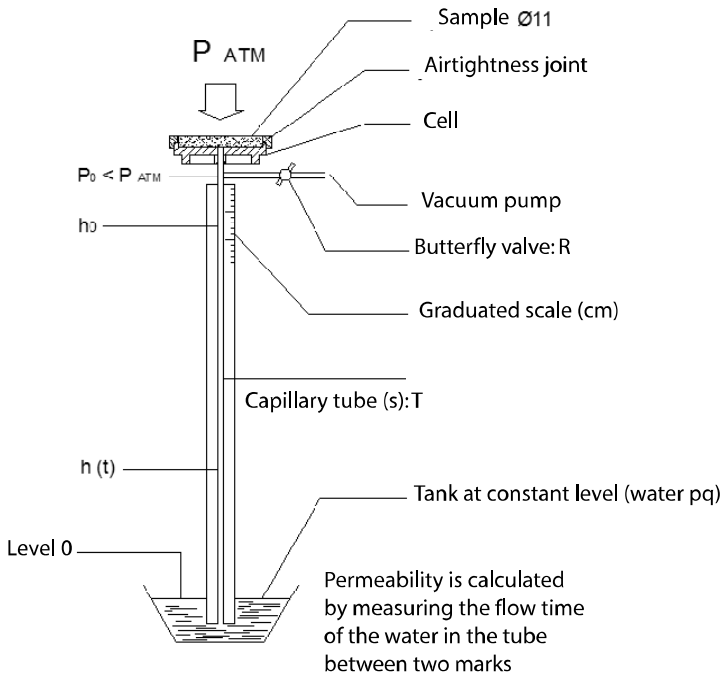

Figure 7.10. *Variable head permeameter [YSS 95]*

7.4. The relationship between permeability and porous structure

As for diffusion, several groups of models relate porous structure to permeability. There are:

– empirical models, in which permeability is calculated from the characteristics of the porous network;

– physical models, where the flow and the geometry of the porous network are modeled; and

– polyphasic models.

In the last category, the models presented in Chapter 6 can be transposed to permeability; this is the case for series and parallel models. However, they are most often used when the material presents strong heterogeneities, as is the case in cracked materials or materials that are partially chemically degraded. These models will not be discussed in this chapter.

7.4.1. *Empirical models*

Empirical models are based on fairly simple relationships between permeability and the characteristics of the porous structure. These relationships present as functions of which the constants and exhibitors are calculated with experimental data in order to obtain the best possible correlation. The characteristics of the porous structure used are principally porosity and the critical or average diameter of the pores[5]. Most of the models proposed concern the relationships between water permeability and porous structure.

In the case of cement materials, several authors [NYA 81, SCH 74] have demonstrated the lack of simple correlation between porosity and permeability. However, the correlations improve when additional parameters (such as the average diameter of the pores) are used. These relationships are presented in Table 7.1.

Relationships	Domain of validity	Authors
$k = 1.82\times10^{-13}.{p_o}^{4.75}.{d_c}^{3.284}$	Cement paste	[DAN 73]
$k = 2.51\times10^{6}.d_c^{3.35}$	Cement paste and mortar	[HAL 95]

Table 7.1. *Empirical models relating gas permeability (in m²) to the characteristics of the porous network (mercury porosity p_o or critical diameter of d_c) [LOB 03]*

7.4.2. *Physical models*

7.4.2.1. *The Carman-Kozeny model*

Kozeny's theory (1927), presented in Chapter 3, is based on the idea of an equivalent environment. The porosity of the material is assimilated into a

5 See section 5.5.1.6 for the definition of these terms.

single rectilinear channel with constant section, a, and length, L_e (see Figure 7.11). The hypotheses are the same as those presented in 3.3.1.

The speed of the fluid in the channel under pressure gradient $\frac{\Delta P}{L_e}$ is given by Poiseuille's law:

$$v_e = \frac{m^2}{h_0 \mu} . \frac{\Delta P}{L_e}$$

where:

– μ is the viscosity of the fluid;

– h_0 is a geometric factor depending on the shape of the section; and

– m is the hydraulic radius of the channel, equal to the ratio between the volume and the area of the channel.

These two last coefficients are adapted to the porosity of the consolidated materials. Thus, the volume of the channel modeled is equal to the volume of voids in the material and its surface lateral to the surface of the voids.

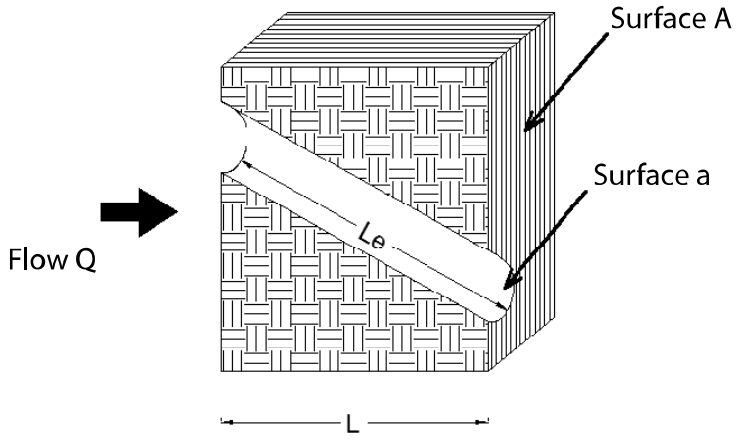

Figure 7.11. *Model equivalent environmental schema according to the Carman-Kozeny theory*

Using these hypotheses and introducing tortuosity, τ, we obtain the Carman-Kozeny relationship:

$$k = \frac{p_o.m^2}{h_0\tau} = \frac{1}{h_0\tau}.\frac{{p_o}^3}{(1-p_o)^2}.\frac{1}{{S_s}^2}$$

where S_s is the specific surface of the porous environment.

This model is frequently used in the case of powders, since the factor $h_0.\tau$ is virtually constant; we can thus calculate the specific surface of a powder using a permeability measurement (see section 3.3.1 with the example of the determination of the specific surface of cement using a Blaine permeameter).

In the case of cement materials, it is very difficult to apply this model, which requires a perfect description of the porous volume participating in the flow through parameters such as h_0, τ and the specific surface of the porous environment.

The Kozeny-Maxwell model [BAR 01] is a variant of the initial model in which we disregard the knowledge of h_0 and τ. $k = \frac{{p_o}^3}{(3-p_o)^2}.\frac{1}{{S_v}^2}$ where S_v is the specific volume surface of the material.

7.4.2.2. *Simple statistical models*

Statistical models are based on a more precise description of the porous network. In place of a single equivalent channel, the porous space is modeled by a group of capillary tubes or flat cracks in three dimensions [SCH 74]. The simplest models are presented in Figure 7.12. The geometric data used are generally taken from mercury porosimetry tests or microscopic observations for cracked materials (the parameter is thus the opening of the crack).

These simple models have difficulty taking into account the complexity of the porous network of cement materials. In particular, they do not take into account the connectivity of pores. There are more advanced statistical models, which will be presented in section 7.4.2.4.

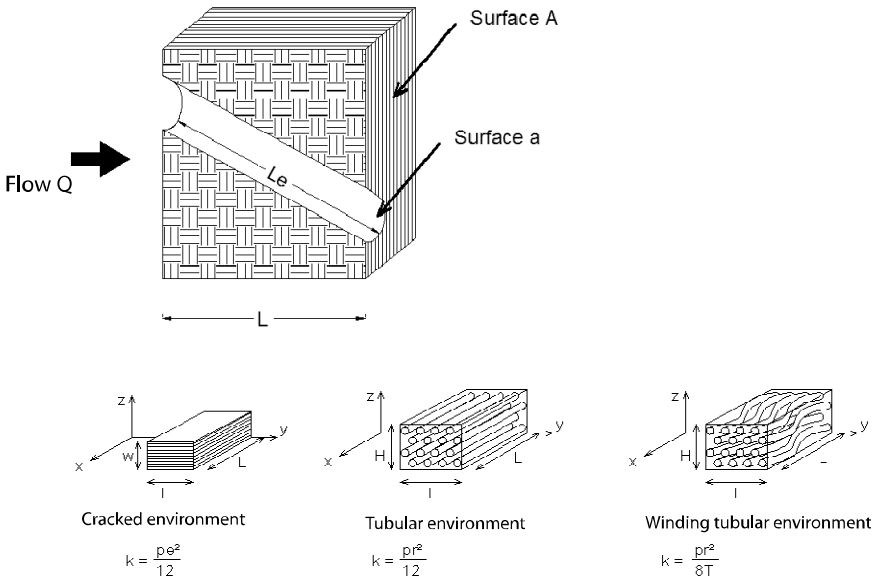

Figure 7.12. *Simple statistical models*

7.4.2.3. *Models based on the percolation theory*

The capacity of a porous material to be traversed by a fluid depends on the probability of the existence of connections between the pores. The preceding models are based on the hypothesis of a strong probability of connection, but in the case of concrete, the probability of conductive links can become very low. We can then apply percolation theory, which is used to define the variation in transport properties with the probability of connection near the percolation threshold.

The *percolation threshold* is defined as the critical probability from which a connected route appears in the porous network; it marks the change of a non-conductive network into a conductive network.

The best known model, originally developed for sedimentary rocks, is that of Katz and Thompson [KAT 86, KAT 87], which proposes a relationship between the intrinsic permeability of the material depending on

the critical diameter of pores, d_c, and the formation factor F: $k = c.d_c^2.\frac{1}{F}$, where c is a constant equal to 1/226. Numerous works [BAN 87, DOU 89, SCH 93], however, have shown that coefficient c varies very strongly with the shape of the pores (spherical, cylindrical, etc.). The formation factor is most often obtained using conductivity measurements [CHR 94].

The application of this model to cement materials gives fairly contrasting results. It would seem that when the capillary network is strongly interconnected (as is the case with materials with high *W/C* ratios), modeling correctly reproduces transport by permeation, while for materials with poorly connected porous networks (low *W/C* ratio, high saturation, etc.) this is not the case, as the results in Figure 7.13 show:

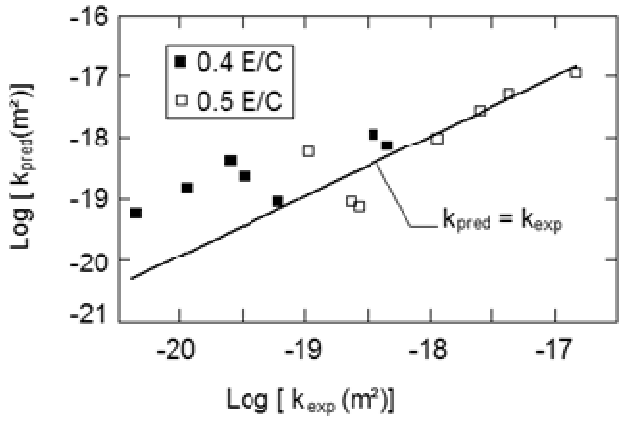

Figure 7.13. *Comparison between the Katz-Thompson model and experimental permeability results for mortars with W/C ratios of 0.4 and 0.5 [HAL 95]*

7.4.2.4. *Statistical models introducing the concept of percolation*

More complex models exist that take into account the distribution of pore diameters, their length, the distance between the pores, and their possible interconnection. These models, which use a more realistic description of the porous network, are, however, fairly complicated to apply. This is because they require the knowledge of parameters that are difficult to access and measure.

In the case of cement materials, Reinhardt and Gaber's work may be cited [REI 90]. These two individuals proposed the following relationship:

$$k = 0.7.p_o.r_{eq}1.5.\exp(-0.7\theta_{water})$$

where:

– k is oxygen permeability;

– p_o is open porosity;

– r_{eq} is an equivalent radius of pores calculated from the average of pore radii obtained by mercury porosimetry; and

– θ_{water} is the volume water content of the material.

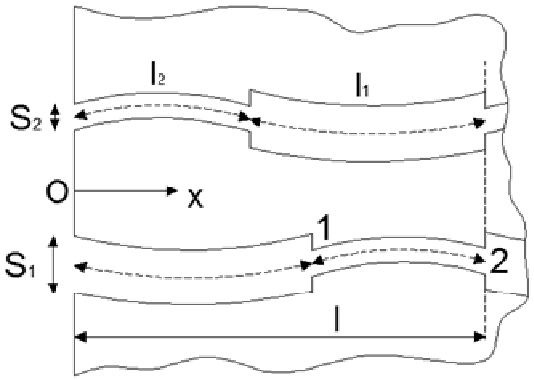

Figure 7.14. *Model of pores [AIT 02]*

Ait-Mokhtar *et al.* [AIT 02] have proposed a model that relates permeability to data taken from a mercury porometry test; specifically, porosity, tortuosity, constrictivity and critical pore radius. The material is modeled by a cube in which the interconnected porous network represents an isotropic porous structure. The pores are assimilated into circular section tubes (S_1 or S_2) representing a bimodal porometric distribution (S_1 representing the middle section of the first porometric distribution peak and S_2 that of the second peak, see Figure 7.14).

Koster *et al.* [KOS 06] have also used a model of cylindrical tube networks, but one built from microtomographic images of cement pastes.

Once the networks are constructed, the various authors apply Darcy's law in each tube. This allows us to estimate the permeability of the environment.

7.5. The drying of concrete

After manufacture, concrete often has an internal hygrometry higher than the average hygrometry of the environment in which it is placed[6]. This imbalance is manifested by a movement of water from the interior of the concrete toward the surrounding environment. This phenomenon, which is very slow (1,000 to 10,000 times slower than thermal diffusion – see Figure 7.15 for an example of water content profiles)in a paired manner causes various phenomena, such as permeation, diffusion, adsorption–desorption and condensation–evaporation. Its modeling is very important since, in addition to transfer properties, drying affects the mechanical properties of concrete [BUR 05], causes major varying deformations (desiccation pullback and warping), and can lead to cracking by hydric gradient [PON 08].

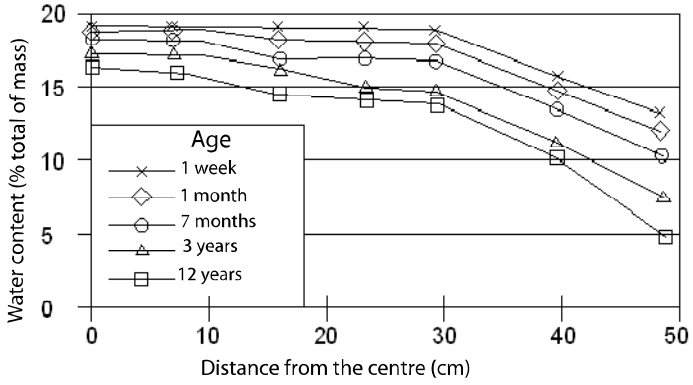

Figure 7.15. *Distribution of water content in a prism of dimensions 100 × 100 × 200 cm drying unidirectionally on a 1 m sample of concrete at different times [ACK 90]*

6 This is not the case for concrete that will be permanently immersed in water.

7.5.1. *Physical mechanisms*

Multiple physical mechanisms contribute to the drying of concrete [BAR 07]:

– *Permeation*: when a pressure gradient is present, fluids (liquid water or water vapor and air) will be displaced. The apparent permeability of the material depends on the pore size, on the pressure gradient, and on the saturation of the material.

– *Molecular diffusion*: at low relative humidity, water will be displaced by diffusion. If the relative humidity exceeds a threshold value, a meniscus of water will form in the pores. Since part of the transport of water occurs in the vapor phase, the process of condensation and evaporation in pores where menisci are formed greatly accelerates the diffusion process. This mechanism is dominant for pores with dimensions of 50 nm to 10 μm, which corresponds to the size of capillary pores (the vestigial pores of water initially present in the concrete).

– *Knudsen diffusion*: nanopores (smaller than 50 nm) correspond to the porosity of cement paste. The dimensions of these pores are smaller than the mean free path of water molecules (around 80 nm). Thus, the flow is governed by Knudsen's law (see section 7.3.2).

– *Surface diffusion*: this mechanism also occurs in nanopores at very low humidity. Indeed, in these nanopores, water molecules are subject to the force fields of the pore walls. A transport mechanism due to the jumps of water molecules between adsorption sites is possible, since the water is essentially adsorbed onto the surface of the pores.

We must complete these mechanisms by studying the auto-desiccation of concrete due to cement hydration. This hydration causes a reduction of volume (the Le Chatelier contraction) which is manifested, when the process has occurred, in the existence of pores that are no longer saturated with water. The lower the *W/C* ratio, the more intense this effect will be. Thus, concrete with low *W/C* ratios will attain a state close to hydric equilibrium with their environment thanks solely to auto-desiccation. Figure 7.16 gives an example of the internal humidities obtained for cement pastes of different *W/C* ratios.

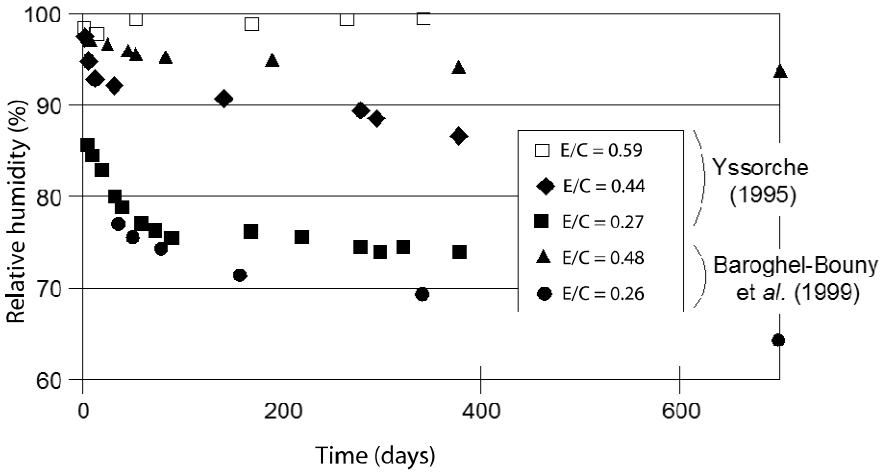

Figure 7.16. *Auto-desiccation of cement pastes with different W/C ratios [BAR 99, YSS 95]*

7.5.2. *Simplified modeling of drying*

Strictly speaking, the modeling of the drying of concrete must consider equations of water conservation in liquid and vapor form and of air (see the books by [GAW 07, MAI 01 and THI 07]). For example, for liquid water we define its speed of flow by Darcy's law:

$$v_l = -\frac{k_l}{\mu_l} grad P_l \qquad [7.11]$$

where:

– k_l is the water permeability of concrete,

– μ_l is the viscosity of water, and

– P_l is the pressure in the liquid.

We replace k_l with the following expression:

$$k_l = k_{vl}.k_{rl}(s)$$

in which k_{vl} is the intrinsic water permeability and $k_{rl}(s)$ is the relative water permeability as defined in section 7.3.2.

For the natural drying of concrete[7], several authors [MAI 99, MES 03, STE 07] have shown that it is reasonable to consider the transport of water only in its liquid phase[8]. Moreover, we can disregard gas pressure, which remains low compared to the liquid pressure. The capillary pressure, P_c, is thus equal to the liquid pressure, P_l. The water speed is thus written as:

$$v_l = -\frac{k_{vl}.k_{rl}(s)}{\mu_l} grad(P_l) = -\frac{k_{vl}.k_{rl}(s)}{\mu_l} grad(P_c) \qquad [7.12]$$

where s is the degree of saturation of the concrete.

The conservation equation of the mass of liquid water

$$\dot{m}_l + div(m_l \mathrm{v}_l) = 0$$

with

$$m_l = \rho_l . p_o . s$$

where p_o is the open porosity of the concrete, leads to:

$$\frac{\partial s}{\partial t} = div\left(k_{rl}(s) \frac{k_{vl}}{\mu_l p_o} \mathrm{grad}(P_c(s)) \right) \qquad [7.13]$$

To solve equation [7.13], we need two additional relationships giving capillary pressure and relative permeability with respect to saturation.

For capillary pressure, we can use the relationship proposed by Van Genuchten [GEN 80]:

$$P_c(s) = a\left(s^{-b} - 1\right)^{1-1/b} \qquad [7.14]$$

7 This will not be the case, for example, for drying in elevated temperature conditions, as in the case of a fire.

8 The error remains limited to 10% of the loss of mass, even for relatively porous concrete, for which the diffusive system of water vapor will be larger [THI 07].

where a and b are parameters dependent on the material. These parameters can be obtained from desorption tests that relate saturation to relative humidity (see Exercise 5.7).

Kelvin's law (see section 5.5.3) then allows us to relate relative humidity to capillary depression. There are other models for desorption curves which, coupled with Kelvin's law, are used to get P_c(s). Therefore, the BSB (Brunauer, Skalny and Bodor) model [BRU 69] expresses the relationship between water content, w, and relative humidity, ψ, by:

$$w(\psi) = \frac{ACV_m\psi}{(1-C\psi)\left[1+(A-1)b\psi\right]}$$

where A, C and V_m are the material parameters.

For the evolution of permeability relative to saturation, we generally use the relationship proposed by Mualem [MUA]:

$$k_{rl}(s) = \sqrt{s}\left[1-\left(1-s^b\right)^{1/b}\right]^2$$

where parameter b is the same as in equation [7.14].

NOTE 7.1.– These equations are also used to estimate permeability k_{rl} by means of an inverse analysis test in which we measure the loss of mass of concrete in controlled conditions (typically 50% relative humidity)

7.6. Physical parameters and performance-based approach

The durability of concrete causes various physical phenomena governing the transfer of water, gas (particularly CO_2), and various ions (chlorides, sulfates, etc.). The current normative approach (norm NF EN 206-1) is mainly a prescriptive approach based on experimentation and which, for a given environment, indicates the minimal quantities of binder and the water/binder ratio. The norm also opens up the possibility of performance-based approaches based on the concept of equivalent performance (concrete must have a durability performance equal to that of a reference concrete formulated according to the prescriptive approach) or a performance-based

concept defining the performances required from the durability of the concrete.

Temporary recommendations for the performance-based approach applied to concrete in works of art [LCP 09] present the methodology of the approach. For example, three indicators have been proposed for the problem of the corrosion of reinforcements:

– water porosity ρ_{water};

– gas permeability k_{gas}; and

– apparent chloride diffusivity D_{app}.

Then, according to the categories of the environment, they set thresholds at these indicators. For example, for an XC4 environment (concrete exposed to air with alternating drying and humidity), the corrosion of reinforcements can be affected by the penetration of CO_2 from the air. The indicators chosen are porosity accessible to water, p_{water}, and gas permeability. The threshold values proposed are $p_{water} \leq 13\%$ and $k_{gaz} \leq 150 \times 10^{-18}$ m².

In the case of an XS2 environment (part of the structure is permanently immersed in seawater), we will examine the penetration of chlorides and thus the pertinent indicator becomes diffusivity. The threshold values given in the recommendations are, in this case, $p_{water} \leq 13\ \%$ and $D_{app} \leq 7 \times 10^{-12}$ m²/s.

Finally, when there is a possible combination between carbonation and the penetration of chlorides, all indicators are used. This is the case with an XS3 environment, which corresponds to tidal zones or to zones subject to projections or spray. In this case, the concrete must have the following performances: $p_{water} \leq 11\%$, $k_{gaz} \leq 150 \times 10^{-18}$ m², and $D_{app} \leq 3 \times 10^{-12}$ m²/s.

All of these thresholds have been established using modeling in order to attain a life span of 100 years for bridges.

Of course, the recommendations also specify the conditions of testing and preparation of the samples. This is particularly important for gas permeability, which depends strongly on the state of saturation of the concrete.

In conclusion, current knowledge of physical transfer phenomena through concrete and their consequences in terms of durability, their modeling, and the mastery of tests used to measure the parameters of these models have allowed us to develop an alternative to the classic prescriptive approach of norm EN 206-1. The performance-based approach is, however, in the early days of its implementation, and will surely be improved in the years to come, both by progress in the modeling of very complex phenomena that occur in concrete, and by the results of experience.

7.7. Bibliography

[ACK 90] ACKER P., MAMILLAN M., MIAO B., "Drying and shrinkage of concrete: the case of massive parts", in: SUPRENANT B.A. (ed.), *Serviceability and Durability of Construction Materials*, ASCE, New York, pp. 1072-1081, 1990.

[AIT 02] AÏT-MOKHTAR A., AMIRI O., DUMARGUE P., SAMMARTINO S., "A new model to calculate water permeability of cement-based materials from MIP results", *Advances in Cement Research*, vol. 14, no. 2, pp. 43-49, 2002.

[BAN 87] BANAVAR J.R., JOHNSON D.L., "Characteristic pore sizes and transport in porous media", *Physical Review B*, vol. 35, pp. 7283-7286, 1987.

[BAR 99] BAROGHEL-BOUNY V., MAINGUY M., LASSABATERE T., COUSSY O., "Characterization and identification of equilibrium and transfer moisture properties for ordinary and high-performance cementitious materials", *Cement and Concrete Research*, no. 29, pp. 1225-1238, 1999.

[BAR 01] BAROGHEL-BOUNY V., "Transferts dans les bétons et durabilité", *Revue Française de Génie Civil*, vol. 5, no. 2-3, pp. 145-146, 2001.

[BAR 07] BAROGHEL-BOUNY V., BENBOUDJEMA F., BURLION N., "Le séchage des bétons", *Référentiel des Connaissances*, *Projet ANR Applet*, pp. 41-49, 2007, http://or.lcpc.fr/applet/.

[BRU 69] BRUNAUER S., SKALNY J., BODOR E.E., "Adsorption on nonporous solids", *Journal of Colloid and Interface Science*, vol. 30, pp. 546-552, 1969.

[BUR 05] BURLION N., BOURGEOIS F., SHAO J.F., "Effects of desiccation on the mechanical behaviour of concrete", *Cement and Concrete Composites*, vol. 27, pp. 367-379, 2005.

[CHR 94] CHRISTENSEN B.J., COVERDALE R.T., OLSON R.A., FORD S.J., GARBOCZI E.J., JENNINGS H.M., MASON T.O., "Impedance spectroscopy of hydrating cement-based materials: measurement, interpretation, and application", *Journal American Ceramic Society*, vol. 77, no. 11, pp. 2789-2804, 1994.

[DOU 89] LE DOUSSAL P., "Permeability versus conductivity for porous media with wide distribution of pole sizes", *Physical Review B*, vol. 39, pp. 4816, 1989.

[GAW 07] GAWIN D., PESAVENTO F., SCHREFLER B., "Modelling creep and shrinkage of concrete by means of effective stresses", *Materials and Structures*, nvol. 40, pp. 579–591, 2007.

[GEN 80] VAN GENUCHTEN M.T., "A closed-form equation for predicting the hydraulic conductivity of unsaturated soils", *Soil Science Society American Journal*, vol. 44, pp. 892–898, 1980.

[GRA 96] GRANGER L., Comportement différé du béton dans les enceintes de centrales nucléaires, Analyse et modélisation, Thesis, Ecole Nationale des Ponts et Chaussées, 1996.

[HAL 95] HALAMICKOVA P.,DETWILER R.J.,BENTZ D.P., GARBOCZI E.J., "Water permeability and chloride ion diffusion in Portland cement mortars: relationship to sand content and critical pore diameter", *Cement and Concrete Research*, vol. 25, no. 4, pp. 790-802, 1995.

[KAT 86] KATZ A.J., THOMPSON A.H., "A quantitative prediction of permeability in porous rock", *Phys. Rev. B*, vol. 24, pp. 8179-8181, 1986.

[KAT 87] KATZ A.J., THOMPSON A.H., "Prediction of rock electrical conductivity from mercury injection measurements", *Journal of Geophysical Research*, vol. 92, no. B1, pp. 599-607, 1987.

[KLI 41] KLINKENBERG L., "The permeability of porous media to liquid and gases", *Drilling and Production Practice*, American Petroleum Institute, pp. 200-213, 1941.

[KOS 06] KOSTER M., HANNAWALD J., BRAMESHUBER W., "Simulation of water permeability and water vapor diffusion through hardened cement paste", *Computational Mechanics* ,vol. 37, pp. 163-172, 2006.

[KUN 75] KUNDT A., WARBURG E., *Phil. Mag*., vol. 50, pp. 53, 1875.

[LCP 09] LCPC, Maîtrise de la Durabilité des Ouvrages d'Art en Béton – Application de l'Approche Performantielle, Temporary Recommendations, LCPC, 2009.

[MAI 99] MAINGUY, M., Modèles de diffusion non-linéaires en milieux poreux. Applications à la dissolution et au séchage des matériaux cimentaires, Thesis, Ecole Nationale des Ponts et Chaussées, Paris, 1999.

[MAI 01] MAINGUY M., COUSSY O., BAROGHEL-BOUNY V., "Role of air pressure in drying of weakly permeable materials", *Journal of Engineering Mechanics*, vol. 127, no. 6, pp. 582–592, 2001.

[MES 03] MESCHKE G., GRASBERGER S., "Numerical modelling of coupled hygromechanical degradation of cementitious materials", *Journal of Engineering Mechanics*, vol. 4, 383-392, 2003.

[MUA 76] MUALEM Y., "A new model for predicting the hydraulic conductivity of unsaturated porous media", *Water Resources Research,* vol. 12, pp. 513–522, 1976.

[OLL 92] OLLIVIER J.P., MASSAT M., "Permeability and microstructure of concrete: a review of modeling", *Cement and Concrete Research*, vol. 22, no. 2-3, pp. 503-514, 1992.

[PON 08] PONS G., TORRENTI J.M., "Retrait et fluage", in: OLLIVIER J.P. and VICHOT A. (eds) *La Durabilité des Bétons*, Presses de l'ENPC, 2008.

[REI 90] REINHARDT H.W., GABER K., "From pore size distribution to an equivalent pore size of cement mortar", *Materials and Structures*, vol. 23, pp.3-15, 1990.

[ROZ 07] ROZIÈRE E., LOUKILI A., PIJAUDIER-CABOT G., CUSSIGH F., "The equivalent performance concept applied to carbonation of concrete", *CONSEC'07*, 4-6th June, Tours, France, 2007.

[SCH 74] SCHEIDEGGER A.E., *The Physics of Flow Through Porous Media*, 3rd edition, University of Toronto Press, 1974.

[SCH 93] SCHWARTZ L.M., "Cross-property relations and permeability estimation in model porous media", *Phys. Rev. E*, vol. 48, no. 6, pp. 4584-4591, 1993.

[SKO 05] SKOCZYLAS F., "Multiphysicsprocesses in concrete", *Revue Européenne de Génie Civil*, vol. 9, no. 5-6, pp.597-618, 2005.

[STE 07] STEFAN L., BENBOUDJEMA F., ROBERT F., MORANVILLE M., "Séchage et retrait: influence de la fissuration induite", *Revue Européenne de Génie Civil*, vol. 11, no. 6, pp. 855-866, 2007.

[THI 07] THIERY M., BAROGHEL-BOUNY V., BOURNETON N., VILLAIN G., STEFANI C., "Modélisation du séchage des bétons – Analyse des différents modes de transfert hydrique", *Revue Européenne de Génie Civil*, vol. 11, no. 5, pp. 541-577, 2007.

[VIL 01] VILLAIN G., BAROGHEL-BOUNY V., KOUNKOU C., HUA C., "Mesure de la perméabilité aux gaz en fonction du taux de saturation des bétons", *Revue Française de Génie Civil*, vol. 5/2-3, pp. 251-268, 2001.

[YSS 95] YSSORCHE M.P., Microfissuration et durabilité des bétons à hautes performances, Doctoral thesis, INSA Toulouse, 1995.

7.8. Exercises

Exercise 7.1: *Permeability and porous structure*

1) *Prediction of permeability in the case of a single group of pores*

We will attempt to model permeation in porous materials by assimilating the porous structure of the solid into a group of n cylindrical tubes that are parallel to the pressure gradient.

Let us first consider the flow of a fluid in a cylindrical tube of radius r. The flow, q, through a tube is given by Poiseuille's law expressed by the following relationship, in which we disregard the weight term and to which we apply an element of length, dx:

$$q = -\frac{\pi r^4}{8\mu} \cdot \frac{dP}{dx}$$

If the pores of the material are assimilated into the pores of the same radius, establish the relationship between permeability k, the radius r of the pores, and the porosity p_o of the material.

2) *Prediction of permeability in the case of several groups of pores*

In reality, not all pores have the same dimensions, and a simple model consists of considering that all the pores are identical and of equal dimensions to the average value of the distribution of dimensions. The model will now be used to predict permeability through hydrated cement paste. The porous structure of hydrated cement pastes is frequently made up of two groups of pores: capillary pores and gel pores.

In the first approximation, we may consider that the porous structure of the cement paste can be broken down into two distinct groups of pores. The first, corresponding to capillary pores, is made up of cylindrical pores of radius r_{cap}, and the second, corresponding to gel pores, is made up of cylindrical pores of radius r_{gel}.

Figure 7.17 shows the cumulative porosity curves obtained by mercury porosimetry on cement pastes made up with weighted W/C ratios of different quantities of cement, C, and water, W. The pastes tested are all 28 days old.

The curves give, in ordinates, the volume of the pores (related to the mass of the samples) of which the dimension is greater than the diameter of the abscissa.

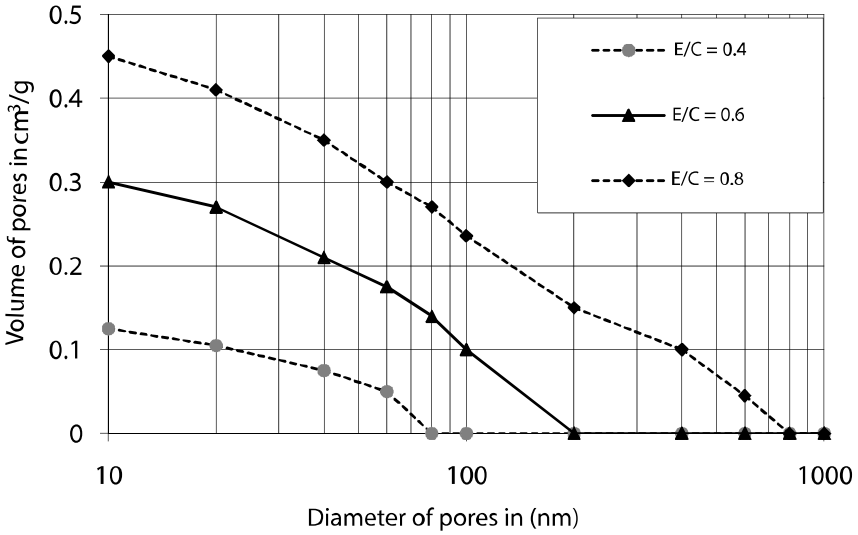

Figure 7.17. *Cumulative porosimetric curves*

a) The apparent densities of the pastes are given in Table 7.2. The limit between capillary pores and gel pores conventionally corresponds to a diameter of 100 nm (100×10^{-9} m). Calculate, in terms of the *W/C* ratio, the variation in capillary porosity p_{cap} and in gel porosity p_{gel}.

W/C	0.4	0.6	0.8
Apparent density (g/cm^3)	1.65	1.26	1.09

Table 7.2. *Apparent density of cement pastes*

b) Supposing that the flow of a fluid through the cement paste is equivalent to the flow through the two families of pores placed in parallel, express permeability in terms of p_{cap}, p_{gel}, r_{cap} and r_{gel}.

c) The radius of gel pores is chosen equal to 10 nm (10^{-8} m). The radius of the capillary pores depends on the *W/C* ratio. The value chosen for

the calculation will be the mathematical mean between the radius of the largest pores in the paste considered and the conventional limit radius between capillary pores and gel pores.

Calculate the permeability of the cement pastes for the different *W/C* values.

3) *Prediction of permeability from a water absorption test*

In the following, we will study a method of evaluating the permeability of a porous material based on a water absorption test. We will be considering a vertical cylindrical pore of radius *r*, the base of which plunges into a layer of water (see Figure 7.18).

When the tube is plunged into the water, the level of water inside the tube rises to a height of h_e, called capillary withdrawal. h_e varies with time, *t*, between 0 at the initial time and a maximum value of H_e.

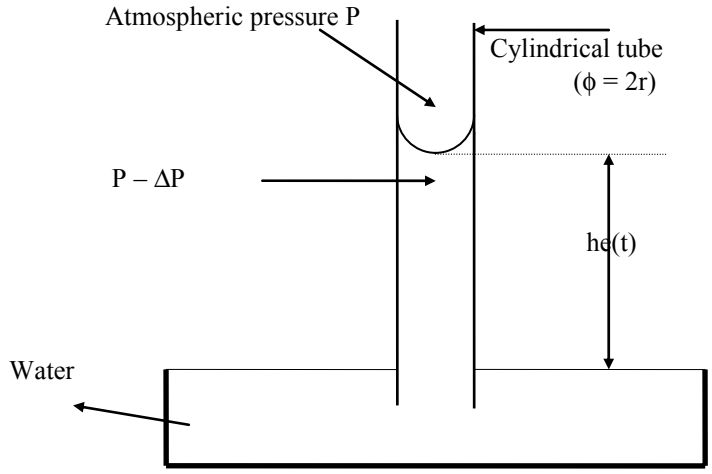

Figure 7.18. *Water absorption test*

Jurin's law expresses the maximum value of capillary withdrawal, H_e:

$$H_e = \frac{2\sigma \cos\theta}{r \rho_e g}$$

Washburn's law expresses capillary withdrawal, h_e, in terms of the square root of time:

$$h_e = \sqrt{\frac{\sigma r \cos\theta}{2\mu_e} t}$$

In these relationships, σ is the surface tension of the water and θ is the connection angle to the right of the meniscus between the water, the solid, and the air. We will consider in the following that $\theta = 0$.

Capillary withdrawal results from the difference in pressure between the two faces of the meniscus $\Delta P = \frac{2\sigma\cos\theta}{r}$. The water-side pressure is lower than ΔP at atmospheric pressure on the air side. ΔP is called the *capillary pressure*.

a) Washburn's law produces the hypothesis that only the capillary forces are responsible for the withdrawal of water in the pore (the force of gravity is disregarded). Expressing that the volume flow of water in the cylindrical tube is given by Poiseuille's law, demonstrate Washburn's law.

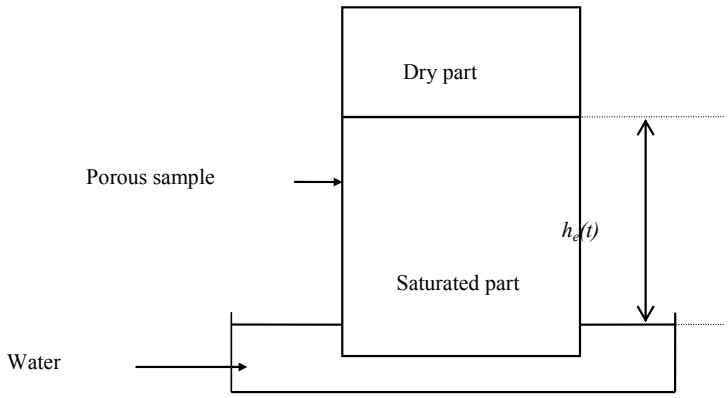

Figure 7.19. *Hypothetical schema of water absorption test*

b) If we now consider a sample of porous material whose base is immersed in water (see Figure 7.19), there is also capillary withdrawal. Ignoring the force of gravity in the column of water, express the hydraulic

gradient that acts on the column of water of height h_e under the effect of capillary pressure. Express the permeability coefficient in terms of porosity p, ascension h_e obtained at time t from this time t and maximum ascension height H_e obtained at the end of an infinite period of time.

c) Assimilating the pores into a group of cylindrical tubes of radius r, express the permeability coefficient with respect to porosity, density and water viscosity, as well as pore radius. Compare with the expression found in question 2.

Exercise 7.2: *The influence of the state of saturation on permeability*

Before measuring the oxygen permeability of concrete, the sample (a cylinder 15 cm in diameter and 5 cm thick) is dried at 60 °C. Table 7.3 indicates the evolutions in mass and permeability with the passage of time. The initial mass of the saturated sample before introduction to the oven is 2,281 g. The last column of the table corresponds to drying at 105 °C carried out until stabilization of mass.

Time of drying (weeks)	0	1	3	6	8	10	12	Drying at 105 °C
Mass of sample (g)	2,281	2,264	2,254	2,244	2,239	2,235	2,232	2,193
Permeability (10^{-18} m^2)	-	0.4	0.5	1.1	1.9	3.1	4.8	92

Table 7.3. *Evolution of gas permeability depending on the state of saturation of the sample*

Complete Table 7.3 with the values of the degree of saturation and water content at each maturity date. What is the open porosity of the concrete?

Exercise 7.3: *Permeability of granular materials: The Carman Kozény model*

We will evaluate the permeability of a granular material using the Carman-Kozény model.

Remember that Poiseuille's law is used to express flow speed, u_e, of a fluid of viscosity μ, under the effect of a difference in pressure P, in a constant section tube (form coefficient h_0), of hydraulic radius m and length L_e as:

$$u_e = \frac{m^2}{h_0.\mu}.\frac{\Delta P}{L_e}$$

The granular material is assimilated into a group of spherical grains of diameter D and density ρ.

1) Express the specific (mass) surface of this material in terms of ρ and D.

2) All of the intergranular voids in the material are assimilated into a tube according to the Carman-Kozény model. The volume of the tube is equal to the volume of the voids and its lateral surface is the same as the exterior surface of the grains.

a) Express the hydraulic radius of this tube in terms of:

– the porosity p of the material;

– the specific surface; and

– the density of the grains.

b) Give the expression of the hydraulic radius in terms of the porosity and diameter D of the grains.

3) To calculate permeability, express that the flow that traverses a thickness L of material and given by Darcy's law is the same as the one that traverses the model tube.

Take: $h = h_0\left(\frac{L_e}{L}\right)^2$.

Give the expression of the permeability of the material in terms of h, D and porosity p.

For grains sized between 1 and 100 μm, Carman has shown that h is equal to 5.

4) The measurement of the specific surface of a material gives 3,000 cm²/g. Applying the relationship demonstrated in the previous question, calculate its permeability if its porosity is equal to 0.48 and knowing that the density of the grains is equal to 2.65 g/cm^3.

Exercise 7.4: ***The basics of Brémont porosimetry (see Figure 7.20)***

1) We will model a porous material with n cylindrical capillaries, of radius r, which are identical and parallel. The material presents in the form of a disk of height L, the pores being perpendicular to the two faces.

After saturation with water, the disk is placed in the cell of a Brémont porosimeter. In the upper part there is atmospheric pressure, and in the lower part there is a pressure P of compressed air. We will write p as the relative pressure, with $p = \Delta P = P - P_{atm}$.

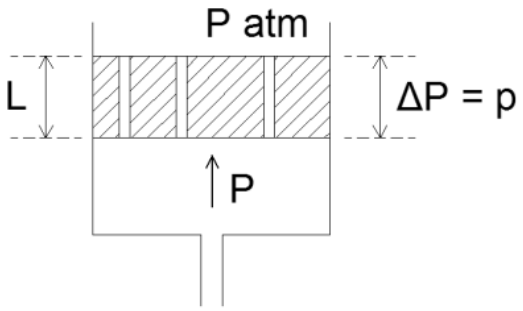

Figure 7.20. *Hypothetical schema of a Brémont porosimeter*

When the pressure p increases from a zero value, the pores are unblocked at a pressure p_d, which is equal to the capillary pressure of the water in the pores.

a) If σ is the surface tension of the water and θ is its angle of connection to the solid, express the value of p_d.

b) When p increases beyond p_d, the pores release air according to a flow system that we will suppose to be viscous. Give the expression of the volume flow q of air for $p > p_d$ in a pore of radius r and length L. Then give the expression of the volume flow Q in the n pores of radius r.

c) Trace the speed of $Q(p)$ in the area $[0, p]$, $p > p_d$.

2) The material is now modeled by n_1 pores of radius r_1 and n_2 pores of radius r_2 ($r_1 < r_2$). The first ones are unblocked at pressure p_{d1}, the second ones at pressure p_{d2}.

a) Give the expression of flows Q_1 and Q_2 of air released in the two groups of pores, specifying the areas of definition and supposing that the flow system remains viscous.

b) Give the expression of the total flow Q_t and trace on the same graph: $Q_1(p)$, $Q_2(p)$ and $Q_t(p)$ in area $[0,p]$ with $p > \max(p_1 ; p_2)$.

c) Taking $p > \max(p_1 ; p_2)$ and Q as the corresponding flow of air, show how we can determine the number and volume of pores of radius r_1 from the recording of $Q_t(p)$.

Exercise 7.5: ***Confinement enclosure: decennial test (from the PSI 2005 modeling test of the X/ENS competition by Benboudjema, Colliat and Torrenti)***

In order to guarantee the security of nuclear facilities, it has been decided to use an external confinement enclosure made of concrete to protect nuclear reactors from natural and accidental threats. In the case of a nuclear accident (risk of dispersion of radioactive elements), environmental protection is ensured by an internal concrete wall 1.2 m thick (for a reactor of REP type 1,400 MWe). It is sized to resist an internal pressure of 0.6 MPa and an approximate temperature of 140 °C, corresponding to the sizing accident APRP (accident by loss of primary refrigerant). A simplified diagram of the two enclosures is given in Figure 7.21.

In order to periodically verify that the enclosure is playing its confinement role in the case of an accident, enclosure tests (the application of an internal pressure of 0.6 MPa in the air and at ambient temperature) are conducted at the end of its construction, and then again every 10 years (the

decennial test). Simply stated, the operator must prove the enclosure's capacity to ensure a rate of leakage that is lower than 1.5% of the total mass of fluids (air plus vapor mixture) contained in the enclosure per 24 hours to security authorities.

In the case of concrete, voids of different sizes are present. These can be pores (voids "naturally" present in concrete) or cracks (accidental situations) that can serve as routes to disperse radioactive elements (in the case of an accident) or air (in the case of the decennial test) into the environment. It is therefore very important to understand the influence of porosity and cracking on the airtightness of confinement enclosures.

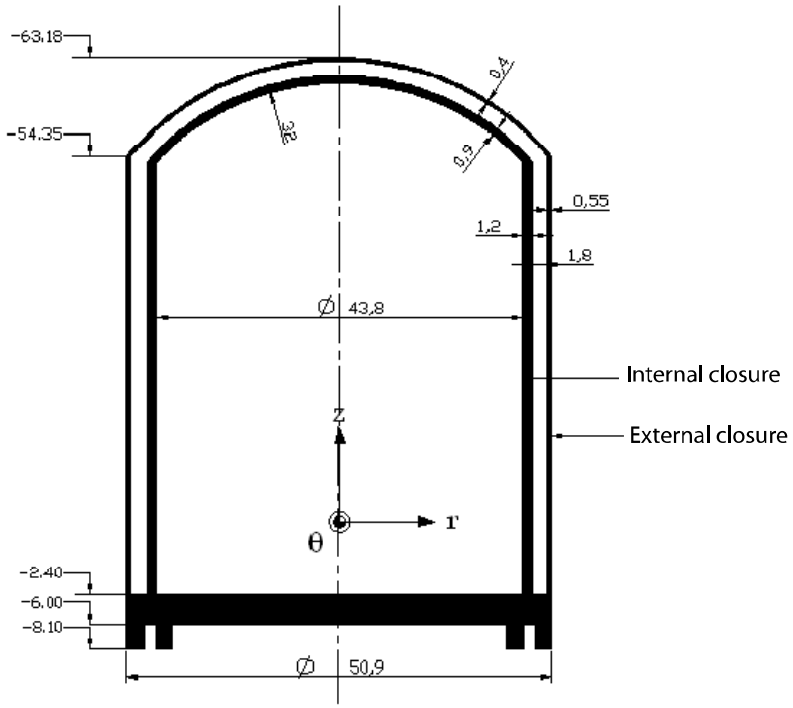

Figure 7.21. *Simplified diagram of the civil engineering part of a nuclear reactor enclosure (French reactor REP 1,400 MWe), with dimensions in meters [GRA 96]*

1) *Permeability in a porous environment*

We will examine a flow of fluid and air in a porous environment. The environment can also be cracked. In order to model the flow of fluid, several hypotheses are considered:

– the effects of gravity are negligible;

– the fluid is considered homogeneous and incompressible, of density ρ and dynamic viscosity $\mu = 0.01818 \times 10^{-3}$ Pa.s;

– the flow system is stationary;

– the flow is unidirectional along axis $\vec{z}$;

– the hydrostatic pressure is written as P.

In this environment, the speed vector $\vec{u}$ of the fluid at point M is written as:

– in Cartesian coordinates $M(x, y, z)$:

$$\vec{u} = u_x(M).\vec{x} + u_y(M).\vec{y} + u_z(M).\vec{z}$$

– in cylindrical coordinates $M(r, \theta, z)$:

$$\vec{u} = u_r(M).\vec{r} + u_\theta(M).\vec{\theta} + u_z(M).\vec{z}$$

The hydrostatic pressure P is written as $P(M) = P(x, y, z)$ in Cartesian coordinates and $P(M) = P(r, \theta, z)$ in cylindrical coordinates.

NOTE 7.2.– The surface forces of viscosity $d\overrightarrow{F_v}$, in a Newtonian fluid oppose flow (see Figure 7.22). They are applicable to lateral surfaces (parallel to flow) and are proportional to the transversal speed gradient. If flow occurs along an axis $\vec{z}$, they are written, in Cartesian coordinates $d\overrightarrow{F_v} = (2.l.dz)\mu.\dfrac{\partial u_z(M)}{\partial y}\vec{z}$, using the following hypotheses:

– the speed u_z does not depend on x;

– there is symmetry with regard to the plan $(O, \vec{x}, \vec{z})$; and

– the width *l* is infinitely greater than the height *h*.

In cylindrical coordinates, it is written as:

$$d\overrightarrow{F_v} = (2\pi.r.dz)\mu.\frac{\partial u_z(M)}{\partial r}\vec{z}$$

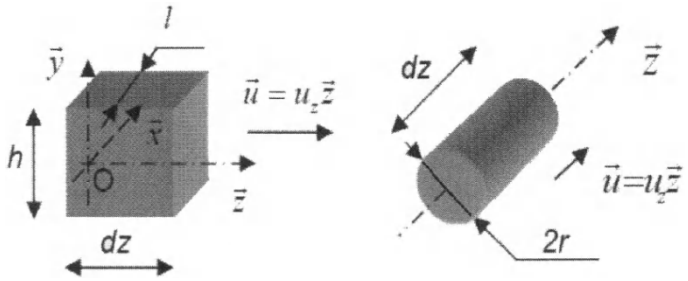

Figure 7.22. *Elements of volume subject to a force of viscosity in Cartesian coordinates*

2) *Preliminary calculations*

We consider the flow in a standard tube of constant section $A = l.x.h$ along an axis $\vec{z}$. We will use Cartesian coordinates.

a) Establish the conservation equation of the mass of fluid in the tube. Simplify this equation by using the calculation hypotheses. Then deduce from it that $u_z(M)$ does not depend on z.

b) Write the conservation of the quantity of movement using the calculation hypotheses. Then show that the pressure P depends only on z.

3) *Flow in a pore – Poiseuille's relationship*

Consider the flow of a fluid, along an axis $\vec{z}$, in a pore, assimilated into a cylinder of radius R and length L. The fluid is subject to a constant pressure P_1 in $z = 0$ and to a pressure P_2 in $z = L$. Take $\Delta P = P_2 - P_1$. A diagram is given in Figure 7.23.

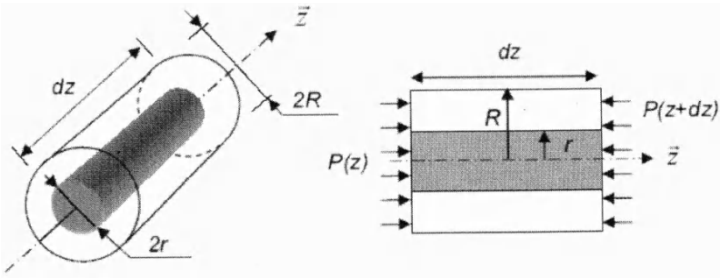

Figure 7.23. *Diagram of a pore*

a) What can we say about the dependence between u_z and θ? Isolating an element of cylindrical volume of radius r and length dz, create a balance of the quantity of movement.

b) Determine the expression of speed u_z with respect to ΔP, μ, r, L and an integration constant.

c) We will suppose that the speed of the fluid in contact with the walls is zero. Comment on this hypothesis. Then deduce the expression of the integration constant, and then the speed u_z from it.

d) Show that the volume flow Q circulating throughout the crack can be written as (Poiseuille relationship):

$$Q = \frac{\pi.R^4.\Delta P}{8.\mu.L} \qquad [7.15]$$

4) *Gas permeability in a porous environment without water: effect of the distribution of porosity*

The pores of this material are assimilated into a group of n cylindrical and parallel tubes. Each cylinder is supposed to be independent of the others and the fluid, circulating along an axis $\vec{z}$, is subject to a constant pressure P_1 where $z = 0$ and to a pressure P_2 where $z = L$. Again, take $\Delta P = P_2 - P_1$. A diagram is given in Figure 7.24.

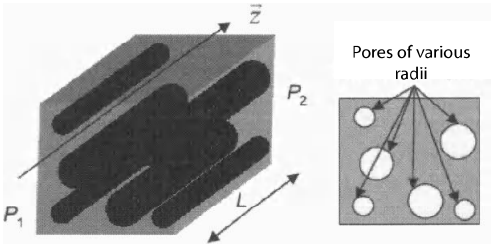

Figure 7.24. *Diagram of a porous environment*

a) Suppose first that all of the pores have the same radius R. Determine the expression relating the porosity p to n, R and A, the section of porous material through which the fluid flows. From this relationship and equation [7.15], establish the relationship between k, R and p.

b) Now consider that the pores do not all have the same radius. Figure 7.25 shows the cumulative porosity curves obtained for three different materials (called 1, 2 and 3). The curves give, in ordinates, the cumulative porosity p_c of the pores larger than the radius R in the abscissa. These curves are modeled by the following equation (i being the number of the material):

$$p_c(\mathbf{R})_i = a_i + b_i.R + c_i.R^2 \quad \text{if} \quad R \leq R_i$$

and

$$(V_{pc})_i = 0 \quad \text{if} \quad R > Ri$$

The values of the coefficients are given in Table 7.4.

	a_i	b_i (nm^{-1})	c_i (nm^{-2})	R_i (nm)
Material 1	8.078×10^{-2}	-6.640×10^{-4}	-4.073×10^{-6}	80
Material 2	2.583×10^{-1}	-2.303×10^{-4}	5.071×10^{-6}	200
Material 3	3.687×10^{-1}	-9.759×10^{-4}	6.035×10^{-7}	600

Table 7.4. *Coefficients used to calculate the cumulative porosity from the radius of pores*

Determine the total porosity of each of these three materials. Then determine the permeability associated with each one of these materials.

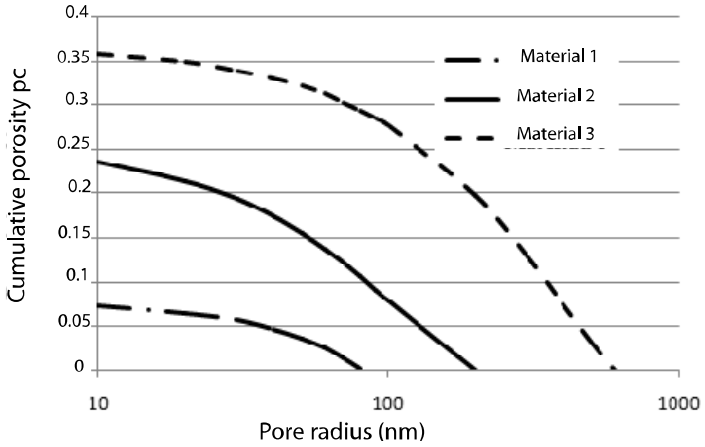

Figure 7.25. *Cumulative porosity p_c*

c) For each of these three materials, calculate the value of the pore radius R_{eq} for which we obtain an identical permeability. For the same overall porosity value, does the pore radius have a significant influence on permeability?

5) *Water in porous environments*

In liquids (and in solids) there are intermolecular cohesion forces acting on very short distances; beyond a few nanometers, the interaction between molecules can be disregarded.

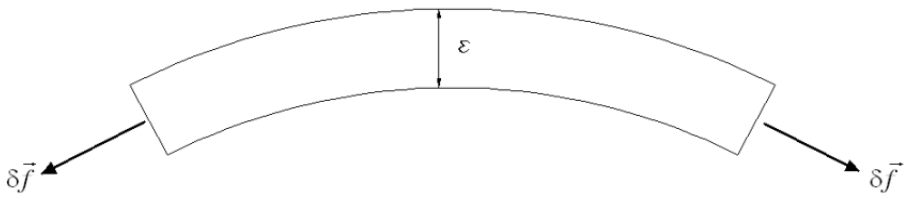

Figure 7.26. *Demonstration of the existence of surface tension*

The layer in which these forces exist has a very low thickness, *e*, and is called the capillary layer. If we consider a vertical facet in this layer (for a free horizontal surface), the force exercised on this facet is horizontal. If we return to a line on the free surface we will have:

$$\delta\vec{f} = w.dl.\vec{n}$$

where:

– w is the surface tension coefficient (a positive value);

– dl is an element of the curve on the free surface; and

– $\vec{n}$ is the normal of this element of the curve (see Figure 7.26).

a) Now consider a cylindrical pore of radius R containing a liquid of anchoring angle θ (see Figure 7.27). Supposing that the meniscus is spherical and has a radius R_{sph}, deduce from this the expression of the difference in pressure $P - P_0$ in terms of w and R_{sph} (this equation is called Laplace's law). Take $Pc = P - P_0$ and $\theta = 0$ (a perfectly anchored liquid), where Pc is the capillary pressure. Then simplify the previous expression and show that capillary pressure corresponds to a depression.

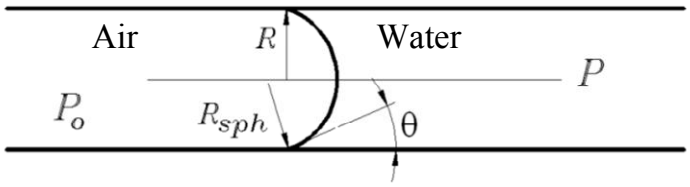

Figure 7.27. *Cylindrical pore*

b) We are considering the case of a porous material here whose porosity can contain liquid water and a gas composed of air and water vapor. The pressure in the liquid will be written as P_l; that in the gas P_g (air plus water vapor); and that in the water vapor P_v. We will also suppose that the transformations are isotherm. Free enthalpy is expressed by the relationship: $G = n\zeta$, where n is the number of moles and ζ is the chemical potential. We also have the Gibbs Duhem identity $S\mathrm{d}T + n\mathrm{d}\zeta - V\mathrm{d}P = 0$ where S is entropy, T is temperature, V is volume, and P is pressure.

Supposing that liquid water is incompressible, show that the chemical potential of liquid water ζ_l can be written as:

$$\zeta_l - \zeta_{l_0} = M(P_l - P_{l_0})/\rho_l$$

where:

– M is the molar mass of water and

– (ζ_{l_0}, P_{l_0}) is a reference state.

Then, supposing that water vapor follows the law of perfect gases ($PV = nR_{gp}T$), show that the chemical potential of water vapor ζ_v can be written as:

$$\zeta_v - \zeta_{v_0} = R_{gp}Tln(P_v/P_{v_0})$$

where R_{gp} is the perfect gases' constant (ζ_{v_0}, P_{v_0}) characterizing a reference state.

c) We will choose water $P_{l_0} = P_g$ as a reference state of liquid and $P_{v_0} = P_{vs}$ (the pressure of saturating vapor) for water vapor. We suppose that at thermodynamic equilibrium, we have $\zeta_l = \zeta_v$. Deduce from this that $\zeta_{l_0} = \zeta_{v_0}$. Defining relative humidity $H(0 \leq H \leq 1)$ as the P_v/P_{vs} ratio, show that we get Kelvin's law:

$$P_c = P_l - P_g = \frac{R_{gp}.T.\rho_l}{M} \ln H$$

d) Introducing into the previous equation Laplace's law (see Part 5a of exercise 7.5.), deduce the expression of the pore radius R_{sat} corresponding to a given relative humidity H at liquid-vapor equilibrium.

6) *Flow in a crack – Poiseuille's relationship*

We will consider the flow of a fluid, along an axis $\vec{z}$, in a crack of length L and opening e, which is assimilated into two infinite parallel planes, such that the width l is infinitely larger than the opening e. The fluid is subject to a constant pressure P_1 with $z = 0$ and to a pressure P_2 with $z = L$.

Take $\Delta P = P_2 - P_1$. A diagram is given in Figure 7.28.

a) What can we say about the dependence between u_z and x? Isolating an element of a certain volume with a width l, length dz, and included between the planes ±y, create a balance of quantity of movement.

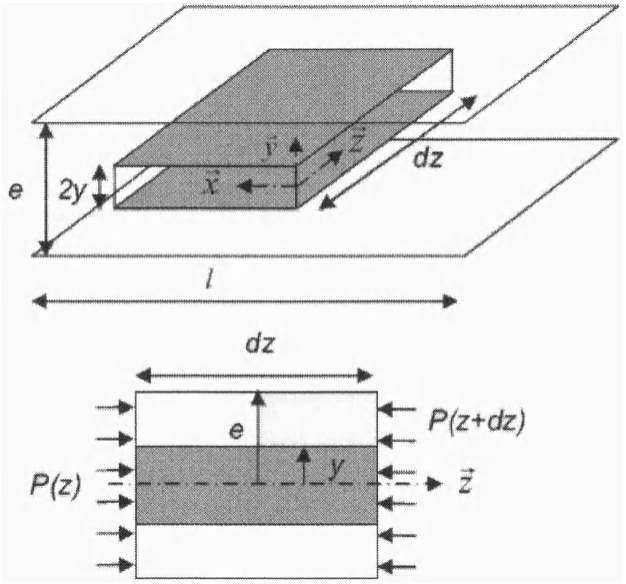

Figure 7.28. *Diagram of a crack*

b) Determine the expression of speed u_z in terms of ΔP, μ, y, L and an integration constant.

c) Suppose that the speed of the fluid in contact with the walls is zero. Deduce the expression of the integration constant, and then of speed u_z.

d) Show that the volume flow, Q, circulating throughout the crack can be written as (Poiseuille relationship):

$$Q = -\frac{e^3 .l.\Delta P}{12.\mu.L} \qquad [7.16]$$

7) *Gas permeability in a cracked environment*

We assimilate each crack into an opening separated by two infinite parallel planes. In order to quantify the number n of cracks in the element of

volume given in Figure 7.29 and its thickness e (which is constant), we define the damage variable of the environment, D, as being the ratio between the area of the cracks A_v (perpendicular to axis $\vec{z}$) and the total area A:

$$D = A_v/A \qquad [7.17]$$

a) Determine the relationship between D, n, h and e.

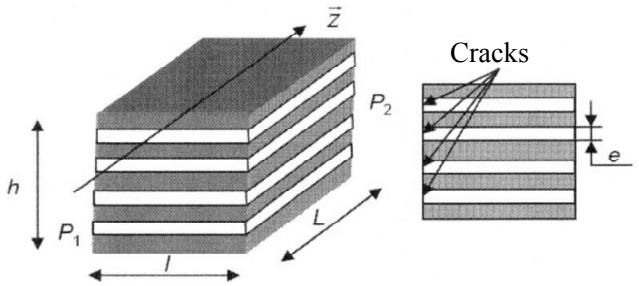

Figure 7.29. *Diagram of a cracked environment*

b) Using relationships [7.16] and [7.17], express the permeability of the cracked environment k in terms of D and e.

c) The approximation proposed for cracks actually does not conform to experimental results. It is suggested that we introduce the correction coefficient χ, in comparison to Poiseuille's equation [7.16]. We give the experimental values in Table 7.5 for a crack where there is a pressure variation P = -100 Pa, and a length L = l = 1 m.

***e* (mm)**	0.00	0.25	0.50	0.75
***Q* (m^3/h)**	0.0	3.6	39.6	140.4

Table 7.5. *Flow measured through a crack depending on the opening*

Suggest a numerical method used to identify the value of the correction coefficient χ. Then calculate this coefficient using the method of your choice.

8) *Application to a confinement enclosure in a peripheral nuclear reactor building*

Consider the case of a decennial test of a confinement enclosure. Assimilate the wall of the enclosure of a parallelipipedic wall (see Figure 7.30). The thickness is L = 1.2 m. Consider an area A = 6,880 m^2 of concrete. The volume of the enclosure is Ve = 75,300 m^3.

Suppose that the enclosure is built of material 1 (see Exercise 7.4). Look first at a case where there is no crack. The fluid circulating in the enclosure is air. Suppose that P_1 = 0.6 MPa and P_2 = 0.1 MPa.

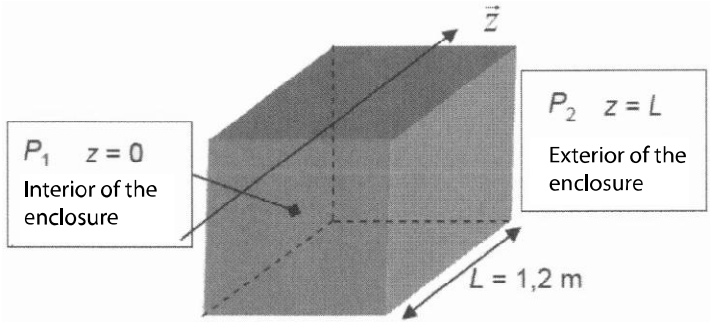

Figure 7.30. *Simplified diagram of an enclosure*

a) Supposing that the pores do not contain any water (see equation [7.1]), calculate the volume flow of air Q_a, and then the volume V_a of air having traversed the wall during a 24-hour period.

b) Now consider that the pores can contain water. The water content in a pore can be assessed via its relative humidity (see point 4). Suppose two cases for the evolution of relative humidity $H(z)$ in the wall of the enclosure (j being the case number):

$$H_j(z) = \alpha_j + \beta_j z + \gamma_j z^2.$$

The values of the coefficients are given in Table 7.6. Using the results obtained in point 5d, consider that if the pore radius R is lower than R_{sat}, the pore is saturated with water (the transport of air is impossible); if not, the

pore does not contain water (the transport of air can be calculated using equation [7.15]).

	α_j	β_j	γ_j
Case 1	1	0	0
Case 2	0.464	1.472	-1.153

Table 7.6. *Coefficients used to estimate relative humidity depending on z*

For the two profile conditions of relative humidity, recalculate the value of permeability, taking into account the presence of water in some pores. Then deduce the volume V_a of air having traversed the wall during a 24-hour period. Compare this result to exercise 7.5 point 8a. We give the perfect gases constant as:

$R_{gp} = 8.314$ J.mol−1.°K^{-1},

$w = 0.073$ N.m^{-1},

$M_H = 1$ g.mol^{-1} and

$M_O = 16$ g.mol^{-1}.

The pores are considered cylindrical and parallel.

c) Now take into account the existence of cracks assimilated into the openings between two parallel planes (supposed to be infinite) separated by a distance e. The value of the damage is D. We will also use the correction coefficient calculated in exercise 7.5 point 5c.

Considering the maximum volume of air traversing the wall determined in exercise 7.5 point 8b, fill out Table 7.7 (giving the volume of air having traversed the wall during a 24-hour period) for the various damage values D and the values of the openings in the cracks e. Explain this calculation and compare these values to the requirements of the enclosures.

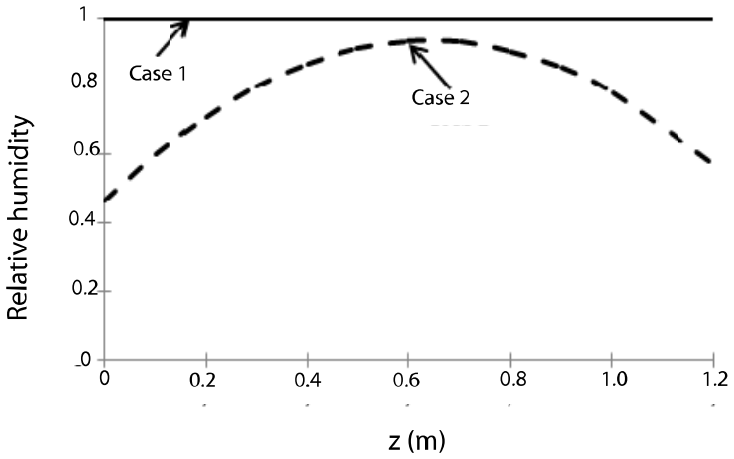

Figure 7.31. *Evolution of relative humidity in the two cases*

	e = 100 μm	e = 300 μm
$D = 50.10^{-10}$		
$D = 100.10^{-10}$		

Table 7.7. *Volume of air having traversed the wall in a 24-hour period depending on damage and the opening of the cracks*

Index

A, B

absorption, 7, 9, 12, 15, 17, 36, 70, 146, 180, 314, 315
  absorption of water, 12
angle of connection, 315, 318
apparent
  coefficient, 240
  volume of granular material, 2
BET, 56, 73-78, 81-86, 125, 137, 163, 165
BJH method, 169-171, 174, 187
Blaine device, 56, 59, 64, 67, 69, 78, 81, 125, 296, 299
Boltzmann transformation, 217, 218
Brownian movement, 195, 196, 198, 201, 202

C

capillarity, 145, 146
capillary
  ascension, 153-155
  condensation, 73, 84, 167, 187
  pressure, 155, 157, 306, 315, 316, 318, 326
carbonation, 223, 227, 256, 262, 308, 311
Carman-Kozeny, 297, 298, 299
CEMBUREAU permeameter, 283, 284
compactness, 102
  isocompactness, 113
  maximum, 98
compaction index, 109
critical radius, 160, 248
cumulative granular curve, 25, 53

D

Darcy's law, 257, 280, 282, 286, 287, 289, 291-293, 295, 303, 305, 317
deflocculation, 119, 120
differential calorimetry, 173
diffusion
  cell, 228, 236, 237, 270
  coefficient, 195, 198-201, 203, 205, 207, 219, 220, 222-232, 235, 237, 238, 240-246, 248-263, 267-272, 276, 277, 279

E, F

effective coefficient, 223
electric field migration, 233
electrochemical potential, 205, 206
electrostatic repulsion, 6, 115, 117
expansion, 116, 117, 144, 178

flocs, 115, 118, 120, 123, 124, 125
fractal dimension, 138, 139, 174

G, H

gas pycnometer, 142, 143
gaseous diffusion, 195, 256, 259, 261
Gibbs Duhem, 326
high-performance concrete, 120, 121, 171, 172, 237, 244

I

image analysis, 140, 141, 164, 165, 175, 176
imbibition, 155, 157, 158, 164
immersion test, 240, 241
ionic diffusion, 205, 208, 219, 222, 243, 244, 260, 265
isocompactness, 113
isotherm, 72-78, 81, 83-85, 166, 169, 170-172, 178, 187, 189, 190, 223, 224, 227, 229, 230, 265, 326
  adsorption, 71, 72, 165, 170

K, L

Kelvin-Laplace, 165, 167-169, 187, 261
Knudsen diffusion, 258-260, 304
Lea and Nurse device, 59, 64, 65, 67, 70
level of saturation, 169

M, N

mercury porosimetry, 145, 156, 161, 163, 164, 187, 194, 248, 299, 302, 312
methylene blue test, 78
model
  with interaction, 106, 114
  compressible packing model, 109
  linear model without interaction, 105
  Powers model, 181, 255
molecular diffusion, 203, 205, 219, 243, 304
Nernst-Planck (relationship), 205, 207-209, 222, 231, 233, 234, 243, 266, 268

P

past, 47, 52, 87, 136, 137, 162, 184, 185, 247, 254, 265, 266, 277, 303-305, 312, 313, 314
penetration, 12, 70, 144, 163, 179, 216, 219, 222-226, 238, 239, 240, 243, 266, 268, 308
performance-based approach, 307-309
permeability coefficient, 279, 281, 282, 316
porosimetry, 145, 158, 163, 164, 184, 318
porosity, 4, 5, 12, 18, 59, 60, 63, 65, 67, 69, 90-93, 95-101, 115, 116, 119, 120, 122-124, 126, 127, 131, 133-136, 139-144, 156, 160, 162, 166, 175, 181-187, 190-194, 221, 223, 226, 244, 246-249, 254, 255, 260, 262, 266, 268, 269, 272, 274, 276, 277, 279, 287, 297, 298, 302, 304, 306, 308, 312, 313, 316-318, 320, 323-326
Powers model, 181, 255

S, T

shape of grain, 19, 20, 21, 87, 124
sieving, 20, 21, 23, 24, 25, 26, 27, 29, 139
specific surface, 55-60, 63, 70, 75-83, 85, 125, 126, 133, 136, 137, 163, 175, 296, 299, 317, 318

state of saturation, 244, 260, 261, 292, 294, 308, 316
superplastifiant, 119
surface tension, 146-148, 150, 152, 154, 167, 173, 179, 185, 194, 315, 318, 325, 326
thermoporometry, 172, 174

V, W

volume of voids, 133, 190, 274, 298
wall effect, 96, 97, 107, 111, 134
water content, 120, 132, 302, 303, 307, 316, 330
water-accessible, 142, 156